Institute of Condensed Matter and Nanosciences

Bio and Soft Matter division

Dynamic Polymer Hydrogels Based on the Orthogonal Combination of Reversible C=N Bonds and Metal-Ligand Coordination Bonds

Hui Yang

Supervisors: **Professor Charles-André Fustin**

Professor Evelyne Van Ruymbeke

Thesis submitted in fulfilment of
the degree of Doctor in Sciences

Louvain-la-Neuve 2021

Institute of Condensed Matter and Nanosciences

Bio and Soft Matter division

Dynamic Polymer Hydrogels Based on the Orthogonal Combination of Reversible C=N Bonds and Metal-Ligand Coordination Bonds

Hui Yang

Members of Jury:

Prof. Charles-André Fustin (UCLouvain), Supervisor
Prof. Evelyne Van Ruymbeke (UCLouvain), Supervisor
Prof. Yann Garcia (UCLouvain), Chairperson
Prof. Michael Singleton (UCLouvain), Secretary
Prof. Jean-François Gohy (UCLouvain)
Prof. Richard Hoogenboon (UGent)
Prof. Michel Cloitre (ESCPI, France)

Thesis submitted in fulfilment of
the degree of Doctor in Sciences

Louvain-la-Neuve 2021

Acknowledgements

The four years I have enjoyed at UCLouvain have been some of the best of my life. This thesis is more than a summary of my PhD work, it is the fruit of all the love and support I have received.

I would like to first and foremost acknowledge my supervisor, Prof. Charles-André Fustin, for his support, guidance, drive and patience throughout the entire period of my PhD studies. His serious and meticulous attitude towards scientific research has deeply impressed me and enabled me to become a better researcher. I am eternally grateful for his many productive discussions, insightful advice and patient assistance in sustaining me through many challenging times. I would also like to thank my co-supervisor, Professor Evelyne Van Ruymbeke, for her pro bono time and efforts in guiding my work. Her profound knowledge of rheology provided informative discussions that were essential to understanding my PhD work.

Many thanks to the members of my thesis jury, Prof. Jean-François Gohy, Prof. Michael Singleton, Prof. Yann Garcia, Prof. Richard Hoogenboon and Prof. Michel Cloitre for taking the time to read my thesis and providing valuable advice to improve it.

To my lab mates, Dr. Jagadeesh malineni, Dr. Atul kumar Sharma, Dr. Sina Ghiassinejad, Clement Coutouly, Rowanne Lyons, Lu Bai, Dr. Miriam Khodeir, Dr. He Jia, Dr. Hamid Taghipour, Alexis Andre, Yanzhao Li, Dr. Naima Sallem, I appreciate all the help and the generous sharing of laboratory resources. A special thanks to Dr. Sina Ghiassinejad for his expert help with rheological measurements and data analysis.

These are some of the most talented people I have had the opportunity to work with and I am grateful for all the collaboration we have had that has made my work here easier and my time here more

enjoyable. I am also thankful to all the people I have met in Louvain-la-Neuve that have made my life rich and fulfilling but are too numerous to list here.

Finally, I would like to give a special acknowledgment to my beloved wife, who has been a constant source of love, encouragement and energy for me. I am also very grateful to my mum, dad, and my younger brother for their love and support.

Financial support from the China Scholarship Council (CSC) is gratefully acknowledged.

Abstract

Dynamic polymer hydrogels crosslinked by dynamic bonds are capable of a controlled lifetime, enhanced toughness, self-healing properties or responsiveness to external stimuli. Dynamic bonds generally fall into two categories: supramolecular interactions and dynamic covalent bonds, which can break and reform spontaneously or in response to external stimuli. Supramolecular interactions (e.g., hydrogen bonds, metal-ligand coordination bonds, host-guest interactions) are labile and reversible, and usually under (fast) continuous equilibrium between associated and dissociated forms. In comparison with supramolecular interactions, dynamic covalent bonds (e.g., C=N bonds, disulfide bonds, boronic ester bonds) are much more robust but also exhibit slower exchange. The pros and cons of these two types of linkages make them a promising complementary toolbox for the design and fine-tuning of the properties of hydrogels. The focus of this dissertation is the development of dynamic polymer hydrogels by the orthogonal combination of dynamic covalent bonds and supramolecular interactions, and the investigation of the contribution of the two types of dynamic bonds to the properties of the hydrogels. Metal-terpyridine coordination bonds (zinc(II)-terpyridine and iron(II)-terpyridine bis-complexes) and reversible C=N bonds (acylhydrazone and oxime) were selected and employed as crosslinks to form hydrogels.

First, we sought to design four interpenetrating polymer network (IPN) hydrogels with tunable combinations by leveraging the differences in lifetime and stability of the two types of dynamic bonds. The dynamic, oscillatory mechanical properties and pH responsiveness of the four hydrogels were systematically investigated using oscillatory rheological methods. Second, we prepared hydrogels with three topological strategies, namely, IPN, dual-crosslinked network (DCN) and double network (DN), using a combination of zinc(II)-terpyridine

bis-complexes and oxime bonds. The dynamic and linear rheological behaviors of hydrogels prepared by these three strategies that allow the integration of two dynamic bonds into one system were explored and compared. Finally, we prepared and compared the rheological properties of two DN hydrogels made from a combination of labile zinc(II)-terpyridine bis-complexes and stable oxime bonds, as well as a combination of less stable acylhydrazone bonds and long-lifetime iron(II)-terpyridine bis-complexes. Overall, this work has demonstrated the feasibility and interest in combining dynamic covalent bonds and supramolecular interactions for the preparation of dynamic polymer hydrogels, and has explored the pros and cons of three network topologies for combining the two crosslinks into a polymer hydrogel.

Table of Contents

List of Abbreviations

AAm: Acrylamide

ADH: Adipic dihydrazide

AFM: Atomic force microscopy

AG: Amino gelatin

Aga: Agarose

AIBN: 2,2'-Azobis(isobutyronitrile)

AIE: Aggregation-induced emission

AMSA: Aldehyde methacrylate sodium alginate

BIS: N,N'-Methylene bis(2-acrylamide)

CAN: Covalent adaptable network

CB[8]: Cucurbit[8]uril

CEC: N-Carboxyethyl chitosan

CMC: Carboxymethyl cellulose

CMCS: Carboxymethyl chitosan

CNCs: Cellulose nanocrystals

Cys: Cysteamine hydrochloride

DA: Diels-Alder reaction

DAAM or DAAm: Diacetone acrylamide

DAMC: Dialdehyde methylcellulose

DB: Dynamic bond

DCB: Dynamic covalent bond

DCC: Dynamic covalent chemistry

DCN: Dual-crosslinked network

DDMAT: S-1-dodecyl-S'-(α,α'-dimethyl-α"-acetic acid) trithiocarbonate

DFO: Deferoxamine mesylate

DLS: Dynamic light scattering

DMA: N,N-Dimethyl acrylamide

DMF: N,N-Dimethylformamide

DN: Double network

DTP: 3,3'-Dithiopropionic acid dihydrazide

DTT: 1,4-Dithiothreitol

EDTA: Ethylenediaminetetraacetic acid

ELP: Elastin-like protein

EPL: Polylysine

EWG: Electron withdrawing group

FCC: N-(furfural)carboxymethyl chitosan

Fe^{2+}-Tpy: Iron (II)-terpyridine bis-complexes

FTIR: Fourier-transform infrared

GC: Glycol chitosan

GE: Gelatin

GelMA: Gelatin methacrylate

GPC: Gel permeation chromatography

HA: Hyaluronic acid

HEMA: 2-Hydroxyethyl methacrylate

HPMA: N-(2-Hydroxypropyl)methacrylamide

HTCC: Chitosan quaternary ammonium salt

IONPs: Iron oxide nanoparticles

IPN: Interpenetrating polymer network

LCST: Lower critical solution temperature

LVE: Linear viscoelastic range

M(II)-Tpy: Metal(II)-terpyridine bis-complexes

MAA: Methacrylic acid

MBA: N,N'-Methylenebisacrylamide

MC: Methylcellulose

MRI: Magnetic resonance imaging

NIPMAM: N-Isopropylmethacrylamide

NIR: Near-infrared

NLVE: Non-linear viscoelastic range

NMR: Nuclear magnetic resonance

NPs: Nanoparticles

OA or OSA: Oxidized alginate

OCMC: Oxidized carboxymethyl cellulose

OD-DA: Oxidized dextran-dopamine

ODex: Oxidized dextrans

OEG: Oligoethylene glycol

OEGMA: Oligo(ethylene glycol) methacrylate

OG: Oxidized gellan gum

P(DMAMEA): Poly(2-(dimethylamino)ethyl methacrylate)

PAA: Polyacrylic acid

PAAm: Polyacrylamide

PBI: Perylene bisimide

PBS: Phosphate buffer saline

PDA: Polydopamine

PDMA: Poly(N,N-dimethyl acrylamide)

PEG: Poly(ethylene glycol)

PEI: Polyetherimide

PETMA: Pentaerythritol tetramercaptoacetate

Phe: Phenylalanine

PHEMA: Poly(2-hydroxyethyl methacrylate)

PiPOx: Poly(2-isopropenyl-2-oxazoline)

PL: Poly-l-lysine

PNIPAAm or PNIPAM: Poly(N-Isopropylacrylamide)

POEGMA: Poly(oligo ethylene glycol methacrylate)

PS: Polystyrene

PTHP: Poly-tetrahydropyrimidine

PVA: Polyvinyl alcohol

QCS: Quaternized chitosan

QMC: Quaternized methacryloyl chitosan

RAFT: Reversible addition-fragmentation transfer

RT: Room temperature

SA: Sodium alginate

SANS: Small-angle neutron scattering

SAOS: Small amplitude oscillatory shear

SCN: Single-crosslinked network

SEC: Size exclusion chromatography

TCN: Triple-crosslinked network

TEA: Triethylamine

TEM: Transmission electron microscopy

TM: Thiol-Michael reaction

TPE: Tetraphenylethylene

Tpy: 2,2':6',2"-Terpyridine

TPy-AM: N-(3-([2,2':6',2"-terpyridin]-4'-yloxy)propyl)-N-methylacrylamide

TPy-DEG-AM: N-(2-(2-([2,2':6',2"-terpyridine]-4'-yloxy)ethoxy)ethyl) acrylamide

Upy or UPys: Ureidopyrimidinones

Zn^{2+}-Tpy: Zinc (II)-terpyridine bis-complexes

γ-PGA: Poly(γ-glutamic acid)

List of Symbols

Đ: Dispersity

E_a: Activation energy

f: Functionality of the crosslinks

G": Loss modulus

G': Storage modulus

G'_p: Experimental plateau modulus

G_N^0: Theoretically plateau modulus

ρ_0: Density of PDMA

$\varphi_{dangling}$: Weight fraction of dangling ends

k_a: Bond association (formation) rate

k_d: Bond dissociation rate

K_{eq}: Thermodynamic equilibrium constant

M_n: Number average molar mass

M_w: Weight average molar mass

M_{xx}: Number-average molar mass of a network strand

N_{Av}: Avogadro's number

γ_c: Critical strain of linear viscoelastic range

γ_L: Limiting strain of linear viscoelastic range

γ_r: Rupture strain of G' and G" crossover point

γ_y: Yield strain of linear viscoelastic range

$\Delta G^{\ddagger}$: Gibbs free energy

$\Delta H^{\ddagger}$: Enthalpy of activation

$\Delta H^{\ominus}$: Standard enthalpy change

$\Delta S^{\ddagger}$: Entropy of activation

$\Delta S^{\ominus}$: Standard entropy change

ν: Number of elastically effective network strands per unit volume

ρ: Network density

τ: Stress relaxation time

$\tau_{Acylhydrazone}$: Average lifetime of the acylhydrazone network

$\tau_{Zn\text{-}Tpy}$: Average lifetime of the Zn^{2+}-Tpy network

ω: Angular frequency

γ: Strain

δ: Loss factor tan

ξ: Mesh size of network

σ: Stress

Chapter 1

Objectives

Abstract

Complementary interactions are, in nature, central to all biological processes and are usually mediated by several reversible chemistries. Inspired by these reversible systems, multiple orthogonal dynamic bonds are incorporated within hydrogel networks to interact in a synergistic manner towards superior properties. In this chapter, the strategies to develop a series of novel dynamic hydrogels with two types of dynamic crosslinks, i.e., reversible C=N bonds and metal-ligand coordination bonds, will be presented. The goal, strategy and methodology of this thesis will be discussed.

1.1. Introduction

In the past decades, dynamic bonds have emerged as a powerful synthetic tool in the preparation of hydrogels.[1, 2] Dynamic bond can be described as any kind of bond which can break and reform autonomously or in response to external stimuli.[3] Dynamic bonds can be classified into two main categories: non-covalent/supramolecular interactions and dynamic covalent bonds (DCB).[4-6] By virtue of their labile and reversible nature, supramolecular interactions are usually under (fast) continuous equilibrium between associated and dissociated forms, which allows supramolecular hydrogels to exhibit high sensitivity to environmental stimuli, and to be capable of self-healing.[7-10] The thermodynamic equilibrium of dynamic covalent bonds is usually much slower than typical supramolecular interactions since the intrinsic covalent linkages are more stable than supramolecular interactions. Thus, most DCB require external stimuli (e.g., addition of a catalyst, heating, light) to achieve equilibrium within acceptable timescales.[11] On the other side, the slow kinetics allows DCB to have greater chemical stability and to be more robust than supramolecular interactions. The pros and cons of these two types of interactions make them promising complementary candidates for synthesizing dynamic hydrogels with tunable properties.

Introducing dynamic bonds into polymer networks can confer them desirable characteristics such as self-healing, shape memory, printability, adaptability, enhanced mechanical properties (such as high compressibility, tensile strength or elasticity).[11-17] Up to now, a broad range of dynamic hydrogels have been investigated, based on either a single type of supramolecular interaction, a single type of dynamic covalent bond, or a combination of two types of supramolecular interactions.[18-21] Very few reports, however, focused on multiple dynamics hydrogels based on DCB, i.e., the combination of two types of DCBs, or of DCB and supramolecular interactions.[1] DCB-based crosslinked polymer networks with multiple dynamic bonds have been

developed within the last decade,[22] but most of these efforts have focused on solid state systems (elastomers, thermosets).[23] Therefore, fundamental and applied investigations on gel-like soft and wet materials[24] remain to be developed.

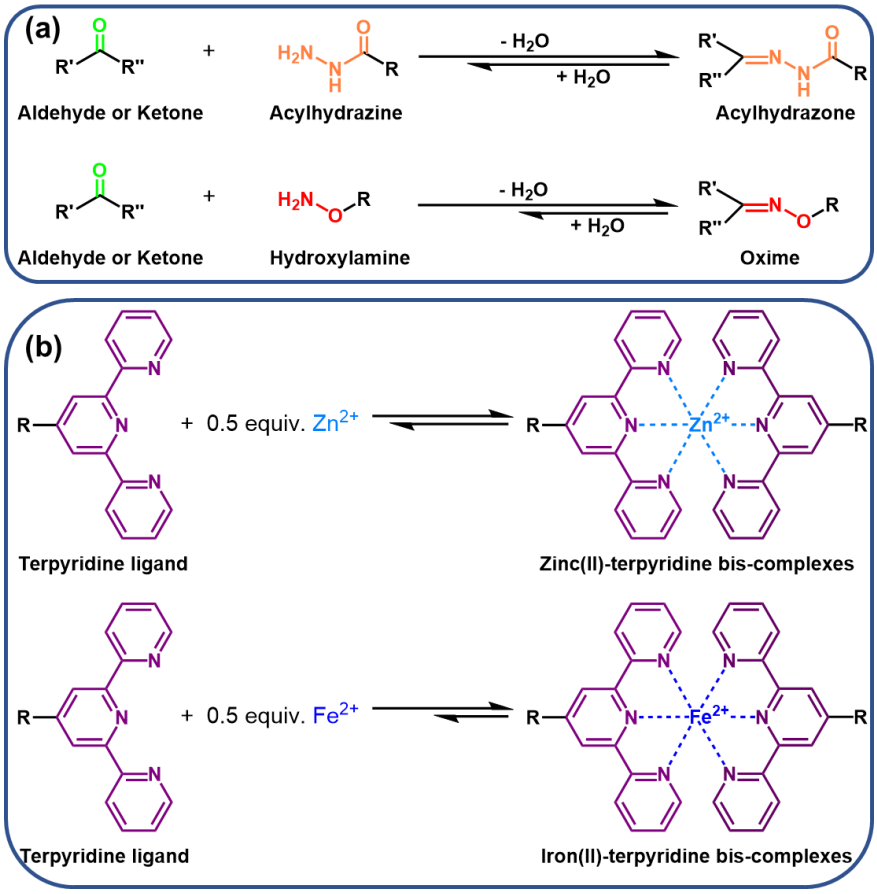

Figure 1.1. Schematic representation of dynamic bonds used in this work: (a) acylhydrazone and oxime reversible C=N bonds; (b) metal-ligand coordination bonds.

As two types of dynamic Schiff base bonds[25] formed by "click" reactions[26] upon the condensation between a acylhydrazine/hydroxylamine and a carbonyl group (aldehyde or ketone), acylhydrazone/oxime bonds (**Figure 1.1a**) are one of the most

successful DCB used so far in dynamic covalent chemistry.[27-29] Due to the improved hydrolytic stability over an imine bond, acylhydrazone/oxime bonds are able to form strong but reversible networks and hydrogels. The integration of these reversible C=N bonds into networks can provide gels with desirable properties including stimuli-responsiveness,[30] self-healing,[31] injectability[32] and high mechanical strength,[33] allowing them to be used in areas such as biomedicine and 3D printing.[34, 35]

Among supramolecular interactions, metal-ligand coordination bonds are particularly interesting because their characteristics (lifetime, strength) can be tuned over several orders of magnitudes simply by changing the metal ions (or the ligand) used,[36] they can be used in a range of solvents, and they may confer additional useful properties (catalytic, magnetic, photoactive,…) to the materials.[37] Terpyridine ligands (**Figure 1.1b**) will be used in this project since several derivatives are commercially available, allowing for easy functionalization of the polymers, and they are able to complex a very broad range of transition metal cations.[38-40] Combination of acylhydrazone/oxime bonds with the terpyridine-metal interactions may bring hydrogels with interesting properties for practical applications.

1.2. Goal and strategy

This thesis therefore aims to investigate the effects of the orthogonal combination of two types of dynamic crosslinks (acylhydrazone/oxime and metal-terpyridine bis-complexes) on the hydrogel properties, and to further understand the impact of network topologies on these hydrogels. To achieve this, one network topology has first to be chosen to build a series of dynamic hydrogels based on various crosslink combinations. This will allow us to evaluate the contribution of each crosslink type to the final hydrogel properties. On

this basis, we will be able to select two of these crosslinks as a representative orthogonal combination, and, based on this combination, to construct hydrogels with various network topologies to study the influence of network topologies on the hydrogel properties.

Our design will have the following advantages: 1) the hydrogels will be based on simple and easily accessible building blocks; 2) the hydrogels could respond to a wide range of (orthogonal) stimuli, which will be crucial for further applications; 3) the design strategy will allow the introduction of a large variety of functional groups to confer additional properties. This strategy will lead to the property/function-driven generation of new adaptive systems that could be further developed for practical applications in diverse fields.

As discussed above, different network topologies will be prepared combining acylhydrazone/oxime and metal-terpyridine bis-complexes in one hydrogel system. The first system is an interpenetrating polymer network (IPN)[41] (**Figure 1.2a**), which comprises two sub-networks, both of which completely fill the available space and mutually interpenetrate, but, structurally at least, appear not to interact or influence one another. Therefore, the two sub-networks will be based on acylhydrazone/oxime crosslinks and on metal-terpyridine bis-complexes crosslinks. Another possibility is to fabricate a dual-crosslinked network (DCN) (**Figure 1.2b**), which is a single network built from two different crosslinks (acylhydrazone/oxime bonds and metal-ligand bonds).

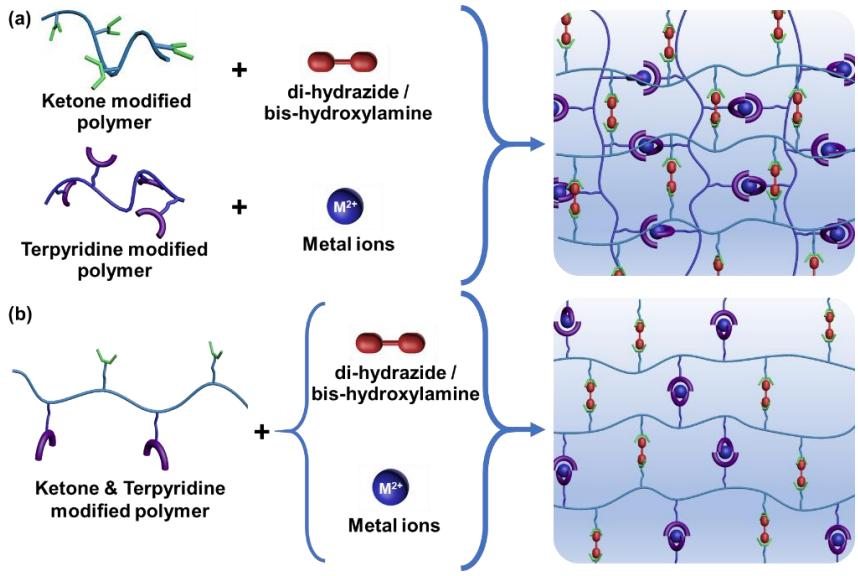

Figure 1.2. Schematic representation of interpenetrating polymer network (IPN) hydrogels (a), and dual-crosslinked network (DCN) hydrogels (b), based on the acylhydrazone/oxime bonds and metal-terpyridine bis-complexes.

As shown in **Figure 1.2a**, IPN hydrogels are fabricated from two polymers, each bearing a different type of functional groups. In comparison, DCN hydrogels are made from only one polymer containing the two types of reactive groups (**Figure 1.2b**). The IPN hydrogels were chosen as the first topology to understand the impact of the different types of crosslinks on the gel properties, because IPNs allow the combination of the desired properties of each network (e.g. stimuli-responsiveness),[42] and even more, because they may show enhanced mechanical properties due to synergistic interactions between the sub-networks that transfer the stress and dissipate mechanical energy upon deformation.[43]

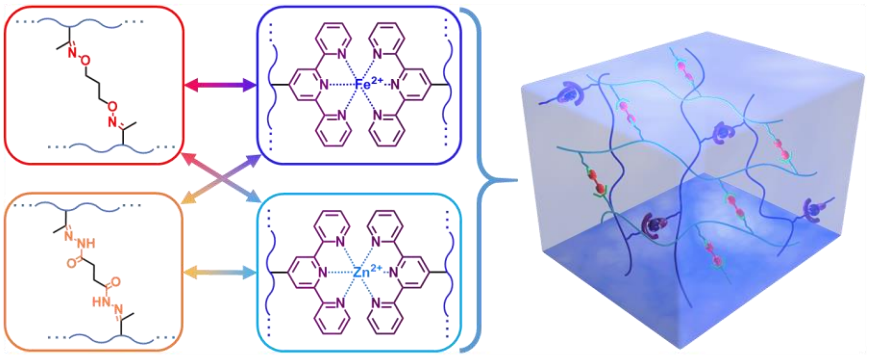

Figure 1.3. The Schiff base bonds and metal-ligand bonds used for preparing IPN hydrogels.

In order to obtain IPN hydrogels with different combinations of crosslinks, we selected two Schiff base bonds and two metal-terpyridine bis-complexes (**Figure 1.3**). The first polymer bears ketone pendant groups and will be crosslinked by di-acylhydrazine/bis-hydroxylamine compounds to form acylhydrazone/oxime bonds to obtain the DCB sub-network. The second polymer bears terpyridine side groups and will be crosslinked by the addition of transition metal cations (Zn^{2+} or Fe^{2+}) to form zinc(II)-terpyridine bis-complexes (Zn^{2+}-Tpy) or iron(II)-terpyridine bis-complexes (Fe^{2+}-Tpy) to obtain the supramolecular sub-network.

Due to the different nature of the crosslinkers, the bond strength and kinetic stability of the DCB (acylhydrazone or oxime) and of the supramolecular interaction (Zn^{2+}-Tpy or Fe^{2+}-Tpy) can be independently tuned. As shown in **Figure 1.3**, four IPN hydrogels can thus been obtained by combining these interactions in different ways. First, a more stable (i.e., characterized by a high equilibrium constant) DCB is combined with a long-lifetime supramolecular interaction (Oxime + Fe^{2+}-Tpy) or with a labile supramolecular interaction (Oxime + Zn^{2+}-Tpy). Second, a less stable DCB is combined with the long-lifetime supramolecular interaction (Acylhydrazone + Fe^{2+}-Tpy), or with the labile supramolecular interaction (Acylhydrazone + Zn^{2+}-Tpy).

After an in depth understanding of the contributions of these various combinations of crosslinks on the IPN properties, we selected the combination of Oxime + Zn^{2+}-Tpy to prepare hydrogels with different topologies. By comparing the properties between DCN and IPN hydrogels with the same dynamic bond combination, we can explore how the network topology affects the properties of the hydrogels.

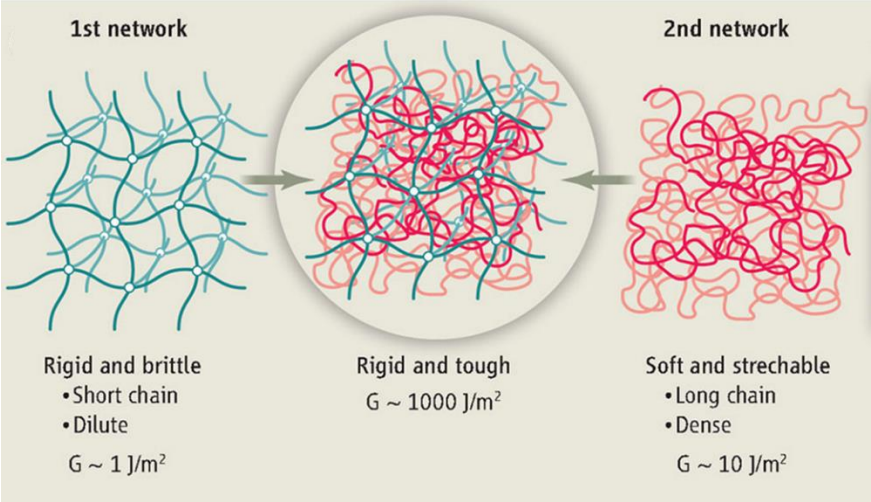

Figure 1.4. Schematic representation of double network by combining two interpenetrated polymer networks.[43]

In addition, as a special case of IPN hydrogels, double network (DN) hydrogels will be also prepared. These hydrogels have received immense interest since Gong and co-workers developed them in 2003 due to their high strength and toughness.[44-47] As shown in **Figure 1.4**, the traditional DN hydrogels consist of two interpenetrating and asymmetric covalently crosslinked polymer sub-networks with contrasting mechanical properties. The first highly stretched and densely crosslinked network is stiff and brittle, and acts as the energy-dissipating sacrificial component. The second flexible network is sparsely crosslinked, and acts as a stretchable network maintaining the

hydrogel integrity during deformation. However, the rupture of the first network on successive loadings will lead to permanent internal damages due to the irreversibility of covalent bonds, making DN hydrogels show stress-induced softening and poor fatigue resistance. To improve the fatigue resistance of DN hydrogels, non-covalently crosslinked sub-networks have been used to design hybrid physically and chemically, or fully physically, crosslinked DN hydrogels.[45-50] Nonetheless, there are still some challenges to design DN hydrogels with superb mechanical properties and versatility.

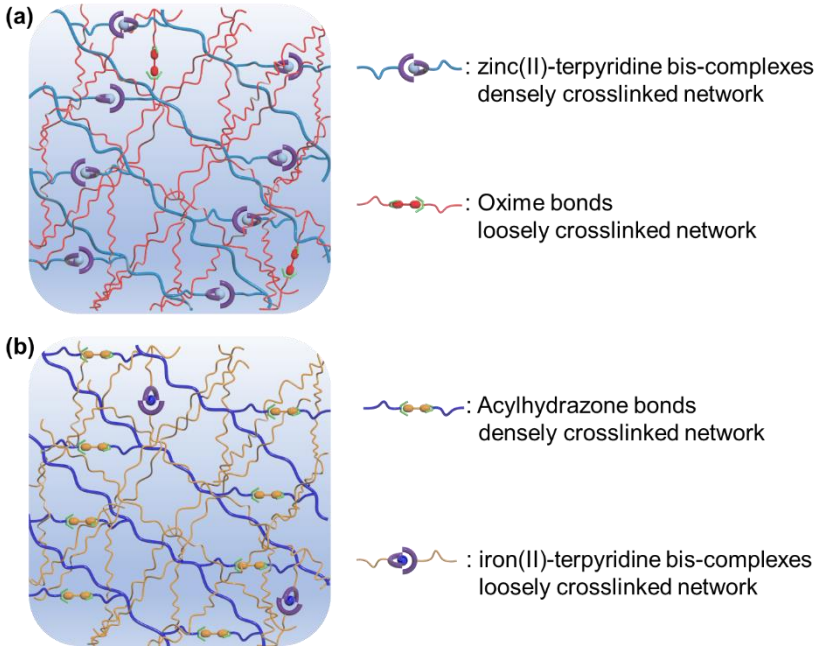

Figure 1.5. Schematic representation of double network (DN) hydrogels based on labile metal-terpyridine bis-complexes with oxime bonds (a), and long-lifetime metal-terpyridine bis-complexes with acylhydrazone bonds (b).

Inspired by the concept of DN hydrogels, our IPN systems could be modified to develop two types of novel dynamic DN hydrogels as shown in **Figure 1.5**. The first system could be prepared from a short chain highly terpyridine-functionalized copolymer crosslinked by zinc

ions to get labile associations as the first network, and a long chain sparsely ketone-functionalized copolymer crosslinked by bis-hydroxylamine to form stable oxime bonds as the second network (**Figure 1.5a**). In contrast, the second system could employ a short chain highly ketone-functionalized copolymer crosslinked by di-acylhydrazine to obtain the less stable acylhydrazone bonds as the first network, and the second network could be made from a longer chain sparsely terpyridine-functionalized copolymer crosslinked with iron ions to give long-lifetime associations (**Figure 1.5b**). Developing these two types of DN hydrogels and comparing their properties will facilitate our understanding of how the location of the different types of dynamic bonds in the double networks influence the properties of the hydrogels. This will be significant for the design of dynamic DN hydrogels with outstanding properties.

1.3. Research methodology

The first step is the synthesis of the different building blocks bearing the desired binding motifs. In this study we have chosen poly(N,N-dimethyl acrylamide) (PDMA) as the backbone polymer for fabricating hydrogels, because PDMA is a hydrophilic biocompatible polymer with good mechanical and film-forming properties, and has numerous applications in molecular biology, DNA sequencing, medical and pharmaceutical fields including contact lenses and drug delivery.[47] The commercially available and nontoxic monomer of diacetone acrylamide (DAAM), which contains a ketone group that can react with di-acylhydrazine/bis-hydroxylamine compounds to form acylhydrazone/oxime bonds, will be employed to create DCB-based networks. A hydrophilic terpyridine-functionalized monomer will be synthesized to form metal-terpyridine bis-complexes with various strengths and labilities in combination with transition metal ions. The copolymers will be prepared by copolymerizing the functionalized monomers, only one of them or both of them, with DMA as the base

monomer. Reversible addition-fragmentation chain transfer controlled radical (RAFT) polymerization will be used to this aim.

In this thesis, the crosslinks used to form reversible C=N bonds (acylhydrazone/oxime) are formed by a condensation reaction between copolymers bearing ketone side groups (electrophilic carbonyl moiety) and succinic dihydrazide/O,O'-(propane-1,3-diyl)bis(hydroxylamine) crosslinkers (α-nucleophile). As shown in **Figure 1.6**, the resulting acylhydrazone or oxime bonds differ from typical Schiff base ligands (**Figure 1.6b**), which have an aryl group bonded to the carbon or nitrogen of the C=N bond.[51] As a result, our designed acylhydrazone or oxime bonds do not form stable complexes with metal ions. This implies that these acylhydrazone or oxime bonds will essentially not compete with the strong terpyridine tridentate ligands for metal ions in the same system. In other words, the acylhydrazone or oxime bonds in this thesis can co-exist with metal(II)-terpyridine bis-complexes without affecting each other.

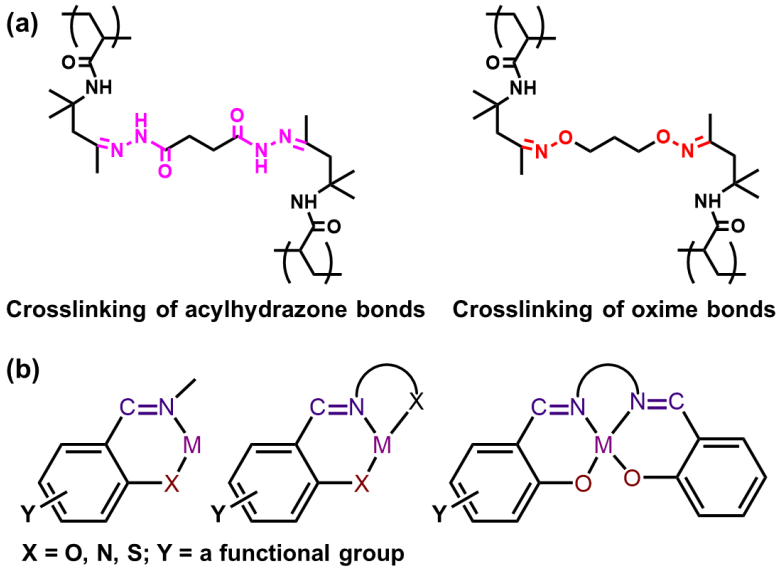

Figure 1.6. Schematic representation of (a) reversible C=N bonds used in this thesis, and (b) typical Schiff base ligands.[51]

The IPN systems are based on two ‘short-chain’ (M_n: 40 ~ 50 kDa) copolymers: The first one bears ketone pendant groups and can be crosslinked by di-acylhydrazine/bis-hydroxylamine compounds to form acylhydrazone/oxime bond-based DCB networks. The second one bears terpyridine side groups and can be crosslinked by the addition of transition metal cations to obtain metal-terpyridine bis-complexes-derived supramolecular networks. The DCN system is based on one copolymer, which bears both ketone and terpyridine groups on the same chain. In order to be comparable to the IPN systems, the copolymer used for DCN should have a comparable molecular weight and functionalization ratio than the two copolymers used for IPN. For the DN hydrogels, a short-chain highly terpyridine-functionalized copolymer (M_n: ~ 50 kDa) and a long-chain sparsely ketone-functionalized copolymer (M_n: ~ 130 kDa) will be used for the system based on a labile densely crosslinked metal-ligand sub-network and a stable loosely crosslinked DCB sub-network. In a contrasting way, a short-chain highly ketone-functionalized copolymer (M_n: ~ 50 kDa) with a long-chain sparsely terpyridine-functionalized copolymer (M_n: ~ 130 kDa) will be used for the system having long-lifetime metal-terpyridine bis-complexes with acylhydrazone bonds. The dynamic mechanical properties of all hydrogels and networks will be characterized by rheology.

The works in this thesis provide some fundamental understanding for the development of novel dynamic hydrogels with tunable properties, not only in the selection of dynamic bonds but also in the design of network topologies. These are essential to design adaptive materials based on multiple dynamic bonds towards potential applications in materials science or mimic biological systems. The detailed work carried out during this thesis is described the next four chapters. In brief, they include:

Chapter 2 is a literature review that will discuss the synthesis, properties and applications of hydrogels of different topologies containing multiple dynamic bonds. To conclude this chapter a special focus will be made on hydrogels based either on reversible C=N bonds or on metal-terpyridine coordination bonds.

In Chapter 3, the contributions of four combinations (Oxime + Fe^{2+}-Tpy, Oxime + Zn^{2+}-Tpy, Acylhydrazone + Fe^{2+}-Tpy, Acylhydrazone + Zn^{2+}-Tpy) of crosslinks on the hydrogels properties of IPN will be discussed.

In Chapter 4, the characteristics of IPN, DCN and DN hydrogels made up of oxime bonds and Zn^{2+}-Tpy will be compared and discussed.

In Chapter 5, the two novel DN hydrogels illustrated in **Figure 1.5** will be compared and discussed.

Finally, the conclusions and future perspectives of this thesis will be discussed.

1.4. References

[1] De Alwis Watuthanthrige, N.; Chakma, C.; Konkolewicz, D. Designing dynamic materials from dynamic bonds to macromolecular architecture. Trends Chem. 2021, doi: 10.1016/j.trechm.2020.12.005

[2] Sattar, M. A.; Patnaik, A. Design Principles of Interfacial Dynamic bonds in self-healing materials: what are the parameters? Chem. Asian J. 2020, 15, 4215-4240.

[3] Wojtecki, R J.; Meador, M. A.; Rowan, S. T. Using the dynamic bond to access macroscopically responsive structurally dynamic polymers. Nat. Mater. 2011, 10, 14-27.

[4] Lehn J. M. Dynamic combinatorial chemistry and virtual combinatorial libraries. Chem. Eur. J. 1999, 5, 2455-2463.

[5] Lehn J. M. From supramolecular chemistry towards constitutional dynamic chemistry and adaptive chemistry. Chem. Soc. Rev. 2007, 36, 151-160.

[6] Rowan, S. J.; Cantrill, S. J.; Cousins, G. R. L.; Sanders, J. K. M.; Stoddart, J. F. Dynamic covalent chemistry. Angew. Chem., Int. Ed. 2002, 41, 899-952.

[7] Appel, E. A.; del Barrio, J.; Loh, X. J.; Scherman, O. A. Supramolecular polymeric hydrogels. Chem. Soc. Rev. 2012, 41, 6195-6214.

[8] Du, X.; Zhou, J.; Shi, J.; Xu, B. Supramolecular hydrogelators and hydrogels: from soft matter to molecular biomaterials. Chem. Rev. 2015, 115, 13165-13307.

[9] Hoque, J.; Sangaj, N.; Varghese, S. Stimuli-Responsive supramolecular hydrogels and their applications in regenerative medicine. Macromol. Biosci. 2019, 19, e1800259.

[10] Saunders, L.; Ma, P. X. Self-Healing supramolecular hydrogels for tissue engineering applications. Macromol. Biosci. 2019, 19, e1800313.

[11] Zhang, Z. P.; Rong, M. Z.; Zhang, M. Q. Polymer engineering based on reversible covalent chemistry: a promising innovative pathway towards new materials and new functionalities. Prog. Polym. Sci. 2018, 80, 39-93.

[12] Li, X.; Sun, Q.; Li, Q.; Kawazoe, N.; Chen, G. Functional hydrogels with tunable structures and properties for tissue engineering applications. Front. Chem. 2018, 6, 499.

[13] Heidarian, P.; Kouzani, A. Z.; Kaynak, A.; Paulino, M.; Nasri-Nasrabadi, B. Dynamic hydrogels and polymers as inks for three-dimensional printing. ACS Biomater. Sci. Eng. 2019, 5, 2688-2707.

[14] Li, Z.; Song, N.; Yang, Y.-W. Stimuli-Responsive drug delivery systems based on supramolecular nanovalves. 2019, 1, 345-368.

[15] Zhang, J.-Y.; Zeng, L.-H.; Feng, J. Dynamic covalent gels assembled from small molecules: from discrete gelators to dynamic covalent polymers. Chin. Chem. Lett. 2017, 28, 168-183.

[16] Zhang, C.; Yang, Z.; Duong, N. T.; Li, X.; Nishiyama, Y.; Wu, Q.; Zhang, R.; Sun, P. Using Dynamic Bonds to Enhance the Mechanical Performance: From Microscopic Molecular Interactions to Macroscopic Properties. Macromolecules 2019, 52, 5014-5025.

[17] Li, Y.; Zhu, C.; Dong, Y.; Liu, D. Supramolecular hydrogels: mechanical strengthening with dynamics. Polymer 2020, 210, 122993.

[18] Patrickios, C. S. Ed.; Amphiphilic polymer co-networks: synthesis, properties, modelling and applications; Polym. Chem. Ser. No. 33; The Royal Society of Chemistry: London, UK, 2020.
[19] Mantooth, S. M.; Munoz-Robles, B. G.; Webber, M. J. Dynamic hydrogels from host-guest supramolecular interactions. Macromol. Biosci. 2019, 19, No. 1800281.
[20] Teng, L.; Chen, Y.; Jia, Y. G.; Ren, L. Supramolecular and dynamic covalent hydrogel scaffolds: from gelation chemistry to enhanced cell retention and cartilage regeneration. J. Mater. Chem. B 2019, 7, 6705-6736.
[21] Picchioni, F. and Muljana, H. Hydrogels based on dynamic covalent and non covalent bonds: a chemistry perspective. Gels 2018, 4, 21.
[22] Hammer, L.; Van Zee, N. J.; Nicolaÿ R. Dually crosslinked polymer networks incorporating dynamic covalent bonds. Polymers 2021, 13, 396.
[23] Jiang, Z.; Bhaskaran, A.; Aitken, H. M.; Shackleford, I. C. G.; Connal, L. A. Using synergistic multiple dynamic bonds to construct polymers with engineered properties. Macromol. Rapid Commun. 2019, 40, 1900038.
[24] Yang, J.; Bai, R.; Chen, B. Suo Z. Hydrogel adhesion: a supramolecular synergy of chemistry, topology, and mechanics. Adv. Funct. Mater. 2019, 1901693.
[25] Chakma, P.; Konkolewicz, D. Dynamic covalent bonds in polymeric materials. Angew. Chem., Int. Ed. 2019, 58, 9682-9695.
[26] Xi, W.; Scott, T. F.; Kloxin, C. J.; Bowman, C. N. Click chemistry in materials science. Adv. Funct. Mater. 2014, 24, 2572-2590.
[27] Skene, W. G, Lehn, J. M. Dynamers: polyacylhydrazone reversible covalent polymers, component exchange, and constitutional diversity. Proc. Natl Acad. Sci. USA 2004, 101, 8270-8275.
[28] Ono, T., Fujii, S., Nobori, T, Lehn, J. M. Soft-to-hard transformation of the mechanical properties of dynamic covalent polymers through component incorporation. Chem. Commun. 2007, 43, 46-48.
[29] Kalia J.; Raines, R. T. Hydrolytic stability of hydrazones and oximes. Angew. Chem. Int. Ed. 2008, 47, 7523-7526.
[30] Deng G.; Tang C.; Li F.; Jiang, H.; Chen, Y. Covalent cross-linked polymer gels with reversible sol-gel transition and self-healing properties. Macromolecules 2010, 43, 1191-1194.
[31] Xu, Y.; Li, Y.; Chen, Q.; Fu, L.; Tao, L.; Wei, Y. Injectable and self-healing chitosan hydrogel based on imine bonds: design and therapeutic applications. Int. J. Mol. Sci. 2018, 19, 2198.
[32] Grover, G. N.; Braden, R. L.; Christman, K. L. Oxime crosslinked injectable hydrogels for catheter delivery. Adv. Mater. 2013, 25, 2937-2942.
[33] Lee, J. H.; Park, J.; Park, J. W.; Ahn, H. J.; Jaworski, J.; Jung, J. H. Supramolecular gels with high strength by tuning of calix[4]arene-derived networks. Nat. Commun. 2015, 6, 6650.
[34] Zhang, Z.; He, C.; Chen, X. Hydrogels based on pH-responsive reversible carbon-nitrogen double-bond linkages for biomedical applications. Mater. Chem. Front. 2018, 2, 1765-1778.
[35] Li, L.; Lin, Q.; Tang, M.; Duncan, A. J. E.; Ke, C. Advanced polymer designs for direct-ink-write 3D printing. Chem. - Eur. J. 2019, 25, 10768-10781.
[36] McConnell, A. J.; Wood, C. S.; Neelakandan, P. P.; Nitschke, J. R. Stimuli-Responsive Metal-Ligand Assemblies. Chem. Rev. 2015, 115,7729-7793.

[37] Wei, P. F.; Yan, X. Z.; Huang, F. H. Supramolecular polymers constructed by orthogonal self-assembly based on host-guest and metal-ligand interactions. Chem. Soc. Rev. 2015, 44, 815-832.
[38] Hofmeier H.; Schubert U. S. Recent developments in the supramolecular chemistry of terpyridine-metal complexes. Chem. Soc. Rev. 2004, 33, 373-399.
[39] Schwarz G.; Haßlauer I.; Kurth D. G. From terpyridine-based assemblies to metallo-supramolecular polyelectrolytes (MEPEs). Adv. Colloid Interface Sci. 2014, 207, 107-120.
[40] Chakraborty, S.; Hong, W.; Endres, K. J.; Xie, T. Z.; Wojtas, L.; Moorefield, C. N.; Wesdemiotis, C.; Newkome, G. R. Terpyridine based, flexible tripods: from a highly symmetric nanosphere to temperature-dependent, irreversible, 3D isomeric macromolecular nanocages. J. Am. Chem. Soc. 2017, 139, 3012-3020.
[41] Dragan, E. Design and applications of interpenetrating polymer network hydrogels. A Review. Chem. Eng. J. 2014, 243, 572-590.
[42] Klymenko, A.; Nicolai, T.; Benyahia, L.; Chassenieux, C.; Colombani, O.; Nicol, E. Multiresponsive hydrogels formed by interpenetrated self-assembled polymer networks. Macromolecules 2014, 47, 8386-8393.
[43] Yu, Z.; Zhang, Y.; Gao, Z. J.; Ren, X. Y.; Gao, G. H. Enhancing mechanical strength of hydrogels via IPN structure. J. Appl. Polym. Sci. 2017, 134, 44503.
[44] Gong, J. P.; Katsuyama, Y.; Kurokawa, T.; Osada, Y. Double-Network hydrogels with extremely high mechanical strength. Adv. Mater. 2003, 15, 1155-1158.
[45] Gong, J. P. Why are double network hydrogels so tough? Soft Matter 2010, 6, 2583-2590.
[46] Gong, J. P. Materials Both Tough and Soft. Science 2014, 344, 161-162.
[47] Chen, Q.; Chen, H.; Zhu, L.; Zheng J. Engineering of tough double network hydrogels. Macromol. Chem. Phys. 2016, 217, 1022-1036.
[48] Wu, J.; Han, S.; Yang, T.; Li, Z.; Wu, Z.; Gui, X.; Tao, K.; Miao, J.; Norford, L. K.; Liu, C.; Huo, F. Highly stretchable and transparent thermistor based on self-healing double network hydrogel. ACS Appl. Mater. Interfaces 2018, 10, 19097-19105.
[49] Yuan, N.; Xu, L.; Wang, H.; Fu, Y.; Zhang, Z.; Liu, L.; Wang, C.; Zhao, J.; Rong, J. Dual physically cross-linked double network hydrogels with high mechanical strength, fatigue resistance, notch insensitivity, and self-healing properties. ACS Appl. Mater. Interfaces 2016, 8, 34034-34044.
[50] Algi, M. P.; Okay, O. Highly stretchable self-healing poly(N,N-dimethylacrylamide) hydrogels. Eur. Polym. J. 2014, 59, 113-121.
[51] Lewiński, J. Prochowicz, D. Assemblies Based on Schiff Base Chemistry. In: Assemblies Based on Schiff Base Chemistry, Atwood J. L. ed.; Elsevier, Oxford 2017.

Chapter 2

State of the art

Abstract

Developments in dynamic chemistry have provided scientists with a powerful toolbox based on both supramolecular interactions and dynamic covalent bonds for the fabrication of dynamic crosslinked polymeric materials, especially hydrogels. There is a growing interest in using multiple dynamic bonds as crosslinks to enhance the functionality of hydrogels or to provide some clues for mimicking nature. This literature review provides an introduction to how multiple dynamic bonds can be introduced into hydrogel network structures from the viewpoint of dynamic bonds and network topologies. In particular, hydrogels of different topologies based on metal-terpyridine coordination bonds and reversible C=N bonds will be presented in more details regarding the synthesis methods, properties and applications.

2.1 Introduction

This chapter consists of two main parts. In the first part, we discuss some basic concepts that are relevant to this thesis. This part covers dynamic hydrogels, dynamic bonds, supramolecular interactions and dynamic covalent bonds (in particular, metal-terpyridine coordination bonds and reversible C=N bonds, which are directly relevant to this thesis). We then discuss available topologies for constructing polymer hydrogel networks using dynamic bonds as crosslinks, and notably the classification of network topologies for incorporating two different dynamic bonds into one hydrogel system. Finally, we discuss one of the popular characterization tools that can be used to systematically study the viscoelasticity, oscillatory mechanical properties, self-healing properties, etc., of dynamic hydrogels, namely rheology. In the second part, we review in detail hydrogels based on metal-terpyridine coordination bonds or reversible C=N bonds. We present a detailed review of the design, properties and developed applications of these two types of dynamic hydrogels, mainly from the perspective of synthetic polymers, dynamic bonds and topologies.

Polymer hydrogels are a type of hydrophilic crosslinked three-dimensional macromolecular networks, which are capable of absorbing and entrapping a large volume fraction of water. Since Wichterle and Lím reported the first hydrogel of poly(2-hydroxyethyl methacrylate) (PHEMA) in 1960,[1] hydrogels have become the subject of intense research in agriculture, food and cosmetics industry as well as in biomedical and biotechnological fields due to the high water absorption capability that resembles natural tissues.[2-4] Hydrogels are therefore valid candidates for water treatment,[5-7] nutrient/drug delivery,[8-10] cell culture,[11,12] wound healing,[13,14] and tissue regeneration.[15,16] Because polymer hydrogels are made of a liquid portion (water) and a solid portion (crosslinked network), their unique physicochemical properties can hence be tuned and optimized by modulating the polymer compositions and by using different types of crosslinks.[17]

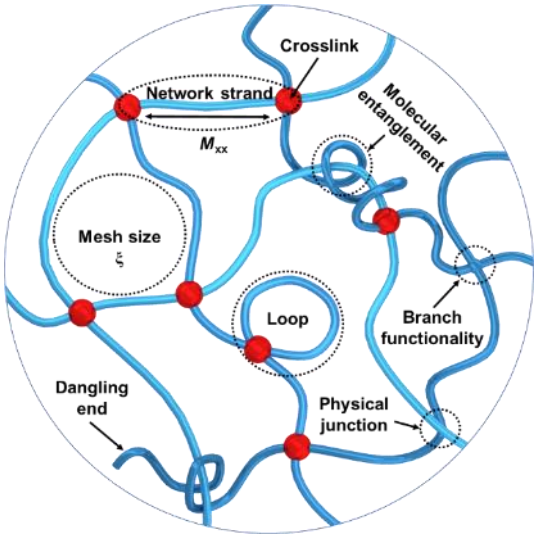

Figure 2.1. Schematic representation of possible structures existing in hydrogel networks. M_{xx} is the number-average molar mass of a network strand (between crosslinks).

For an aqueous polymer network, many potential structural parameters (**Figure 2.1**) can be used for characterizing the hydrogel.[18, 19] For example, the length of the strands (ν) between crosslinks and the mesh size (ξ) are relevant for the swelling behavior of hydrogel.[20] The elastic modulus of a hydrogel can be estimated from ν and ξ by applying the affine or phantom network models.[21] Understanding and controlling the network composition and structure allow the manipulation of the hydrogel properties from a (macro)molecular level.[19] However, the structure is usually difficult to modify or alter once a percolated network is formed by permanent covalent bonds. Another simple way to regulate the properties of the gels is to introduce dynamic crosslinking. Traditionally, hydrogels can be classified into chemical and physical hydrogels based on covalent and non-covalent crosslinking mechanisms respectively.[22] As dynamic covalent chemistry (DCC) develops, an increasing number of reactions are being found to be reversible.[23, 24] Scientists are now integrating dynamic covalent bonds (DCBs) into polymeric network materials such as

gels,[25] elastomers,[26-28] thermosets,[24] thermoplastics,[29] and vitrimers[30] to give to these materials dynamic properties such as self-healing or stimuli responsiveness. Thus, chemical (covalent) hydrogels actually include both permanent covalent and dynamic covalent hydrogels. Depending on the reversibility of crosslinking, therefore, hydrogels can be further divided into two main families: conventional (permanent/static) gels and dynamic gels[31] (**Figure 2.2**).

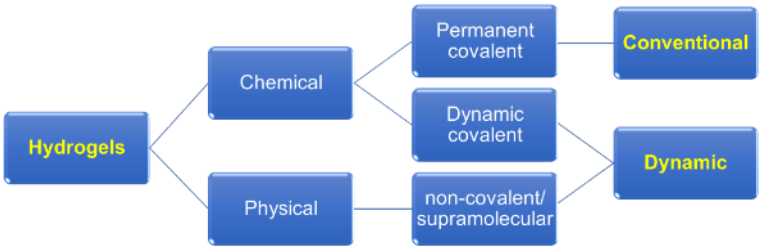

Figure 2.2. Classification of hydrogels based on the nature of crosslinking.

The conventional hydrogels are 3D networks crosslinked with permanent covalent bonds and swollen in water. These networks are formed by chemical reactions between complementary functional groups (between polymer chains or between polymer chains and crosslinkers) or by free radical polymerization of vinyl monomers in the presence of crosslinkers.[32] Due to the formation of permanent covalent bonds during the gelation, the processability of this type of gel is very poor.[33] Despite being permanently covalently crosslinked, conventional hydrogels without topological optimization are not always strong (fracture energy < 10 J/m^2).[34] Besides, static networks often prevent the spontaneous healing of the hydrogels after external damage. These drawbacks restrict the scope of their usage in real-world applications.

In the case of dynamic hydrogels, the networks are crosslinked by at least one type of dynamic bond (DB).[35-37] Such hydrogels can undergo topological rearrangement of the network either spontaneously, or under given stimulus conditions by reversible crosslinking formation,

breakage or exchange.[38, 39] Because the network can efficiently dissipate energy under deformation through the breakage and reformation, or exchange of DBs, these hydrogels sometimes possess high mechanical strength.[40] More importantly, the nature of DBs also endow gels with desirable properties such as stimuli-responsiveness, shape-memory, self-healing, degradability, or injectability. Integration of these properties with anti-freezing, adhesive, bio-compatible, bio-active, conductive, tough, flexible or stretchable polymer constituents, make hydrogels useful materials for applications such as 3D or 4D printing,[41] bio-sensor,[42] soft machine and actuator,[43] wearable and implantable device,[44] nanogenerator,[45] flexible energy storage device,[46] artificial skin, muscle and nerve.[47, 48]

The DBs used for dynamic hydrogels, can be described as any kind of bond which can break and reform spontaneously or in response to external stimuli.[49] These bonds can be classified into two main categories: non-covalent/supramolecular interactions (e.g., hydrogen bonds, metal-ligand coordination bonds, hydrophobic associations, crystallization, etc.) and dynamic covalent bonds (DCBs) (e.g., reversible C=N bonds, boronic ester bonds, disulfide bonds, Diels-Alder reactions).[50, 51] Due to the weak non-covalent character, supramolecular interactions usually exchange rapidly under ambient conditions, but this fast kinetics can also make polymer networks susceptible to irreversible creep.[52] DCB involves reversible but robust covalent bond, with slower formation/cleavage kinetics than supramolecular interactions, facilitating the formation of strong networks.[53] Although these two types of bonds are considered as interesting crosslinks for producing dynamic networks, the use of a single type of bonds limit hydrogels to a comparatively narrow range of properties, making them unsatisfactory for the desired applications. To tackle this shortcoming, crosslinking strategies such as DB combined with permanent covalent bonds and multiple DBs have been designed for tailored networks during the last decade.[54-56]

Incorporating two or more types of bonds into one hydrogel system to obtain the desired functionality requires addressing several points. The first issue is: how to select suitable DBs as crosslinks to build the polymer networks? The following question that needs to be answered is: what kind of topology can be chosen to construct networks based on multiple bonds. In this literature review, we will begin by discussing the chemistry of DB, especially the metal-ligand bonds and reversible C=N bonds used for this thesis. We will then turn to the topologies that could be used for dynamic hydrogels. Finally, possible applications and the future perspectives of the area are discussed.

2.2 Dynamic Bonds

2.2.1. General considerations

The behavior of the aqueous polymer network will depend on the nature of the dynamic bond (DB), which is related to the thermodynamic/kinetic parameters and to the bonding mechanism. These parameters and mechanisms also determine, to a large extent, the type and manner in which the hydrogel realizes its dynamic response.[49] Therefore, the understanding of the dynamics and chemistry of DB is of importance to understand the way in which these DBs contribute to the final properties of dynamic hydrogels.

As shown in **Figure 2.3a**, the association (i.e., bonding reactions to form DB) of functional moieties on linear polymers can lead to inter-chain crosslinking, and thus the formation of a 3D network of hydrogels. Conversely, dissociation of the DBs can lead to disruption of the network structure, causing changes in the volume, shape or color of the hydrogel, or even a complete gel-sol transition.[35-40] Thus, the intrinsic reversibility of DB can confer controllable mechanical properties, stimulus responsiveness, shape memory, etc. to hydrogels. The reversibility of DB also facilitates the exchange of functional moieties

on polymer chains under certain conditions, thus bringing self-healing properties to the hydrogels.[34, 39] Dynamic exchange of DBs can occur through either associative or dissociative pathways.[56] In an associative pathway, bond breakage and reformation occur simultaneously (**Figure 2.3b, I**), keeping the network at a constant crosslinking density throughout the dynamic exchange process. In a dissociative pathway, the bond first dissociates, and after a period of time forms a new linkage (**Figure 2.3b, II**). In this pathway, due to the reduction in the number of linkages, the network crosslinking density decreases dramatically and even in the most extreme cases depolymerises into linear chains. The mechanical strength of the hydrogel is therefore likely to change significantly in the process.

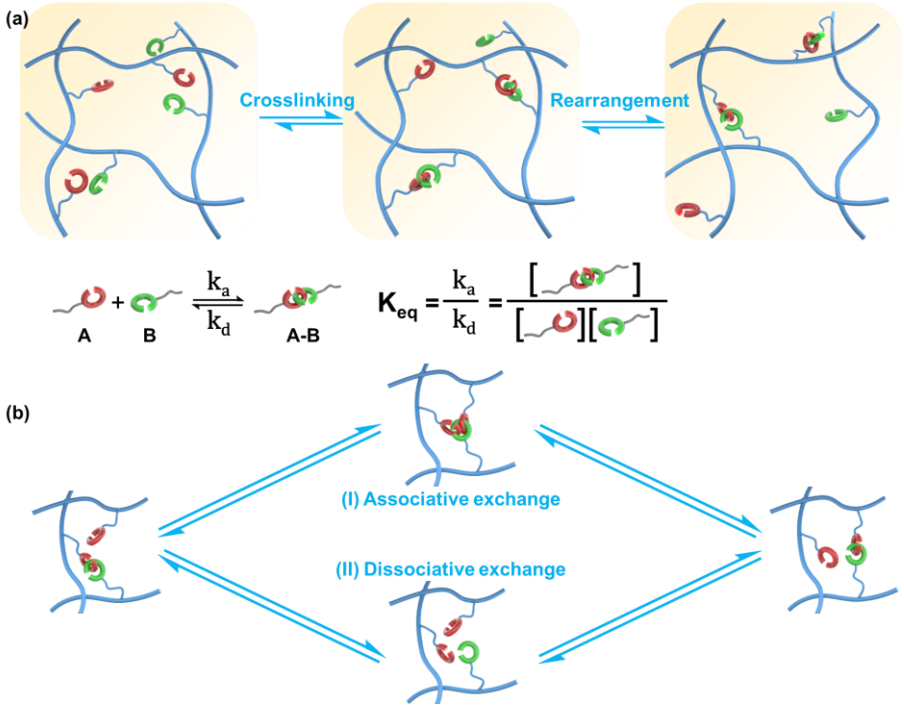

Figure 2.3. (a) Schematic representation of the crosslinking and rearrangement of dynamic networks, which are governed by the thermodynamic and kinetic parameters of the dynamic bonds. (b) Schematic representation of associative and dissociative exchange of dynamic bonds (DBs).

The gelation process of a dynamic hydrogel occurs upon the formation of crosslinks, which is governed by the reaction equilibrium of the DB. To achieve the creation of a network, the thermodynamic and kinetic parameters of the DBs must be taken into account. The thermodynamic equilibrium constant (K_{eq}) (**Figure 2.3**) quantifies the amount of associated DBs compared to the initial functional moieties.[57] In other words, K_{eq} directly reflects the degree to which DBs are effectively formed in the crosslinking of polymer networks, and determines the relative stability of the dynamic hydrogels. Because the DBs are reversible bonds, the bond stability and strength are affected by many environmental parameters such as temperature, pH, ionic strength, etc.[58] Besides, the stability of DBs in the networks depends on the number of functionalities, crosslinking density, polymer molecular weight, and polymer concentration.[59] As shown in **Figure 2.3**, the kinetic parameters are the DB association (formation) (k_a) or dissociation rates (k_d), and are related to the equilibrium constant by the equation $K_{eq} = k_a/k_d$. The k_a of DB is primarily responsible for the formation of networks or self-healing kinetics of the hydrogels. The k_d depicts the dissociation rate of DB and greatly impacts the stress relaxation of the polymer networks. Therefore, these kinetic parameters are related to crosslinking kinetics and they play an integral role in determining the response speed of hydrogels. Since K_{eq} is the ratio of k_a to k_d, a high K_{eq} usually indicates a network with sluggish exchange between crosslinks and a low K_{eq} means a faster exchange.[60]

To understand the role of DB dynamics in determining the behavior of hydrogel networks, it is necessary to know the driving forces for the formation and dissociation of DB. For DBs, either supramolecular interactions or dynamic covalent bonds, the processes of formation, dissociation and reconstruction of reversible bonds are driven by thermodynamically controlled process under the given environmental conditions.[58, 59] The equilibrium constants of DB and the crosslinking density of the network are therefore temperature dependent. A particularly important parameter is the activation energy (E_a) of the

association and dissociation processes.[59] It allows for a relatively more stable DB to be formed (**Figure 2.4a**).

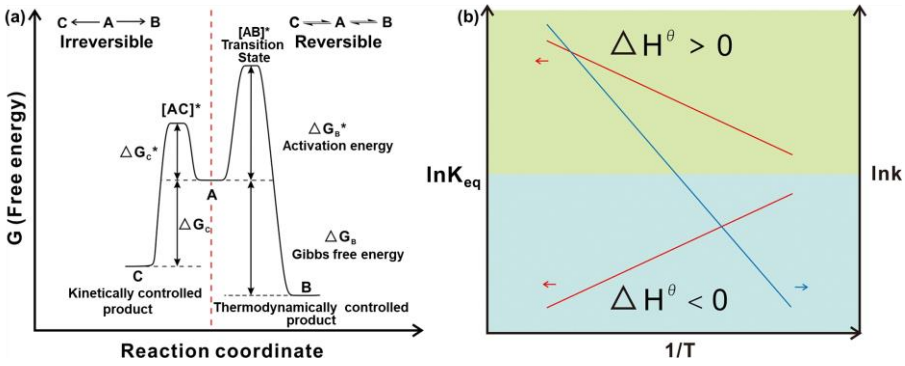

Figure 2.4. (a) Free energy profile of irreversible and reversible reactions under kinetic and thermodynamic controls, respectively. (b) Dependences of chemical equilibrium constant and reaction rate constant on reaction temperature.[58]

Typically, the relationship between the thermodynamic equilibrium constant (K_{eq}), standard enthalpy change, (ΔH^{Θ}), and standard entropy change (ΔS^{Θ}), and the relationship between temperature-dependent rate constant (k), Gibbs free energy ($\Delta G^{\ddagger}$), enthalpy of activation ($\Delta H^{\ddagger}$), entropy of activation ($\Delta S^{\ddagger}$) and activation energy (E_a) obeys the following equations:

$$\ln K_{eq} = -\Delta H^{\theta}/RT + \Delta S^{\theta}/R \quad (2.1)$$

$$k = \frac{k_B T}{h} \exp\left(-\frac{\Delta G^{\ddagger}}{RT}\right) \quad (2.2)$$

$$k = \frac{k_B T}{h} \exp\left(-\frac{\Delta S^{\ddagger}}{R}\right) \exp\left(-\frac{\Delta H^{\ddagger}}{RT}\right) \quad (2.3)$$

$$k = A\exp\left(-\frac{E_a}{RT}\right) \quad (2.4)$$

where k_B is Boltzmann's constant, T is temperature, h is Plank's constant, R is gas constant and A represents the pre-exponential factor. **Figure 2.4b** graphically depicts the relationship between equilibrium constant, rate constant and enthalpy change. For an exothermic

reversible reaction, increasing the temperature causes the rate constant to increase and the equilibrium constant to decrease, thus pushing the equilibrium to move in the inverse direction (i.e., the direction of bond dissociation). According to equation (2.4), the reaction would also be accelerated by lowering the activation energy (e.g., incorporation of catalyst).

Furthermore, the judicious choice of the initial functional moieties is of critical importance when selecting the DB to be used as crosslink for constructing dynamic hydrogels. The initial functional moieties fundamentally determine the mechanism of association and dissociation of the bonding reaction to form DB. For example, as illustrated in **Figure 2.5**, the initial moieties can be identical components (self-complementary)[59] or can be two different groups (hetero-complementary)[49] to obtain final crosslinks. In the case of self-complementary crosslinking (**Figure 2.5a**), the polymer network can be crosslinked in the presence of only one initial component such as hydrogen-bonding between two ureidopyrimidinones (UPys), or disulfide bond formed by the coupling of two thiol groups. The hetero-complementary (**Figure 2.5b**) crosslinks form can be either two moieties through A-B bonding (e.g., imine bond, host-guest complexation), or A-C-A bonding (e.g., metal-terpyridine bis-complexes). In this case, only in the presence of both components can the crosslinking of the network be enabled. The presence of self-complementary functional groups between individual polymer chains, or the installation of hetero-complementary components on the same polymer chain, may result in a high risk of intrachain loops formation. These two main crosslinking methods, therefore, allow researchers to use the DB toolbox to build customizable networks that manipulate the performance of hydrogels.

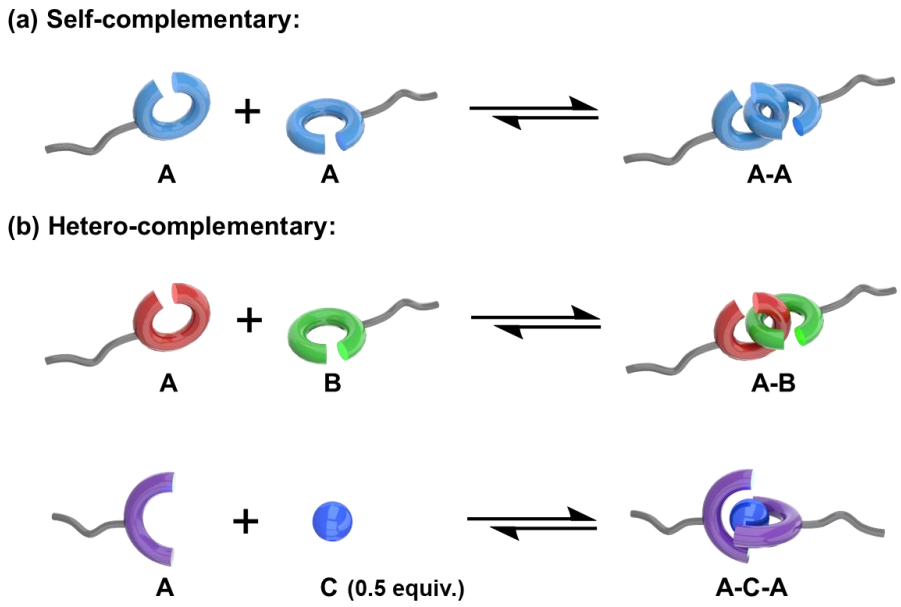

Figure 2.5. The two major classes of DB-based crosslinking: (a) self-complementary, and (b) hetero-complementary.

Briefly, in order to develop the desired dynamic gel, the DB should meet the following requirements. (1) The dynamic equilibrium has to be in the direction of DB formation in order to favor the construction of the crosslinked network. (2) Relatively rapid association and dissociation rates to facilitate the desired macroscopic response of the hydrogel within a reasonable time scale. (3) A reasonable choice of initial components (reactive functional groups) is required to control the structural parameters of the gel network on demand.

2.2.2. Types of dynamic bonds

Since D. J. Cram, C. J. Pedersen and J.-M. Lehn, were jointly awarded the Nobel Prize "for their development and use of molecules with structure-specific interactions of high selectivity" in 1987, supramolecular interactions have been recognized as a powerful tool and were used in a plethora of applications.[61] The critical feature of supramolecular interactions derives from their dynamic nature. Supramolecular interactions are correlated with non-covalent bonds concerning ions and molecules in complexes,[62] and most of them are labile and reversible. Extending the dynamic features of supramolecular interactions into the molecular domain yields dynamic covalent bonds (DCBs)[23] that combine the dynamic reversibility of supramolecular interactions with the stability and robustness of covalent bonds. However, the thermodynamic equilibrium processes of DCBs are usually much slower than supramolecular interactions. The slower kinetics of the reactions associated with DCB formation usually mean that they require extra stimuli (e.g., addition of a catalyst, heating, light) to equilibrate to thermodynamically stable bonds within an acceptable time scale.[53] Therefore, the DB, containing supramolecular interaction and DCB, can be defined as a class of bonds that can selectively and reversibly be broken and reformed under equilibrium conditions.[63] These DBs with exceptional dynamics and a wide range of thermodynamic strengths provide us with a versatile toolbox for the design and manipulation of a broad range of materials, including polymer networks. **Table 2.1** offers some representative DBs that have been used in the preparation of networks.

Table 2.1. Typical dynamic bonds.[55, 64]

Dynamic bond types	Reversibility tuning conditions
Supramolecular interactions (hydrogen bonding, hydrophobic interactions, electrostatic interactions, and metal-ligand coordination)	Generally, under continuous equilibrium, highly susceptible to environment change.
Imine formation and exchange: 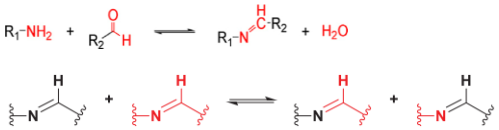	Formation (condensation): 22 °C Exchange: 50~110 °C, acid. Catalysts: aniline/acid catalyst. Stimulus: temperature, pH.
Hydrazone formation and exchange: 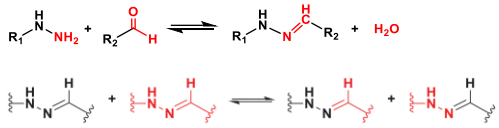	Formation (condensation): 25 °C, pH 7.4. Exchange: 75 °C, acid. Catalysts: aniline/acid catalyst. Stimulus: temperature, pH.
Oxime formation and exchange: 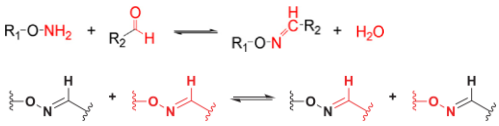	Formation (condensation): 25 °C, pH 6.4~8.3. Exchange: acid, >50 °C. Catalysts: aniline/acid catalyst. Stimulus: temperature, pH.
Boronic/borate ester formation and exchange: 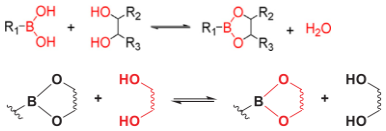	Formation (condensation): 25 °C, pH ≤ 7. Exchange: 25 °C (ambient self-healing). Cis-diol concentration affects rates. Stimulus: temperature, pH.

Table 2.1. Continued.

Dynamic bond types	Reversibility tuning conditions
Disulfide formation and exchange, and thiol-disulfide exchange: 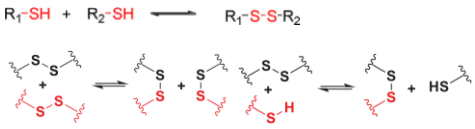	Formation (addition) and exchange both possible; conditions suitable for exchange vary widely. Catalysts: none or base, nucleophiles, radical generators. Stimulus: temperature, pH, and light.
Alkoxyamine dissociation and exchange: 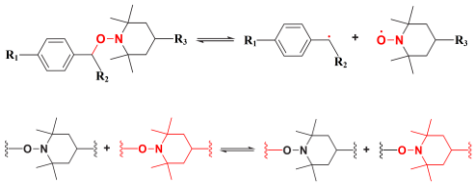	Dissociation (addition): stable below 60 °C. Exchange: typical reversibility at 100 °C, reaction time up to 24 h. No catalysts. Stimulus: temperature.
Diels-Alder reaction (DA): 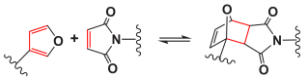	Formation (addition): reversibility at 90~150 °C, minutes to hours. Possible above 150 °C. No catalysts. Stimulus: temperature.
Cycloadditions [2 + 2]: cinnamate and coumarin derivatives: 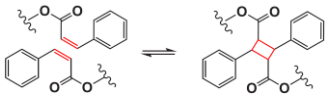	Formation (addition): RT, triggered by light: λ > 260 nm forward, λ < 260 nm reverse. Stimulus: light.
Cycloadditions [4 + 4]: anthracene: 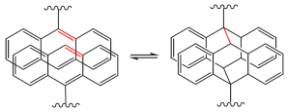	Formation (addition): λ > 300 nm forward, λ < 300 nm reverse. Stimulus: light and/or temperature.

Table 2.1. Continued.

Dynamic bond types	Reversibility tuning conditions
Thiol-Michael reaction (TM): 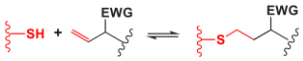 (EWG: electron withdrawing group)	Formation (addition): reversibility optimal at >90 °C, Reaction time: 1~16 h, pH 4~10. Catalysts: bases and nucleophiles. Stimulus: temperature, pH.
Thiol-thioester exchange (transthioesterification): 	Exchange: facile exchange at RT, Catalysts: bases and nucleophiles. Increased reaction rates at elevated temperature. Stimulus: temperature.
Transesterification: 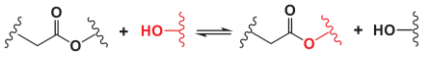	Exchange: usually >150 °C for a couple of hours. Catalysts: bases [1,5,7-triazabicyclo [4,4,0] dec-5-ene (TBD)], Lewis acids (zinc acetate), phosphines (triphenylphosphine). Stimulus: temperature.
Urea-amine exchange: 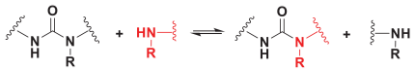	Exchange: can occur as low as 37 °C, typically above 100 °C. Catalysts: bases or free amines. Stimulus: temperature.
Urethane, urea, thiourethane reversions: 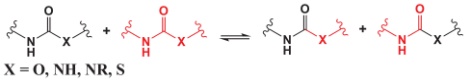 X = O, NH, NR, S	Addition: 100~190 °C, minutes to hours. Catalysts: stannous organo-compounds. Stimulus: temperature.
Transcarbomylation, transcarbonation: 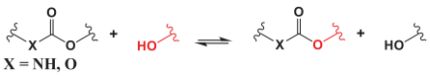 X = NH, O	Exchange: >100 °C, typically 150~180 °C in minutes to hours. Catalysts: stannous organo-compounds. Rates depend on OH concentration. Stimulus: temperature, strain.

The nature of DBs in crosslinking determines the formation and rearrangement of polymer networks. Networks crosslinked by supramolecular interactions are intrinsically dynamic and active, and have relatively rapid exchange under ambient conditions. Most of the dynamic covalent bonds usually maintain the stabilities of networks in the absence of external stimuli.[64] The chemical composition of systems containing DBs may undergo changes over time or in response to stimuli,[24] and therefore the introduction of DBs could promote stress relaxation, self-healing ability, or stimulus responsiveness of the polymer networks.[65] The presence of steric hindrance, electronic effect, etc. in the polymer network, in turn, affects the dissociation and exchange of DBs.[57] The dynamic properties exhibited by the final material arise from the synergistic interactions between the various components of the system.

2.2.3. Metal-terpyridine coordination bonds

The supramolecular interactions in polymer networks lead to hydrogels and are responsible for their function. Supramolecular networks are based on weak non-covalent interactions including hydrogen bonds, metal-ligand coordination bonds, van der Waals forces, π-π stacking, dipole-dipole interactions, etc. As presented in **Figure 2.6**, most of these interactions are usually weaker than covalent bonds (ca. 150 kJ/mol to 450 kJ/mol for single bonds).[66-68] Among the various supramolecular interactions, metal-ligand coordination bonds are considered to be the most tunable, and their bond strength can vary over an extensive range (tens kJ/mol to hundreds kJ/mol).[68, 69] Thus, the bonds can be made dynamic or permanent with the appropriate selection of ligands and metal ions. Moreover, the metal-ligand complexes can display various interesting functions, such as optical, magnetic, redox, electrochemical, and catalytic behaviors.[70, 71]

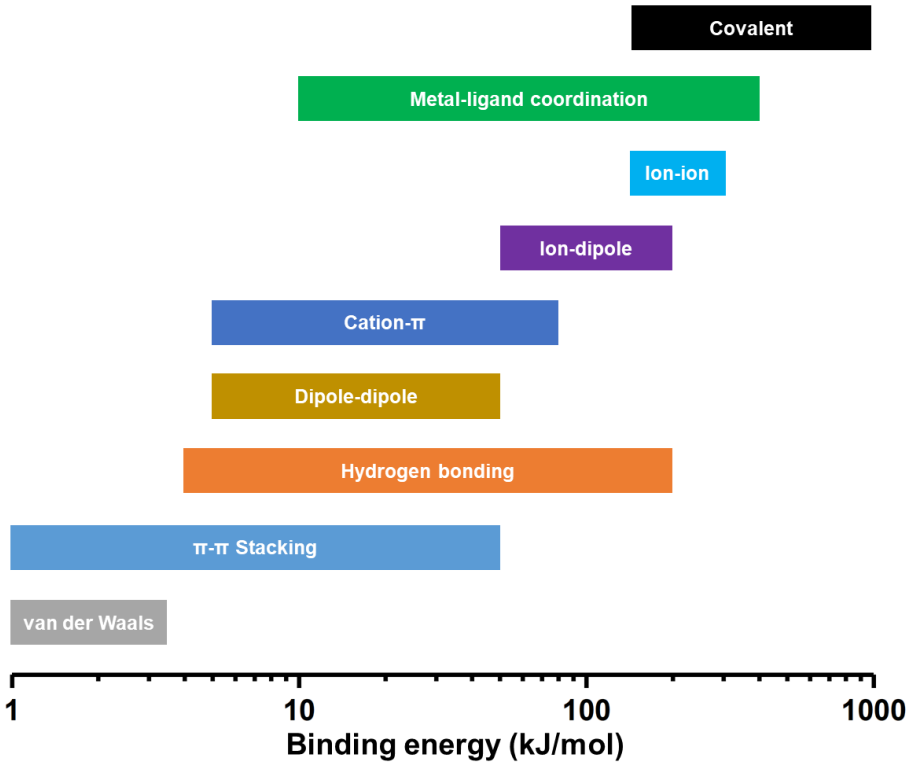

Figure 2.6. Summary of binding energies for different interactions.[66-68]

When a ligand donates a non-bonding pair of electrons to one of the empty d-orbitals of a metal ion, metal-ligand coordination bonds are formed. These ligands are usually nitrogen/oxygen-containing functional groups, such as pyridine (including bipyridine and terpyridine), catechol, carboxylate, histidine, phosphate or iminodiacetate grafted onto polymeric backbones.[72, 73] Networks can be created if two or three of these groups are able to form metal-ligand bis-complexes or tris-complexes with metal ions. Since metal coordination bonds are susceptible to external environments and their thermodynamic parameters depend strongly on the oxidation state of the metal ions, the network can be degraded or rearranged in response to external stimuli (e.g. pH, temperature, acoustic treatment, redox potential). Therefore, metal-ligand bonds are vastly employed in the

preparation of self-healing and shape memory hydrogels and networks.[50, 74]

The terpyridine (Tpy), one of the most broadly exploited ligands to complex transition metal ions, has also been utilized as building block for the manufacture of polymer networks. Tpy has three nitrogen atoms and is thus a tridentate ligand which forms stable bis-complexes of pseudo-octahedral geometry by chelating a broad range of transition metal ions in their low oxidation states.[75] According to the Irving-Williams Series, the relative stabilities of bis-complexes of divalent first-row transition metal ions generally follow the order: Zn(II) < Cu(II) < Co(II) < Fe(II) < Ni(II).[76] Consequently, the complexes formed by these metal ions with Tpy exhibit a wide range of tunable thermodynamic and kinetic parameters (**Table 2.2**).[76-79] The $K_{eq,\,1}$ and $K_{eq,\,2}$ (**Figure 2.7**) are the thermodynamic equilibrium constants of the metal-terpyridine mono- and bis-complexes, respectively.

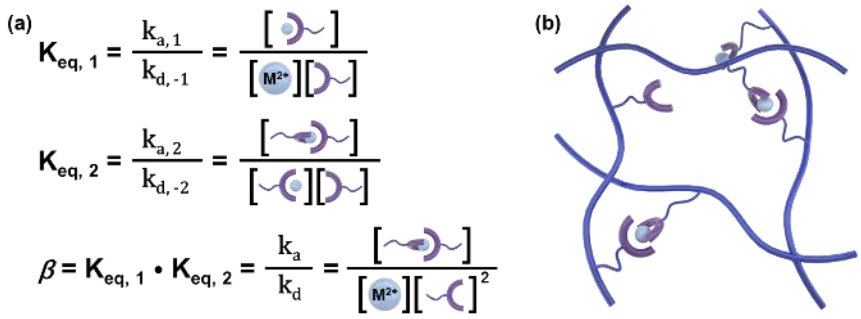

Figure 2.7. (a) Representation of thermodynamic and kinetic parameters of mono- and bis-complexes. (b) Schematic representation of dynamic network based on metal-terpyridine coordination bonds.

Table 2.2. Thermodynamic and kinetic equilibrium constants and binding enthalpies of metal-terpyridine mono- and bis-complexes.[76-79]

Metal ion	$K_{eq,\,1}$ (M^{-1})	$k_{a,\,1}$ ($M^{-1}\bullet s^{-1}$)	$k_{d,\,-1}$ (s^{-1})	$K_{eq,\,2}$ (M^{-1})	$k_{a,\,2}$ ($M^{-1}\bullet s^{-1}$)	$k_{d,\,-2}$ (s^{-1})	β
Mn (II)	$10^{4.4}$	$10^{5.0}$	$10^{0.6}$	n.a.	n.a.	n.a.	n.a.
Fe (II)	$10^{7.1}$	$10^{4.9}$	$10^{-2.2}$	$10^{13.8}$	$10^{7.0}$	$10^{-6.8}$	$10^{20.9}$
Co (II)	$10^{8.4}$	$10^{4.4}$	$10^{-4.0}$	$10^{9.9}$	$10^{6.7}$	$10^{-3.2}$	$10^{18.3}$
Ni (II)	$10^{10.7}$	$10^{3.1}$	$10^{-7.6}$	$10^{11.1}$	$10^{5.3}$	$10^{-5.8}$	$10^{21.8}$
Cu (II)	~ 10^{12}	~ $10^{7.3}$	~ $10^{-4.7}$	> 10^{6}	n.a.	n.a.	> 10^{18}
Zn (II)	$10^{6.0}$	$10^{6.1}$	$10^{0.1}$	$10^{5.2}$	n.a.	n.a.	$10^{11.2}$

The kinetic and thermodynamic equilibrium constants were determined by a stopped-flow procedure in water. The binding enthalpies were determined by ITC in CH_3CN.

These varying thermodynamic and kinetic parameters of the coordination bonds define the degree of terpyridine ligand participation in network formation and in the dynamics of materials. Therefore, the mechanical and dynamic response of the materials can be regulated by varying the type and amount of incorporated metal ions in the terpyridine-containing system.[80] For example, metallo-supramolecular hydrogels with maximum elastic modulus can be obtained when coordination bonds with long lifetimes are used and the stoichiometric ratio of the metal is half that of the Tpy ligands.[81] In addition, it is to be noted that the composition and length of the polymers, ligand substituents, steric interactions, electronic effects, solvents, and concentrations could also affect the strength and lifetime of the ligand bonds in the network.[82] Lohmeijer et al. measured the pH-stability of metal-terpyridine bis-complexes of 4'-(2-(2-methoxyethoxy)ethoxy)-2,2':6',2''-terpyridine in buffer solutions at different pH by using UV-spectra.[83] It was found that most of the complexes remain intact when varying the pH from 3 to 10 (**Table 2.3**). This information can provide us with a reference when using metal-terpyridine coordination bonds in selecting the appropriate pH for network preparation in water.

Table 2.3. pH-stability of the metal-terpyridine bis-complexes.[83]

Metal ion	pH = 1.0	pH = 3.0	pH = 5.0	pH = 7.0	pH = 10.0	pH = 13.0
Mn (II)	-	-	+	+	+	-
Fe (II)	-	+	+	+	+	-
Co (II)	-	+	+	+	+	-
Ni (II)	+	+	+	+	+	+
Cu (II)	-	+	+	+	+	-
Zn (II)	-	+	+	+	+	-
Ru (II)	+	+	+	+	+	+
Cd (II)	-	+	+	+	+	-
Hg (II)	-	+	+	+	+	-

The '+' represents an intact complex, whereas the '-' indicates the dissociation of the complex or that UV/vis-spectrum resembled that of the protonated ligand.

2.2.4. Reversible C=N bonds

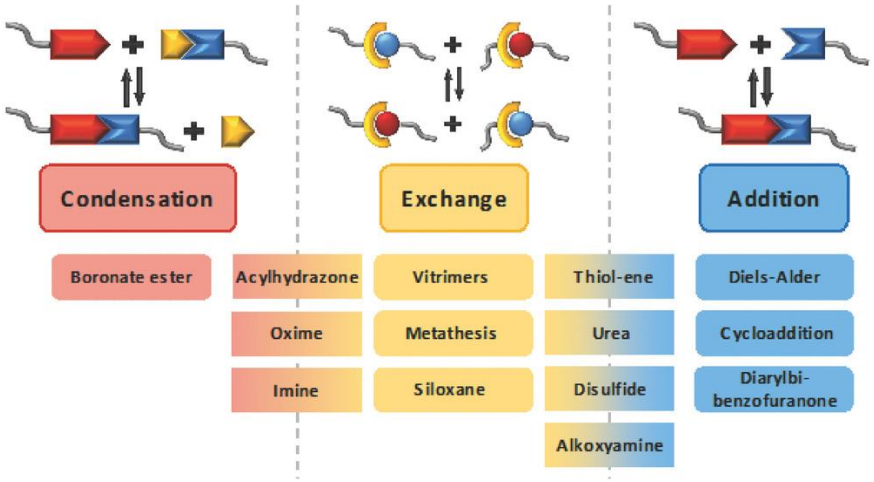

Figure 2.8. Categorization of dynamic covalent bond types.[87]

As another subset of dynamic bonds (DB), dynamic covalent bonds (DCBs) combine the reversibility and sensitivity of supramolecular

interactions with the prolonged life span and improved stability of chemical bonds. Based on these exceptional characteristics, DCBs have been exploited extensively in recent years for the purpose of preparing covalent adaptable networks (CANs).[84-86] The configurations and physicochemical properties of networks can be regulated by changing the thermodynamically controlled reactions of the DCBs. Based on the underlying chemistry used and the mechanism of action, DCBs can be broadly classified into three main groupings, namely, condensation, exchange and addition-based DCBs (**Figure 2.8**).[87] Among various DCBs, the reversible C=N bonds, including imine, hydrazone and oxime bonds, are undoubtedly the most special, because these bonds cannot only be reversibly formed and broken, but also the components of the system can be restructured by means of bond exchanges under certain conditions (**Table 2.1**).

A typical condensation reaction between a carbonyl electrophile (aldehyde or ketone) and a primary amine (α-nucleophilic reagent) produces a reversible C=N bond, i.e., the imine bond. This reaction is also called as Schiff base reaction,[88] from the name of the German chemist, Hugo Schiff, who first discovered the reaction in 1864. The imine bond is also known as Schiff base bond, especially when the amine is an aniline derivative.[89] The formation of imine and their N-substituted derivatives (hydrazone, oxime) has a similar mechanism (**Figure 2.9a**).[90] Generally, the nucleophilic attack of the amino group on the electrophilic carbon of the carbonyl group first results in the formation of a tetrahedral intermediate (hemiaminal). Subsequently, water is eliminated from the hemiaminal and a C=N bond is produced.[91] In most cases, the step of the formation of tetrahedral intermediate is a fast reaction and is not rate limiting. The rate-determining step of the reaction is dehydration of the hemiaminal and it is highly pH-dependent in water.[92]

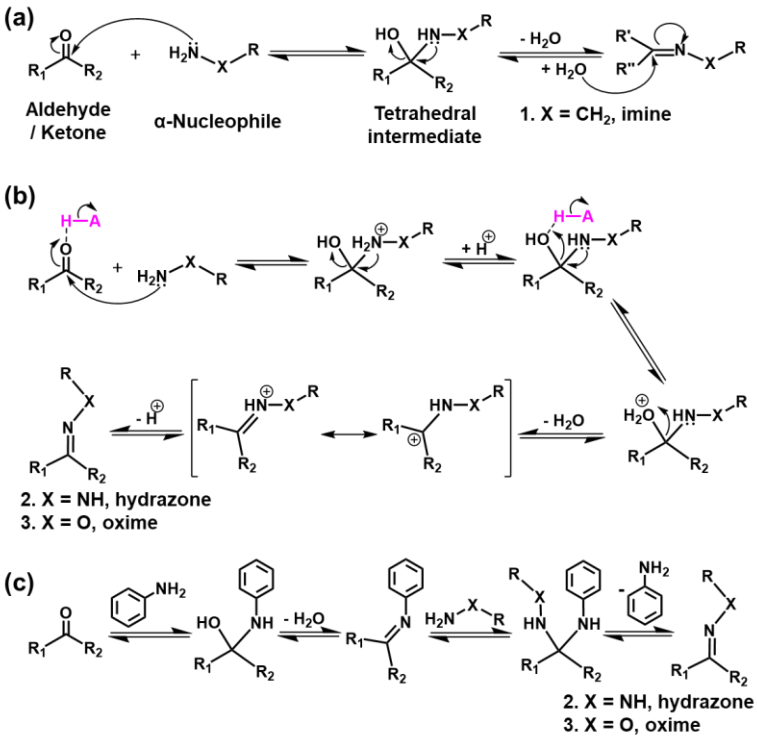

Figure 2.9. (a) The general mechanism for the formation of imine. (b) Mechanism for the formation of hydrazone or oxime catalyzed by acids. (c) Mechanism for the formation of hydrazone or oxime catalyzed by aniline.

At acidic pH conditions, the C=N bond production step can be described as concerted proton transfer and nucleophilic addition.[89] Specifically, the initial electrophile attack is promoted by favoring the protonation of the carbonyl oxygen atom, enhancing the electrophilicity on the carbon atom. The subsequent C=N bond formation step is also promoted at acidic pH, which makes it easier to dehydrate due to the proton transfer to the OH group of the tetrahedral intermediate (**Figure 2.9b**). This explains why the formation of C=N bonds can be accelerated by using an acid (acetic acid, trifluoroacetic acid) as a catalyst. Nevertheless, in order to accelerate the dynamic formation and exchange rate of C=N bonds (especially hydrazone and oxime), it is usually necessary to control the pH of the system in the range of 4.0 ~

6.0 (a pH of ca. 4.5 is typically advantageous),[93] and the efficiency of the reaction decreases sharply at pH outside these levels.[94] Particularly, under high acidity (pH < 3) conditions, the nitrogen atoms of α-nucleophilic reagents undergo protonation, causing lower nucleophilicity.[95] This results in slower formation of hemiaminal or even failure to form C=N bonds.[96]

Moreover, in an acidic[96, 97] or neutral[98] environment, the nucleophilic catalyst aniline can reduce the barrier to the highest transition state to increase the reaction rate by adding rapidly to the carbonyl group and effective yielding the tetrahedral intermediate after the attack of the α-effective nucleophilic reagents (**Figure 2.9c**). For example, Dirksen et al. found that the formation rate of acylhydrazone bond can be enhanced 20-fold with the addition of aniline under a pH of approximately 4.5.[97] Meanwhile, some new low-toxic and soluble nucleophilic amine-based catalysts such as anthranilates and phosphanilates have been found to be more efficient catalysts to replace aniline.[99-101]

As seen in **Figure 2.9a**, the reverse reaction of the C=N bonds can proceed by their hydrolysis. The hydrolytic stability of the C=N bonds is influenced by the electronic factors in the vicinity of the linkage, especially the N-substitution of the α-nucleophile. There are two major explanations for the higher stability of hydrazone and oxime compared to imine. The explanation in the textbook is that the electron delocalization of lone pair of electrons on the nitrogen-adjacent heteroatom X in hydrazone and oxime, i.e., through the α-effect, improves their stability.[89] As shown in **Figure 2.10**, the contribution of resonance form reduces the electrophilicity of the sp^2 carbon atom in hydrazone and oxime, the thereby making them not susceptible to attack by nucleophiles such as water or amines.[102] The protonation of the imine nitrogen can promote the reverse reaction (**Figure 2.9b**), water can serve as a proton source as well as a nucleophile, thus both factors accelerate the hydrolysis of imine in water. This implies that reducing the electrophilicity of the carbon atom in the C=N bond could improve

its inherent stability. For example, the stability of oxime bond obtained from different carbonyl group derivatives following the order: acetone < cyclohexanone ~ furfural ~ benzaldehyde < pyruvic acid (**Figure 2.11**).[98, 103]

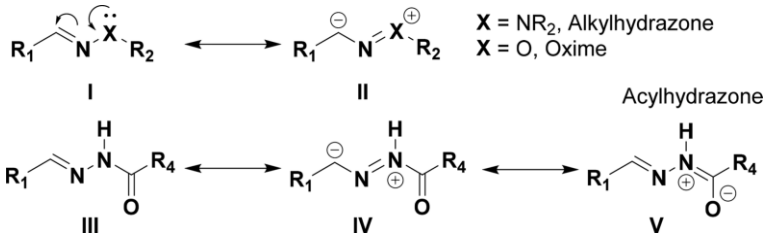

Figure 2.10. Major resonance forms of C=N bonds.[102]

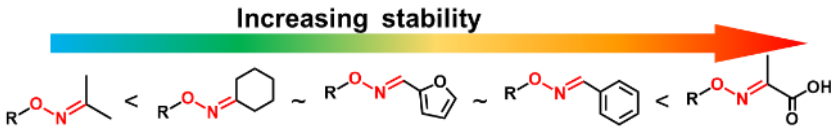

Figure 2.11. Stability trend in a series of oximes.[98]

Moreover, in a mechanistic study conducted by Kalia and Raines, they found that the negative inductive effect of the nitrogen-adjacent heteroatomic X moiety directly affects the stability of the corresponding C=N bond.[104] The X atom in hydrazone and oxime is more electronegative than the adjacent alkyl carbon atoms of typical imines, thereby reducing the basicity of the C=N bonded nitrogen atom and further making hydrazone and oxime more resistant to protonation than imines. This electronegative effect also explains why the oxime bond is more stable than hydrazone since the electronegativity of oxygen is higher than nitrogen. Likewise, based on the electronegativity differences of the substituents attached to the amine in the α-nucleophile, the typical C=N bonds have the following order of stability (**Figure 2.12**): imine < alkylhydrazone < acylhydrazone < semicarbazone < oxime.[104-106]

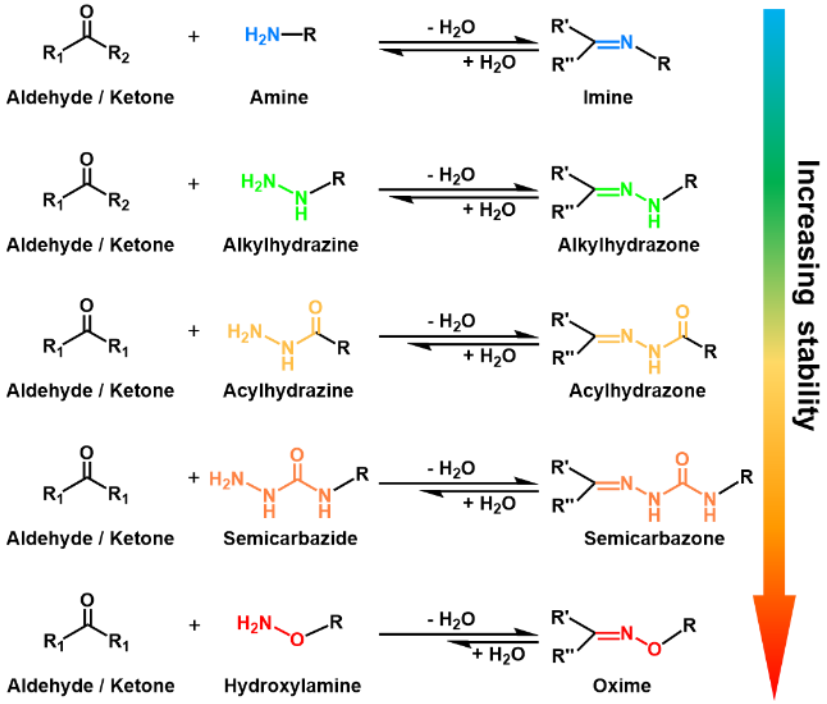

Figure 2.12. The hydrolytic stability of typical C=N bonds.

Among the typical C=N bonds, hydrazone and oxime have higher hydrolytic stability than imine, in other words, imine bond is the most reversible and dynamic bond formed by reversible reactions under thermodynamic control.[107] Imine bonds are thus the most extensively implemented crosslinking strategy in reversible C=N bonds used in dynamic polymers and their composite materials.[108-111] Due to the electronegative heteroatomic X moiety, which reduces the basicity of the amino groups in the nucleophiles, the formation of hydrazone and oxime bonds is therefore usually relatively slow. Despite this, stable hydrazone and oxime bonds are advantageous for many conjugation reactions of biomolecules and biomaterials that require more stable linkages.[112-114] Moreover, the rate of formation and hydrolysis of hydrazone and oxime bonds can be increased by heating,[115] regulating the pH (by addition of Brønsted acids[90] or enzymes[116]) or adding catalysts.[117] These properties of reversible C=N bonds provide us with

the possibility to regulate polymer networks on a large scale in terms of linkage design and kinetic control. Besides, some aryl group bonded to C=N bonds, that can be used as Schiff base ligands (such as Salen ligands) to chelate metal ions, have been comprehensively reviewed and are not discussed here.[118-120]

2.3 Classifications of Network Topologies

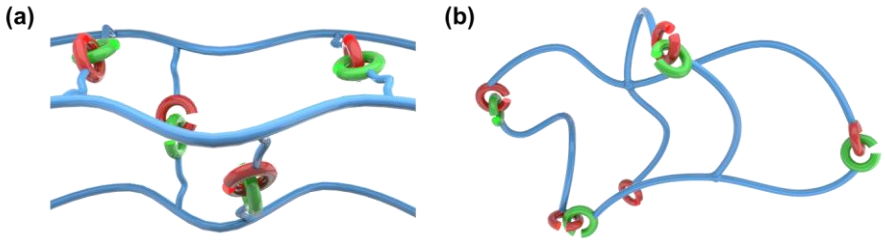

Figure 2.13. Schematic representation of polymer network based on crosslinks (a) in the side chain, or (b) in the main chain.

Typically, the three-dimensional architecture of hydrogel networks can be formed by crosslinking linear polymers via side functional groups (**Figure 2.13a**). The crosslink can be formed by functional groups between polymer chains or by additional free molecules as crosslinkers via the form of self-complementary or hetero-complementary bonding. Polymer main chains can also be crosslinked in the presence of functionalized molecules with multiple (i.e. >2) attachment sites or of multibranched chain-end functionalized polymers (**Figure 2.13b**). Both of these crosslinking methods are responsible for the formation of most of the basic polymer networks. They mainly, but not exclusively, control the final network topologies, which offers the possibility of enhanced functionality (e.g. mechanical toughness) to hydrogels.

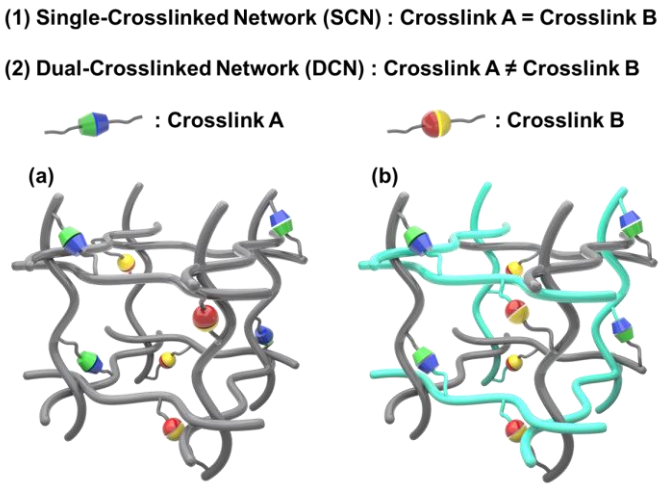

Figure 2.14. Schematic representation of the topologies of single-crosslinked network (SCN) and dual-crosslinked network (DCN) based on (a) one, or (b) two polymers.

Depending on the number of crosslink types, the network topology can be mainly divided into single-crosslinked networks (SCNs) and dual-crosslinked networks (DCNs) for systems made from only one network (**Figure 2.14**). The SCN, the simplest type of network topology, is constructed by one type of crosslink (either static covalent bonds or dynamic bonds). DCNs, which are also called dual networks[121-123] or dual-crosslinked single networks,[124] are usually crosslinked by two types of bonds, one of them at least being formed by dynamic bonds. As presented in **Figure 2.14a** and **2.14b**, both SCN and DCN are a topology where the whole system is a single network that can be built from one or two (or more) polymers by inter-chain crosslinking. In the presence of two (or more) polymers, the crosslinking always happens between different base polymers. Because it is a single network, if the dynamic crosslinks in SCN are cleaved under certain stimuli, the network will hence be destroyed, resulting in a gel-sol transition. However, the damage to the architecture of DCN is related to the position of the crosslink in the polymer chain. If two crosslinks are in the side positions of the polymer chains (like shown in **Figure 2.13a**)

and only one of the bonds is broken, the network still has the opportunity to keep the hydrogel in a solid-like state. When the DCN is constructed by crosslinking the polymer main chain (like shown in **Figure 2.13b**) through two different bonds, the breakage of either of these bonds can lead to a completely collapsed network. Sometimes, a single network may contain more than two types of crosslinks, such as a triple-crosslinked network (TCN), and can give the material even more dynamic properties.[55]

When a system has more than one network and the same crosslinks occur only between the same polymers, the network topology will potentially become a so-called interpenetrating polymer network (IPN) (**Figure 2.15a**). According to the definition of the IUPAC compendium of chemical terminology, an IPN is "A polymer comprising two or more networks that are at least partially interlaced on a molecular scale but not covalently bonded to each other and cannot be separated unless chemical bonds are broken".[125] IPNs are combinations of polymer networks, at least one of which is synthesized or crosslinked in the presence of the other,[126] it is not a simple blending of two or more pre-formed networks. If there are un-crosslinked linear or branched macromolecules that are dispersed in the IPN and that can be separated from the network without breaking chemical bonds, then this topology is called a semi-IPN.[127] An IPN where both networks are based on the same polymer chains, i.e., the same monomer or the same non-functional part of the backbone, the IPN is called a homo-IPN.[128] For homo-IPNs, the phase separation can be almost completely avoided and a full interpenetrating of polymer chains is obtained since the networks are thermodynamically miscible.[129] Compared with SCNs and DCNs, a synergistic effect of all components is observed in IPNs,[130] which often exhibit improved mechanical properties over single network hydrogels.[131] In addition, IPNs have shown advantages in terms of thermal stability, chemical resistance, and suppression of creep and flow of the hydrogels.[132]

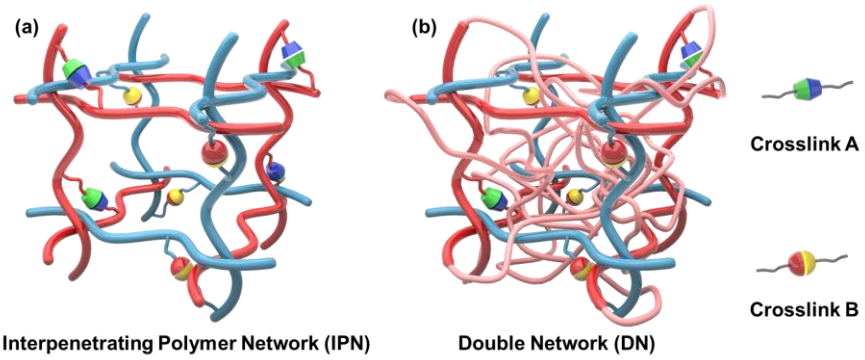

Figure 2.15. Schematic representation of the topologies of (a) interpenetrating polymer network (IPN), and (b) double network (DN).

Benefiting from the readily adjustable chemical composition, chain length and crosslinking density of the individual networks in the IPN topology, Gong has pioneered the development of the double network (DN) (**Figure 2.15b**) hydrogels,[133] which consist of two asymmetric interpenetrating polymer networks with contrasting mechanical properties.[134] The short-chain network (the first network) is a densely crosslinked and brittle network for energy dissipation under large deformations (**Figure 2.16**), while the long-chain network (the second network) is a loosely crosslinked and stretchable network for maintaining elasticity, thus a DN hydrogel exhibits high strength and toughness.[135] Although the advantage of static covalent sacrificial bonds is high bond energy, and low temperature and deformation rate dependency,[136] their irreversibility makes them unusable once broken. Dynamic bonds, particularly supramolecular interactions, have been introduced into DN hydrogels as sacrificial bonds being able to recover after damage.[137-139] Gong's double network theory starts with, but is not limited to, double network hydrogels and can be extended to the design of macromolecular topologies for tough materials, provided they have sacrificial bonds to dissipate energy and can retain the integrity of the materials after large deformations. For example, a weak and strong bond crosslinked DCN hydrogel can have similar mechanical behaviors

as double network hydrogels by dissipating energy through weak bonds while strong bonds maintain the integrity of the gel.[140]

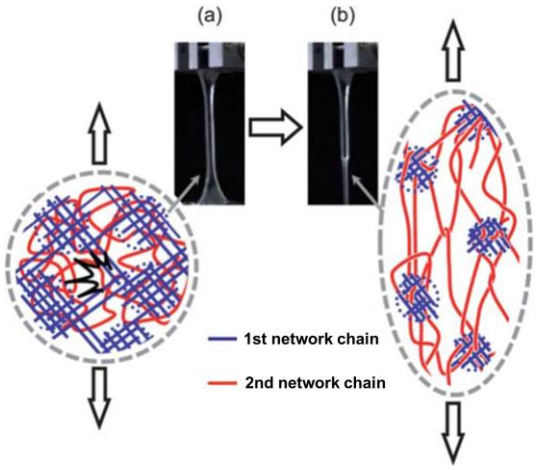

Figure 2.16. Schematic representation of the effect of deformation on a DN (a) before necking, and (b) after necking.[135]

Based on the previous discussion, the installation of two or more dynamic bonds into a hydrogel network can be implemented with the topologies of DCN, TCN, IPN and DN. Macromolecules functionalized with two or more dynamic bonding sites can be prepared as hydrogels with DCN or TCN topologies, while chains containing only a single dynamic bonding site can be used with other functionalized polymers to synthesize IPN or DCN hydrogels. These multi-dynamic crosslinking network strategies can be applied not only to build gels but also to prepare elastomers with tunable response properties and excellent mechanical properties.[56] For example, Bao and co-workers reported a DCN elastomer based on Eu(III)-curcumin coordination bonds and on hydrogen bonds between urethane groups.[141] This elastomer is capable of self-healing and has excellent mechanical properties (tensile stress ~ 1.8 MPa and strain capability ~ 900%). Peng et al. prepared an IPN elastomer based on a polyurethane network crosslinked by Fe(III)-catechol coordination bonds and on an epoxy network crosslinked by imine bonds.[142] By virtue of the synergistic

effect between the two individual networks and the pH sensitivity of the two dynamic bonds, the obtained IPN elastomer showed enhanced mechanical properties and excellent underwater self-healing capacity over a wide pH range from acidic to alkaline. Since there have been many comprehensive reviews discussing multi-dynamic polymer systems based on dynamic bond types,[50-52, 55, 56] this chapter will focus on aqueous polymer network systems containing metal-terpyridine coordination and reversible C=N bonds in hydrogels from the network topology perspective.

2.4 Rheological Characterization of Hydrogels

Before starting the discussion on various types of dynamic hydrogels, it is necessary to introduce an important characterization tool that is often used for such materials, namely rheology. Rheological characterizations can give information directly related to the dynamics and mechanical properties of hydrogels, which are always presented in the discussions about dynamic hydrogels.[143] The dynamics of hydrogels basically exhibit time- or temperature-dependent rheological behaviors such as creep, stress relaxation, and dynamic actuation depending on the lifetime and number of dynamic crosslinks.[85] Connecting the dynamic bonds and network topologies in dynamic hydrogel architectures to their rheological behaviors will help us to better recognize the relationship between structure and properties of such materials.

An ideal viscous fluid exhibits a Newtonian behavior following Newton's law of viscosity. An ideal elastic material exhibits a Hookean behavior, i.e., rapid deformation when stress is applied and immediate recovery once the stress is removed. A hydrogel is composed of an aqueous solution and a solid 3D network portion, possessing both liquid-like and solid-like nature.[21] A hydrogel is therefore viscoelastic and exhibits both viscous and elastic mechanical response upon

deformation. Viscoelasticity defines a hydrogel's ability, under an applied load, to resist mechanical deformation (solid-like behavior) and to dissipate energy (liquid-like behavior).[144] Rheological characterization is an appropriate approach to characterize the viscoelasticity of the hydrogel since it is fast, sensitive, requires minute amount of sample, and can provide insight into gelation kinetics, mechano-responsiveness, and relaxation timescale of the hydrogel. These rheological characteristics are related to storage modulus (G′) (qualitatively the hydrogel stiffness, solid-like elastic properties), loss modulus (G″) (qualitatively the hydrogel energy dissipation, liquid-like or flow response of hydrogel), and loss factor tan δ (Tan δ = G″/G′), measured as functions of time, applied oscillatory strain and angular frequency.[145] If tan δ < 1 (i.e. G′ > G″), the sample behaves more like an elastic solid, while if tan δ > 1 (i.e. G′ < G″), the sample behaves more like a viscous liquid.[146]

Rheological properties of hydrogels are typically evaluated by using small amplitude oscillatory shear (SAOS) measurements.[147] In this experiment, a sample is placed between two parallel plates or a cone and a disk, a small amplitude torsional oscillation deformation is applied to the sample. and the material response (strain or stress) is given as a sinusoidal output (**Figure 2.17b**). If the rheometer is strain-controlled, a shear strain is applied to the sample in a sinusoidal oscillation, $\gamma(t) = \gamma_o (\sin \omega t)$, and the measured shear stress is a phase-shifted sine wave $\sigma(t) = \sigma_o (\sin \omega t + \delta)$, where ω is the applied angular frequency and $\delta \in [0, \pi/2]$ is the phase difference between the strain and stress waves.[147] For a viscoelastic material like a hydrogel, the phase lag between the applied strain and the resulting stress curves will fall between the limits (i.e., $0 < \delta < \pi/2$).[146] If the sample is a purely elastic material, the stress and strain waves are in phase (i.e., $\delta = 0$). If the sample is a purely viscous material, the two waves are out of phase by $\pi/2$ (i.e., $\delta = \pi/2$). Similarly, in the case of a stress-controlled rheometer, the shear stress is applied as $\sigma(t) = \sigma_o (\sin \omega t)$ and the resulting shear strain is measured as $\gamma(t) = \gamma_o (\sin \omega t + \delta)$. The equation

related to shear stress and shear strain are given by $\sigma(\omega, t) = G'.\gamma_o.(\sin \omega t) + G''.\gamma_o.(\cos \omega t)$, with the coefficients G' and G'', respectively denoting the energy stored elastically and the energy lost through flow per cycle when the oscillatory shear is applied to a viscoelastic sample like a hydrogel.[145]

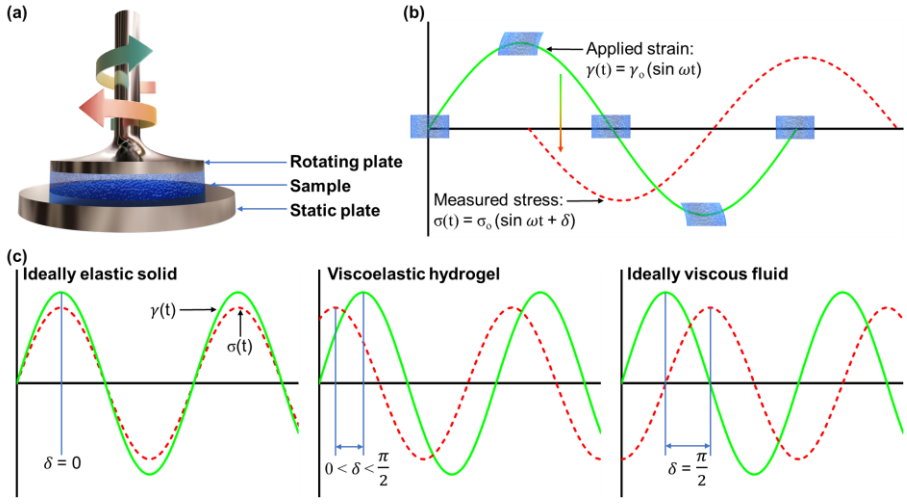

Figure 2.17. (a) Schematic representation of a shear rheometer equipped with a plate-plate geometry. (b) The measure response when oscillatory deformation is applied to the sample. A complete period of oscillation is equal to 2π radians.[148] (c) The behavior of the three materials: $\gamma(t)$ and $\sigma(t)$ as a function of time dependence.

Typically, three types of rheological measurements can be performed to characterize hydrogels. Generally, the rheological parameters of a hydrogel are independent of the applied strain amplitude up to the limiting strain (γ_L) level.[146] In some papers, limiting strain is also referred to as critical strain (γ_c)[149] or yield strain (γ_y),[150] which are described as the strain at which G' starts to decrease and are used to define the limit of the linear viscoelastic (LVE) range. The SAOS behaviors of hydrogels are typically investigated within the LVE regime. Beyond the γ_L, the behavior of the hydrogel is non-linear (NLVE). Thus, oscillatory strain amplitude sweep measurement at a fixed frequency to determine the LVE range is a good first step in

characterizing the rheological behavior of hydrogels. In typical strain sweeps (**Figure 2.18a**), the variation of the modulus is a function of the strain amplitude. Usually, G′ and G″ of the hydrogel are constant in a small range of LVE. G′ is always larger than G″ in the LVE region, indicating that the hydrogel exhibits a solid-like behavior. As the strain is higher than γ_L, G' gradually decreases and G" gradually increases, suggesting that the hydrogel transforms from a solid-like behavior to a liquid-like behavior. The G' and G" crossover point is then observed when the rupture strain (γ_r) is reached. Once the strain is beyond γ_r, G' falls below G", demonstrating that the hydrogel network is completely damaged and exhibits liquid-like characteristics.

With the LVE range established, oscillatory frequency sweeps at a fixed strain amplitude (in the LVE region) can be performed. By measuring the moduli as a function of frequency, the behavior of hydrogels can be observed at short versus long timescales. For robust hydrogels based on strong or long lifetime bonds, G' is nearly frequency independent and is always greater than G" over a range of oscillation frequencies[151] (**Figure 2.18b**, dashed curves). However, for some dynamic hydrogels whose crosslinking bonds are more reversible under a certain condition (such as pH, temperature, …), the variation of G' and G" may depend on the frequency. Such hydrogels may display a solid-like behavior (G' > G") at high frequencies (fast timescale), while at lower frequencies or longer timescales, the hydrogels behave more like a liquid-like response (G' < G") and flow easily (**Figure 2.18b**). By taking the reciprocal of the frequency at which G"(ω) reaches its peak, the stress relaxation time scales of the network (τ) may be found.[152] In dynamic hydrogels, the stress relaxation time (τ) is often linked to the dissociation rate (k_d) of the dynamic bonds.[60]

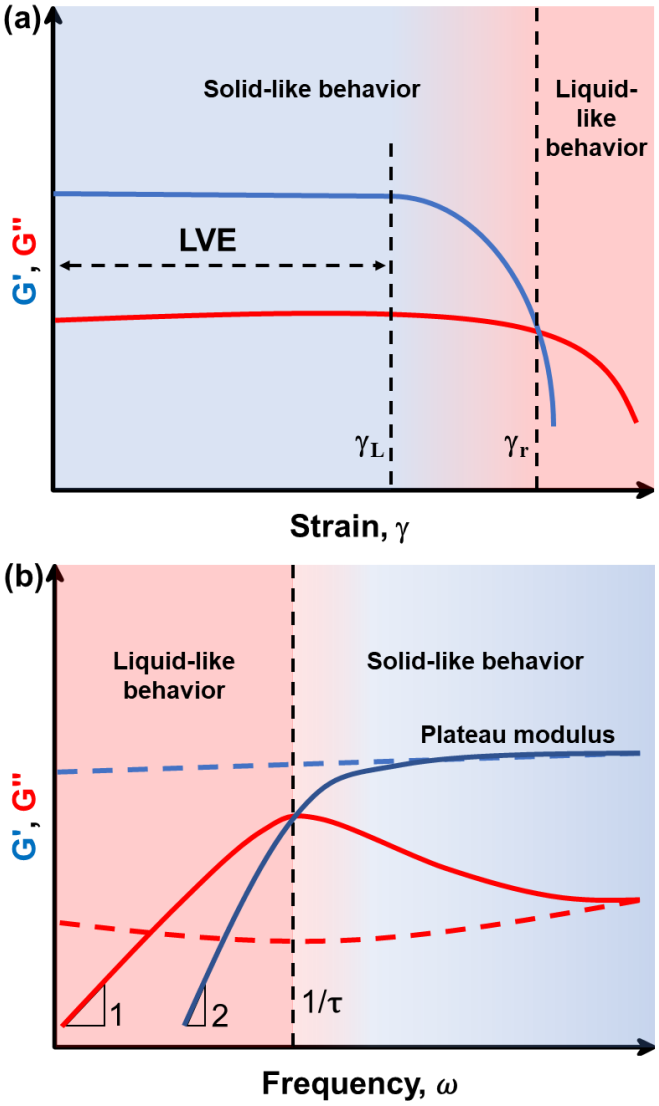

Figure 2.18. Rheological experiments on hydrogels at a constant temperature: (a) oscillatory strain sweeps at a fixed frequency amplitude, (b) oscillatory frequency sweeps at a fixed strain amplitude.

Besides, the frequency sweep data also provide the experimental plateau modulus (G'_p), which could be compared with the theoretically expected value (G_N^0) according to the affine and phantom network models.[21, 80, 152] The affine network model is based on a polymer

network of Gaussian chains, where the displacement of the crosslinked points at both ends of each elastic network strand is identical to the macroscopic deformation of the entire network.[143] Unlike the affine model, the phantom network model considers fluctuations in the crosslinking points.[21] The theoretical shear modulus given by the two network models are respectively:

$$G_N^0 = \nu k_B T = \frac{\rho R T}{M_{XX}} \text{ (affine network)} \quad (2.5)$$

$$G_N^0 = \nu k_B T \frac{f-2}{f} = \frac{\rho R T}{M_{XX}}\left(1 - \frac{2}{f}\right) \text{ (phantom network)} \quad (2.6)$$

where ν is the number of elastically effective network strands per unit volume, ρ is the network density (mass per unit volume), f is the functionality of the crosslinks, M_{xx} is the number-average molar mass of a network strand. However, it is important to note that both equations assume that the number of elastically effective strands $\nu = \rho N_{Av}/M_{xx}$ (N_{Av} is Avogadro's number) for an ideal network and ignore the contribution of trapped entanglements. In reality, it is hardly possible to eliminate defects such as loops, dangling ends, and network misconnections, which are not elastically effective. In addition, the G' value of static covalent hydrogels is mainly influenced by the crosslinking density, whereas in dynamic hydrogels, the crosslinking density, K_{eq} and crosslinks exchange kinetics all could influence the value of G'.[40, 60]

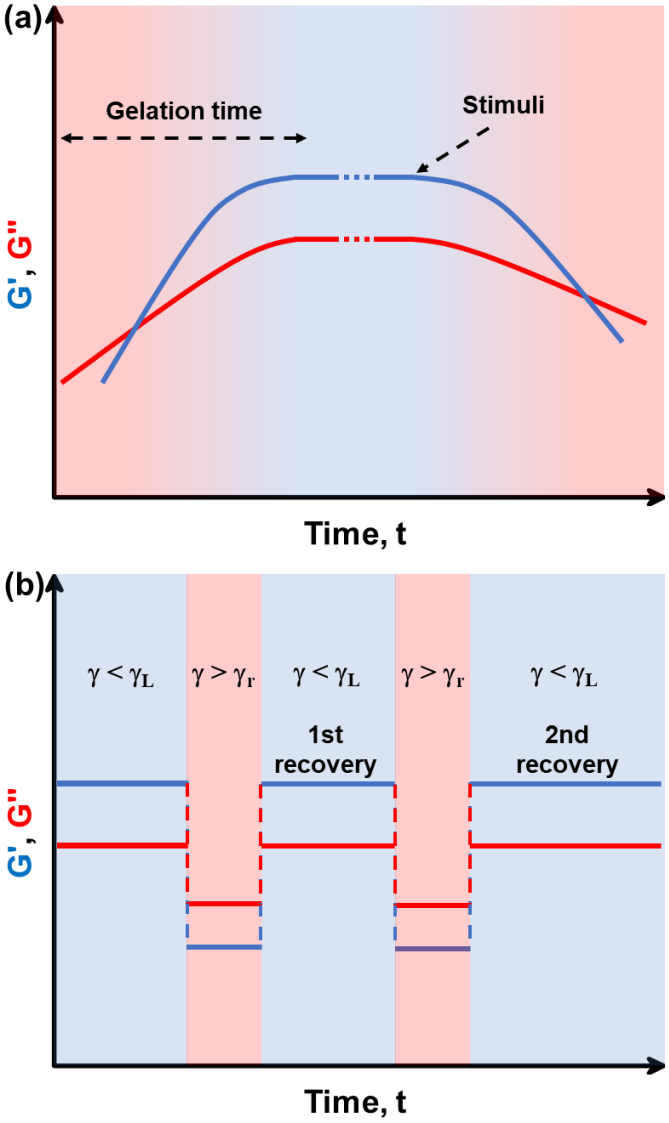

Figure 2.19. Rheological experiments on hydrogels at a constant temperature: (a) oscillatory time sweeps under fixed frequency and strain amplitude for gelation process and gel-sol transition in response stimuli, (b) oscillatory time sweeps at a fixed frequency and strain amplitude with repeated step strain (from $\gamma < \gamma_L$ to $\gamma > \gamma_r$, then, back to $\gamma < \gamma_L$).

The third rheological measurement commonly used to characterize hydrogels is the oscillatory time sweeps under fixed frequency and strain amplitude. In practice, time sweeps at constant small shear amplitudes and frequencies are often required to monitor gel samples before performing other tests to ensure sample equilibrium. The test can also be used to track the gelation time from precursor solution to hydrogel as well as the gel-sol transformation process of responsive hydrogels upon receipt of the stimuli (**Figure 2.19a**).[151] For hydrogels with self-healing properties, self-healing performance can be assessed by performing time sweeps with cyclic strain amplitude and repeated several times to check the reproducibility of the self-healing ability (**Figure 2.19b**). The self-healing efficiency of hydrogels can be determined by comparing the recovered G' value with the initial G' value.

2.5 Hydrogels Based on Metal-Terpyridine Coordination and Reversible C=N Bonds

Because the hydrogels are composed of water and aqueous polymer networks, which are crosslinked hydrophilic polymers, at least the main backbone of which must be hydrophilic to render them water-swellable. The choice of the hydrophilic polymer is a fundamental factor that has to be taken into account when designing hydrogels. These hydrophilic polymers can be synthetic polymers made from the polymerization of water-soluble monomers, or they can be naturally derived biomolecules. The primary hydrophilic part of the hydrogel network can therefore be constituted by pure synthetic polymers, biopolymers, or the combination of them. Before proceeding to discuss multiple bonding hydrogels based on metal-terpyridine complexes and reversible C=N bonds, we will introduce the SCN hydrogels prepared by them to learn which hydrophilic polymers can be used as backbones for installing

these two types of dynamic bonds, and what properties or behaviors the obtained hydrogels have.

2.5.1. SCN hydrogels

As mentioned in section 2.3, a common method of constructing polymer networks is to introduce side functional groups onto the linear copolymer backbone. Such side-chain functionalized hydrophilic polymers can be synthesized by copolymerizing functional monomers with water-soluble monomers or post-modification of hydrophilic polymers possessing reactive groups. In addition, functional groups can also be grafted onto the main chain of a hydrophilic polymer, such as on the chain-ends of a multi-armed hydrophilic polymer. As a result, terpyridine groups or amine/carbonyl groups can be used in the above three ways to develop functional polymers for the construction of SCN hydrogels based on metal-terpyridine coordination or reversible C=N bonds.

2.5.1.1. SCN based on metal-terpyridine coordination bonds

With the appropriate selection of metal ions, the strengths and reversibility of metal-terpyridine coordination bonds can be varied over a wide range. Consequently, these crosslinks allow the networks to exhibit a range of stability from dynamic to permanent.[153] However, networks were often used to prepare organogels and very few studies have been devoted to hydrogels due to the hydrophobicity of terpyridine entities.[154-158] **Table 2.4** lists some of the reported Tpy-functionalized polymers that can be used to construct hydrogels.

Table 2.4. Representative hydrophilic polymers and metal ions for the preparation of hydrogels based on metal-terpyridine coordination bonds.

Polymer	Metal ion	Properties	Ref.
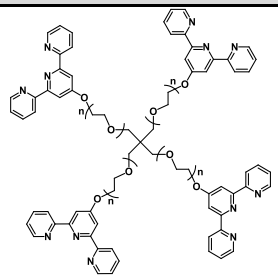	Fe^{2+}	NH_3-Responsiveness	[159]
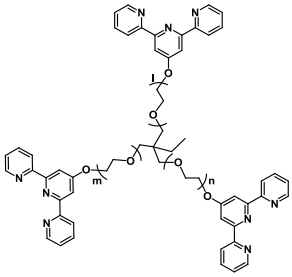	Co^{2+}, Fe^{2+}	Oxidation/reduction-responsiveness; self-healing	[160]
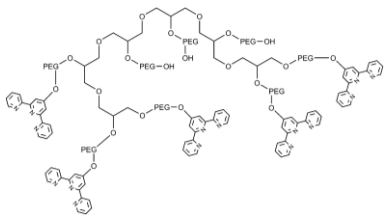	Zn^{2+}, Co^{2+}, Fe^{2+}, Ni^{2+}	Zn^{2+}-Tpy gels show thermo-reversible sol-gel transition	[166]
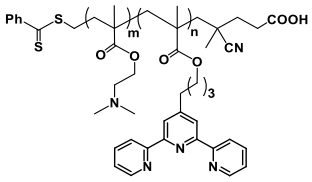	Co^{2+}	Stress relaxation	[170]
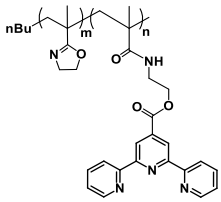	Zn^{2+}, Co^{2+}, Fe^{2+}, Ni^{2+}	Self-healing and moldable, Zn^{2+}-Tpy and Co^{2+}-Tpy gels show thermo-reversible sol-gel transition	[171]

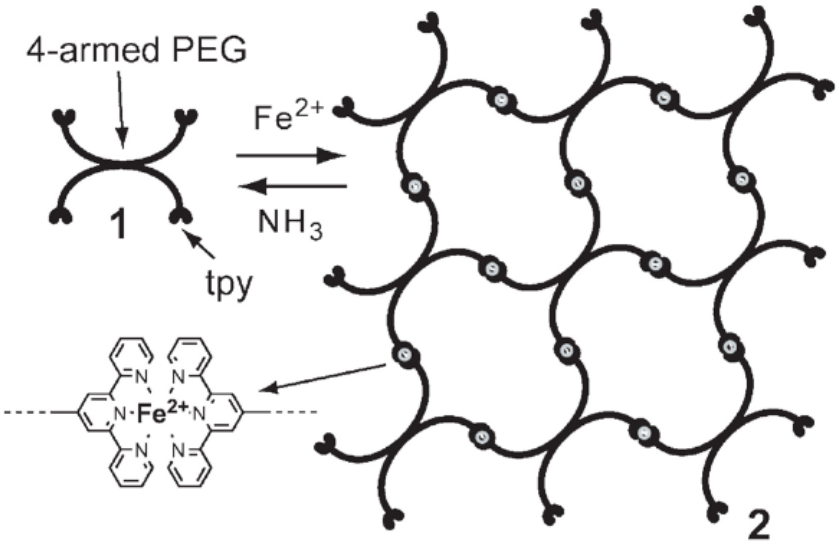

Figure 2.20. Schematic representation of the formation of hydrogels based on Fe^{2+}-Tpy crosslinked four-arm PEG and ammonia-induced collapse.[159]

Telechelic star poly(ethylene glycol) (PEG) having terpyridine termini have been developed as promising aqueous polymer precursors for metal-ligand coordination hydrogels. Kimura et al. used a four-armed PEG end-capped with terpyridine moieties to synthesize a Fe^{2+}-Tpy crosslinked network (**Figure 2.20**), which can swell in water to obtain a hydrogel.[159] The hydrogel was very stable when varying the pH in the range of 1 ~ 13 or heating up to 90 ℃, but the addition of aqueous NH_4OH solution resulted in a decomplexation of Fe^{2+}-Tpy bis-complexes and a induced gel-sol transition. The hydrogel containing 0.1 M KCl also displayed reversible Fe^{2+}/Fe^{3+} couple at $E_{1/2}$ = +0.77 V vs. Ag/AgCl, indicating the potential of electrically controllable network variations. Kikuchi et al. synthesized a series of metal-terpyridine coordination hydrogels by using the terpyridine terminated three-arm PEG (tris-PEG-Tpy) with Co^{2+} and Ni^{2+}.[160] Because the Co^{2+}-Tpy bis-complexes are kinetically labile and Co^{3+}-Tpy bis-complexes are kinetically inert (slow ligand exchange), the sol-gel transition can be achieved by exposing the system to air to oxidize Co^{2+}

to Co^{3+}. Conversely, the addition of Ascorbic acid can also transform Co^{3+}-Tpy bis-complexes into Co^{2+}-Tpy bis-complexes to achieve a reversible gel-sol transition. A hydrogel ($Co_{85}Ni_{15}$, where the indices are the molar percentages of each metal ions) containing both redox responsive Co^{2+} and non-oxidizable Ni^{2+} with tris-PEG-Tpy can undergo reversible sol-gel transition and has self-healing properties, which were attributed to the oxidation/reduction of cobalt ions and kinetically unstable bis-complexes, respectively. Tpy-terminated four-arm PEG are ideal precursors for the construction of model supramolecular hydrogels because such star polymers form networks with well-defined topology showing very little spatial inhomogeneity, and because the binding strength and dynamics of the metal-ligand complexes can be easily tuned by changing the transition metal ions.[81] With such polymer architecture, Seiffert's group developed a variety of terpyridine functionalized star-PEG for model-network gels.[161-165] For example, they found that Zn^{2+}-Tpy crosslinked star-shaped PEG networks show rheological relaxation similar to the sticky Rouse model, where the presence of stickers delays Rouse relaxation and terminal relaxation.[163] The understanding of the model network relaxation can allow a rational design of the self-healing and mechanical properties of the materials in relation with the dynamic crosslink strength and network topology.

Wang et al. synthesized an eight-arm PEG partially substituted with terpyridine entities to study the metallo-supramolecular assembly behaviors with the transition metal ions Zn^{2+}, Co^{2+}, Fe^{2+}, and Ni^{2+}.[166] The large differences in dissociation rate constants of the various M(II)-Tpy bis-complexes largely determine the formation of nanoparticle at low concentrations and of hydrogel properties at higher concentrations (> 5 wt.%). Due to the thermodynamic stability of Fe^{2+}-Tpy and Ni^{2+}-Tpy, the hydrogels formed by them were elastic and were stable in the range of 5 to 60 °C. As the Co^{2+} and Zn^{2+} complexes are kinetically labile, the loss moduli of the hydrogels were largely temperature-dependent, and a reversible gel-sol transition of the Zn^{2+}-Tpy hydrogel at 25°C was observed. Interestingly, such temperature-responsiveness

of the Zn^{2+}-Tpy hydrogel was independent of the polymer concentration. Subsequently, Wang et al. synthesized another terpyridine end-functionalized 8-arm PEG by using the reaction of a 4'-aminopentanoxy substituted terpyridine with a p-nitrophenyl chloroformate activated PEG-$(OH)_8$.[167] Based on the uncomplexed and complexed state of Fe^{2+}-Tpy, they studied the biocompatibility and potential cytotoxicity of the polymer conjugate, nanogels, and hydrogels by using bovine chondrocytes. Since the bonding of Fe^{2+}-Tpy is almost as strong as a covalent bond, the stable complexes are not cytotoxic when the metal ions are embedded in the hydrogel network. However, the polymer conjugate with free ligands may be toxic to cells due to depletion of essential Fe^{2+}. Importantly, the work of Wang et al. was the first biological evaluation of terpyridine-based PEG hydrogels, providing a start for the application of such hydrogels in potential biomedical or pharmaceutical applications.

Walther et al. reported a supramolecular fluorescent hydrogel formed by mixing solutions of a terpyridine-modified 4-arm polymer and Zn^{2+}.[168] The functional aqueous polymer was a Tpy-terminated 4-arm poly(triethylene glycol methyl ether acrylate) (p(mTEGA)) star polymer with a fluorescent perylene bisimide (PBI) core (**Figure 2.21**). Due to the dynamic and thermally reversible nature of Zn^{2+}-Tpy, the hydrogel allows for rapid self-healing at room temperature and can be 3D printed by extruding it at 40 °C onto a plate at room temperature.

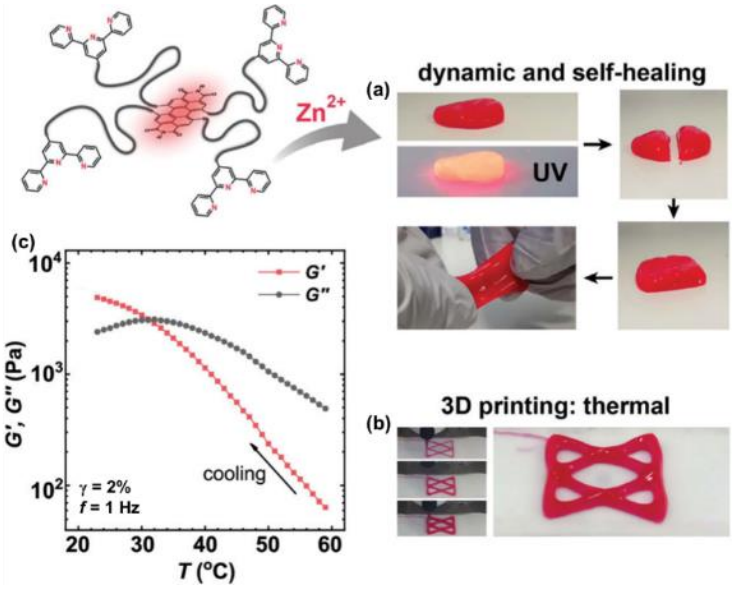

Figure 2.21. Schematic illustration of a dynamic and thermo-reversible fluorescent hydrogel based on Zn^{2+}-Tpy, (a) showing self-healing at room temperature and (b) 3D printing at 40 °C. (c) Temperature-dependent dynamic rheological behavior.[168]

Besides, the synthesis of side-chain terpyridine-functionalized hydrophilic copolymers via copolymerization of Tpy monomers with aqueous monomer represents a good alternative and has been explored by our group to prepare M(II)-Tpy hydrogels.[169] Brassinne et al. synthesized a side-chain terpyridine-functionalized poly(2-(dimethylamino)ethyl methacrylate) (P(DMAMEA)) via controlled radical copolymerization of 2-(dimethylamino)ethyl methacrylate and terpyridine-functionalized methacrylate comonomers.[170] In the work, the Co^{2+} was selected to form crosslinks of moderate strength, resulting in a transient Co^{2+}-Tpy hydrogel (**Figure 2.22**). The obtained hydrogel shows stress relaxation and self-restructuring abilities that were probed by rheology. This work uses terpyridine functional monomers to synthesize copolymers and add metal ions to prepare M(II)-Tpy crosslinked hydrogels in a similar way to the preparation of hydrogels in this thesis, so reference can be made to their monomer and polymer synthesis operations. In addition, the analysis of dynamic rheology in

the paper can also be applied to our study to help in the understanding of our dynamic hydrogel systems.

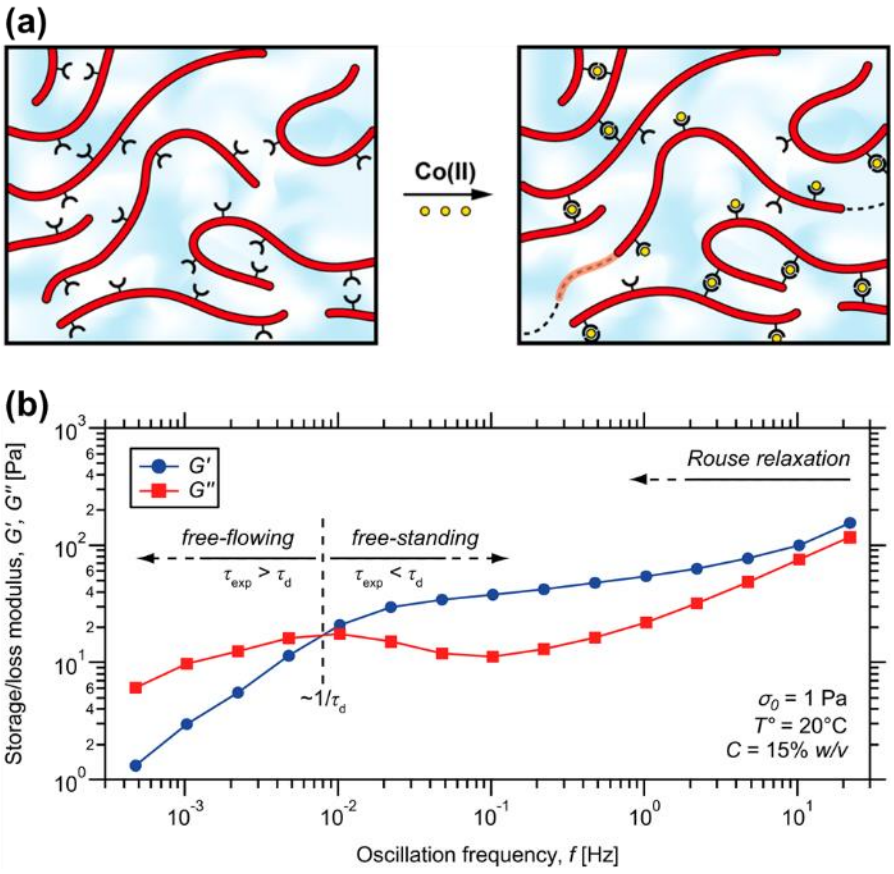

Figure 2.22. (a) Schematic representation for the network of Co^{2+}-Tpy hydrogel prepared from side-chain Tpy functionalized P(DMAMEA). (b) Oscillatory frequency sweep on the obtained hydrogel.[170]

Xu et al., reported a facile and straightforward strategy to synthesize side-chain terpyridine-modified precursors, which were prepared by the ring-opening addition reaction of poly(2-isopropenyl-2-oxazoline) (PiPOx) with a commercially available 2,2′:6′,2″-terpyridine-4′-carboxylic acid.[171] A series of M (II)-Tpy hydrogels were obtained by the addition of divalent transition metal ions (Zn^{2+},

Co^{2+}, Fe^{2+}, and Ni^{2+}). All prepared hydrogels exhibited self-healing and moldable capacity even at higher crosslinking density. The Zn^{2+}-Tpy and Co^{2+}-Tpy hydrogels also show thermo-reversible sol-gel transition due to the higher kinetic lability of their complexes.

Recently, Es Sayed and coworkers reported a method to control emulsion stability by an advanced class of microgel emulsifiers.[172] The microgel network was formed by a two-step surfactant-free dispersion copolymerization of N-isopropylmethacrylamide (NIPMAM) in the presence of a terpyridine-based comonomer (TpyAm) (**Figure 2.23**). After 4 h of polymerization, a linear NiPMAM-*co*-TpyAm polymer can be obtained in the mixture of water and oil, and followed by the addition of $FeCl_2 \cdot 4H_2O$ to induce the formation of Fe^{2+}-Tpy crosslinked microgel. The Fe^{2+}-Tpy microgels were able to stabilize creamed emulsions for months. However, the addition of H_2O_2 and potassium persulfate resulted in a completely phase-separated within a few hours due to the oxidation of Fe(II) complexed with the terpyridine units to Fe(III). The oxidation reaction produced Fe(III)-Tpy bis-complexes that were kinetically labile and led to the collapse of the network, thereby depriving the microgel of its emulsion stabilizing ability.

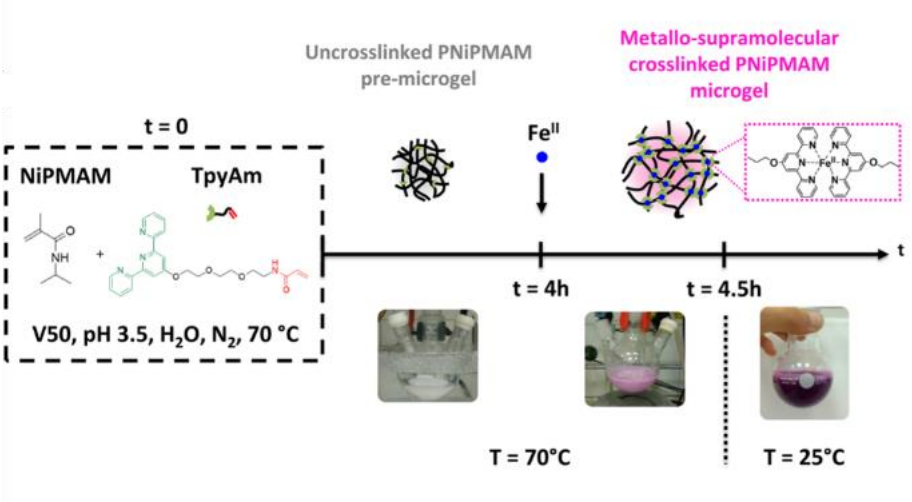

Figure 2.23. Schematic representation of the reaction pathway for the synthesis of Fe^{2+}-Tpy microgels.[172]

2.5.1.2. SCN based on reversible C=N bonds

The SCN hydrogels crosslinked by reversible C=N bonds (including imine, hydrazone and oxime bonds) have been extensively studied in the last two decades due to the availability of carbonyl groups (aldehyde or ketone groups) which are common in biomolecules. Moreover, hydrophilic polymers can be readily modified using facile methods to include carbonyl groups or α-effect nucleophiles. Given the abundant sources of functional polymers for such hydrogels, we will mainly focus on synthetic polymer-derived SCNs for the purpose of this thesis since there are already many reviews discussing reversible C=N bonding hydrogels from biopolymers.[173-178] This type of hydrogels will be sequentially introduced in the order of imine, hydrazone (including alkylhydrazone, acylhydrazone, semicarbazone), and then oxime.

Compared to other types of reversible C=N bonds, imine bonds are the most unstable and are prone to cleavage in aqueous environments. In addition, many biopolymers have the natural availability of primary amines and functional groups that are easily modified by aldehydes and ketones. Therefore, according to reported literatures, SCN hydrogels based on imine bonds are mostly prepared from biopolymers and few efforts have been devoted to utilize synthetic polymers.[179] Various biopolymers such as chitosan, dextran, hyaluronic acid, gelatin, amylopectin, alginate, cellulose, pullulan, konjac glucomannan, gum Arabic, chondroitin sulfate, agar and collagen have been widely explored to form imine-based SCN hydrogels for biomedical applications.[180-192] For example, by the formation of imine bonds between the amino groups of chitosan and the benzaldehyde end-groups of linear PEG (**Figure 2.24**), Wei et al. prepared SCN hydrogels with multi-responsive and rapid self-healing ability due to the pH-responsive and reversible nature of imine bonds.[180] The hydrogels also can be used to encapsulate and control the release of small bioactive molecules such as lysozyme without compromising its bioactivity.

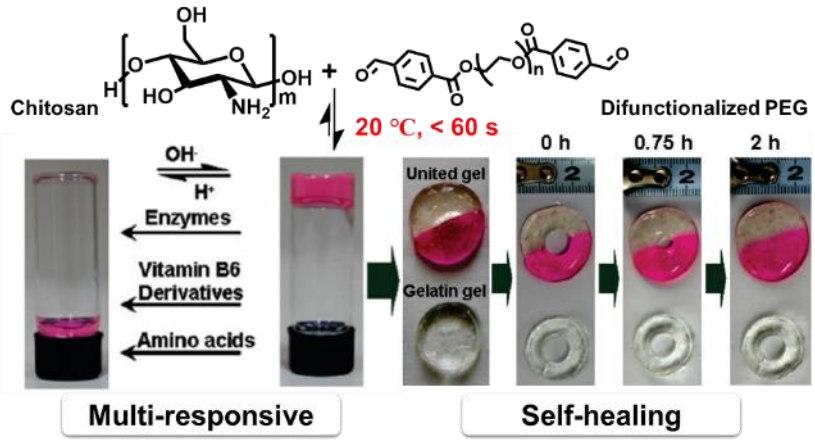

Figure 2.24. The multi-responsive and self-healing SCN hydrogels based on imine bonds formed by the chitosan and a dibenzaldehyde-terminated PEG.[180]

Aldehyde groups on polysaccharides can be easily obtained by an old but still widely used method, i.e. oxidative cleavage of vicinal diols with sodium periodate.[175-177] Shokrolahi and colleagues, reported a class of SCN hydrogels based on imine bonds, in which gelatin was the amine-sharing part and oxidized amylopectin was the aldehyde-providing part (**Figure 2.25**).[183] These gels combine properties of rapid forming, self-healing, injectability, and proper durability. Notably, the authors demonstrated the biocompatibility and biological applications of the imine hydrogels.

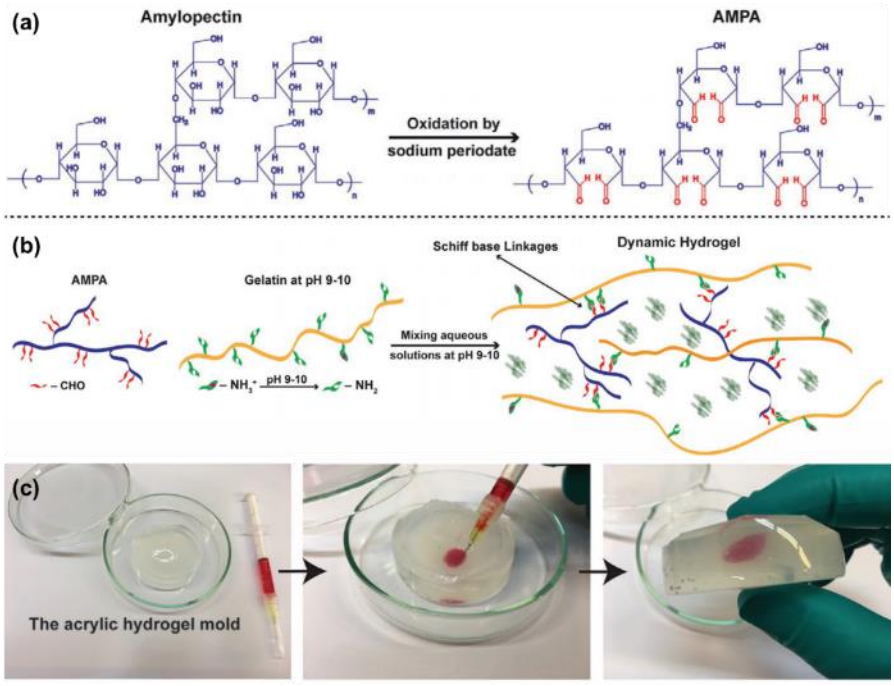

Figure 2.25. (a) Synthesis of amylopectin multiple aldehyde (AMPA). (b)Schematic representation of the formation of SCN hydrogels from aldehydes of AMPA and imines of gelatin. (c) The injectability of SCN hydrogels based on imine bonds.[183]

In addition, some natural small molecules with aldehyde groups can also be introduced on the side chains of polymers to prepare SCN hydrogels. Cong and coworkers synthesized a poly(N,N-dimethylacrylamide) (PDMA)-based copolymer by using the benzaldehyde group of vanillin, which can react with amino-modified poly-tetrahydropyrimidine (PTHP) to rapidly form an SCN hydrogel based on imine bonds (**Figure 2.26**).[193] The obtained hydrogels were injectable, biocompatible, antimicrobial and self-healing, and can be used to cure the suppurative subcutaneous infection.

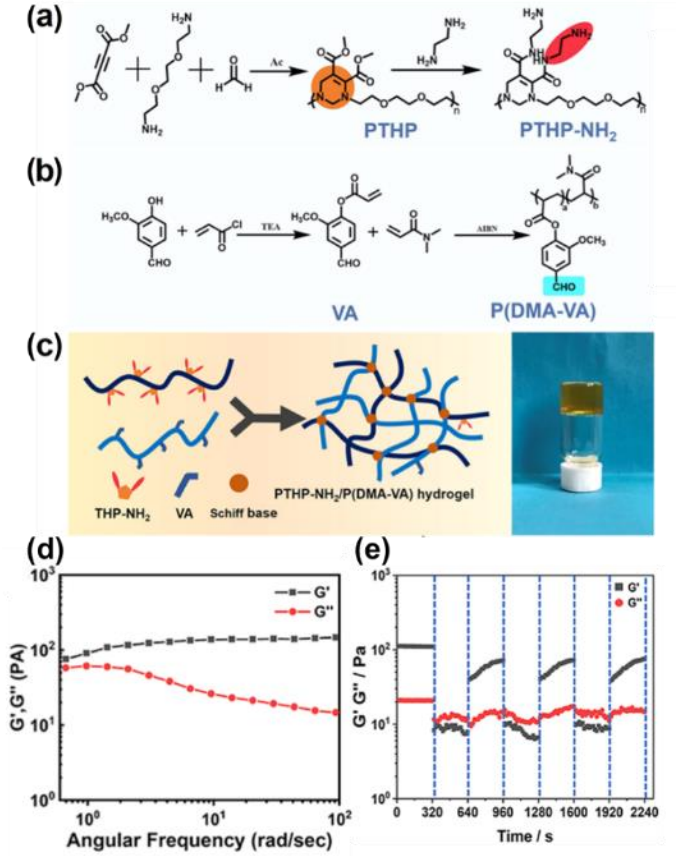

Figure 2.26. (a) Synthesis of aminated PTHP. (b) Synthesis of vanillin functionalized PDMA. (c) Schematic representation of the formation of SCN hydrogels based on imine bonds. (d) Frequency sweeps on hydrogel. (e) Times sweeps with alternative shear strains for characterizing self-healing property.[193]

Ketone groups can also be included into the macromolecular structure as precursors for the preparation of imine crosslinked hydrogels. Yuan et al. prepared a thermo-responsive self-healing hydrogel by the formation of imine bonds between the acetoacetate groups in the four-armed star-shaped poly(2-(dimethylamino)ethyl methacrylate-*co*-2-hydroxyethyl methacrylate) modified with tert-butyl acetoacetate (t-BAA), SP(DMAEMA-*co*-HEMA-AA) and amine groups in polyetherimide (PEI).[194] By dispersing polydopamine nanoparticles (PDA NPs) in the hydrogel, the nanocomposite hydrogels

show phase transition and volume shrinkage under near-infrared (NIR) radiation (**Figure 2.27**). The authors exploited this property to develop an efficient synergistic thermo-chemotherapy for the delivery of anticancer drugs from such imine gels controlled by NIR laser irradiation.

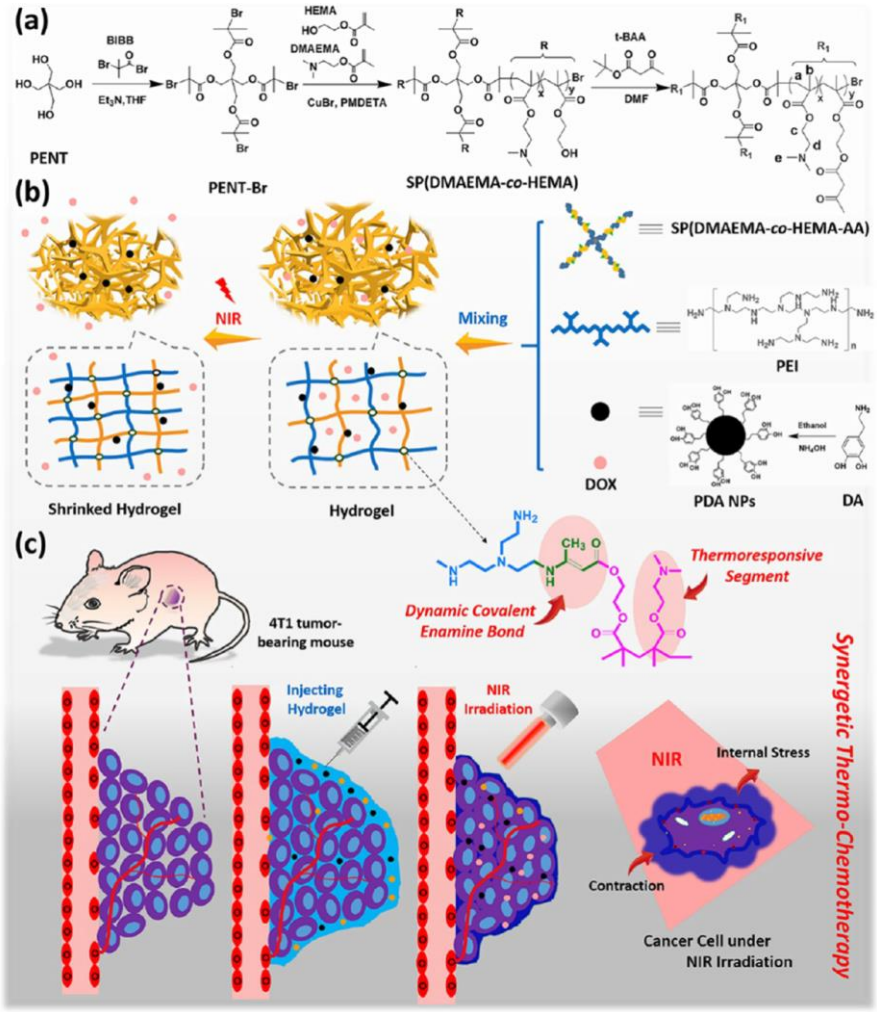

Figure 2.27. Schematic representation for (a) synthesis of the ketone modified SP(DMAEMA-*co*-HEMA-AA), (b) preparation of the imine hydrogel loaded with PDA NPs and DOX; and (c) synergistic thermo-chemotherapy process of nanocomposite hydrogels under NIR Irradiation.[194]

Because hydrazone and oxime bonds possess higher hydrolytic stability than imine bonds, they were more suitable for introduction into synthetic polymers for the preparation of SCN hydrogels than imine bonds. Since Deng and co-workers first discovered the dynamic nature of acylhydrazone bonds in gels in 2010, such dynamic covalent polymer materials have rapidly developed.[29, 195-197] They found that adjusting pH < 4 can achieve gel-sol transition and demonstrated that acylhydrazone gels have self-healing properties. **Figure 2.28** and **Figure 2.29** present some of the synthetic polymers that have been used to prepare SCN hydrogels based on reversible C=N bonds of hydrazone and oxime, and **Table 2.5** summarizes the properties and applications of the hydrogels prepared by the combination of these polymers.

Similar to the synthesis of Tpy polymer precursors, the electrophilic carbonyl moieties (ketone or aldehyde) and α-nucleophilic reagents (hydrazide or hydroxylamine) can be introduced into the side chain of polymers by copolymerization or modification, and at the chain-ends of a PEG backbone by grafting the functional groups. In fact, these functional polymers can be used between each other by the reaction of carbonyl and nucleophilic groups to form 3D networks for the preparation of SCN hydrogels as long as all precursors were not a linear chain like PC10 (**Figure 2.28**). The mentioned synthetic polymers as precursors can not only bring to the hydrogel the dynamic properties of reversible C=N bonds and the properties of the polymer backbone, but can also impart additional functions to the hydrogel by introducing certain functional segments into the polymer precursor by copolymerization or chemical modification. For example, Qin et al. introduced the tetraphenylethylene (TPE) moiety, which has the aggregation-induced emission (AIE) property, to the main chain of copolymer of PC11 (**Figure 2.28**), and produced aggregation-induced emissive acylhydrazone hydrogels.[226]

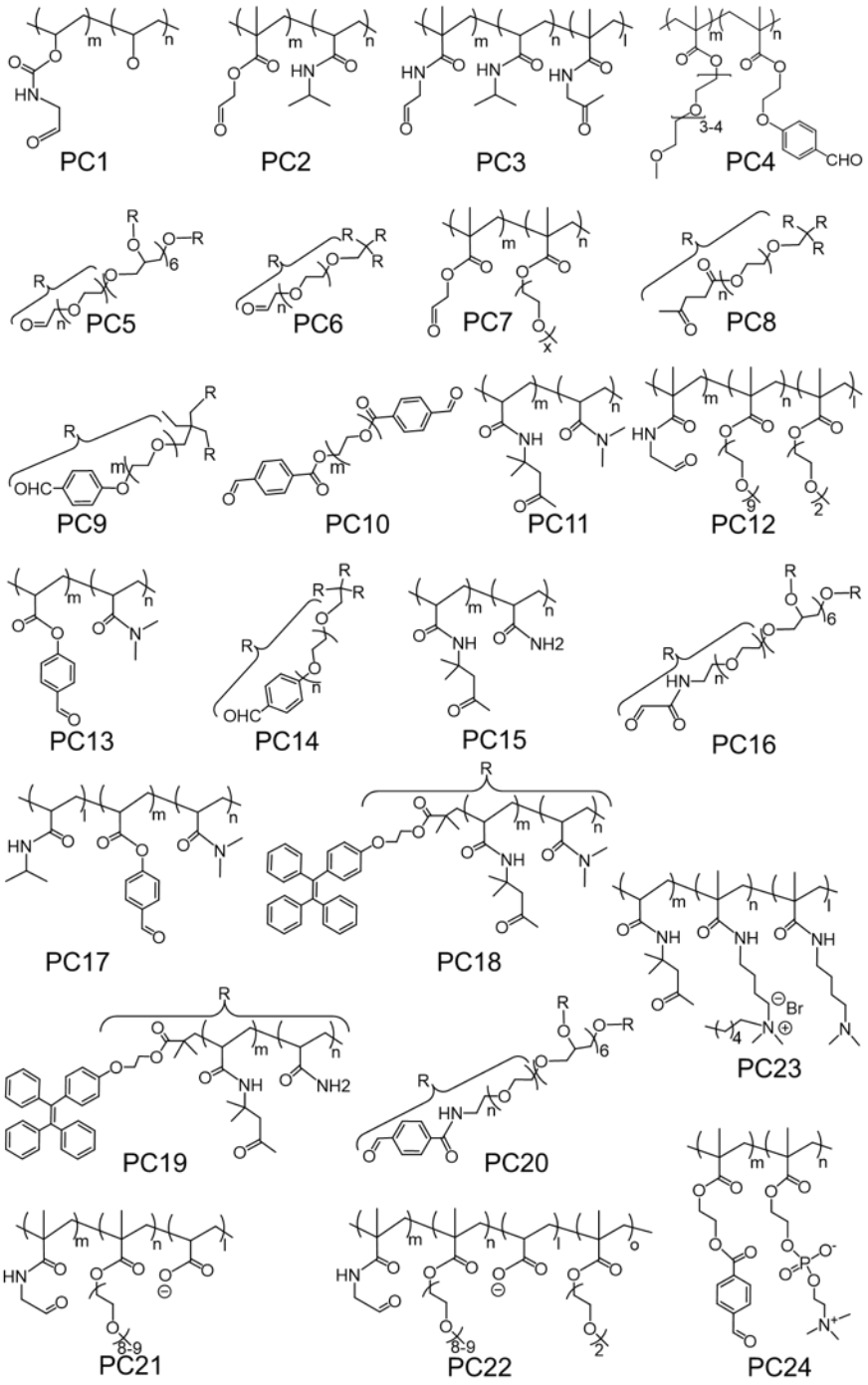

Figure 2.28. Synthetic polymer structures as electrophilic carbonyl reagents for SCN hydrogels based on hydrazone or oxime.

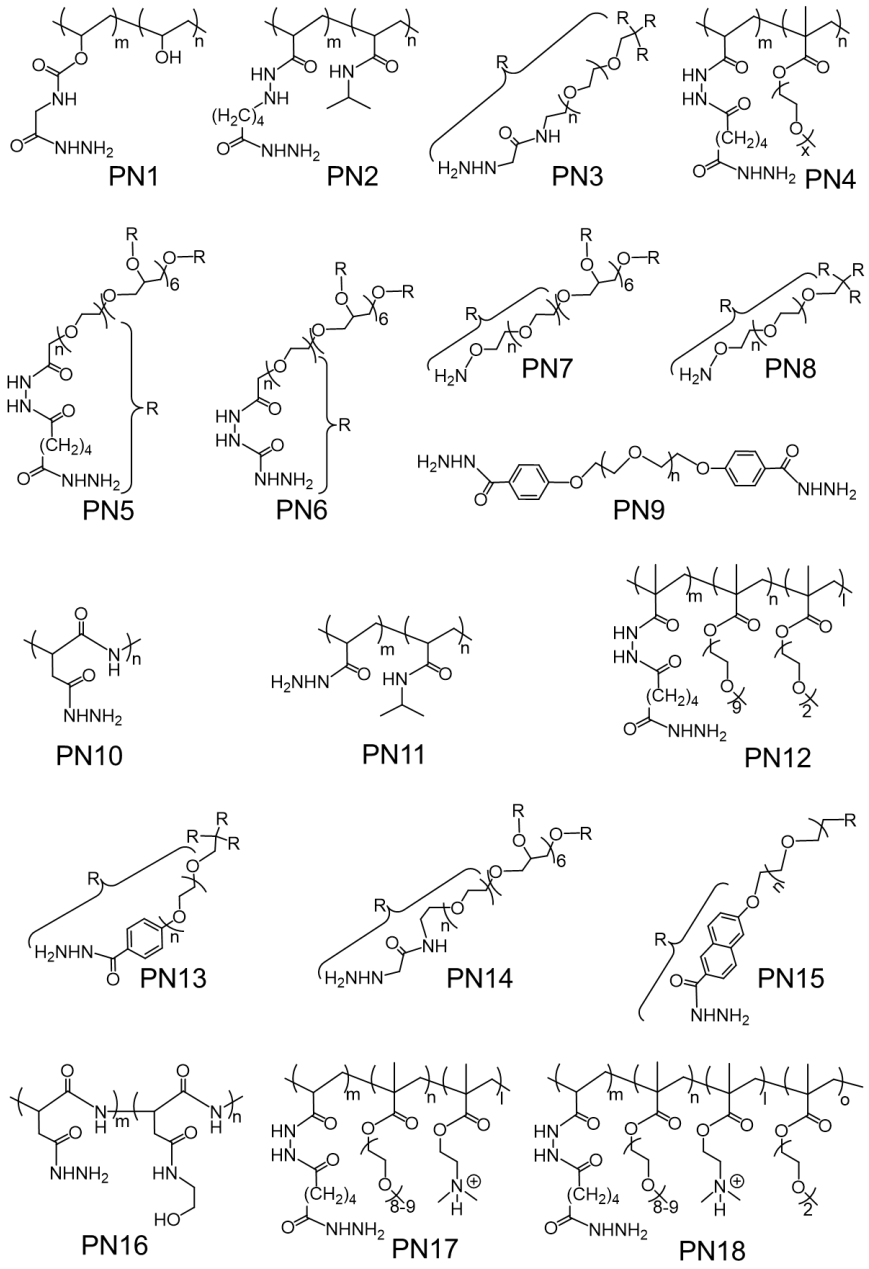

Figure 2.29. Synthetic polymer structures as α-nucleophilic reagents for SCN hydrogels based on hydrazone or oxime.

Table 2.5. Properties and applications of SCN hydrogels based on hydrazone and oxime bonds prepared from synthetic polymer precursors.

Network composition[a]	Bond type	Properties	Ref.
PC1 + PN1	Acylhydrazone	Injectability, degradability, and biocompatibility	[198]
PC2 + PN2	Acylhydrazone	Thermo-responsiveness, degradability, Injectability, and biocompatibility	[199]
PC3 + PN2	Acylhydrazone	Injectability; cytocompatibility; tunable gelation rates, degradation rates, opacities, and mechanical properties	[200]
PC4 + succinic dihydrazide	Acylhydrazone	Thermo-responsiveness	[201]
PC5/PC6 + PN3	Alkylhydrazone	Cytocompatibility; tunable modulus and stress relaxation; cell culture application	[202-204]
PC7 + PN4	Acylhydrazone	Injectability; tunable mechanics, degradation times, and phase transition behaviors	[205-207]
PC5 + PN5; PC5 + PN6; PC5 + PN7	Acylhydrazone; Semicarbazone; Oxime	Biocompatibility; the degradation time of hydrogels can be controlled by varying the α-nucleophilic reagents	[208]
Glutaraldehyde + PN7	Oxime	Biocompatibility; cell adhesion; tunable mechanical properties, gelation kinetics, and water swelling ratios	[209]

Table 2.5. Continued.

Network composition[a]	Bond type	Properties	Ref.
PC8/oxidized-hyaluronic acid/oxidized-alginate + PN8	Oxime	Injectability; catheter delivery application	[210]
PC9 + PN9	Acylhydrazone	Macroscopic self-assembly of the organogel and hydrogel, self-healing	[211]
PC10 +PN10	Acylhydrazone	Biocompatibility, biodegradability, Injectability; local cancer chemotherapy application	[212]
PC11 + O,O'-1,3-propanediylbishydroxylamine	Oxime	Stress relaxation, self-healing	[213]
PC10 + PN11	Acylhydrazone	Thermo-responsiveness, self-healing	[214]
PC12 + PN12	Acylhydrazone	Injectability, degradability	[215]
PC13 + PN9	Acylhydrazone	Degradability, pH-responsiveness, self-healing	[216, 217]
PC14 + PN13	Acylhydrazone	Tunable gelation time and self-healing	[218]
PC15 + hexanedihydrazide	Acylhydrazone	pH-Responsiveness, self-healing	[219]

Table 2.5. Continued.

Network composition[a]	Bond type	Properties	Ref.
PC11 + PN9/ hexanedihydrazide	Acylhydrazone	pH-Responsiveness, self-healing	[220, 221]
PC16 + PN14	Alkylhydrazone	Self-healing, biocompatibility, injectability; chemotherapeutic agent delivery application	[222]
PC17 + PN9	Acylhydrazone	Thermo-responsiveness, biocompatibility, self-healing, degradability	[223]
PC15 + PN15	Acylhydrazone	Thermo-responsiveness, self-healing	[224]
PC18 + PN9/PN15	Acylhydrazone	Thermo-responsiveness, biocompatibility, self-healing, light emission; drug delivery application	[225-227]
PC19 + PN15	Acylhydrazone	Thermo-responsiveness, self-healing, light emission	[228]
PC10 + PN16	Acylhydrazone	Self-healing, biocompatibility	[229]
PC20/PC5+ PN14	Alkylhydrazone	stress relaxation	[230]
PC21 + PN17	Acylhydrazone	pH-Responsiveness, degradability	[231]
PC22 + PN18	Acylhydrazone	Injectability, thermo-responsiveness, pH-responsiveness, degradability, cell adhesion	[232]
PC23 + PN15	Acylhydrazone	Self-healing and antimicrobial properties	[233]

Note: [a] The network compositions were made up of polymers with the same chemical structures, and the actual monomer fractions and polymer weights may vary.

As shown in **Table 2.5**, hydrogels based on reversible C=N bonds can be crosslinked between polymers or between polymer and small molecule, they can also be prepared from functional polymers and nanoparticles since they all can be modified. Zeng and coworkers reported a nanocomposite hydrogel based on C=N bonds from the PC24 (**Figure 2.28**) and amine-modified silica nanoparticles (**Figure 2.30a**).[234] Hoare et al. used hydrazide functionalized poly(oligo ethylene glycol methacrylate) (POEGMA) and aldehyde-functionalized cellulose nanocrystals (CNCs) to prepare an acylhydrazone crosslinked hydrogel (**Figure 2.30 b**).[235] Thus, C=N bonds crosslinked hydrogels were available with a remarkably abundant source of precursors.

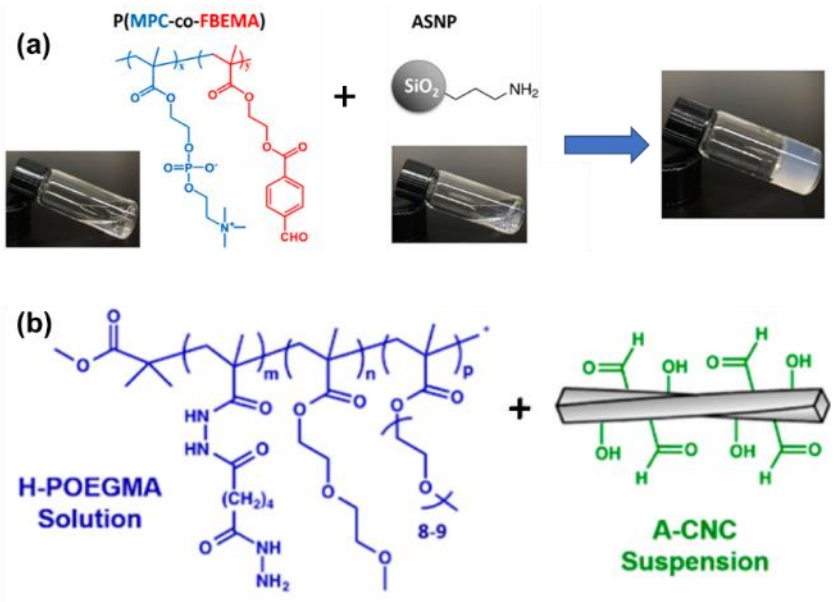

Figure 2.30. The C=N bonds crosslinked hydrogels prepared from polymers and (a) silica nanoparticles,[234] and (b) cellulose nanocrystals.[235]

It is worthwhile mentioning that aldehyde groups can not only be introduced into polymer precursors for direct utilization, but can also be generated in situ from other functional moieties on polymers, and

further used to react with nucleophilic reagents to build gel networks. For example, the 2-nitrobenzyl alcohol is photoreactive and can form 2-nitrosobenzaldehyde when exposed to UV-visible light (365-405 nm). Anseth and coworkers used this in situ photogenerated aldehyde and its reaction with alkylhydrazine to prepare an alkylhydrazone crosslinked PEG hydrogel (**Figure 2.31**).[236] The four-arm PEG end-capped with 2-nitrobenzyl alcohol moieties was used as photoresponsive compound to form aldehydes in situ, which were then captured by an alkylhydrazine-functionalized four-arm PEG to form alkylhydrazone crosslinked networks. The gelation kinetics and final moduli of the hydrogel can be readily controlled by the light intensity and exposure time. Based on a similar photo liberation mechanism, DeForest et al. synthesized a 8-arm telechelic PEG precursors modified with 2-(2-nitrophenyl)propoxycarbonyl-photocaged alkoxylamines, which can release alkoxylamines under near UV irradiation and then react with a benzaldehyde terminated 8-arm PEG (same structure as PC20 in **Figure 2.28**) to produce oxime crosslinked hydrogels.[237] The aldehyde group can also be generated in situ from a furan precursor using a photosensitizer (such as methylene blue) under red light (625 nm, I = 20 mW/cm^2). Truong et al. exploited this property and synthesized a four-arm PEG capped by furans that could generate aldehydes under red light irradiation and further react with another hydroxylamine-terminated four-arm PEG (same structure as PN8 in **Figure 2.29**) to yield oxime crosslinked hydrogels.[238] Like other biocompatible PEG hydrogels, the obtained alkylhydrazone and oxime hydrogels also can be used as cell culture matrices.[236-238]

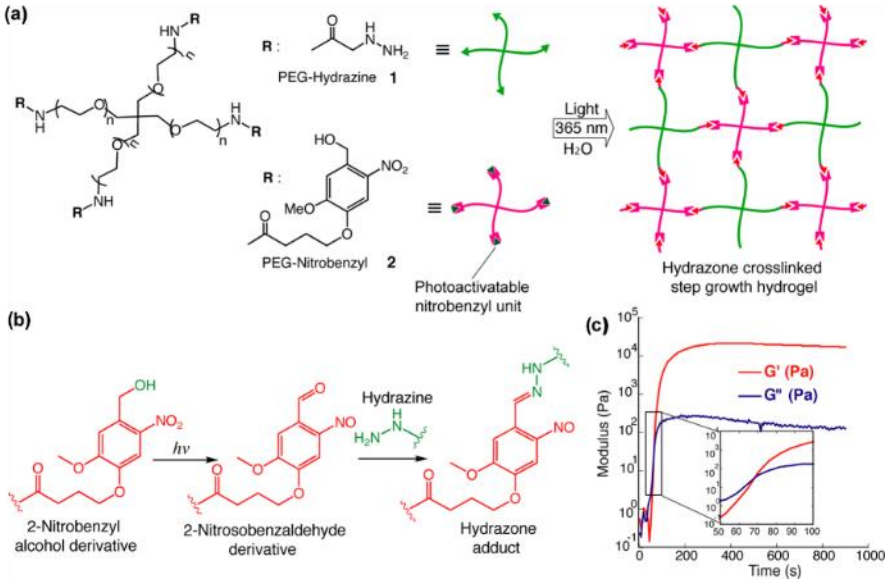

Figure 2.31. (a) Photo-driven formation of PEG hydrogels based on alkylhydrazone bonds. (b) The formation of 2-nitrosobenzylaldehyde is photoinduced from 2-nitrobenzyl alcohol and the aldehyde is immediately trapped by alkylhydrazine to form the alkylhydrazone bond. (c) Oscillatory time sweeps for the formation of hydrogels from solutions containing both precursors under UV light.[236]

It can be seen that the reported methods for constructing SCN hydrogels based on reversible C=N bonds generally start with carbonyl- or amino-modified macromolecules as precursors. Michálek et al. synthesized acylhydrazone pre-crosslinked bis-methacrylate monomers as crosslinkers with N-(2-hydroxypropyl)methacrylamide (HPMA) for copolymerization to form acylhydrazone crosslinked SCN structures (**Figure 2.32**).[239] The synthesized SCN hydrogels exhibited the degradability conferred by the pH-sensitive acylhydrazone. This suggests that reversible C=N hydrogels can also be synthesized by pre-forming C=N bonds in monomers, followed by polymerization.

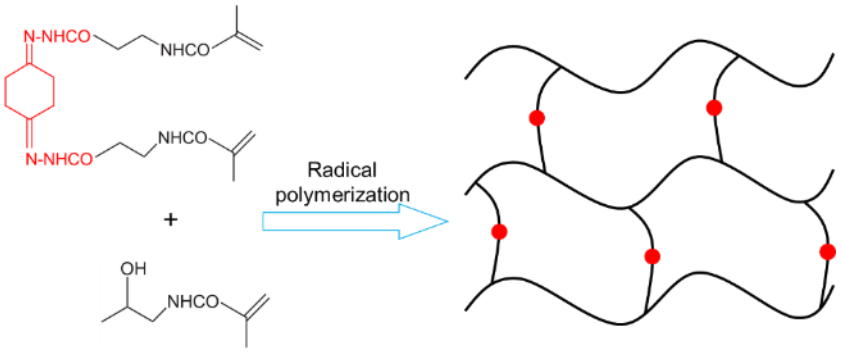

Figure 2.32. Schematic representation of the formation of SCN hydrogels from acylhydrazone crosslinkers.[239]

2.5.2. DCN hydrogels

As described previously, the 3D structure of DCN is a single network involving two types of crosslinks between polymer chains, at least one of the crosslinks is caused by dynamic bonds. Therefore, one type of crosslink in DCN hydrogels could be based on M(II)-Tpy or reversible C=N bond, while the other type would be based another static covalent bond or dynamic bond. This section will discuss the DCN hydrogels composed of either M(II)-Tpy or reversible C=N bond with a static covalent bond, and then switch to either M(II)-Tpy or reversible C=N bond with other types of dynamic bond.

2.5.2.1. DCN based on metal-terpyridine coordination bonds

The utilization of static covalent bond as a crosslink with M(II)-Tpy to form DCN hydrogels is perhaps one of the easiest approaches to achieve because the stability and insensitivity of static covalent bonding may not readily affect the formation of M(II)-Tpy. Zhou and coworkers used two routes to introduce Ru(II)-Tpy bis-complexes into a covalently crosslinked poly(N-Isopropylacrylamide) (PNIPAAm) SCN hydrogel (**Figure 2.33**).[240] Although the Ru^{2+}-Tpy they used did not work as the crosslinking in the gel network, it showed the potential of

such metal-ligand bonds to construct DCN hydrogels together with covalent bonds. The two synthetic routes they used also demonstrate the feasibility of M(II)-Tpy bis-complexes as crosslinkers to be pre-formed in the monomer and then incorporated into the polymer network by polymerization.

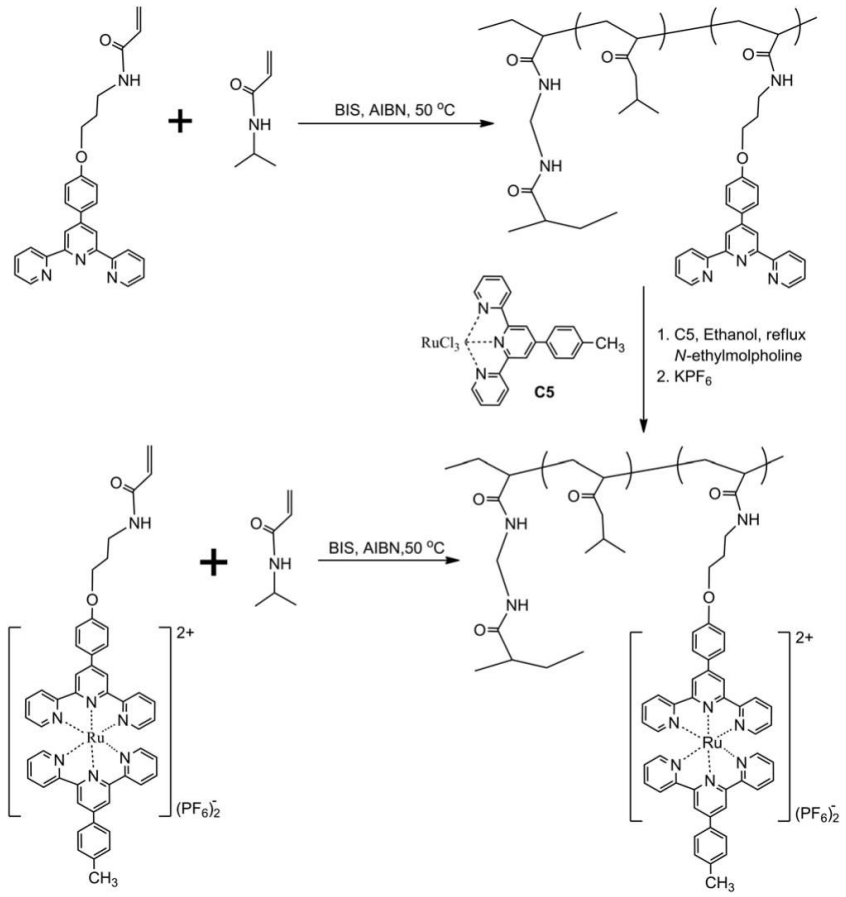

Figure 2.33. The two synthetic routes for Ru^{2+}-Tpy functionalized hydrogels.[240]

Seiffert' group has developed a series of DCN hydrogels by using four-arm PEG based on the orthogonal combination of M(II)-Tpy and static covalent bonds.[80, 81, 150, 241] For example, they synthesized both azide and Tpy functionalized linear PEG, which can be covalently crosslinked by the cyclooctene end-capped four-arm PEG by strain-

promoted azide-alkyne cycloaddition (**Figure 2.34a**).[150] The addition of metal(II) ions then leads to the generation of DCN hydrogels with both static covalent and M(II)-Tpy crosslinks. Such M^{2+}-Tpy DCN allows the dynamic M(II)-Tpy crosslinks to break first for dissipating the strain energy under large deformation, and increase thus the toughness of the hydrogel. Oscillation frequency sweeps on pure covalent SCN hydrogels show a purely elastic response of G', which was independent of frequency and greater than G" (**Figure 2.34b**). The Zn^{2+}-Tpy crosslinked DCN hydrogel, by contrast, shows larger viscous modulus and the frequency at the peak of G"(ω) matches the measured dissociation rate constant of Zn^{2+}-Tpy (k_{diss}) (**Figure 2.34c**). In addition, they show that the plateau modulus (G'_p) of DCN hydrogels was approximately twice higher than that of covalent SCN hydrogels. Their work has demonstrated that the DCN topology not only preserves the dynamics of Zn^{2+}-Tpy but also allows for an increase in the elastic modulus of the hydrogel by at least a factor of two.

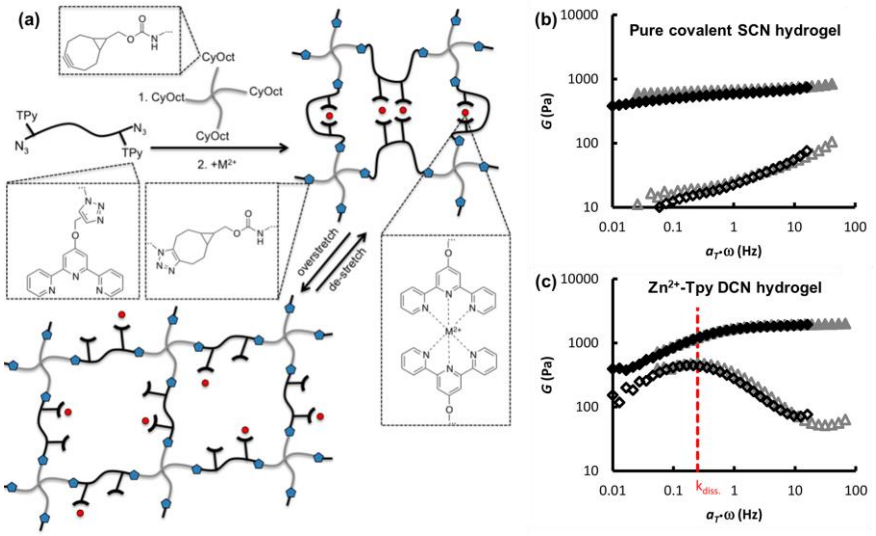

Figure 2.34. (a) Schematic representation of the formation of DCN hydrogels based on M(II)-Tpy and static covalent bonds and the topological crosslinking changes upon overstretching. Oscillatory frequency sweeps on (b) only static covalent bonding crosslinked pure covalent SCN hydrogel, and (c) both Zn^{2+}-Tpy and static covalent bonding crosslinked DCN hydrogel.[150]

Another DCN hydrogel system consisting of M(II)-Tpy and static covalent bonds was reported by Xu et al.[242] They used Tpy-modified PiPOx polymer (**Table 2.4**) to first prepare covalently crosslinked SCN hydrogels by reaction with azelaic acid (nonanedioic acid). Subsequently, DCN hydrogels crosslinked by covalent bonds and M(II)-Tpy were obtained by swelling the covalent SCN hydrogel in different aqueous solutions of divalent transition metal ions (**Figure 2.35a**). DCN hydrogels formed from strong binding metal ions (e.g. Fe^{2+}, Ni^{2+} and Co^{2+}) have lower mechanical stability and higher brittleness than the covalent SCN hydrogel. The authors attribute this to the higher thermodynamic and kinetic stability of the corresponding complexes, leading to kinetically trapped monocomplexes and ineffective intramolecular crosslinking. Different from other M^{2+}-Tpy DCN hydrogels, the Zn^{2+}-Tpy DCN hydrogel was found to have excellent mechanical properties (maximum compression strength: 9 MPa, toughness: 99 MJ/m^3) and excellent self-recoverability due to the dynamic nature of Zn^{2+}-Tpy. This suggests that due to the fast kinetics of Zn^{2+}-Tpy, DCN containing Zn^{2+}-Tpy has the opportunity to achieve higher toughness than other M(II)-Tpy crosslinked DCNs.

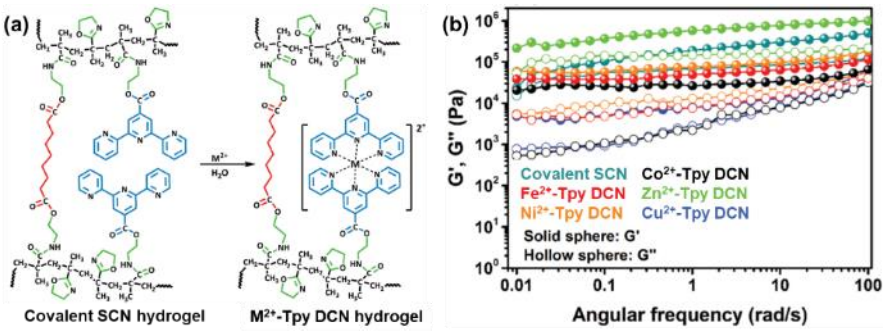

Figure 2.35. (a) Schematic representation of the formation of DCN hydrogels by swelling the covalent SCN hydrogel in a solution of metal(II) ion. (b) Oscillatory frequency sweeps on the SCN and DCN hydrogels.[242]

Es Sayed and co-workers synthesized covalent SCN microgels with free Tpy entities on the networks (MG-Tpy) by dispersion

copolymerization of Tpy end-capped PEG monomethacrylate (PEGMA-Tpy), N-isopropylacrylamide (NIPAM) and the covalent crosslinker N,N'-methylenebisacrylamide (MBA).[243] Such microgels can then undergo macro-aggregation to form macrogels in water by forming Fe^{2+}-Tpy or Co^{2+}-Tpy crosslinked DCN in Fe^{2+} or Co^{2+} solution (**Figure 2.36**). The obtained Fe^{2+}-Tpy DCN macrogels can be further transferred into individual microgels by oxidizing Fe(II) to Fe(III) using potassium persulfate because the unstable Fe(III)-Tpy complexes disconnect the microgel particles.

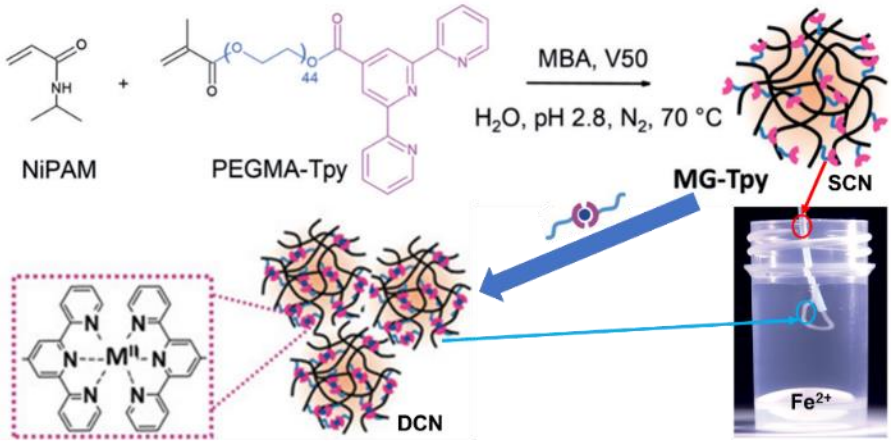

Figure 2.36. Schematic illustration of the synthesis of covalent SCN microgels containing Tpy and further macroscopic aggregation into DCN macrogels in water in the presence of Fe^{2+}.[243]

Another effective strategy to construct M(II)-Tpy DCN hydrogels was by combining this type of bond with other kinds of supramolecular interactions (e.g., hydrogen bonds and hydrophobic interactions) as dual-crosslinking. Seiffert and coworkers developed a strategy to construct DCN hydrogels on the basis of M(II)-Tpy and hydrogen bonding.[244] They used partially azidized linear polyglycerol, which can react with alkyne-functionalized diaminotriazines, cyanurates, and terpyridines via strain-promoted azide-alkyne cycloaddition to yield water-soluble polymers functionalized with multipoint H-bond arrays and terpyridine ligands. They thus obtained linear polyglycerols modified with either diaminotriazine and terpyridine or with cyanurate and terpyridine on the side chain. After mixing aqueous solutions of both functional polymers and the addition of Fe^{2+}, DCN hydrogels with hydrogen bonds (multipoint hydrogen-bonded arrays between the cyanurate and diaminotriazine moieties) and Fe^{2+}-Tpy bonds (bis-complexes between Fe and two terpyridine moieties) were formed (**Figure 2.37**). The stimulus responsiveness of hydrogen bonding and metal-ligand bonds allows this DCN hydrogel to respond to a wide range of stimuli. For example, the addition of acetic acid can disrupt the hydrogen-bonded network within hours without affecting the Fe^{2+}-Tpy network, and the addition of EDTA/H_2O_2 can degrade the terpyridine-based network on a similar time scale without affecting the hydrogen-bonded network. The dual crosslinked network, however, can be degraded by sulfuric acid within a few minutes. These results are interesting because they show that the properties of the two dynamic bonds used to crosslink DCN hydrogels can be modulated separately without affecting the other bond. This allows the hydrogel to display multi-stimuli responsiveness by giving the DCN the responsiveness of each of the two bonds themselves. Because it is dual dynamically crosslinked, the complete degradation of the gel can be achieved by breaking both bonds together under a certain set of conditions. These properties are not easily obtained in static covalent DCN or in DCN containing with only one type of dynamic bond.

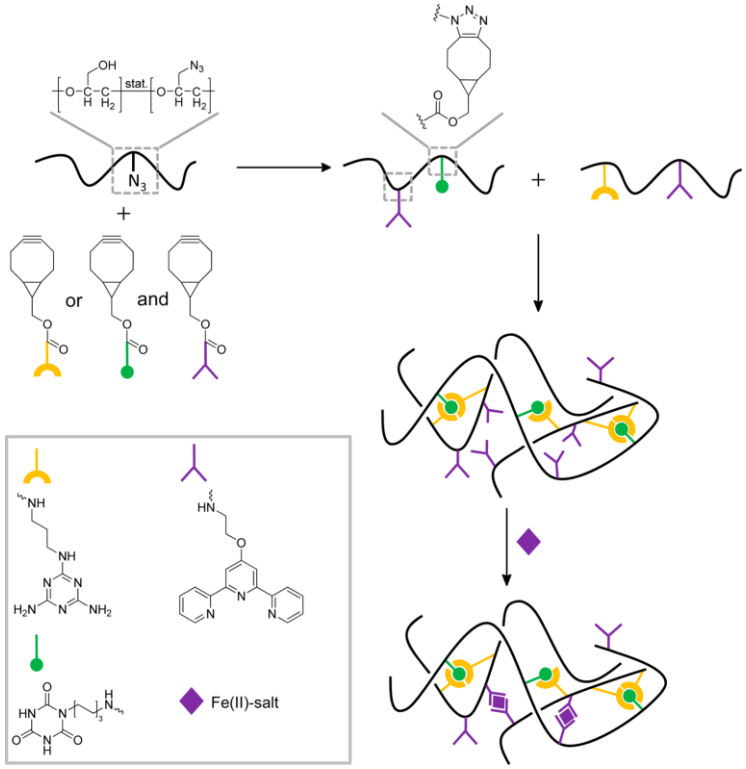

Figure 2.37. Schematic illustration of the preparation of functional copolymers for fabricating DCN hydrogels based on hydrogen bonds and Fe^{2+}-Tpy bonds.[244]

Polymers modified by Tpy on the main chain can also be used for the synthesis of DCN hydrogels. Our group developed a series of DCN-like hydrogels based on the orthogonal combination of hydrophobic and coordinative interactions to tune the rheological properties and responsiveness of hydrogels.[245-253] Those studies involve Tpy end-capped amphiphilic diblock copolymers that were able to form micellar DCN-like hydrogels in the presence of metal ions in semi-dilute or concentrated aqueous solutions. These DCN-like hydrogels were obtained by a two-step process. First, the block copolymers self-assemble in an aqueous solution by hydrophobic interactions to form micelles bearing ligands at the surface. Subsequently, the added transition metal ions lead to hydrogels by forming M(II)-Tpy bis-complexes as crosslinks between micelles. For example, Brassinne et

al. reported a class of hydrogels with the combination of hydrophobic interactions and coordinative bonds through the synthesis of Tpy end-functionalized polystyrene-block-poly-(N-isopropylacrylamide) block copolymers (PS-b-PNIPAAm-tpy).[248] These amphiphilic block copolymers were found to be easily dispersible to water at low temperature and give rise to opalescent micellar solutions (**Figure 2.38**). Subsequently, the addition of metal ions leads to the formation of crosslinked gel networks by the formation of terpyridine bis-complexes. These reported studies have focused on micelles with a PS core. Such hydrophobic polymers are known to form frozen micelles in aqueous solutions. As a result, the viscoelastic response of the obtained DCN-like hydrogels depends not only on the type of metal ion but also on the hydrophobic chain segment length of the diblock copolymer.

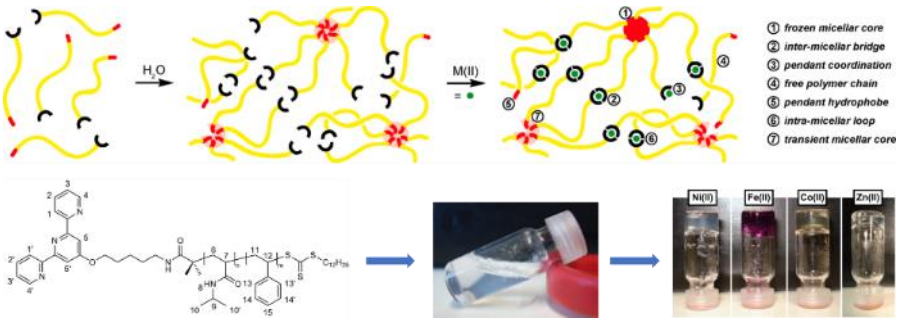

Figure 2.38. Schematic illustration of the preparation of micellar DCN-like hydrogels based on hydrophobic interactions and Fe^{2+}-Tpy bonds.[248]

Unlike the works of Brassinne et al., Piogé and coworkers reported that copolymer micelles functionalized with terpyridine groups can be formed from thermally responsive block copolymers.[254] They prepared well-defined poly(N,N-dimethylacrylamide)-b-poly(N-isopropylacrylamide-*co*-2-vinyl-4,4-dimethyl-azlactone) (Tpy-PDMA-*b*-P(NIPAM-*co*-VDM)) thermo-responsive double hydrophilic block copolymers bearing a terpyridine at one chain end by sequential reversible addition fragmentation chain transfer (RAFT)

polymerization. Due to the LCST-type thermosensitive block, the metal-terpyridine bis-complexes of the block copolymers can self-assemble in concentrated aqueous solution at a temperature above the LCST to form both Fe^{2+}-Tpy and micelle crosslinked DCN-like hydrogels (**Figure 2.39**). Based on the same crosslinking mechanism, the same group subsequently reported similar DCN-like hydrogels via thermo-induced micellar aggregation of M(II)-Tpy bis-complexes from poly(N,N-dimethylacrylamide)-b-poly(N-isopropylacrylamide) (Tpy-PDMA-*b*-PNIPAM).[255] Thermo-rheological experiments show that the thermally reversible sol-gel transition temperature across the LCST was about 34°C, which indicates the formation of a frozen percolating 3D network ensured by the aggregation of PNIPAM blocks. This also validates the important crosslinking role of micelles in DCN formation.

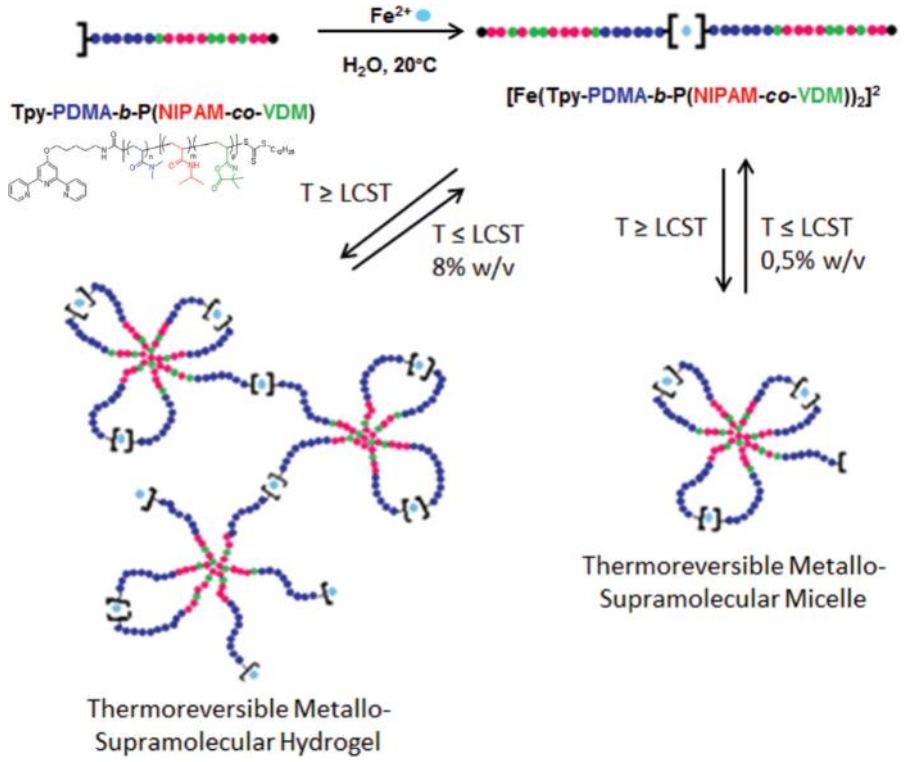

Figure 2.39. Schematic representation of reversible metallo-terpyridine copolymer micelles and hydrogels elaborated from Tpy-PDMA-b-P(NIPAM-*co*-VDM) in the diluted (0.5% w/v) and concentrated regimes (8% w/v), respectively.[254]

2.5.2.2. DCN based on reversible C=N bonds

As discussed previously, hydrogels based on reversible C=N bonded biopolymers are the most studied systems due to the large distribution of carbonyl or amino groups in natural macromolecules and the ease of modification with acyl hydrazide or hydroxylamine groups. Therefore, the currently reported DCN hydrogels based on C=N bonds are mainly focused on hydrogel systems using biopolymers.

Similar to the previously discussed DCN hydrogels based on metal-terpyridine coordination bonds, DCN hydrogels crosslinked by both reversible C=N bonds and static bonds also exhibit properties superior to those of SCN hydrogels. Mo et al. reported a series of injectable DCN hydrogels based on the aldehyde methacrylate sodium alginate (AMSA) and amino gelatin (AG) using both imine bonds and static covalent bonds as crosslinks.[256] The AMSA was synthesized by the reaction of oxidized alginate with 2-aminoethyl methacrylate through EDC/NHS coupling reaction. By mixing the aqueous solution of AMSA and AG, a primary network of imine crosslinking was formed rapidly (120 s) between the amino groups of AG and the aldehyde groups of AMSA, followed by a radical reaction of the methacrylate groups in AMSA triggered by a 365 nm irradiation (15 min) to generate the secondary network (**Figure 2.40**). Compared to the imine crosslinked SCN hydrogels, both imine and covalently crosslinked DCN hydrogels exhibited higher crosslinking density, enhanced mechanical properties, lower swelling ratio, and lower degradation rate. In addition, the in vitro cytotoxicity activity of cells on the hydrogels surface tests showed that the DCN hydrogels were more suitable for tissue repair.

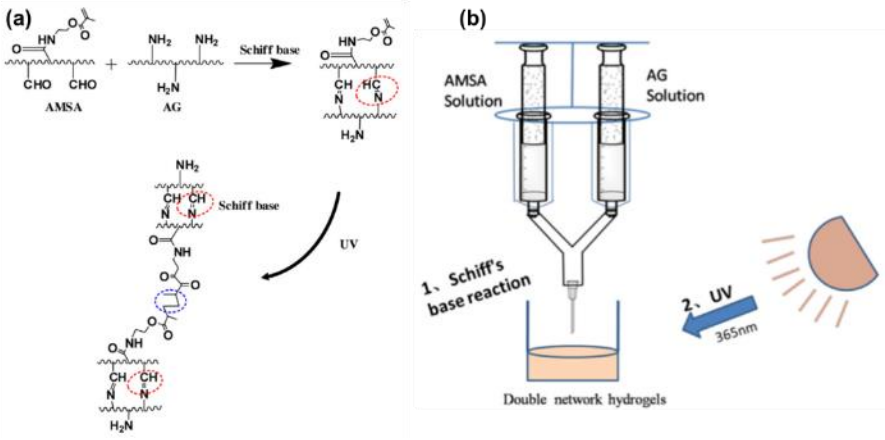

Figure 2.40. Schematic representation of (a) the formation of DCN hydrogels, and (b) the preparation procedure of such hydrogels.[256]

Similarly, Wang and Lee et al. prepared a series of imine bonds and static covalent bonds crosslinked DCN hydrogels.[257] Two biocompatible building blocks: a quaternized methacryloyl chitosan (QMC) and a four-arm benzaldehyde-terminated PEG (BPEG) were employed (**Figure 2.41**). The DCN hydrogels were formed by mixing the QMC solution with the BPEG solution to first form the imine bonds, followed by the photo-induced crosslinking of methacrylate bonds. The DCN hydrogels have enhanced mechanical properties (tensile modulus: 157.4 kPa) compared to SCN hydrogels crosslinked with only imine bonds. The free quaternary ammonium and protonated amino groups on the DCN structure provided excellent antimicrobial performance to the hydrogel. The residual aldehyde groups in the hydrogel matrix can form reversible C=N bonds with the amino groups on tissue surface to improve the adhesion of the hydrogel to biological tissues. In addition, hydrogels have demonstrated biocompatibility and self-healing ability, which combined with the desirable mechanical properties and antimicrobial capacity demonstrating an application for enhanced healing of infected wounds.

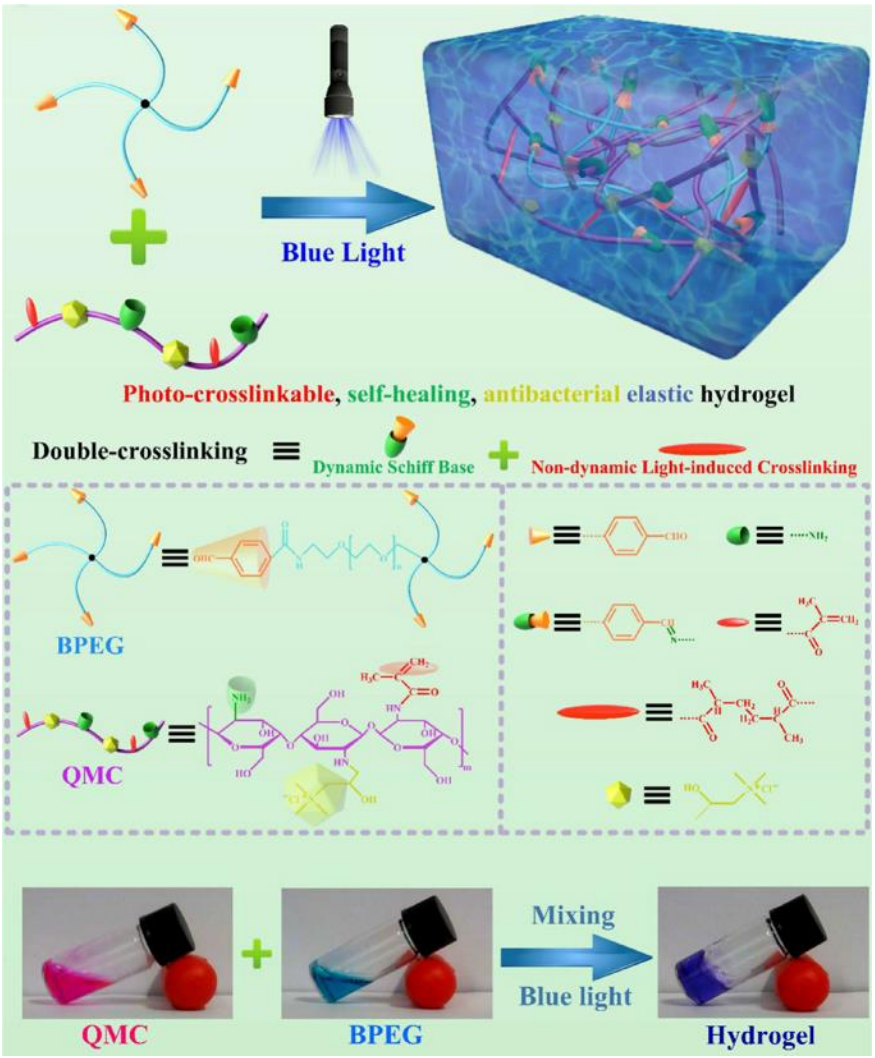

Figure 2.41. Schematic representation for the formation of DCN hydrogels based on imine bonds and static C=C bonds.[257]

Combining the reversible C=N bonds with alternative dynamic covalent bonds was another good strategy for the preparation of DCN hydrogels. Among these, the introduction of disulfide bonds together with acylhydrazone bonds is probably the easiest orthogonal combination to obtain.[54, 94, 220, 221, 216] Otto and Rodriguez-Docampo demonstrated in 2008 that hydrazone and disulfide bonds were

compatible with each other in one system and can be selectively activated or deactivated depending on pH.[258] In particular, commercially available dithiodipropionic acid dihydrazide is easily synthesized and often used as crosslinkers directly or after modification to react with multi-carbonyl functionalized polymers to generate both acylhydrazone and disulfide DCN hydrogels.[54, 220, 221, 216, 259-262] The embedded disulfide bonds in the crosslinkers can also serve as dynamic covalent crosslinks in 3D networks to impart further stimulus responsiveness to the hydrogel. Deng and co-workers firstly introduced this crosslinker to react with a three-arm benzaldehyde-capped PEG to synthesize both acylhydrazone and disulfide bonds crosslinked DCN hydrogels (**Figure 2.42a**).[54] Since the dynamics of hydrogels were dominated by acylhydrazone exchange under acidic conditions and disulfide bond exchange under alkaline conditions, the hydrogels exhibit viscous response in the low-frequency region (**Figure 2.42b**) and can achieve self-healing (**Figure 2.42c**) under either acidic or alkaline environments. However, the added catalytic aniline during the preparation process can accelerate the acylhydrazone exchange reaction and thus promote the self-healing of the hydrogel under neutral conditions. Besides, due to the redox-responsiveness of the disulfide bonds, the hydrogels also shown reversible gel-sol transitions triggered by 1,4-dithiothreitol (DTT) and H_2O_2. This suggests that the introduction of disulfide bonds into DCNs containing reversible C=N bonds not only preserves the intrinsic stimuli-responsiveness of the C=N bond, but also confers additional redox-responsiveness on the hydrogel. More prominently, the introduction of disulfide bonds extends the pH range where self-healing occurs, which suits a wider range of application conditions. This again confirms the advantages of dual dynamic crosslinking compared to single dynamic crosslinking.

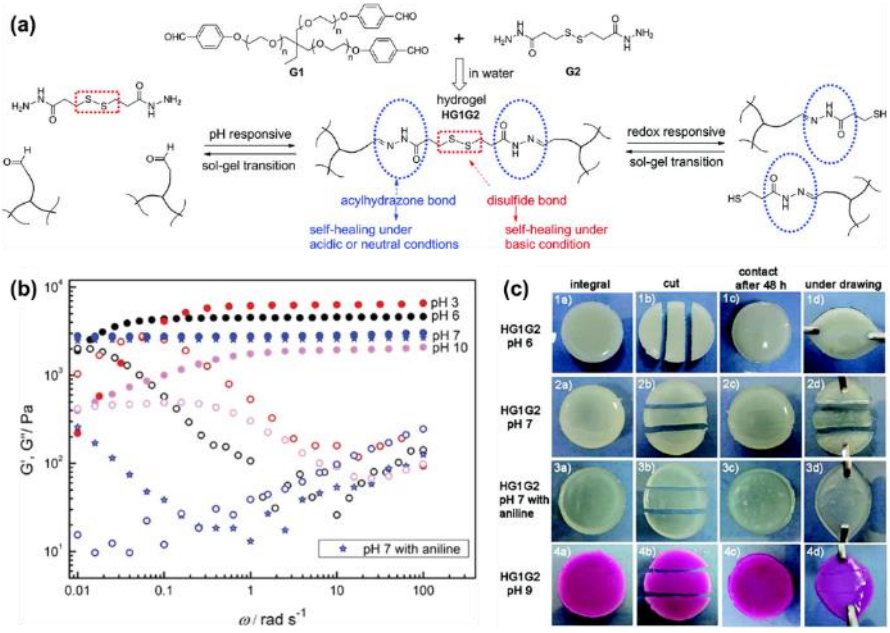

Figure 2.42. (a) Formation of DCN hydrogels from three-arm PEG end-capped with benzaldehyde groups and dithiodipropionic acid dihydrazide. (b) Oscillatory frequency sweeps on DCN hydrogels at different pH. (c) Self-healing ability of DCN hydrogels at different pH.[54]

In addition to the common method described above for introducing disulfide crosslinkers into reversible C=N bond-based DCN, disulfide bonds can also be created by the reaction of thiols within C=N crosslinked networks. Zhou and coworkers showed that cysteamine hydrochloride (Cys) can also be used as a crosslinker to prepare imine crosslinked hydrogels.[263] The aldehyde groups on the oxidized hyaluronic acid can readily react with the amino groups at both ends of Cys to result in a gel network crosslinked by imine bonds. The obtained hydrogels showed pH responsiveness, injectability and excellent self-healing ability (100% recovery within 10 min). Although the function of the disulfide bonds embedded in the network was not discussed in the paper, the Cys as crosslinker was certainly another option for constructing both imine and disulfide crosslinked DCN hydrogel networks. In addition, Zhao et al. reported a DCN hydrogel prepared

from the cysteine modified poly(amido-amine) dendrimers (Gn-PAMAM-NH_2-X, n and X represent the generation of PAMAM and the proportion of -NH_2 at the periphery of the Gn-PAMAM-NH_2-X respectively) and oxidized dextrans (ODex) (**Figure 2.43**).[264] The disulfide bond crosslinks were formed automatically by the reaction of thiols with cysteine-rich subdomains of the Gn-PAMAM-NH_2-X. The imine crosslinked network was then created between the amine groups of the Gn-PAMAM-NH_2-X and the aldehydes of the ODex. These DCN hydrogels exhibit injectability, adhesion, and biocompatibility.

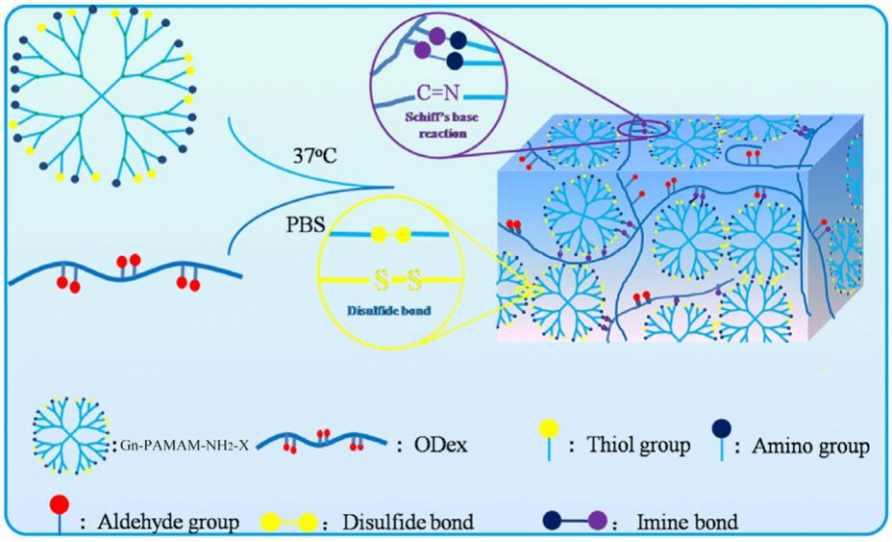

Figure 2.43. Schematic representation for the formation of DCN hydrogels based on imine bonds and disulfide bonds.[264]

Reversible C=N bonds with boronic/borate ester bonds is another common combination for the preparation of DCN hydrogels. As early as 2004, Jayakrishnan et al. reported that periodate oxidized alginate (alginate dialdehyde) and gelatin undergo self-crosslinking in the presence of borax to form hydrogels.[265] As shown in **Figure 2.44**, the hydrogel was established as a result of DCN formation due to the creation of imine bonds between gelatin and alginate dialdehyde and the formation of boronic ester bonds between alginate dialdehyde and

borax. These hydrogels were injectable, biocompatible and biodegradable.[266] Furthermore, the authors showed that these hydrogels can adhere well with the cartilage tissue.[267] Subsequently, Pettignano et al. showed that DCN hydrogels prepared from these precursors have self-healing properties.[268] They found that pH has an important effect on the reconstruction of the damaged hydrogel interface, confirming that imine bonds play a fundamental role in the repair process of DCN hydrogels.

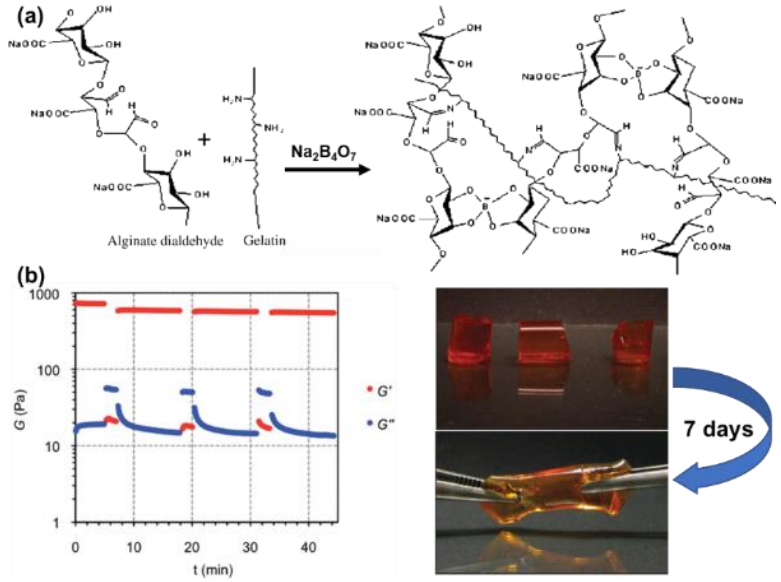

Figure 2.44. (a) The formation of DCN hydrogels based on imine and boronic ester bonds.[265] (b) The self-healing properties of such DCN hydrogels.[268]

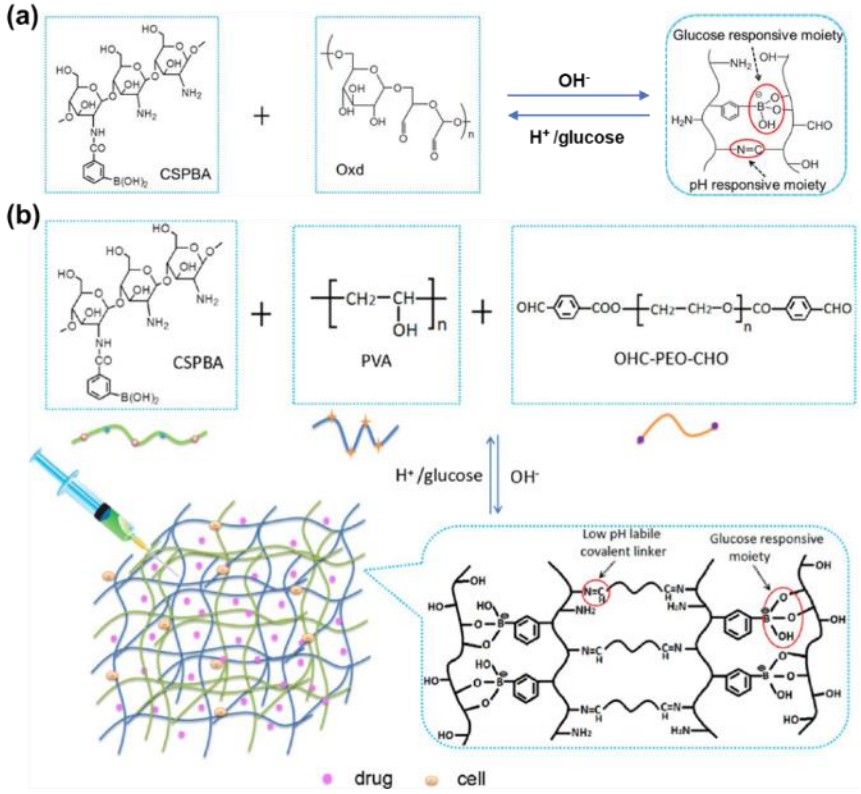

Figure 2.45. The formation of DCN hydrogels based on imine and boronic ester bonds from phenylboronic modified chitosan with (a) oxidized dextran,[269] (b) polyvinyl alcohol and benzaldehyde terminated linear PEG.[270]

In the previous example, borate ester bonds were formed by the addition of a crosslinker (borax). However, this type of bond can also be generated in-situ by the direct reaction between functionalized macromolecules without the addition of external crosslinkers. Zhao et al. proposed phenylboronic modified chitosan and oxidized dextran to prepare injectable DCN hydrogels based on crosslinking of imine and borate ester bonds (**Figure 2.45a**).[269] Due to the pH sensitivity of imine bonds and to the fact that borate ester bonds can be dissociated using another competitive diol (such as glucose), these DCN hydrogels have pH- and glucose-triggered drug release capabilities. Hydrogels also exhibited good biocompatibility and can be used to culture and

proliferate cells. Based on the same crosslinking mechanism, the same team also reported that phenylboronic modified chitosan together with polyvinyl alcohol and benzaldehyde terminated linear PEG can form both borate ester and imine bonded DCN hydrogels (**Figure 2.45b**). The obtained DCN hydrogels also showed pH/glucose triggered release of protein drugs and live cells and demonstrated self-healing properties. DCN hydrogels crosslinked with both borate ester bonds and reversible C=N bonds show once again that two dynamic bonds can retain their respective stimuli-responsiveness when incorporated in a DCN.

Another DCN hydrogel crosslinked by imine and borate ester bonds was proposed by Tao et al. using multifunctional PEG (MF-PEG) with both benzaldehyde groups and phenylboronic acid groups at the two ends of the linear chain.[271] The MF-PEG as a polymeric crosslinker can form DCN hydrogels within seconds by creating imine bonds with glycol chitosan (GC) and borate ester bonds with polyvinyl alcohol (PVA) (**Figure 2.46**). By adjusting the concentration of GC and PVA, the ratio of crosslinking types can be easily adjusted (Gel 2 ~ Gel 5 in **Figure 2.46**). For example, SCN hydrogels crosslinked by single borate ester or imine bonds can be obtained by selectively adding only PVA or GC to the MF-PEG, respectively. Due to the different formation kinetics and thermodynamic stability of borate ester and imine bonds, the borate ester crosslinked SCN (Gel 1 in **Figure 2.46**) has a shorter gelation time and weaker mechanical strength than the imine crosslinked SCN (Gel 6 in **Figure 2.46**) (**Figures 2.46b** and **2.46c**). The gelation time and mechanical properties of DCN hydrogels can hence be adjusted by varying GC/PVA. Compared to the two SCN hydrogels, these DCN hydrogels have enhanced strength and mucosal adhesion capacity. These DCN hydrogels also have self-healing properties, biocompatibility and biosafety, and can be used as injectable drug carriers.

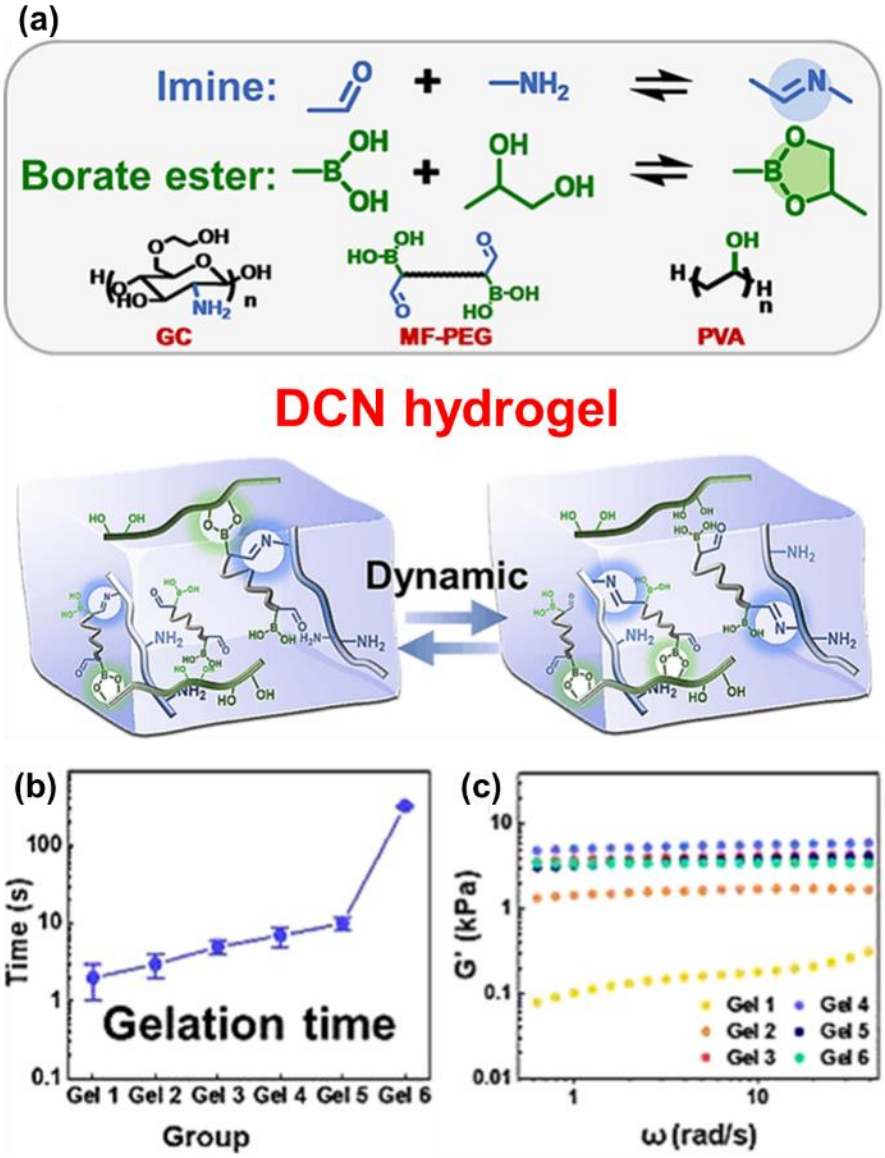

Figure 2.46. (a) Schematic representation for the formation of DCN hydrogels based on imine and borate ester bonds from the MF-PEG with GC/PVA. Gelation time (b) and frequency sweeps (c) on hydrogels varying the ratio of GC/PVA.[271]

Tan and Chen et al. synthesized phenylboronic- and ketone-functionalized diblock copolymers P(N-isopropyl acrylamide-*co*-N-acryloyl-3-aminophenylboronic acid)-b-(N-isopropyl acrylamide-*co*-

diacetone acrylamide) (PAD) for both acylhydrazone and borate ester crosslinked DCN hydrogels.[272] As shown in **Figure 2.47a**, The addition of PVA was used for forming borate ester bonds with the PAD, and the adipic dihydrazide (ADH) was employed as crosslinker to react with the ketone groups of the PAD to form acylhydrazone crosslinked network. Based on the respective stimuli-responsiveness of these two dynamic bonds, DCN hydrogels showed pH-triggered (HCl/NEt_3) reversible gel-sol transition, and irreversible gel-to-sol transition due to the addition of an excess ADH or fructose. Interestingly, the more dynamic borate ester linkage endows the DCN hydrogel with fast gelation kinetics and self-healing ability, and the stable acylhydrazone linkage imparts hydrogel with enhanced mechanical properties. The single borate ester-crosslinked SCN hydrogel had a typical frequency-dependent behavior, and the acylhydrazone crosslinked SCN hydrogel showed almost frequency-independent behavior (**Figure 2.47b**). The DCN hydrogel also demonstrated frequency-dependent behavior, especially at low frequency. Compared to the two SCN hydrogels (33 kPa and 28 kPa), the DCN hydrogel (55 kPa) exhibited higher breaking stress (**Figure 2.47c**). These results suggest that the stress relaxation behavior of a DCN hydrogel constructed from two reversible bonds with different dynamics is primarily linked to the bond with the faster kinetics. The DCN has higher mechanical strength, but a limited deformability compared to one of the SCNs crosslinked by a single dynamic bond (as shown in **Figure 2.47c**, the rupture strain of DCN is between the two SCNs).

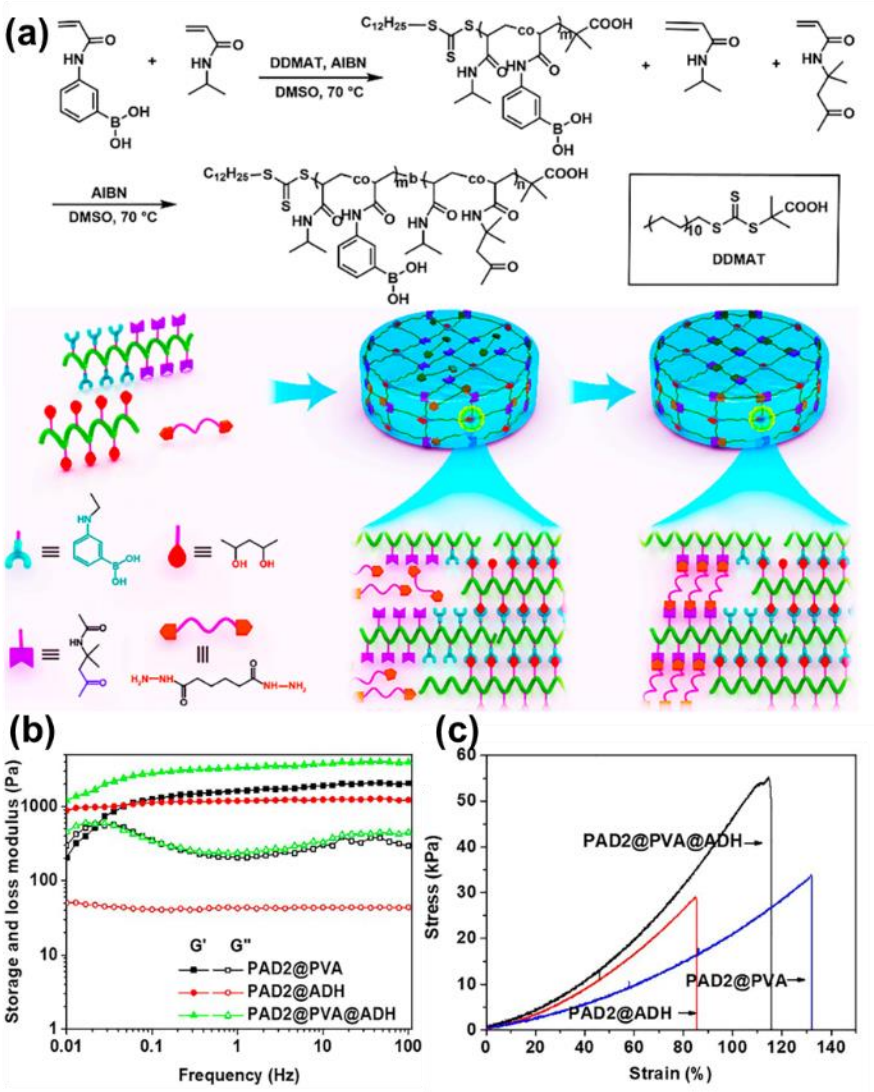

Figure 2.47. (a) Schematic representation for the formation of DCN hydrogels based on imine and borate ester bonds from the PAD with PVA/ADH. Oscillatory frequency sweeps (b) and tensile tests (c) on hydrogels of either imine or borate ester crosslinked SCN and both imine and borate ester crosslinked DCN.[272]

Very recently, Narain and coworkers synthesized a new type of imine crosslinked SCN hydrogel, boronic ester crosslinked SCN hydrogel and both imine and boronic ester crosslinked DCN hydrogel by mixing two poly(2-methacryloyloxyethyl phosphorylcholine) [poly(MPC)]-based functionalized polymers (**Figure 2.48a**).[273] The DCN and both SCN hydrogels demonstrated the frequency-dependent behavior of the dynamic hydrogels (**Figure 2.48b**). Compared to the two SCN hydrogels, DCN hydrogels have enhanced mechanical properties (**Figure 2.48c**). Due to the coexistence of stimuli-responsive imine and boronic ester in DCN hydrogel, the hydrogel showed pH-triggered (HCl/NaOH) reversible gel-sol transition, and exhibited responsiveness to sugar (fructose). As the benzoxaborolate complex could be oxidized and cleaved upon the addition of oxidants, the DCN hydrogels exhibited sensitive responsiveness to H_2O_2 using it as a typical model for reactive oxygen species (ROS). In addition, DCN hydrogels were self-healing and biocompatible and have the potential to be used as cell culture scaffolds.

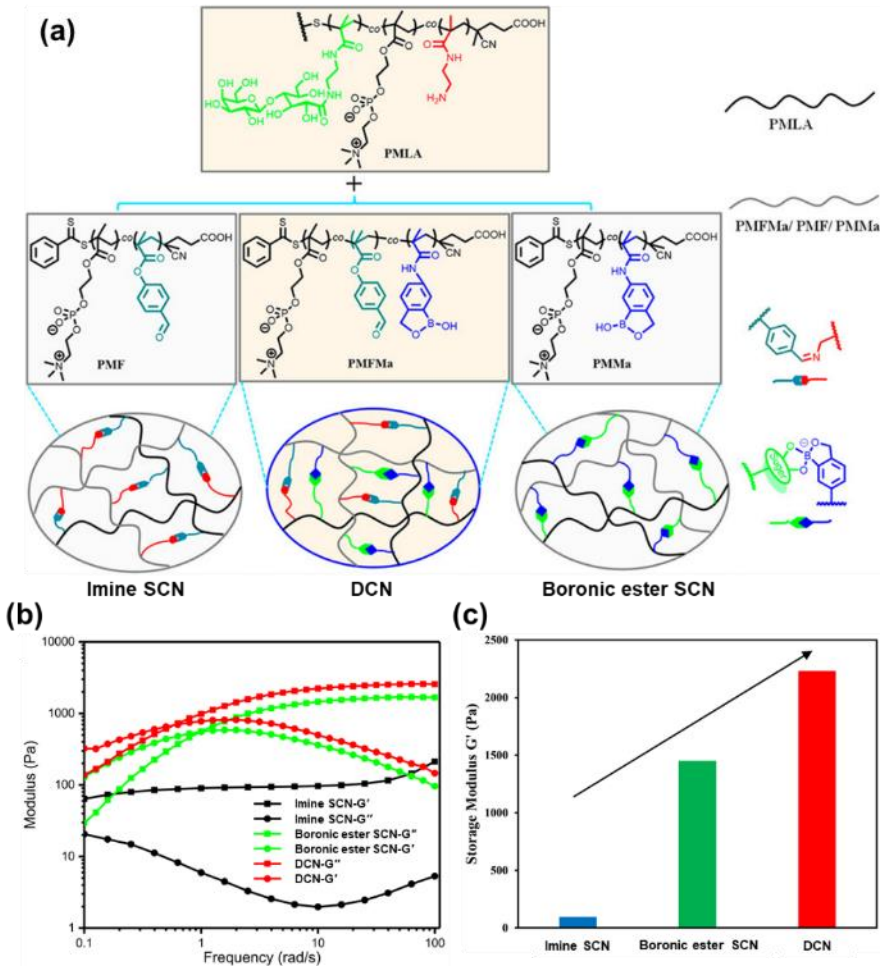

Figure 2.48. (a) Schematic representation for the formation of SCN and DCN hydrogels based on imine and borate ester bonds from two poly(MPC)-based polymers. (b) Oscillatory frequency sweeps on DCN and two SCN hydrogels. (c) The G′ values of hydrogels collected at a frequency of 10 rad/s.[273]

Wang et al. proposed a crosslinking strategy for DCN hydrogels by combining Diels-Alder (DA) adducts and imine bonds.[274] Here, N-(furfural)carboxymethyl chitosan (FCC) and oxidized dextran (ODex) were synthesized as precursors to react with dimaleimide-terminated telechelic PEG (Mal-PEG-Mal) (**Figure 2.49a**). The imine crosslinked SCN hydrogel was prepared from the FCC and ODex, while the DA crosslinked SCN hydrogel was prepared from the FCC and Mal-PEG-Mal. The swelling ratio of DCN was found to be higher than that of DA crosslinked SCN, but lower than that of imine crosslinked SCN hydrogel (**Figure 2.49b**). The authors suggested that the higher crosslinking density of DA SCN hydrogels than DCN hydrogels was due to the two-step crosslinking process of DCN. The first crosslinking step was the formation of imine bonds, which is fast (**Figure 2.49c**) and already leads to a gel. This limits thus the efficiency of the second step (DA reaction), and ultimately leads to a slight decrease in mechanical properties of DCN hydrogels compared to DA SCN hydrogels. These results suggest that the difference in the rate of formation of the two types of bonds in DCN can also have an effect on the crosslinking of the sub-networks. The first network formed by the faster bonds may affect the crosslinking efficiency of the slower bonds, thus affecting the mechanical properties of the final DCN gel. Therefore, in order to obtain the desired high mechanical strength, the difference in gelation time between the two dynamic networks should not be too large.

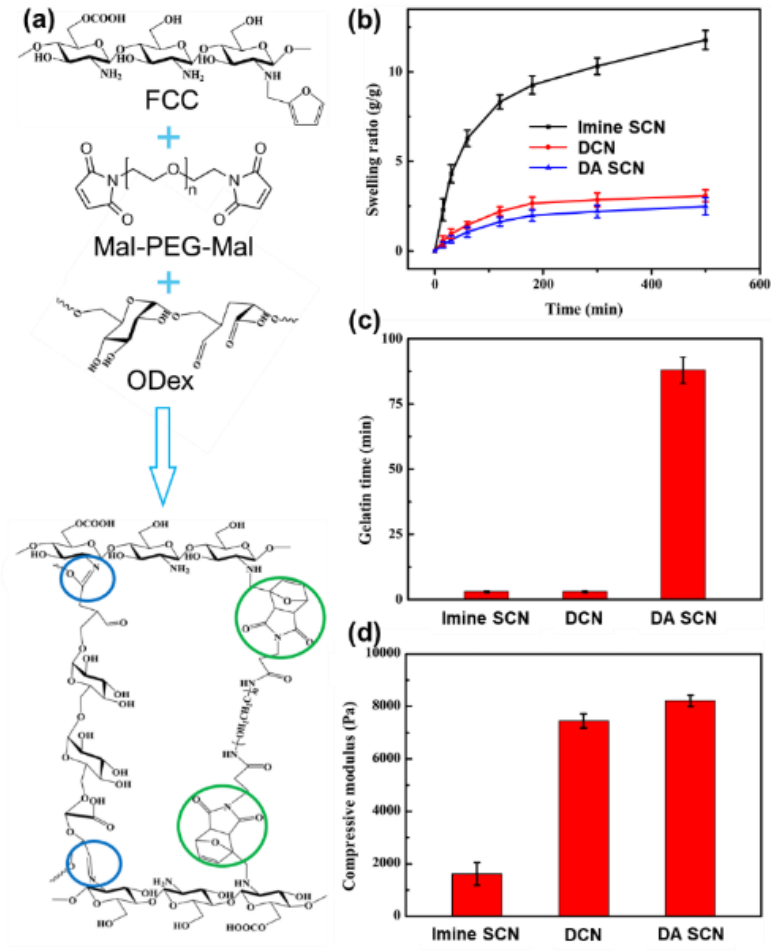

Figure 2.49. (a) The formation of DCN hydrogels based on imine bonds and DA reaction. Swelling curve (b), gelation time (c) and compressive modulus (d) of hydrogels.[274]

Wang et al. established a DCN hydrogel through the formation of catechol-catechol adducts as well as imine bonds.[275] The imine crosslinks were created between aldehyde groups in oxidized dextran-dopamine (OD-DA) and amino groups in chitosan quaternary ammonium salt (HTCC). The dopamine in OD-DA was readily oxidized to dopaquinone, which subsequently undergoes a reverse dismutation reaction with dopamine to generate semiquinone free

radicals and eventually produce the catechol-catechol adducts via coupling (**Figure 2.50a**). The obtained DCN hydrogels exhibited excellent mechanical strength, self-healing, adhesive and injectable properties. In addition, the authors developed an application of such DCN hydrogels for wound dressings (**Figure 2.50b**).

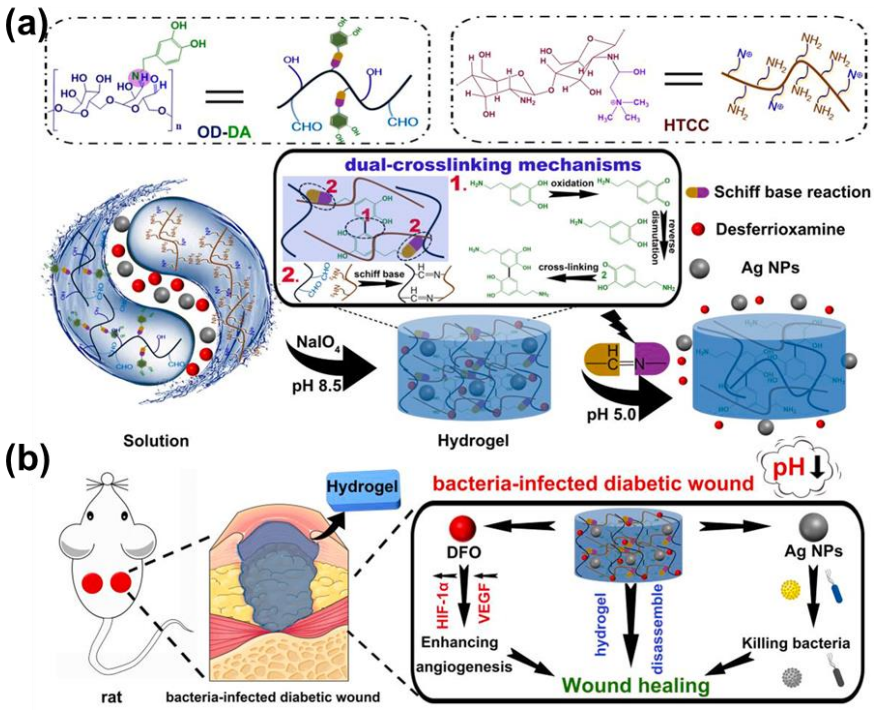

Figure 2.50. (a) Schematic representation for the formation of hydrogels. (b) Diagram showing the antibacterial and wound healing mechanisms of hydrogels.[275]

It is well known that hydrogen bonding is a supramolecular interaction formed between hydrogen atoms and highly electronegative atoms, such as nitrogen (N) or oxygen (O) atoms. Although this weak force is not stable in an aqueous environment, it can be stabilized by the polymer providing strong solvation effects through hydrophobic interactions or by forming multiple hydrogen bonding interactions to increase the bond strength, so that hydrogen bonds can act as interchain crosslinks in the hydrogel network.[276] Hydrogen bonds can therefore

also be combined with reversible C=N bonds for the purpose of DCN hydrogel fabrication.[277-283] For example, Connal et al. synthesized copolymers of oligo(ethylene glycol) methacrylate (OEGMA) and methacrylic acid (MAA), and grafted benzaldehyde units onto the polymer by further esterification with 4-hydroxybenzaldehyde.[279] The hydrogen bonds can be formed between the Bronsted acid MAA and Lewis basic OEGMA on the obtained copolymers, and can be further stabilized by hydrophobic interactions provided by the long-chain oligo(ethylene glycol) side chains and hydrophobicity provided by benzaldehyde. The addition of ethylenediamine (EDA) can therefore lead to the generation of imine bonds between benzaldehyde groups on the polymer chains to yield DCN hydrogel (**Figure 2.51a**). These DCN hydrogels showed enhanced mechanical properties after freeze-thawing due to the freeze-thaw process which further enhances hydrogen bonding and increases the transport of water molecules in the hydrogel network. These freeze-thawed DCN hydrogels exhibit excellent mechanical properties (including strength, toughness, fatigue resistance) in addition to fast and effective self-healing, programmable shape changing and memory effects.

Guo and his coworkers have developed another DCN hydrogel based on hydrogen bonds and acylhydrazone bonds from synthetic polymers.[281] The DCN hydrogels were prepared from the mixed solution of poly(N-vinylpyrrolidone) (PVP), diacetone acrylamide (DAAm) monomer, acrylamide (AAm) monomer and adipic acid dihydrazide (ADH) crosslinker (**Figure 2.51b**). The acylhydrazone crosslinked network formed between P(AAm-*co*-DAAm) and ADH, while the hydrogen bonding network created between P(DAAm-*co*-AAm) and PVP. DCN hydrogels demonstrated excellent mechanical properties (maximum tensile stress: 369.7 KPa, maximum compressive stress: 73.2 MPa, tear energy: 5724 J/m^2), self-healing, injectability and biocompatibility. These works show that reversible C=N bonds can also co-exist with supramolecular interactions in the same system and enhance the properties of hydrogels.

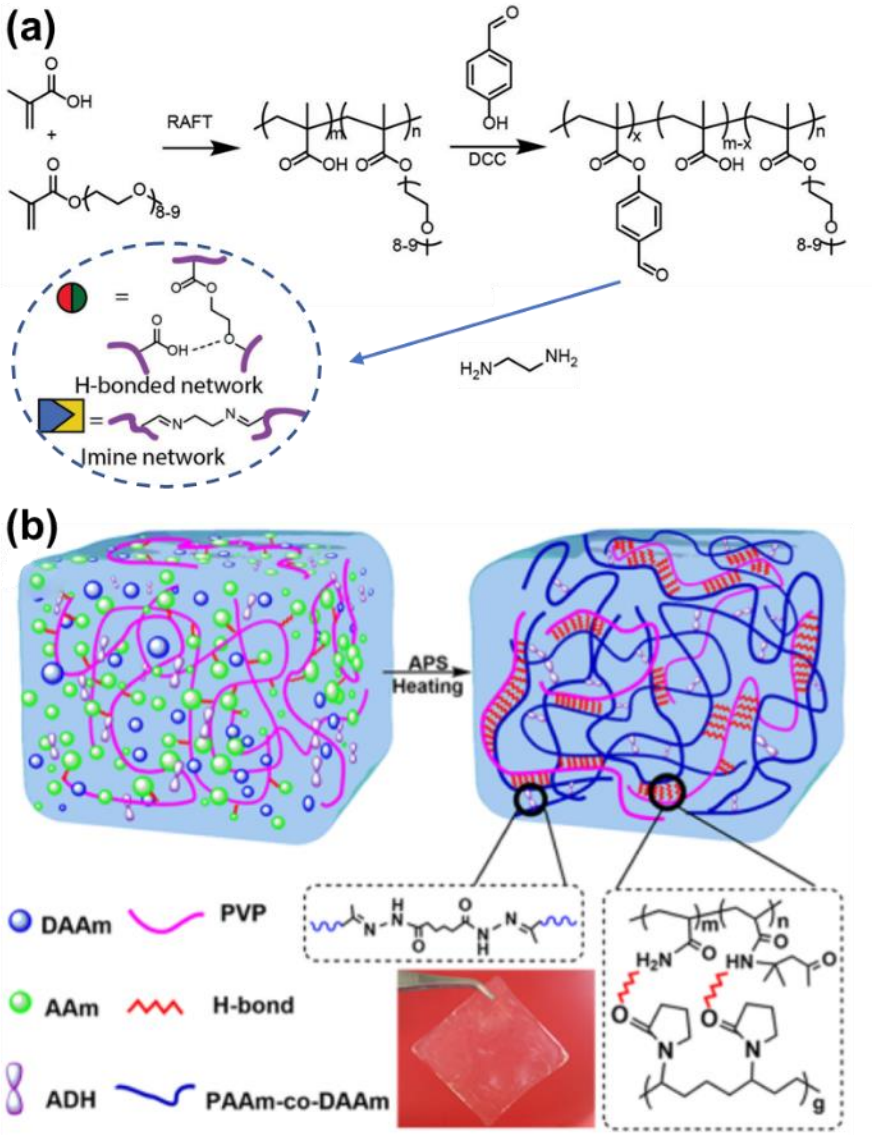

Figure 2.51. Schematic representation for the formation of DCN hydrogels based on hydrogen bonding and imine bonds (a)[279] or acylhydrazone bonds (b).[281]

Similar to the M(II)-Tpy DCN hydrogels mentioned above, the polymer micelles could also serve as a type of crosslinks to be combined with reversible C=N bonds for fabricating DCN hydrogels.[284-287] For example, Guo et al. synthesized benzaldehyde

capped Pluronic F127 (PF127-CHO) capable of self-assembling into micelles by hydrophobic interactions in water (**Figure 2.52**).[284] The aldehyde groups on the surface of the formed micelles can rapidly react with quaternized chitosan (QCS) to form imine crosslinked DCN hydrogels. The prepared DCN hydrogels displayed stretchable, compressible, shear-thinning, self-healing and recoverable mechanical properties due to the dynamic imine bonding and physically crosslinked micelles that can act as energy dissipators. The curcumin-loaded DCN hydrogels showed good antioxidant capacity and pH-responsive release profiles, and can be used as wound dressings.

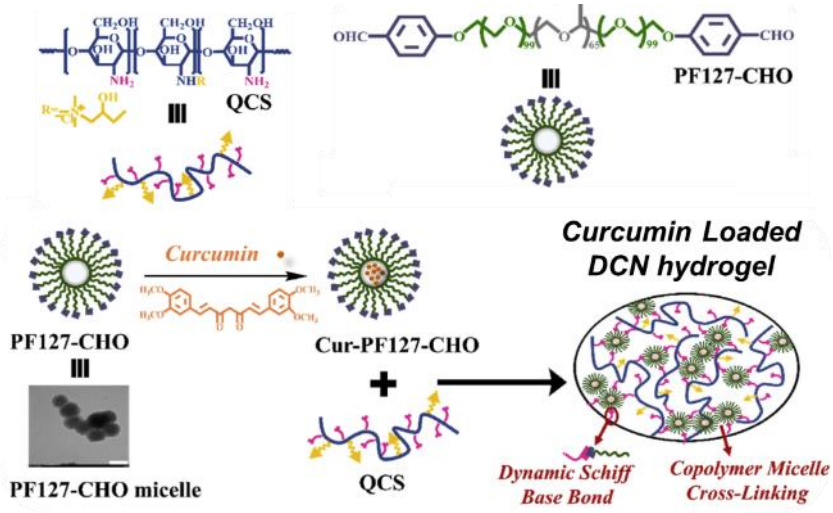

Figure 2.52. Schematic representation for the formation of curcumin-loaded DCN hydrogels based on micelles and imine bonds.[284]

In fact, the micelles formed due to the hydrophobic part of the polymer can also be seen as a case where hydrophobic interactions are used as crosslinks. Hydrophobic interactions can also be directly used in some polymers as interchain crosslinks combined with reversible C=N bonds to prepare DCN hydrogels.[288-291] For example, Yeo and Park synthesized dialdehyde methylcellulose (DAMC) derivative by oxidation of methylcellulose (MC) with sodium periodate (**Figure 2.53**).[290] The aldehyde groups on DAMC can react with the amino

groups on the water-soluble chitosan oligomer (CHI-O) to form imine bonds, while the hydrophobic groups of DAMC constitute the hydrophobic interactions between the chains. Eventually, DCN hydrogels consisting of imine bonds and hydrophobic interactions were obtained. Due to the reversibility of the imine bonds, the obtained DCN hydrogels exhibited better self-healing properties than the MC/CHI-O blended hydrogels. In addition, this DCN hydrogel can be used for the release of two model drugs (adenosine and vitamin C).

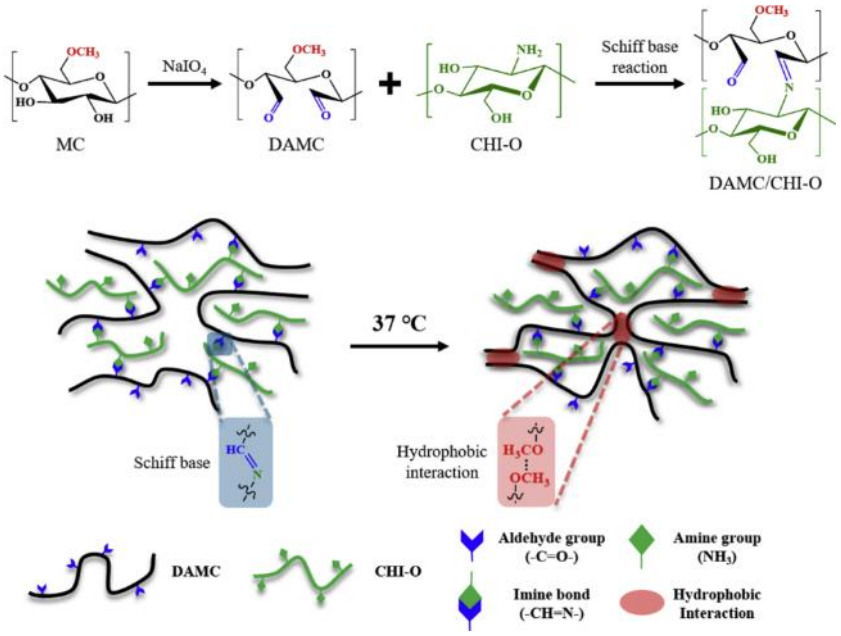

Figure 2.53. Schematic representation for the formation of DCN hydrogels based on imine bonds and hydrophobic interactions.[290]

Tan and Chen et al. have demonstrated that reversible C=N bonds can also be combined with host-guest interactions for the exploitation of DCN hydrogels.[292] They synthesized phenylalanine functionalized ε-polylysine (Phe-EPL) and dialdehyde functionalized PEG (DF-PEG) as precursors. The phenylalanine groups of Phe-EPL could be crosslinked by cucurbit[8]uril (CB[8]) to form CB[8] host-guest network, and the rest of the amine groups on Phe-EPL could react with

the aldehyde groups on DF-PEG to form the imine network (**Figure 2.54a**). Compared to two single networks, DCN hydrogels have higher modulus (**Figures 2.54b** and **2.54c**) and faster self-healing rate.

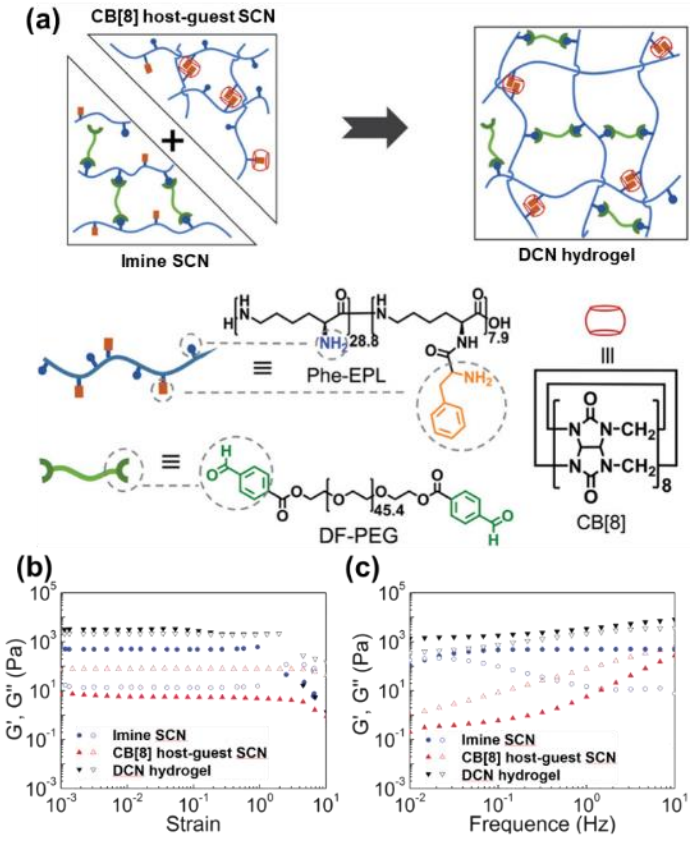

Figure 2.54. (a) Schematic representation for the formation of DCN hydrogel based on imine bonds and CB[8] host-guest interactions. Strain sweeps (b) and frequency sweeps (c) on DCN hydrogel and its single networks.[292]

Noh et al. proposed a DCN hydrogel based on both imine bonds and ionic interactions.[293] The imine bonds were formed between sodium periodide oxidized carboxymethyl cellulose (CMC) and glycol chitosan (GC) (**Figure 2.55**), and the ionic interactions were formed between the acid groups of CMC and the amine groups of GC by using a phosphate buffer saline (PBS) solution at pH 7.0. Evaluation of

cytotoxicity assay showed that DCN hydrogels were biocompatible. In particular, DCN hydrogels with precursor polymer ratios (1:1) exhibited high printability (continuous extrusion) and post-printing stability (without secondary crosslinking).

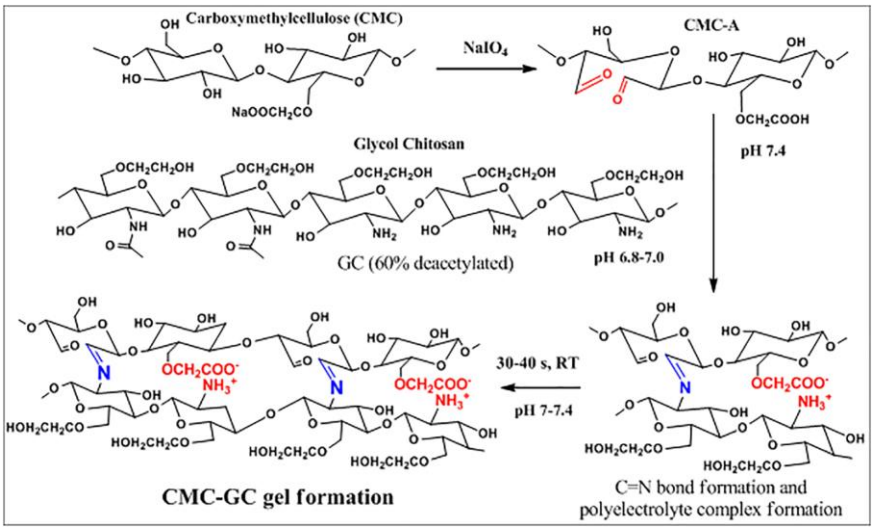

Figure 2.55. The formation of DCN hydrogels based on imine bonds and ionic interactions.[293]

During the last two years, DCN hydrogels based on reversible C=N bonds and metal-ligand coordination bonds have been well developed.[294-298] Zhao et al. developed DCN hydrogels crosslinked by both imine bonds and Fe^{3+}-catechol coordination bonds.[294] The imine linkages could be formed between catechol-modified ε-poly-l-lysine (PL-Cat) and oxidized dextran (ODex), and the addition of Fe^{3+} could result in Fe^{3+}-catechol bis- or tris-complexes between PL-Cat chains at pH ~ 8 (**Figure 2.56**). The obtained DCN hydrogels exhibit the desirable functions of dissolution on demand, repeatable adhesiveness, adhesive and mechanical strength sufficient for wound closure, injectability, and good biocompatibility. Such DCN hydrogel bio-adhesives were able to effectively close open wounds. Due to the fact that imine bonds and Fe^{3+}-catechol bonds are pH-sensitive and Fe^{3+}-

catechol bis- or tris-complexes can be quickly dissociated after adding the medical Fe^{3+} chelating agent such as deferoxamine mesylate (DFO), the DCN hydrogel bio-adhesive can be facilely removed after closing skin incisions by dissolving in DFO, or repeatedly close the reopened wounds with only the help of water. Therefore, the DCN hydrogel bio-adhesives demonstrated great potential in dealing with skin wounds, such as groin and hands skin wounds.

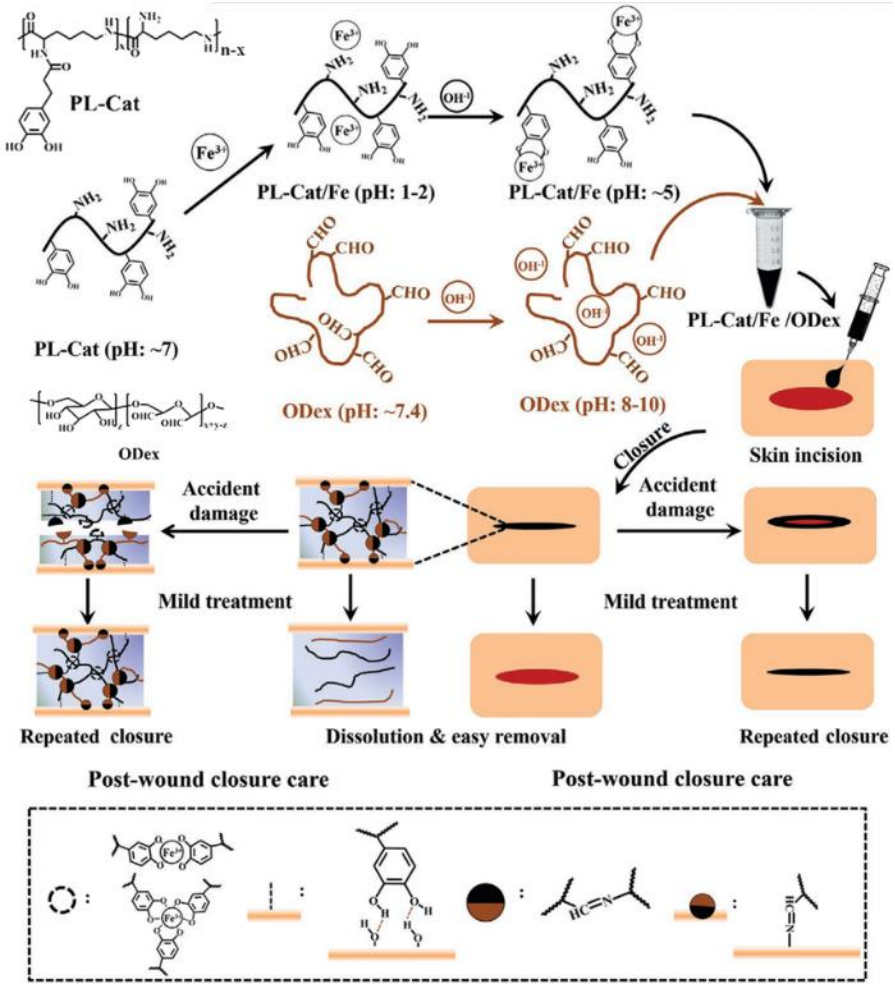

Figure 2.56. Schematic representation for the formation procedures of imine and Fe^{3+}-catechol crosslinked DCN hydrogels for closing open wounds and post-wound closure care.[294]

Liu et al. synthesized a series of polyaspartic hydrazide-*co*-aspartic acid polymers (PHAs) by ring-opening reactions.[295] By copolymerizing diacetone acrylamide (DAAm) and acrylamide (AAm) monomers in PHAs solution as the method shown in **Figure 2.51b**, acylhydrazone crosslinked SCN hydrogels between P(AAm-*co*-DAAm) and PHAs were obtained. Both acylhydrazone bonds and Fe^{3+}-carboxylate complexes crosslinked DCN hydrogels were then obtained by completely soaking the acylhydrazone SCN hydrogels into the Fe^{3+} solution. Similarly, Tan and Li et al. prepared DCN hydrogels using oxidized gellan gum (OG) pre-crosslinked with calcium ion and carboxymethyl chitosan (CMCS) crosslinked by imine bonds.[296] The authors demonstrated that DCN hydrogels containing drugs (antibacterial drugs, tetracycline hydrochloride and silver sulfadiazine) can be used as a wound dressing to avoid wound infection.

Recently, Qiu et al. reported both imine and Fe^{3+}-carboxylate complexes crosslinked DCN hydrogels prepared from oxidized alginate (OA), gelatin (Geln) and butene-modified polyacrylic acid (PAA).[297] The imine bonds were formed between Geln and OA/PAA, and the complexes were created between OA and/or PAA chains (**Figure 2.57**). By varying the concentration of PAA, DCN hydrogels with proper elasticity (up to 37.04 ± 2.75 kPa) and high ionic conductivity (up to $35.36 \pm 7.72 \times 10^{-3}$ S/cm) can be attained. Some DCN hydrogels have been shown to be biocompatible, electrically stable during large strains (~ 50% maximum compressive strain, ~ 150% maximum tensile strain), stretchable (> 500% strain), compressible (> 85% strain), and self-healing. These DCN hydrogels can therefore be used as hydrogel-based engineered cardiac patch.

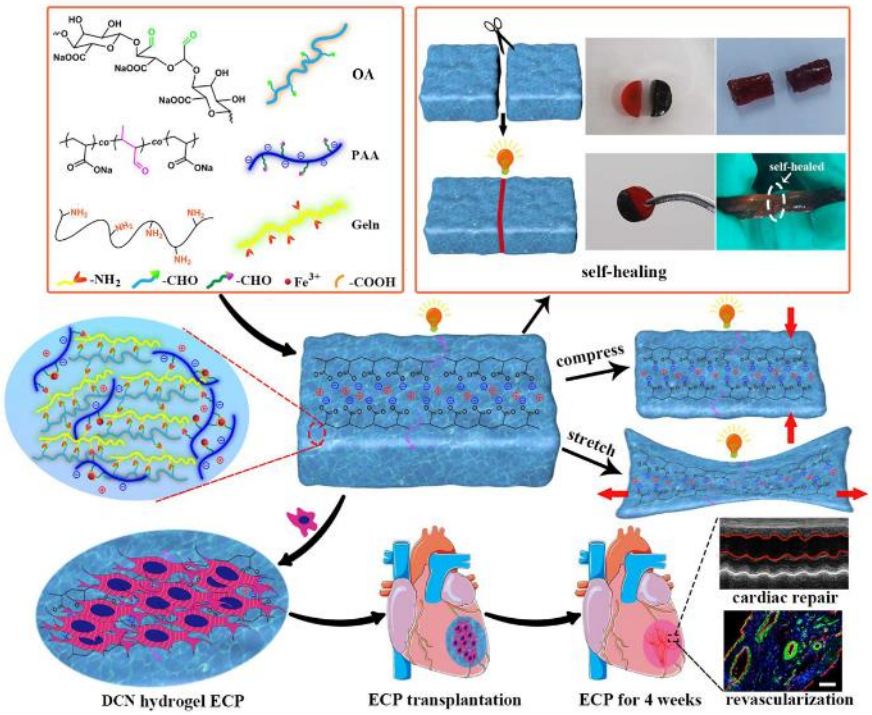

Figure 2.57. Schematic representation for the formation of imine and Fe^{3+}-carboxylate crosslinked DCN hydrogel and its application in myocardial infarction repair.[297]

In 2021, Guo et al. reported on a series of adhesive antioxidant antibacterial DCN hydrogels based on imine bonds and Fe^{3+}-catechol coordination bonds.[298] The stable Fe^{3+}-catechol tris-complexes were first synthesized and then used to crosslink quaternized chitosan (QCS) by forming imine bonds, eventually resulting in DCN hydrogels (**Figure 2.58**). The DCN hydrogel presents injectability, self-healing capability, biocompatibility, antimicrobial activity, adhesiveness, and NIR responsiveness. The antimicrobial capacity of quaternized chitosan and NIR-assisted photothermal ablation could synergistically improve the antimicrobial efficiency of the DCN hydrogel. Similar to the work of Zhao et al,[294] DCN hydrogels based on imine and Fe^{3+}-catechol bonds were not only effective in sealing skin incision, but could also be removed on demand with the intervention of DFO or acidic solution.

Different from Zhao et al DCN hydrogels (**Figure 2.56**), the hydrogels in this work were more sensitive because simply breaking either of the two crosslinks will cause the gel network to collapse.

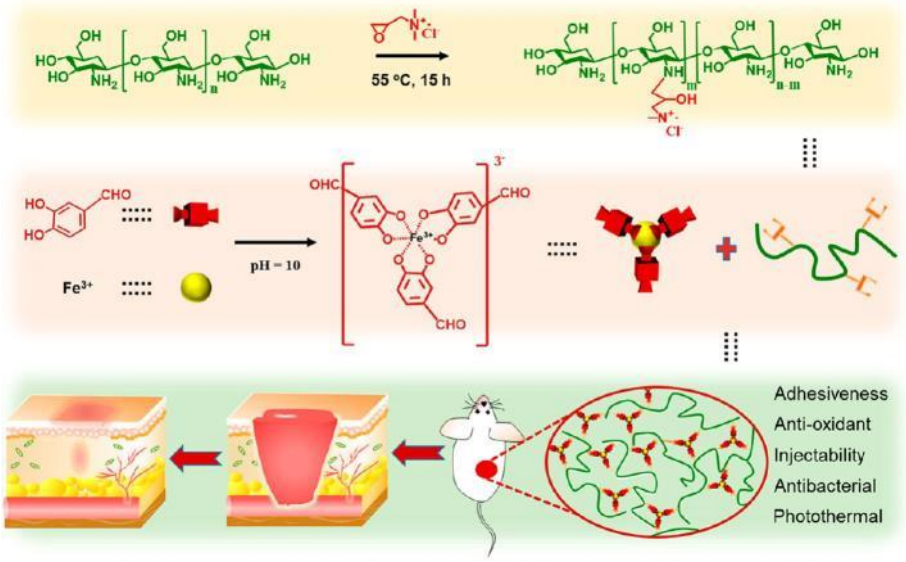

Figure 2.58. Schematic representation for the formation of imine and Fe^{3+}-catechol crosslinked DCN hydrogel and its application in wound closure and post-wound-closure care.[298]

Based on the above works on combining reversible C=N bonds and metal-ligand coordination bonds to construct DCN hydrogels,[294-298] it can be seen that these two types of bonds can be used, not only to make dynamic DCN hydrogels, but also to verify the fact that they can co-exist in the same system. This also implies that the reversible C=N bond and the metal-terpyridine coordination bond combination in this thesis will not have competition problems.

As the reversible C=N bonds can also be adjusted from susceptible bonds (such as imine) to more stable bonds (such as oxime) by varying the nucleophile, some DCN hydrogels were also prepared using the same two types of bonds but with different thermodynamic stability. For example, Li and Nan et al. prepared both imine and acylhydrazone

crosslinked DCN hydrogels.[299] The reaction of aldehyde groups of oxidized alginate (OSA) with amino groups of gelatin (GE) produced the imine network and the acylhydrazone network was formed between OSA chains and adipic acid dihydrazide (ADH) crosslinkers (**Figure 2.59**). The gelation time of DCN hydrogels can be adjusted by altering the ratio of OSA, GE and ADH. The DCN hydrogels have excellent injectability, in situ gelation in vivo, self-healing and tissue biocompatibility as well as support cell survival, proliferation and migration.

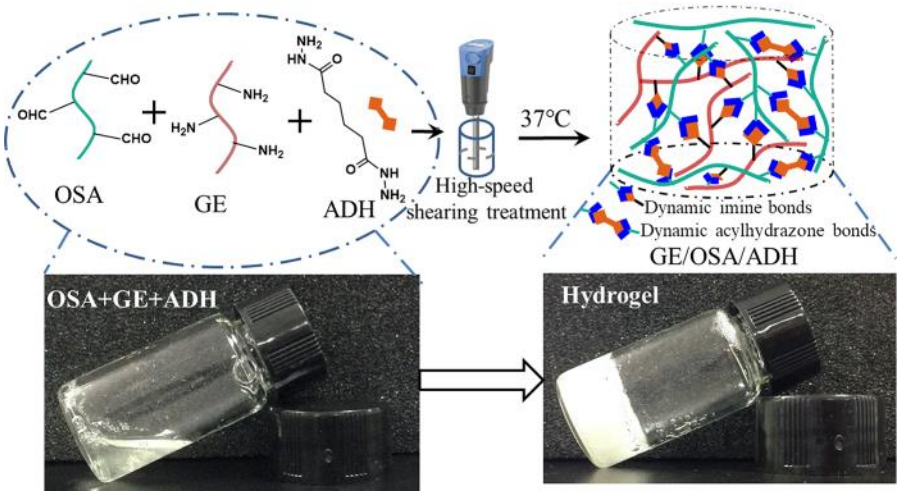

Figure 2.59. Schematic representation for the formation of DCN hydrogel based on imine and acylhydrazone bonds.[299]

2.5.3. IPN or DN hydrogels

To the best of our knowledge, there are no reports of IPN or DN hydrogels containing M(II)-Tpy. Only IPN or DN hydrogels based on reversible C=N bonds will be discussed in this subsection. Among these IPN hydrogels, the IPN is mainly composed of two sub-networks, hence they are also referred to as DN hydrogels most of the time in literature. One of these two networks is connected by the reversible C=N bonds and the other one is crosslinked by static covalent or other types of dynamic bonds.

IPN or DN hydrogels containing reversible C=N bonds most commonly consist of a network of reversible C=N bonds interpenetrated with a static covalent network. Zhang and Ouyang et al. proposed a crosslinking strategy for imine and covalent interlocked DN hydrogels.[300] In this work, the imine bond crosslinked network between gelatin and oxidized dextran (ODex) served as the first network. The second network, crosslinked by static covalent bonds, was formed by exposing the gelatin methacrylate (GelMA) solution to 30 mW/cm^2 UV light (365 nm) for 3 min. As a result, DN hydrogels were formed by the interpenetration of imine and covalent networks (**Figure 2.60**). Compared to statically covalently bonded SCN hydrogels, the storage modulus of DN hydrogels was approximately three times higher. In addition, the DN hydrogels showed lower swelling ratio, higher crosslinking density, and smaller pore size. Due to the reversible nature of the imine network, the DN hydrogels also exhibited rapid recovery ability. In addition, the authors demonstrated that large-scale formation of reversible C=N bonds between amino groups of hog casing tissue surface and excess aldehyde groups in the hydrogel improved the adhesion of DN hydrogels to the tissue. These tough tissue-adhesive DN hydrogels also show good biocompatibility and enhanced ability for the formation of hyaline cartilage-like tissues. These properties suggest that DN hydrogels containing dynamic bonds, similar to the

DCNs mentioned above, also have enhanced toughness and do not lose the dynamic nature of the dynamic bonds themselves.

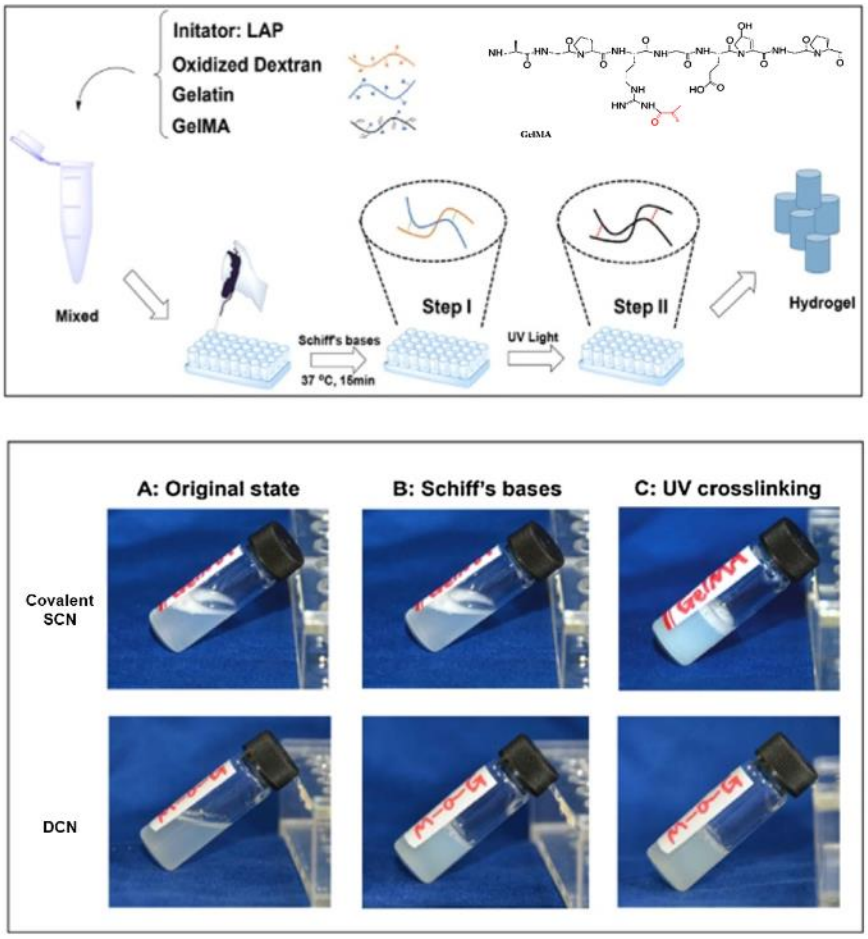

Figure 2.60. Schematic representation for the formation of DN hydrogel composed of an imine network (between oxidized dextran and gelatin) and a static covalent network (between GelMA chains).[300]

Similarly, both imine and covalent crosslinked DN hydrogels were prepared by Wang et al.[301] These DN hydrogels were prepared in the presence of N-carboxyethyl chitosan (CEC) and benzaldehyde terminated linear PEG (DAPEG) by a one-step in situ free-radical polymerization of monomeric acrylamide (AAm) and N,N'-

methylenebisacrylamide (MBA) (**Figure 2.61**). Due to the dynamic and pH-responsive imine bonds, and the large number of amino and hydroxyl groups on chitosan that can chelate various metal ions, DN hydrogels are not only self-healing but also have a repeatable shape memory function with dual responsiveness to pH and metal ions. In addition, DN hydrogel has excellent mechanical properties (tensile strength: 460 kPa, strain at break: 4600%) and the self-healing efficiency of hydrogels can reach 84.2% (elongation at break) and 93.2% (strength at break) with the help of alkali stimulation.

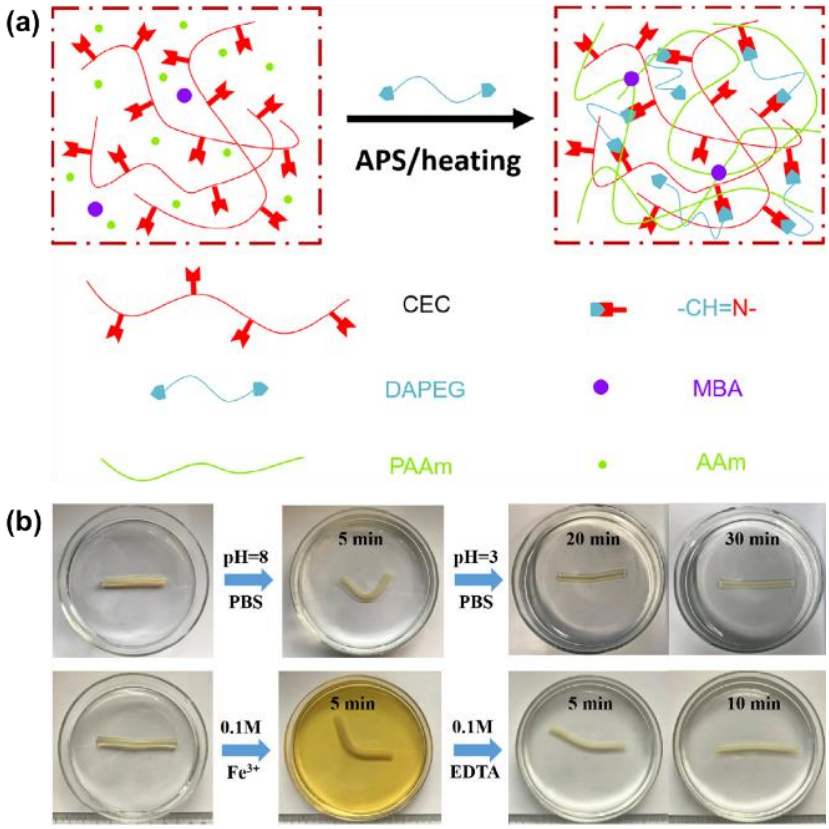

Figure 2.61. (a) Schematic representation for the formation of DN hydrogel composed of an imine network (between CEC and DAPEG) and a static covalent network (between PAAm chains). (b) The pH- and metal ions-induced shape memory abilities of DN hydrogels.[301]

Zhang et al. prepared a series of imine and static covalent crosslinked IPN hydrogels by cryogelation technique.[302] The first network was built by imine crosslinking between an oligoethylene glycol-based dendronized polymer side-functionalized with primary amines (PG1A) and a linear PEG end-capped with benzaldehyde groups (PEG-DA) (**Figure 2.62a**). The second one was a covalent crosslinked network constructed by the free radical polymerization of acrylamide (AAm) or N, N-dimethylacrylamide (DMA) with N,N'-methylenebisacrylamide (MBA). In this study, the IPN hydrogels were prepared by two strategies: (1) two-step method. The covalently crosslinked network was first synthesized and then immersed in the solution of PG1A (pH 10) to swell and form the imine crosslinked network in the frozen state after the addition of PEG-DA. (2) one-pot method. Both networks were formed simultaneously from the mixed precursor solutions of PG1A, PEG-DA, AAm and MBA by independent, non-interfering imine and covalent crosslinking. Compared to IPN hydrogels prepared with covalent PAAm as the second network, PDMA-based IPN hydrogels were weaker, whether they were prepared by a two-step or one-step method. The authors attribute this difference to the weaker hydrogen bonding of the PDMA than the PAAm network. Compared to the imine crosslinked SCN hydrogels (G': ~3 KPa), the mechanical properties of the IPN hydrogels obtained after the introduction of the PAAm covalent network were increased (G' > 4 kPa). IPN hydrogels with the same composition of imine and PAAm covalent networks but prepared by the two different methods show similar G' when the imine network content was equal to or greater than half. The G' of IPN hydrogels prepared by the "two-step method" was much higher than that of the hydrogel prepared by the "one-pot method" when the imine network content was less than half, i.e., the PAAm covalent network was the major component. Based on the pH-responsiveness of the imine bonds and the characteristic thermal response behavior of OEG-based dendrimers, the prepared IPN hydrogels also show a remarkable pH-/thermo- dual shape memory behavior (**Figure 2.62b**). These results suggest that not only do IPN hydrogels have a higher

elastic modulus than single crosslinked networks, but that the crosslinking sequences can also have an important effect on the mechanical properties of the gels. Also, the stimuli-responsiveness of the dynamic crosslinks does not affect the thermal responsiveness of the polymer backbone.

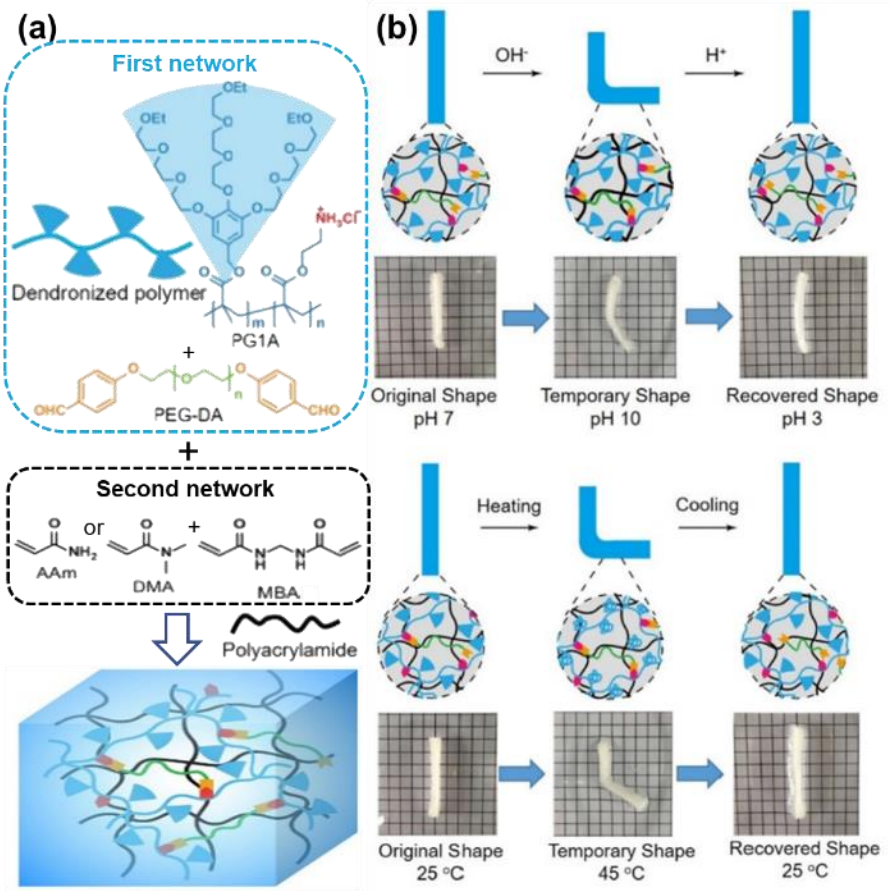

Figure 2.62. (a) Schematic representation for the formation of IPN hydrogel composed of an imine network (between PG1A and PEG-DA) and a static covalent network (between PAAm or PDMA chains). (b) The pH- and thermo-induced shape memory abilities of IPN hydrogels.[302]

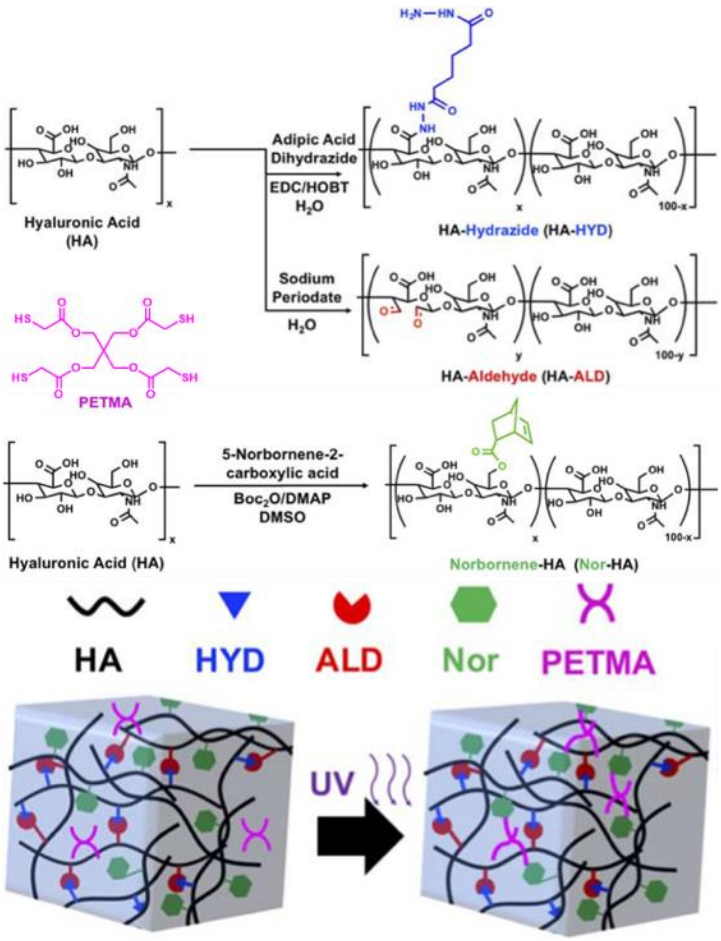

Figure 2.63. Schematic representation for the formation of DN hydrogel composed of an acylhydrazone network (between HA-HYD and HA-ALD) and a static covalent network (between Nor-HA and PETMA).[303]

Similarly, Burdick et al. demonstrated that DN hydrogels composed of an acylhydrazone network and a static covalent network can have superior mechanical properties compared to single networks (**Figure 2.63**).[303] They prepared an acylhydrazone crosslinked SCN hydrogel from a hyaluronic acid-hydrazide (HA-HYD) and a hyaluronic acid-aldehyde (HA-ALD) for 3D printing. To obtain printed hydrogels with enhanced mechanical properties, a covalently crosslinked second network was formed using a norbornene-modified

hyaluronic acid (Nor-HA) crosslinked with pentaerythritol tetramercaptoacetate (PETMA) under UV light. Compared to acylhydrazone SCN hydrogels, the G' of DN hydrogels increased from ~500 Pa to 5 kPa. The Young's modulus and failure stress of 5 mm printed SCN hydrogel discs increased from 1 kPa to 3 kPa and from 10 kPa to 30 kPa, respectively, after the DN hydrogels formed under UV irradiation.

Chi and co-workers reported another IPN hydrogel composed of interlocked acylhydrazone and covalent networks.[304] The hyaluronic acid-aldehyde (HA-CHO) and hydrazide-functionalized poly(γ-glutamic acid) (γ-PGA-ADH) constructed the first network through the formation of acylhydrazone bonds. The second network was established by the photopolymerization of methacrylate-functionalized poly(γ-glutamic acid) (γ-PGA-GMA). Compared with the imine network (~52% fracture strain with a maximum compressive stress of ~35 kPa), the γ-PGA-GMA covalent network (~74% fracture strain with a maximum compressive stress of ~110 kPa) was more flexible and robust. Precursor solutions loaded with cells and/or drugs can be injected via dual-chamber syringes equipped with mixing tips (γ-PGA-ADH and γ-PGA-GMA solutions in one syringe and HA-CHO solution in the other syringe) to first form the imine semi-IPN (SIPN) hydrogel, and then induce the covalent crosslinking under ultraviolet light to form strong IPN hydrogels (**Figure 2.64**). The lack of a covalently crosslinked γ-PGA-GMA network and the fact that the polymer chains were only entangled in the first imine network resulted in a loose SIPN hydrogel structure and a lower storage modulus than that of the IPN hydrogel. The stiffness of the IPN hydrogels could be regulated by altering the content of the γ-PGA-GMA covalent network. In addition to injectability and good mechanical properties, IPN hydrogels have also been shown to be biocompatible and enzymatically degradable for drug delivery and 3D cell culture.

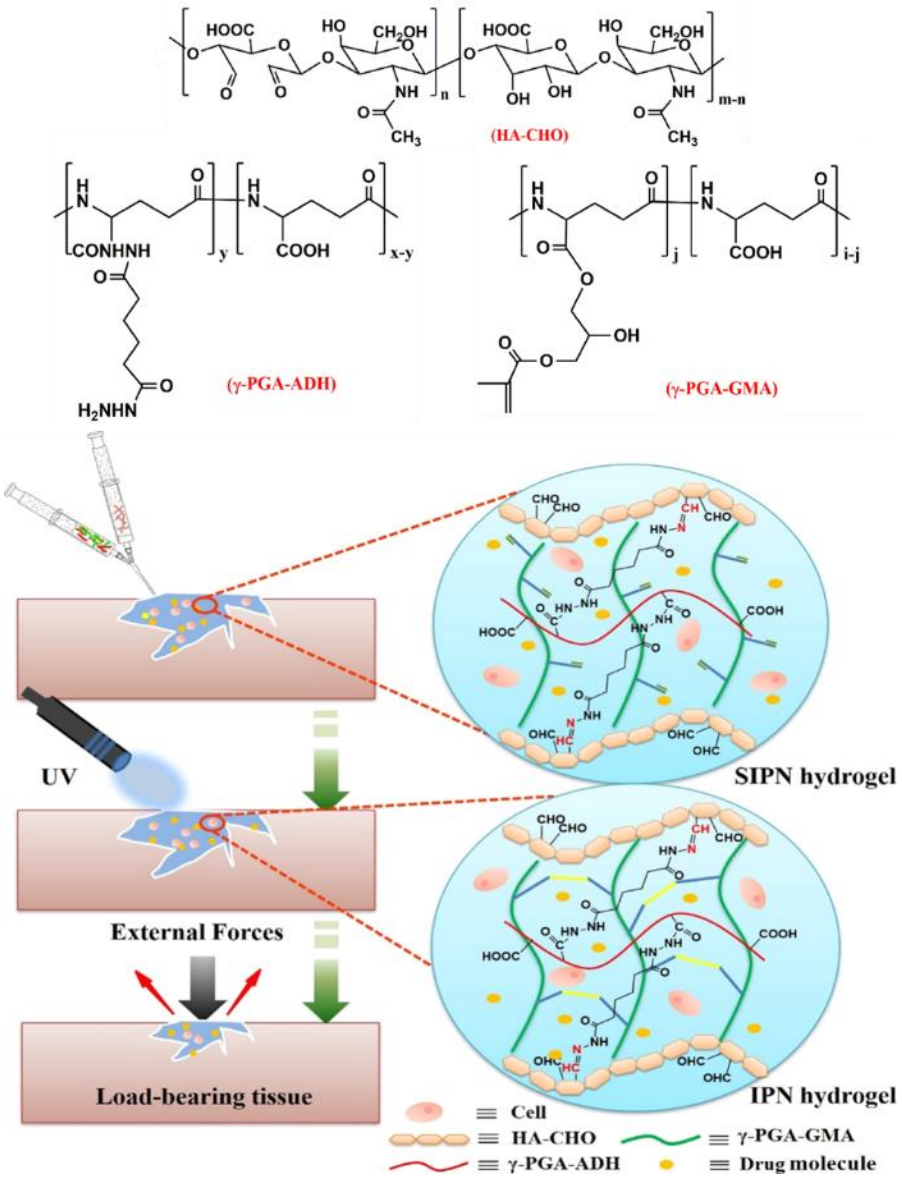

Figure 2.64. Schematic representation for the formation of IPN hydrogel composed of an acylhydrazone network (between HA-CHO and γ-PGA-ADH) and a static covalent network (between γ-PGA-GMA chains).[304]

Ossipov et al. proposed an IPN hydrogel composed of an acylhydrazone network and a disulfide network from four derivatives of hyaluronic acid (HA) bearing hydrazide (HA-hy), aldehyde groups

(HA-al), 2-dithiopyridyl (HA-SSPy), and thiol (HA-SH) respectively (**Figure 2.65a**).[305] The precursor solutions of these four HA derivatives were mixed as shown in **Figure 2.65a** to simultaneously form in situ IPN hydrogels consisting of an acylhydrazone network between HA-hy and HA-al and a disulfide network between HA-SSPy and HA-SH. The rheological results showed that the G′ of IPN was three times higher than that of pure acylhydrazone individual network and twice as high as that of pure disulfide individual network. The storage moduli of the single acylhydrazone network containing HA-SSPy and of the single disulfide network containing HA-al were both smaller than that of the corresponding pure individual network (**Figure 2.65b**). The authors suggest that the presence of a third component that may cause interfering steric effects during the crosslinking reaction result in a lower crosslinking density of the three-component single networks than in the pure individual networks, thus reducing their mechanical strength. This is a very special crosslinking condition in IPN or DN systems, where one of the networks is formed in the presence of another polymer. This causes one of the dynamic bonds to be crosslinked in the presence of another non-crosslinked polymer. The dilutive screening effect caused by the presence of the non-crosslinked polymer reduces the effective crosslinking of the dynamic bonds. They also show that IPN hydrogels (G': ~5.5 kPa) encapsulated with water-soluble iron oxide nanoparticles (IONPs) have enhanced mechanical properties compared to pure IPN hydrogels (G': ~4.2 kPa). As the mesh size of the IPN was smaller than the size of the IONPs, this allows the nanoparticles to be retained in the matrix under equilibrium swelling conditions. These nanoparticles could also be released upon enzymatic degradation, suggesting that the iron oxide hybridized IPN hydrogels could be useful in non-invasive imaging in vivo by magnetic resonance imaging (MRI) and in hyperthermia cancer therapy. In addition, the acylhydrazone network could be disassembled by sodium periodate and the disulfide network could be destroyed by dithiothreitol (DTT). Thus, although the gel-sol transition was not visible with $NaIO_4$ and DTT

separately, it was still possible to soften the hydrogel and release the IONPs from the IPN.

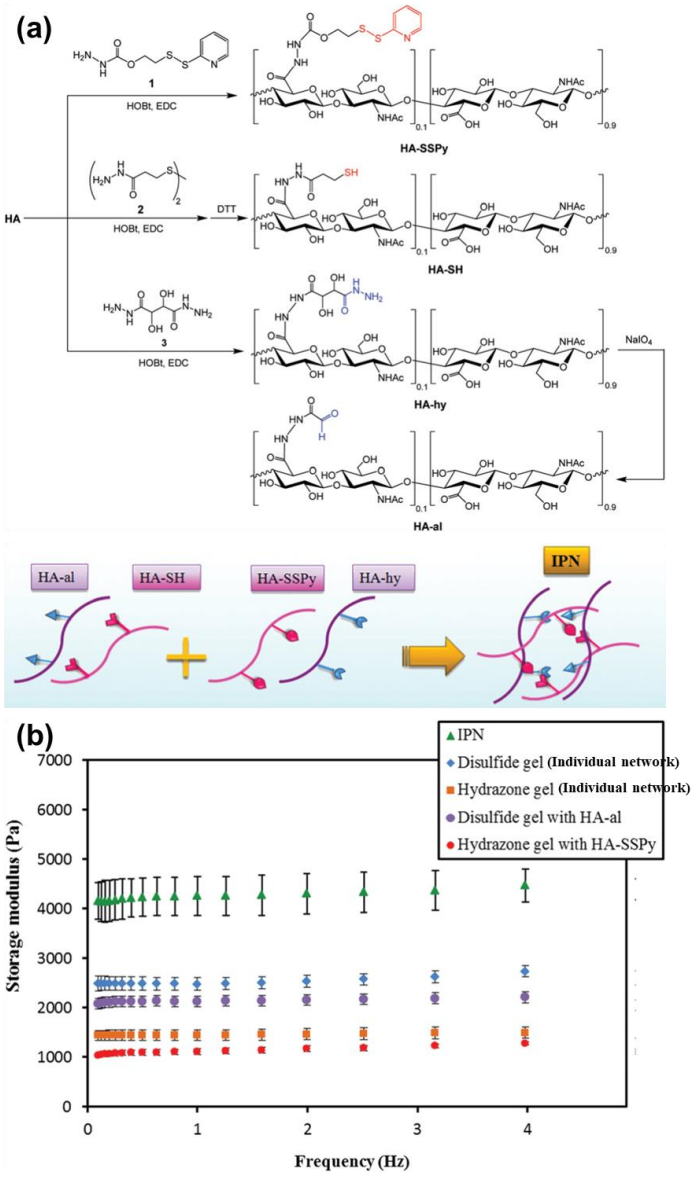

Figure 2.65. (a) Schematic representation for the formation of the IPN hydrogel composed of an acylhydrazone network (between HA-hy and HA-al) and a disulfide network (between HA-SSPy and HA-SH). (b) Frequency sweeps on IPN hydrogel and its pure SCN hydrogels and SCN hydrogels with un-crosslinked polymer.[305]

Zhang and Yang et al. introduced a 3D-printable IPN hydrogel composed of an acylhydrazone network and a borate ester network for creating responsive bio-ink materials.[306] Four copolymers based on N,N-dimethylacrylamide (DMA) were synthesized by RAFT polymerization (**Figure 2.66**). The benzaldehyde grafted PDMA and the hydrazide pendent PDMA were employed for forming the acylhydrazone network, and the dopamine functionalized PDMA and the phenylboronic acid modified PDMA were used for creating the borate ester network. IPN hydrogels could be obtained by mixing two functional polymers that do not react with each other through a dual chamber syringe equipped with a mixing tip. The thermodynamic equilibrium constant of the borate ester bonds was much greater than that of the acylhydrazone bonds. Under acidic conditions, the network was dominated by the formation of acylhydrazone bonds. Under neutral conditions both acylhydrazone and borate ester bonds took part in the construction of the networks. Under alkaline conditions, the network was mainly formed by borate ester bonds. Therefore, the gelation time and mechanical properties of IPN hydrogels can be adjusted by pH or polymer precursor concentration. In the pH range from 3 to 7, the gelation time decreases as the pH increases. In the pH range from 7 to 10, the gelation time increases slightly with increasing pH. The exchange of acylhydrazone bonds at pH 3 was responsible for the self-healing of IPN hydrogels, while the exchange of borate ester bonds at pH 10 also confers self-healing properties. In contrast, the kinetically locked state of the acylhydrazone and borate ester bonds under neutral conditions (pH ~ 7) prevented self-healing. When the pH of the hydrogels was lowered to 1 using 0.1 M HCl solution, the hydrogels showed a gel-to-sol phase transition, and returned to the gel state when the pH was adjusted back above 3 using 0.1 M NaOH solution. This suggests that the dynamic characteristics of the acylhydrazone and borate ester bonds are also preserved in the IPN system as they are in the DCN.

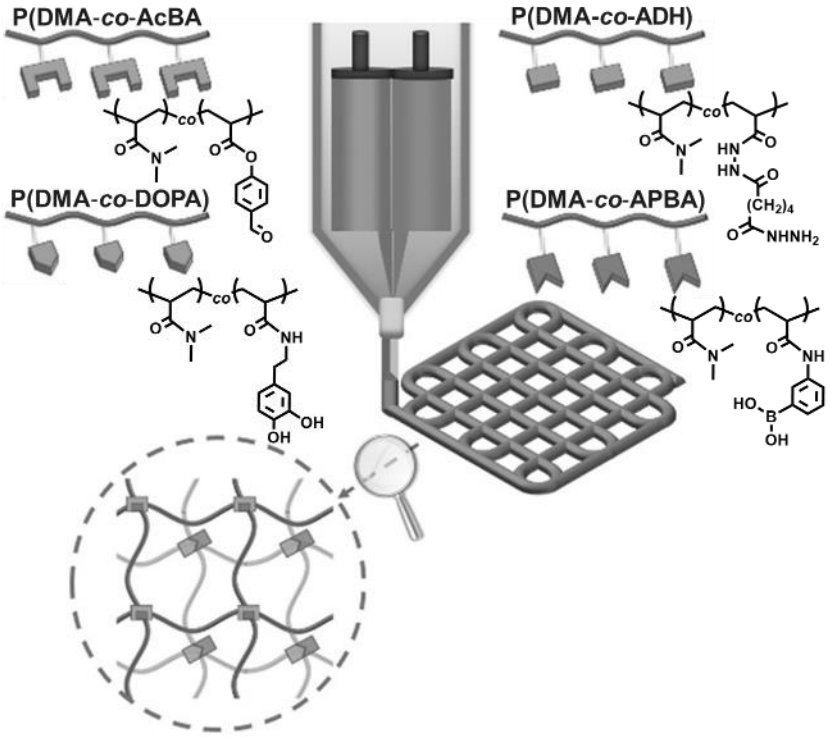

Figure 2.66. Schematic representation for the formation of the IPN hydrogel composed of an acylhydrazone network (between P(DMA-*co*-AcBA) and P(DMA-*co*-ADH)) and a borate ester network (between P(DMA-co-DOPA) and P(DMA-co-APBA)).[306]

Cho and Ooya developed a "one-pot" method to prepare DN hydrogels composed of a hydrogen bonding network and an imine crosslinked network.[307] The agar was crosslinked by hydrogen bonding at 37°C as the first network and the second network was constituted by the formation of imine bonds between oxidized carboxymethyl cellulose (OCMC) and glycol chitosan (GC) (**Figure 2.67**). The DN hydrogel (67% fracture strain with a maximum compressive stress of 43.4 kPa) exhibited enhanced mechanical properties compared to the agar SCN hydrogel (31% fracture strain with a maximum compressive stress of 6.6 kPa) with only hydrogen bonds crosslinking, and the OCMC/GC SCN hydrogel (42% fracture strain with a maximum compressive stress of 16.2 kPa) with only imine bonds

crosslinking. The fracture energy of the DN hydrogel was calculated to be 619.8 kJ/m^3, which was more than 9 and 6 times greater than that of the hydrogen bonding and imine networks, respectively. No significant decrease in maximum stress and hysteresis was observed for DN hydrogels during the 5 cycles of loading-unloading experiments. DN hydrogels also demonstrated injectable, self-healing and biocompatible properties with controlled cell attachment and increased protein adsorption. This work also demonstrates that two different types of dynamic bonds, supramolecular interactions and dynamic covalent bonds, can also co-exist in DN or IPN systems.

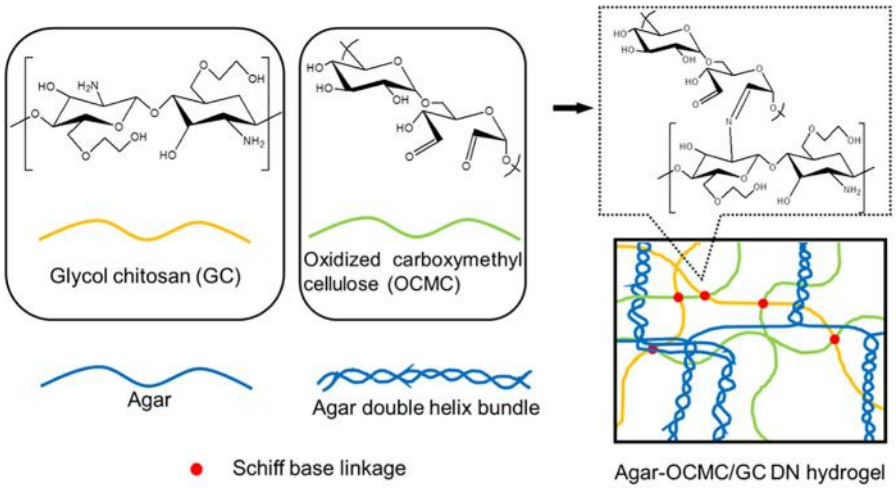

Figure 2.67. Schematic representation for the formation of the DN hydrogel composed of an imine network (between OCMC and GC) and a hydrogen bonding network (between agar chains).[307]

Similarly, Wang et al. prepared another DN hydrogel composed of a hydrogen bonding network (first network) and an acylhydrazone crosslinking network (second network).[308] As shown in **Figure 2.68**, a solution of oxidized sodium alginate (SA-CHO) and agarose (Aga) in PBS was first heated, and then cooled down to 50°C while adding adipic acid dihydrazide (ADH) to produce the acylhydrazone crosslinked second network (SA-CHO gel) between SA-CHO chains. Subsequently,

after the system was further cooled down to room temperature, the densely crosslinked Aga gel was formed as the first network between the Aga chains through hydrogen bonding, resulting in a SA-CHO/Aga DN hydrogel. Due to the reversible transition of Aga's coil-helix crosslinks between low and high temperatures, as well as the dynamic nature of the acylhydrazone bonds, these DN hydrogels exhibited thermally reversible, recyclable, recurrently shapeable and self-healing properties. The DN hydrogels showed a maximum compressive stress and modulus (1.65 MPa and 1.85 MPa) that were 17 and 15 times higher than acylhydrazone SCN hydrogels, as well as 20 and 9 times higher than hydrogen bonding SCN hydrogels, respectively. The DN hydrogels also have excellent fatigue resistance and maintain an almost constant maximum compressive stress during cyclic loading-unloading processes.

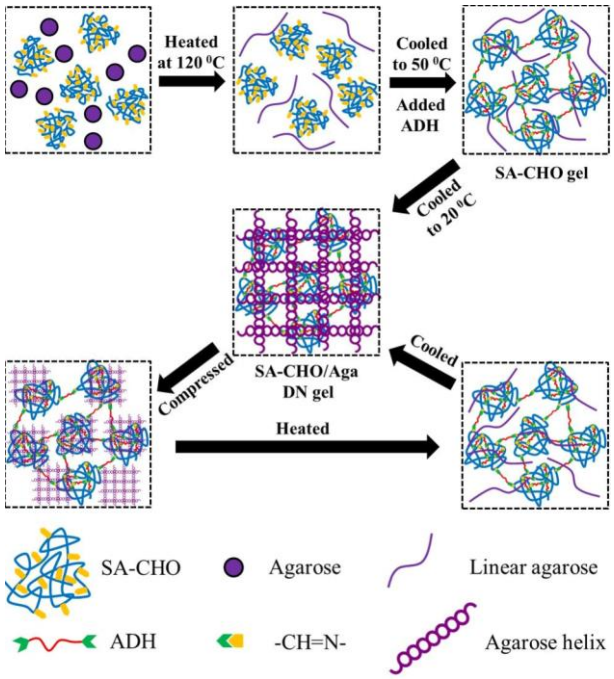

Figure 2.68. Schematic representation for the formation of the DN hydrogel composed of an acylhydrazone network (between SA-CHO chains) and a hydrogen bonding network (between agarose chains).[308]

An example of a DN hydrogel composed of a reversible C=N bond network and a metal-ligand coordination bond network was reported by Wang and Qu et al in 2017.[309] The glycol chitosan (GC) and dibenzaldhyde capped poly(ethylene oxide) (OHC-PEO-CHO) were synthesized for building the imine crosslinked network (GC gel) as the first rigid network, and the Ca^{2+}-carboxylate complexes crosslinked alginate network (Alg gel) has been selected as the second soft network (**Figure 2.69**). Based on the dynamic nature of the crosslinks in the two networks, DN hydrogels can be formed from precursor solutions by injection mixing. Likewise, any of the networks in the DN hydrogels can be selectively broken, i.e., the imine network can be broken by using HCl (pH = 5) or the Ca^{2+}-carboxylate network can be disrupted by chelating Ca^{2+} using EDTA. The gelation time and injectability of the hydrogels could be adjusted by the polymer concentration and the ratio between the crosslinkers and the polymers. With the same precursor solution ratios, the gelation time basically decreases in the order of GC gel > DN gel > Alg gel. The storage modulus (G') of DN hydrogels was much higher than either imine or Ca^{2+}-carboxylate SCN hydrogels (GC gel or Alg gel) at the same frequency. Due to the synergistic effect of the two asymmetric networks; the hydrogen bonding network maintains the imine network while it resists an elastic deformation, the combination of the two networks allows DN hydrogels to retain their integrity against a 90% compressive strain and to obtain a fracture energy of 410 J/m^2. The DN hydrogels showed fatigue resistance properties in 100 cycles of loading-unloading tests where the maximum stress and hysteresis loops did not show a significant decrease. In addition, DN hydrogels have been shown to be biocompatible, allowing in situ cell encapsulation and proliferation in the DN hydrogel matrix. Subsequently, the same group developed GC/Alg DN hydrogels for the encapsulation and co-culture vascular endothelial cells and human bone marrow mesenchymal stem cells.[310]

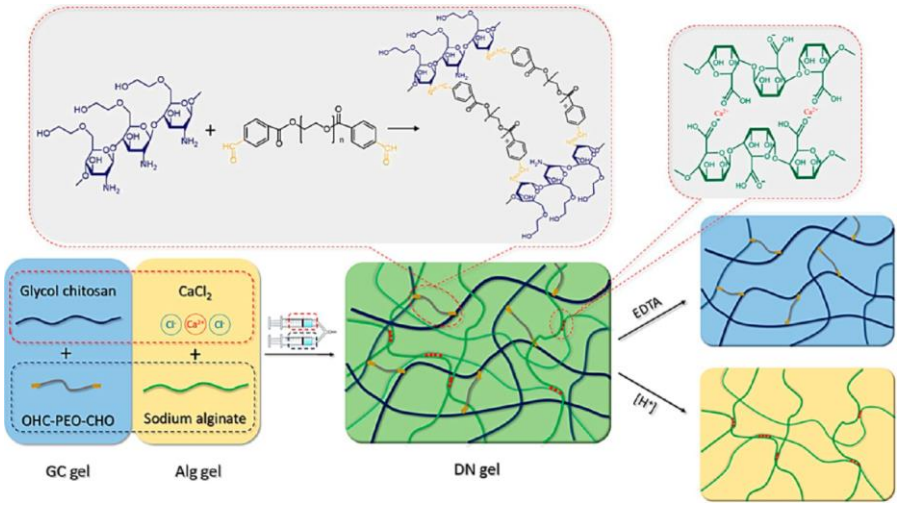

Figure 2.69. Schematic representation for the formation of the DN hydrogel composed of an imine network (between glycol chitosan chains) and a hydrogen bonding network (between sodium alginate chains).[309]

2.5.4. Other topology hydrogels

In order to impart more versatility to hydrogels, more than two dynamic bonds have also been used in the preparation of hydrogels. There are few reports of hydrogels prepared using three types of crosslinks among which metal-terpyridine coordination bonds or reversible C=N bonds.

Xia et al. proposed a TCN hydrogels based on the combination of imine bonds, boronic ester bonds and Ca^{2+}-carboxylate complexes (**Figure 2.70**).[311] The AG hydrogel was first fabricated by the formation of imine bonds between oxidized sodium alginate (Ald-alginate) and gelatin, and boronic ester bonds between Ald-alginate and borax. The AG hydrogel was then immersed in a $CaCl_2$ solution to form further Ca^{2+}-carboxylate complex crosslinks between the Ald-alginate chains leading to the resultant TCN hydrogel. The prepared TCN hydrogels displayed stretchable, compressible, twistable and self-healing mechanical properties and exhibited anti-freezing, high ion

conductivity as well as strong and reversible adhesion to metal, skin, glass and plastic. This suggests that three different types of dynamic bonds, namely imine bonds, boronic ester bonds and Ca^{2+}-carboxylate complexes, can also co-exist in the same system.

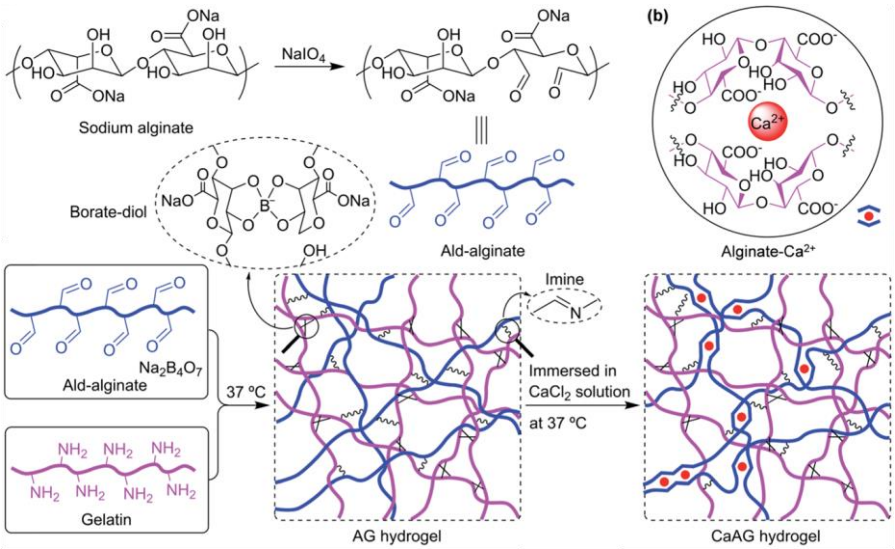

Figure 2.70. Schematic representation for the formation of the TCN hydrogel based on imine bonds, boronic ester bonds and Ca^{2+}-carboxylate complexes.[311]

Since the metal-terpyridine coordination bonds can be varied from labile bonds to long lifetime bonds by changing the metal ions, and the stability of reversible C=N bonds can also be adjusted by varying the nucleophile, some TCN hydrogels were also prepared by combining two types of metal-terpyridine coordination bonds or reversible C=N bonds with another bonds. For example, Seiffert and Ahmadi built DCN hydrogels based on covalent bonds and M(II)-Tpy bonds.[80] When the metal ions used to form M(II)-Tpy were replaced with two different metal ions, the resulting linkages were two different bis-complexes, which have different bond energies. This DCN could also thus be considered as a TCN. As shown in **Figure 2.71a**, the TCN hydrogels were first crosslinked by covalent bonds and then crosslinked by both Zn^{2+}-Tpy and Co^{2+}-Tpy. The SCN hydrogel crosslinked only by

covalent bonds shown flat storage modulus in the frequency sweeps (**Figure 2.71b**), indicating no source of energy dissipation. However, since the Zn^{2+}-Tpy and Co^{2+}-Tpy complexes have different dissociation rates, the appearance of two peaks in the loss modulus demonstrated a dual relaxation process in the TCN (**Figure 2.71c**).

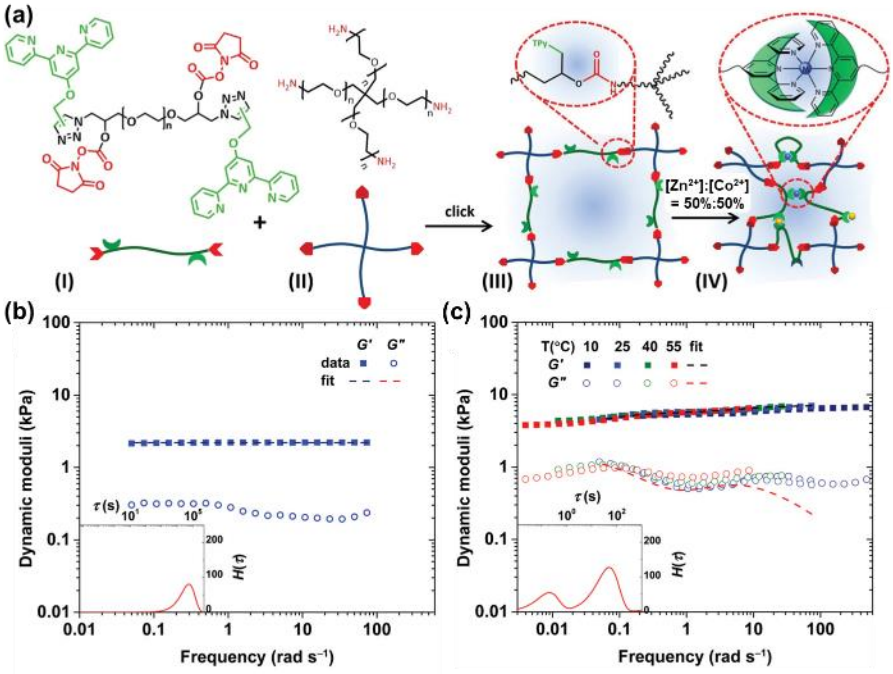

Figure 2.71. (a) Schematic representation for the formation of the TCN hydrogel based on covalent bonds, Zn^{2+}-Tpy and Co^{2+}-Tpy bis-complexes. Dynamic frequency sweeps on pure covalent SCN hydrogel (b), and TCN hydrogel (c).[80]

Liu and Chen et al. developed a TCN hydrogel based on imine, acylhydrazone and disulfide bonds.[312] The 3,3′-dithiopropionic acid dihydrazide (DTP) was used as crosslinker to react with oxidized alginate (OSA) to build a network by both acylhydrazone and disulfide crosslinked, and the imine bonds formed between the OSA and carboxymethyl chitosan (CMC) formed additional crosslinks (**Figure 2.72**). The TCN hydrogel (maximum compressive stress: 65 kPa) shows enhanced mechanical strength compared to the acylhydrazone

and disulfide crosslinked OSA-DTP hydrogel (maximum compressive stress: 40 kPa) and only the imine crosslinked CMC-OSA hydrogel (maximum compressive stress: 25 kPa). Owning to the exchange behaviors of the dynamic bonds, the hydrogel exhibited injectability and self-healing capacity. Based on the pH responsiveness of the imine and acylhydrazone bonds, the TCN hydrogels showed reversible sol-gel transitions at pH=1 (adding HCl) and pH=7 (adding triethylamine), and exhibited reduction (1,4-dithiothreitol)/oxidation (H_2O_2) responsiveness due to the presence of disulfide bonds in the network.

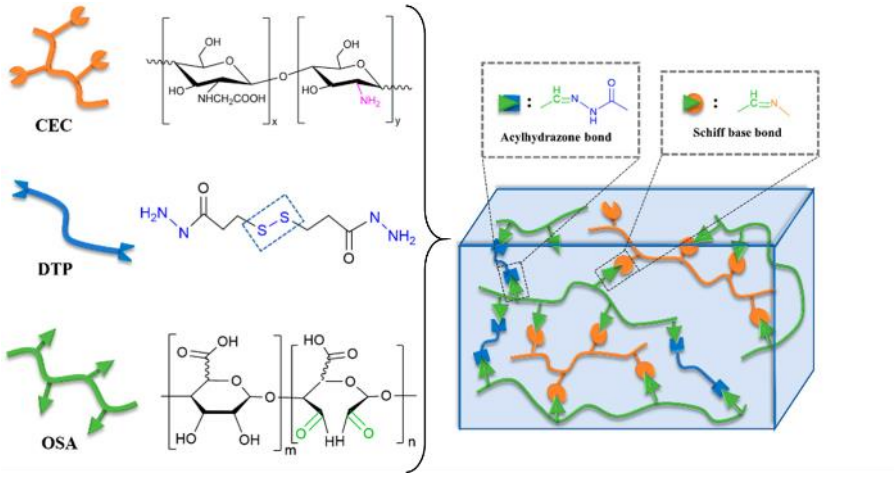

Figure 2.72. Schematic representation for the formation of the TCN hydrogel based on imine bonds, acylhydrazone and disulfide bonds.[312]

In fact, more than just the designed bonds may act as crosslinks in the polymer networks. Entanglements between chains cannot slip or move after the crosslinks are formed. Entanglements can therefore also act as crosslinks and increase their impact on the bulk properties (e.g. elastic modulus) of hydrogels.[127] In addition, some weak interactions between chains (non-covalent interactions) may also act as additional crosslinks. For example, Zhang and Dang et al. designed DCN hydrogels constructed through the formation of imine bonds between collagen and dialdehyde guar, and boronic ester bonds between guar

and borax.[313] However, Fourier transform infrared spectroscopy, sodium dodecyl sulfate polyacrylamide gel electrophoresis, and DSC showed the presence of hydrogen bonding between the macromolecules in addition to the two crosslink types mentioned above, which all contributed to the self-healing of the hydrogels. Besides, they found that the formation of imine and boronic ester bonds leads to entanglement points in DCN, and therefore increases the complex viscosity of the hydrogel. Pourjavadi et al. synthesized a DN hydrogel composed of a covalently crosslinked polyacrylamide network and an imine network between oxidized sodium alginate and glycidyl methacrylate grafted ethylenediamine.[314] The dynamic imine bonds crosslinking the first network, as well as the hydrogen bonds between both networks, provided the hydrogel with self-healing properties. The covalently crosslinked second network was used to withstand stress and stiffen the structure. As a result, the DN hydrogel exhibited high strength, stretchability, self-healing and self-adhesive properties. Liu and Chen et al. reported a TCN hydrogel based on hydrogen bonding, imine bonds and static covalent bonds.[315] The formation of hydrogen and imine bonds between dopamine-grafted oxidized sodium alginate and polyacrylamide chains bestowed on the hydrogel effective self-healing ability (80% mechanical recovery within 6 hours). These two dynamic crosslinks combined with the covalently crosslinked polyacrylamide network were responsible for the TCN hydrogel abilities to withstand large deformations and maintain its elasticity (maximum tensile strain: 2550%, maximum tensile strength: 0.109 MPa).

Heilshorn et al. presented an injectable DN-like hydrogel by using aldehyde-modified hyaluronic acid (HA-ALD) and a hydrazine-modified elastin-like protein (ELP-HYD).[316] The novelty of this method is the use of elastin-like protein (ELP), which is thermo-responsive, cell-adhesive and enzymatically degradable. The hydrazine modified ELP-HYD not only formed the hydrazone crosslinked first network with HA-ALD, but also formed a secondary enhanced network by hydrogen bonding and hydrophobic interactions upon heating due to the thermally responsive phase separation of ELP (**Figure 2.73**). The

use of dynamic hydrazone crosslinking allows the hydrogel to be shear-thinning and protects the cells from the mechanically damaging forces experienced during the injection. The thermal phase separation of the ELP results in the second network which enhances the toughness of the hydrogel and reduces the corrosion rate.

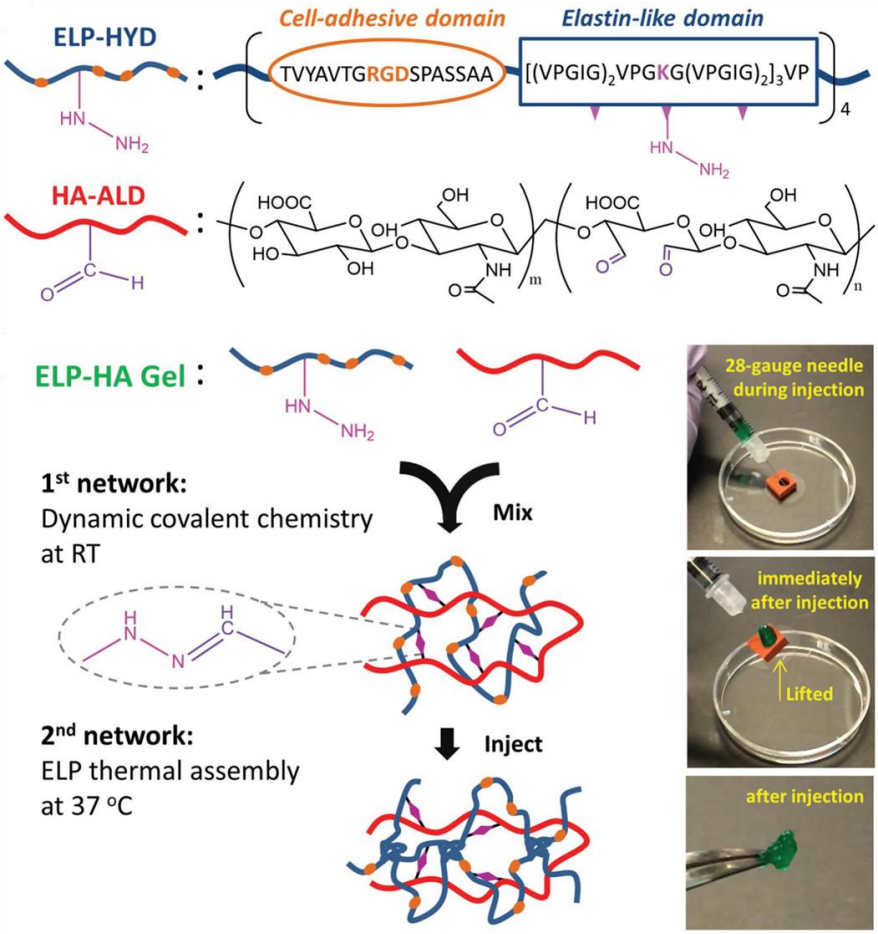

Figure 2.73. Schematic representation for the formation of the DN-like hydrogel based on hydrazone bonds, hydrogen bonds and hydrophobic interactions.[316]

2.6 Conclusion

As discussed above, the intention to use one type of dynamic bonds as crosslinks to produce a 3D gel network can be chosen from the SCN topology, or combined with static covalent bonds to produce a DCN, IPN or DN topology. For combining two or more types of dynamic bonds into a gel system, DCN, IPN and DN are available candidates. Precursors for the synthesis of these hydrogels can be functionalized monomers, synthetic polymers, biopolymers or even nanoparticles or fibers. The properties of the resulting hydrogels depend not only on the nature of the polymer backbone in the final hydrogel, but also benefit from the nature of crosslinks. From the discussion of hydrogels with various topologies based on metal-terpyridine coordination and reversible C=N bonds, it is clear that the introduction of dynamic bonds could provide the hydrogels with the responsiveness of the dynamic bonds to stimuli. In addition, due to the dynamics of these bonds (formation/dissociation/exchange), the networks are dynamic and able to supply hydrogels with properties such as self-healing, shear-thinning, stress relaxation, etc. More importantly, the combination of relatively thermodynamically more unstable bonds with stable bonds (high bond energy or static covalent bonds) in DCN, IPN or DN allows for energy dissipation in the hydrogels which exhibit thus higher mechanical properties (e.g. elastic modulus, toughness, stretchability) than SCN hydrogels crosslinked by a single type of bonds.

In general, by introducing two different types of dynamic bonds into a DCN, IPN or DN hydrogel, the resulting hydrogel has the opportunity to acquire both types of dynamic properties. In addition, it is possible to obtain high mechanical strength hydrogels if there are significant differences in the kinetic and thermodynamic stability of the two dynamic bonds used as crosslinks. For example, using a strong linkage with bond energy and stability close to that of a static covalent bond is responsible for the stability of the structure, while the thermodynamically weak crosslink ruptures during deformation and

dissipates energy.[136] However, the differences in how the three topologies of DCN, IPN and DN affect the dynamic and mechanical properties of hydrogels crosslinked by dynamic bonds have never been investigated.

This thesis therefore aims to combine metal-terpyridine coordination bonds and reversible C=N bonds with different thermodynamic stabilities to construct hydrogels and to understand the contribution of these two types of bonds as network crosslinks to the dynamic and mechanical properties of hydrogels. On these bases, the differences between the three network topologies of DCN, IPN and DN for the construction of dynamic hydrogels will be compared under suitable conditions (e.g. polymer chain length, polymer concentration, crosslink concentration, bond type). We hope that these investigations will provide insights into the selection of multiple dynamic bonds and suitable topologies to achieve the desired hydrogel properties.

2.7 Reference

[1] Wichterle, O.; Lím, D. Hydrophilic gels for biological use. Nature 1960, 185, 117-118.

[2] Demitri, C.; Scalera, F.; Madaghiele, M.; Sannino, A.; Maffezzoli, A. Potential of cellulose-based superabsorbent hydrogels as water reservoir in agriculture. Int. J. Polym. Sci. 2013, 2013, 1-6.

[3] Klein, M.; Poverenov, E. Natural biopolymer-based hydrogels for use in food and agriculture. J. Sci. Food Agric. 2020,100, 2337-2347.

[4] Morin-Crini, N.; Lichtfouse, E.; Torri, G.; Crini, G. Applications of chitosan in food, pharmaceuticals, medicine, cosmetics, agriculture, textiles, pulp and paper, biotechnology, and environmental chemistry. Environ. Chem. Lett. 2019, 17, 1667-1692.

[5] Mittal, H.; Ray S. S.; Okamoto, M. Recent progress on the design and applications of polysaccharide-based graft copolymer hydrogels as adsorbents for wastewater purification. Macromol. Mater. Eng. 2016, 301, 496-522.

[6] Shalla, A. H.; Yaseen, Z.; Bhat, M. A.; Rangreez, T. A.; Maswal, M. Recent review for removal of metal ions by hydrogels. Sep. Sci. Technol. 2019, 54, 89-100.

[7] Jayakumar, A.; Jose, V. K.; Lee, J. M. Hydrogels for medical and environmental applications. Small Methods 2020, 4, 1900735.

[8] Guilherme, M. R.; Aouada, F. A.; Fajardo, A. R.; Martins, A. F.; Paulino, A. T.; Davi, M. F. T.; Rubira, A. F.; Muniz, E. C. Superabsorbent hydrogels based on polysaccharides for application in agriculture as soil conditioner and nutrient carrier: A review. Eur. Polym. J. 2015, 72, 365-385.

[9] Quattrone A.; Czajka A.; Sara S. Thermosensitive hydrogel mask significantly improves skin moisture and skin tone: bilateral clinical trial. Cosmetics 2017, 4, 17.

[10] Hoare, T. R.; Kohane, D. S.; Hydrogels in drug delivery: progress and challenges. Polymer 2008, 49, 1993-2007.

[11] Utech, S.; Prodanovic, R.; Mao, A. S.; Ostafe, R.; Mooney, D. J.; Weitz, D. A. Microfluidic generation of monodisperse, structurally homogeneous alginate microgels for cell encapsulation and 3D cell culture. Adv. Healthcare Mater. 2015, 4, 1628-1633.

[12] Chaudhuri, O. Viscoelastic hydrogels for 3D cell culture. Biomater. Sci. 2017, 5, 1480-1490.

[13] Boateng, J. S.; Matthews, K. H.; Stevens, H. N.; Eccleston, G. M. Wound healing dressings and drug delivery systems: a review. J. Pharm. Sci. 2008, 97, 2892-2923.

[14] Pourshahrestani, S.; Zeimaran, E.; Kadri, N. A.; Mutlu, N.; Boccaccini, A. R. Polymeric hydrogel systems as emerging biomaterial platforms to enable hemostasis and wound healing. Adv. Healthcare Mater. 2020, 9, 2000905.

[15] Singh, Y. P.; Moses, J. C.; Bhardwaj, N.; Mandal, B. B. Injectable hydrogels: a new paradigm for osteochondral tissue engineering. J. Mater. Chem. B 2018, 6, 5499-5529.

[16] Chimisso, V.; Aleman Garcia, M. A.; Yorulmaz Avsar, S.; Dinu, I. A.; Palivan, C. G. Design of bio-conjugated hydrogels for regenerative medicine applications: from polymer scaffold to biomolecule choice. Molecules 2020, 25, 4090.
[17] Deng, G.; Wong, W.-T.; Huang, M.; Wu, R.; Lai, W.-F. Chapter 8: Self-healing properties of hydrogels based on natural polymers. In Hydrogels based on natural polymers. Chen, Y. Ed.; Elsevier, 2019, pp 223-245.
[18] Aswathy, S. H.; Narendrakumar, U.; Manjubala, I. Commercial hydrogels for biomedical applications. Heliyon 2020, 6, e03719.
[19] Gu, Y.; Zhao, J.; Johnson, J. A. A (macro)molecular-level understanding of polymer network topology. Trends Chem. 2019, 1, 318-334.
[20] Ganji, F.; Vasheghani-Farahani, S.; Vasheghani-Farahani, E. Theoretical description of hydrogel swelling: a review. Iran. Polym. J. 2010, 19, 375-398.
[21] Sakai, T. Definition of polymer gels and rubber elasticity. In physics of polymer gels. Sakai, T. Ed.; Wiley-VCH, 2020, pp 45-76.
[22] Ullah, F.; Othman, M. B. H.; Javed, F.; Ahmad, Z.; Akil, H. M. Classification, processing and application of hydrogels: a review. Mater. Sci. Eng. C 2015, 57, 414-433.
[23] Rowan, S. J.; Cantrill, S. J.; Cousins, G. R. L.; Sanders, J. K. M.; Stoddart, J. F. Dynamic covalent chemistry. Angew. Chem., Int. Ed. 2002, 41, 899-952.
[24] Schaufelberger, F.; Timmer, B. J. J.; Ramström, O. Principles of dynamic covalent chemistry. In Dynamic covalent chemistry: principles, reactions, and applications. Zhang, W.; Jin, Y. Ed.; John Wiley & Sons; 2017, pp 1-30.
[25] Zhang, J.-Y.; Zeng, L.-H.; Feng, J. Dynamic covalent gels assembled from small molecules: from discrete gelators to dynamic covalent polymers. Chin. Chem. Lett. 2017, 28, 168-183.
[26] Amaral, A. J. R.; Pasparakis, G. Stimuli responsive self-healing polymers: gels, elastomers and membranes. Polym. Chem. 2017, 8, 6464-6484.
[27] Utrera-Barrios, S.; Verdejo, R.; López-Manchado, M. A.; Hernández Santana, M. Evolution of self-healing elastomers, from extrinsic to combined intrinsic mechanisms: a review. Mater. Horiz. 2020, 7, 2882-2902.
[28] Wang, Z.; Lu, X.; Sun, S.; Yu, C.; Xia, H. Preparation, characterization and properties of intrinsic self-healing elastomers. J. Mater. Chem. B 2019, 7, 4876-4926.
[29] Zheng, N.; Xu, Y.; Zhao, Q.; Xie, T. Dynamic covalent polymer networks: a molecular platform for designing functions beyond chemical recycling and self-healing. 2021, 121, 1716-1745.
[30] Van Zee, N. J.; NicolaÿR. Vitrimers: Permanently crosslinked polymers with dynamic network topology. Prog. Polym. Sci. 2020, 104, 101233.
[31] Barui, A. Synthetic polymeric gel. In polymeric gels; Pal, K.; Banerjee, I. Ed.; Elsevier, 2018, pp 55-90.
[32] Wang, W.; Narain, R.; Zeng, H. Chapter 10: Hydrogels. In polymer science and nanotechnology; Narain, R. Ed.; Elsevier, 2020, pp 203-244.
[33] Thakur, G.; Rodrigues, F. C.; Dathathri, E.; Nayak, S. K.; Pal, K. Protein-based gels: preparation, characterizations, applications in drug delivery, and tissue engineering. In polymeric gels; Pal, K.; Banerjee, I. Eds.; Elsevier, 2018; pp 31-54.
[34] Wang, W.; Narain, R., Zeng, H.; Rational design of self-healing tough hydrogels: a mini review. Front. Chem. 2018, 6, 497.

[35] Xiao, T.; Xu, L.; Zhou, L.; Sun, X.-Q.; Lin, C.; Wang, L. Dynamic hydrogels mediated by macrocyclic host-guest interactions. J. Mater. Chem. B 2019, 7, 1526.
[36] Picchioni, F.; Muljana, H. Hydrogels based on dynamic covalent and non covalent bonds: a chemistry perspective. Gels 2018, 4, 21.
[37] Mantooth, S. M.; Munoz-Robles, B. G.; Webber, M. J. Dynamic hydrogels from host-guest supramolecular interactions. Macromol. Biosci. 2019, 19, e1800281.
[38] Zhao, D.; Zhu, Y.; Cheng, W.; Xu, G.; Wang, Q.; Liu, S.; Li, J.; Chen, C.; Yu, H.; Hu, L. A dynamic gel with reversible and tunable topological networks and performances. Matter. 2020, 2, 390-403.
[39] Perera, M. M.; Ayres, N. Dynamic covalent bonds in self-healing, shape memory, and controllable stiffness hydrogels. Polym. Chem. 2020, 11,1410-1423.
[40] Li, Y.; Zhu, C.; Dong, Y.; Liu, D. Supramolecular hydrogels: mechanical strengthening with dynamics. Polymer 2020, 210, 122993.
[41] Ryan, K. R.; Down, M. P.; Banks, C. E. Future of additive manufacturing: overview of 4D and 3D printed smart and advanced materials and their applications. Chem. Eng. J. 2021, 403, 126162.
[42] Olvera, D.; Monaghan, M. G. Electroactive material-based biosensors for detection and drug delivery. Adv. Drug Deliv. Rev. 2021, 170, 396-424.
[43] Liu, X.; Liu, J.; Lin, S.; Zhao, X. Hydrogel machines. Mater. Today 2020, 36, 102-124.
[44] Li, S.; Zhou, X.; Dong, Y.; Li, J. Flexible self-repairing materials for wearable sensing applications: elastomers and hydrogels. Macromol. Rapid Commun. 2020, 41, 2000444.
[45] Dzhardimalieva, G. I.; Yadav, B. C.; Kudaibergenov, S. E.; Uflyand, I. E. Basic approaches to the design of intrinsic self-healing polymers for triboelectric nanogenerators. Polymers 2020, 12, 2594.
[46] Guo, Y.; Bae, J.; Zhao, F.; Yu, G. Functional hydrogels for next-generation batteries and supercapacitors. Trends Chem. 2019, 1, 335-348.
[47] Fu, R.; Tu, L.; Zhou, Y.; Fan, L.; Zhang, F.; Wang, Z.; Xing, J.; Chen, D.; Deng, C.; Tan, G.; Yu, P.; Zhou, L.; Ning, C. A tough and self-powered hydrogel for artificial skin. Chem. Mater. 2019, 31, 9850-9860.
[48] Kong, W.; Wang, C.; Jia, C.; Kuang, Y.; Pastel, G.; Chen, C.; Chen, G.; He, S.; Huang, H.; Zhang, J.; Wang, S.; Hu, L. Muscle-inspired highly anisotropic, strong, ion-conductive hydrogels. Adv. Mater. 2018, 1801934.
[49] Wojtecki, R J.; Meador, M. A.; Rowan, S. T. Using the dynamic bond to access macroscopically responsive structurally dynamic polymers. Nat. Mater. 2011, 10, 14-27.
[50] Sattar, M. A.; Patnaik, A. Design principles of interfacial dynamic bonds in self-healing materials: what are the parameters? Chem. Asian J. 2020, 15, 4215-4240.
[51] De Alwis Watuthanthrige, N.; Chakma, C.; Konkolewicz, D. Designing dynamic materials from dynamic bonds to macromolecular architecture. Trends Chem. 2021, 3, 231-247.
[52] Creton, C. 50th anniversary perspective: networks and gels: soft but dynamic and tough. Macromolecules 2017, 50, 8297-8316.
[53] Zou, W.; Dong, J.; Luo, Y.; Zhao, Q.; Xie, T. Dynamic covalent polymer networks: from old chemistry to modern day innovations. Adv. Mater. 2017, 29, 1606100.

[54] Deng, G. H.; Li, F. Y.; Yu, H. X.; Liu, F. Y.; Liu, C. Y.; Sun, W. X.; Jiang, H. F.; Chen, Y. M. Dynamic hydrogels with an environmental adaptive self-healing ability and dual responsive sol-gel transitions. ACS Macro Lett. 2012, 1, 275-279.
[55] Jiang, Z.; Bhaskaran, A.; Aitken, H. M.; Shackleford, I. C. G.; Connal, L. A. Using synergistic multiple dynamic bonds to construct polymers with engineered properties. Macromol. Rapid Commun. 2019, 40, 1900038.
[56] Hammer, L.; Van Zee, N. J. NicolaÿR. Dually crosslinked polymer networks incorporating dynamic covalent bonds. Polymers 2021, 13, 396.
[57] Huang, S.; Kong, X.; Xiong, Y.; Zhang, X.; Chen, H.; Jiang, W.; Niu, Y.; Xu, W.; Ren, C. An overview of dynamic covalent bonds in polymer material and their applications. Eur. Polym. J. 2020, 141, 110094.
[58] Zhang, Z. P.; Rong, M. Z.; Zhang, M. Q. Polymer engineering based on reversible covalent chemistry: a promising innovative pathway towards new materials and new functionalities. Prog. Polym. Sci. 2018, 80, 39-93.
[59] Appel, E. A.; del Barrio, J.; Loh, X. J.; Scherman, O. A. Supramolecular polymeric hydrogels. Chem. Soc. Rev. 2012, 41, 6195-6214.
[60] Feliciano, A. J.; van Blitterswijk, C.; Moroni, L.; Baker, M. B. Realizing tissue integration with supramolecular hydrogels. Acta Biomater. 2021, 124, 1-14.
[61] Ariga, K.; Kunitake, T. Ed.; Supramolecular chemistry fundamentals and applications: advanced textbook. Springer-Verlag Berlin Heidelberg, 2006.
[62] Lehn, J.-M. Ed.; Supramolecular chemistry, concepts and perspectives. VCH Verlagsgesellschaft mbH: Weinheim, Germany, 1995.
[63] Aeridou, E.; Díaz Díaz, D.; Alemán, C.; Pérez-Madrigal, M. M. Advanced functional hydrogel biomaterials based on dynamic B-O bonds and polysaccharide building blocks. Biomacromolecules 2020, 21, 3984-3996.
[64] Podgórski, M.; Fairbanks, B. D.; Kirkpatrick, B. E.; McBride, M.; Martinez, A.; Dobson, A.; Bongiardina, N. J.; Bowman, C. N. Toward stimuli-responsive dynamic thermosets through continuous development and improvements in covalent adaptable networks (CANs). Adv. Mater. 2020, 32, 1906876.
[65] Winne, J. M.; Leibler, L.; Du Prez, F. E. Dynamic covalent chemistry in polymer networks: a mechanistic perspective. Polym. Chem. 2019, 10, 6091-6108.
[66] Steed, J. W.; Turner, D. R.; Wallace, K. Ed.; Core concepts in supramolecular chemistry and nanochemistry. John Wiley & Sons: 2007.
[67] van Ruymbeke, E. Preface: special issue on associating polymers. J. Rheol. 2017, 61, 1099-1102.
[68] Potaufeux, J.-E.; Odent, J.; Notta-Cuvier, D.; Lauro, F.; Raquez, J.-M. A comprehensive review of the structures and properties of ionic polymeric materials. Polym. Chem., 2020, 11, 5914-5936.
[69] Lewis C. L.; Dell, E. M.; A review of shape memory polymers bearing reversible binding groups. J. Polym. Sci., Part B: Polym. Phys. 2016, 54, 1340-1364.
[70] Gohy, J.-F. Metallo-supramolecular block copolymer micelles. 2009, 253, 2214-2225.
[71] Ruben, M.; Rojo, J.; Romero-Salguero, F. J.; Uppadine, L. H.; Lehn, J.-M. Grid-type metal ion architectures: functional metallosupramolecular arrays. Angew. Chem. Int. Ed. 2004, 43, 3644-3662.
[72] Shi, L.; Ding, P.; Wang, Y.; Zhang, Y.; Ossipov, D.; Hilborn, J. Self-healing polymeric hydrogel formed by metal-ligand coordination assembly: design,

fabrication, and biomedical applications. Macromol. Rapid Commun. 2019, 40, 1800837.
[73] Lu, W.; Le, X.; Zhang, J.; Huang, Y.; Chen, T. Supramolecular shape memory hydrogels: a new bridge between stimuli-responsive polymers and supramolecular chemistry. Chem. Soc. Rev. 2017, 46, 1284-1294.
[74] Gyarmati, B.; Szilágyi, B. Á.; Szilágyi, A. Reversible interactions in self-healing and shape memory hydrogels. Eur. Polym. J. 2017, 93, 642-669.
[75] McWhinnie, W. R.; Miller, J. D. The chemistry of complexes containing 2,2′-bipyridyl, 1, 10-phenanthroline, or 2,2′,6′,2″-terpyridyl as ligands. Adv. Inorg. Chem. Radiochem. 1970, 12, 135-215.
[76] Winter, A.; Schubert, U. S. Synthesis and characterization of metallo-supramolecular polymers. Chem. Soc. Rev. 2016, 45, 5311-5357.
[77] Holyer, R. H.; Hubbard, C. D.; Kettle, S. F. A.; Wilkins, R. G. The kinetics of replacement reactions of complexes of the transition metals with 2,2′,2"-terpyridine. Inorg. Chem. 1966, 5, 622-625.
[78] Calì, R.; Rizzarelli, E.; Sammartano, S.; Siracusa, G. Thermodynamics of 2,2′,2″-terpyridinecopper(II) complexes in aqueous solution. Transit. Met. Chem. 1979, 4, 328-332.
[79] Dobrawa, R.; Ballester, P.; Saha-Möller, C. R.; Würthner, F. Thermodynamics of 2,2′:6′,2″-terpyridine-metal ion complexation. ACS Symp. Ser. 2006, 928, 43-62.
[80] Ahmadi, M.; Seiffert, S. Thermodynamic control over energy dissipation modes in dual-network hydrogels based on metal-ligand coordination. Soft Matter 2020, 16, 2332-2341.
[81] Ahmadi, M.; Seiffert, S. Dynamic model metallo-supramolecular dual-network hydrogels with independently tunable network crosslinks. J. Polym. Sci. 2020, 58, 330-342.
[82] Rodgers, M. T.; Armentrout, P. B. Noncovalent metal-ligand bond energies as studied by threshold collision-induced dissociation. Mass Spectrom. Rev. 2000, 19, 215-247.
[83] Lohmeijer, B. G. G. Playing LEGO with macromolecules: connecting polymer chains using terpyridine metal complexes. Technische Universiteit Eindhoven. 2004. https://doi.org/10.6100/IR581839.
[84] Bowman, C. N.; Kloxin, C. J. Covalent adaptable networks: reversible bond structures incorporated in polymer networks. Angew. Chem. Int. Ed. 2012, 51, 4272-4274.
[85] McBride, M. K.; Worrell, B. T.; Brown, T.; Cox, L. M.; Sowan, N.; Wang, C.; Podgorski, M.; Martinez, A. M.; Bowman, C. N. Enabling applications of covalent adaptable networks. Annu. Rev. Chem. Biomol. Eng. 2019, 10, 175-198.
[86] Wu, Y.; Wei, Y.; Ji, Y. Polymer actuators based on covalent adaptable networks. Polym. Chem. 2020, 11,5297-5320.
[87] Dahlke, J.; Zechel, S.; Hager, M. D.; Schubert, U. S. How to design a self-healing polymer: general concepts of dynamic covalent bonds and their application for intrinsic healable materials. Adv. Mater. Interfaces 2018, 5, 1800051.
[88] Layer, R. W. The chemistry of imines. Chem. Rev. 1963, 63, 489-510.
[89] Carey, F. A.; Sundberg, R. J. Ed.; Advanced organic chemistry, Vol. A, 5th ed. Springer, New York, 2007, pp. 645-653.
[90] Jiao, T.; Wu, G.; Zhang, Y.; Shen, L.; Lei, Y.; Wang, C. -Y.; Fahrenbach, A. C.; Li, H. Self-assembly in water with N-substituted imines. Angew. Chem. Int. Ed. 2020, 59, 18350-18367.

[91] Jencks, W. P. Ed.; Mechanism and catalysis of simple carbonyl group reactions. In Progress in physical organic chemistry, Volume 2. John Wiley & Sons, lnc. 1964, pp. 63-128.
[92] Ciaccia, M.; Di Stefano, S. Mechanisms of imine exchange reactions in organic solvents. Org. Biomol. Chem. 2015,13, 646-654.
[93] Agten, S. M.; Suylen, D. P. L.; Hackeng, T. M. Oxime catalysis by freezing. Bioconjugate Chem. 2016, 27, 42-46.
[94] Yang, X.; Liu, G.; Peng, L.; Guo, J.; Tao, L.; Yuan, J.; Chang, C.; Wei, Y.; Zhang, L. Highly efficient self-healable and dual responsive cellulose-based hydrogels for controlled release and 3D cell culture. Adv. Funct. Mater. 2017, 27, 1703174.
[95] Egberink, H.; van Heerden, C. The mechanism of the formation and hydrolysis of cyclohexanone oxime in aqueous solutions. Anal. Chim. Acta 1980, 118, 359-368.
[96] Cordes, E. H.; Jencks, W. P. Nucleophilic catalysis of semicarbazone formation by anilines. J. Am. Chem. Soc. 1962, 84, 826-831.
[97] Dirksen, A.; Dirksen, S.; Hackeng, T. M.; Dawson, P. E. Nucleophilic catalysis of hydrazone formation and transimination: implications for dynamic covalent chemistry. J. Am. Chem. Soc. 2006, 128, 15602-15603.
[98] Kölmel, D. K.; Kool, E. T. Oximes and hydrazones in bioconjugation: mechanism and catalysis. Chem. Rev. 2017, 117, 10358-10376.
[99] Crisalli, P.; Kool, E. T. Water-soluble organocatalysts for hydrazone and oxime formation. J. Org. Chem. 2013, 78, 1184-1189.
[100] Larsen, D.; Pittelkow, M.; Karmakar, S.; Kool, E. T. New organocatalyst scaffolds with high activity in promoting hydrazone and oxime formation at neutral pH. Org. Lett. 2015, 17, 274-277.
[101] Zhou, Y.; Piergentili, I.; Hong, J.; van der Helm, M. P.; Macchione, M.; Li, Y.; Eelkema, R.; Luo, S. Indoline catalyzed acylhydrazone/oxime condensation under neutral aqueous conditions. Org. Lett. 2020, 22, 6035-6040.
[102] Pifferi, C.; Daskhan, G. C.; Fiore, M.; Shiao, T. C.; Roy, R.; Renaudet, O. Aminooxylated carbohydrates: synthesis and applications. Chem. Rev. 2017, 117, 9839-9873.
[103] Jencks, W. P. Studies on the mechanism of oxime and semicarbazone formation. J. Am. Chem. Soc. 1959, 81, 475-481.
[104] Kalia J.; Raines, R. T. Hydrolytic stability of hydrazones and oximes. Angew. Chem. Int. Ed. 2008, 47, 7523-7526.
[105] Hafeez, S.; Ooi, H.; Morgan, F.; Mota, C.; Dettin, M.; van Blitterswijk, C.; Moroni, L.; Baker, M. Viscoelastic oxidized alginates with reversible imine type crosslinks: self-healing, injectable, and bioprintable hydrogels. Gels 2018, 4, 85.
[106] Sims, M. B.; Patel, K. Y.; Bhatta, M.; Mukherjee, S.; Sumerlin, B. S. Harnessing imine diversity to tune hyperbranched polymer degradation. Macromolecules 2018, 51, 356-363.
[107] Belowich, M. E.; Stoddart, J. F. Dynamic imine chemistry. Chem. Soc. Rev. 2012, 41, 2003-2024.
[108] Collins, J.; Xiao, Z.; Connal, L. A. Tunable degradation of polyethylene glycol-like polymers based on imine and oxime bonds. J. Polym. Sci., Part A: Polym. Chem. 2017, 55, 3826-3831.
[109] Liu, Y.; Tang, Z.; Chen, Y.; Wu, S.; Guo, B. Programmingdynamic imine bond into elastomer/graphene composite toward mechanically strong, malleable,

and multi-stimuli responsive vitrimer. Compos. Sci. Technol. 2018, 168, 214-223.
[110] Hajj, R.; Duval, A.; Dhers, S.; Avérous, L. Network design to control polyimine vitrimer properties: physical versus chemical approach. Macromolecules 2020, 53, 3796-3805.
[111] Tao, Y.; Cai, K.; Liu, S.; Zhang, Y.; Chi, Z.; Xu, J. Pseudo target release behavior of simvastatin through pH-responsive polymer based on dynamic imine bonds: promotes rapid proliferation of osteoblasts. Mater. Sci. Eng. C Mater. Biol. Appl. 2020, 113, 110979.
[112] Hermanson, G. T. Hydrazine and hydrazide derivatives. In bioconjugate techniques, 3rd ed., Academic Press, 2013, pp. 251-252.
[113] Kool, E. T.; Park, D. H.; Crisalli, P. Fast hydrazone reactants: electronic and acid/base effects strongly influence rate at biological pH. J. Am. Chem. Soc. 2013, 135, 17663-17666.
[114] Spicer, C. D.; Pashuck, E. T.; Stevens, M. M. Achieving controlled biomolecule-biomaterial conjugation. Chem. Rev. 2018, 118, 7702-7743.
[115] Wahbeh, J.; Milkowski, S.; The use of hydrazones for biomedical applications, SLAS Technol. 2019, 24, 161-168.
[116] Li, P.; Zhong, Y.; Wang, X.; Hao, J. Enzyme-regulated healable polymeric hydrogels. ACS Cent. Sci. 2020, 6, 1507-1522.
[117] van der Helm, M. P.; Klemm, B.; Eelkema, R. Organocatalysis in aqueous media. Nat. Rev. Chem. 2019, 3, 491-508.
[118] Vigato, P. A.; Tamburini, S. The challenge of cyclic and acyclic Schiff bases and related derivatives. Coord. Chem. Rev. 2004, 248, 1717-2128.
[119] Cozzi, P. G. Metal-salen Schiff base complexes in catalysis: practical aspects. Chem. Soc. Rev. 2004, 33, 410-421.
[120] Miroslaw, B. Homo- and hetero-oligonuclear complexes of platinum group metals (pgm) coordinated by imine Schiff base ligands. Int. J. Mol. Sci. 2020, 21, 3493.
[121] Zhou, B.; Zuo, C.; Xiao, Z.; Zhou, X.; He, D.; Xie, X.; Xue, Z. Self-healing polymer electrolytes formed via dual-networks: a new strategy for flexible lithium metal batteries. Chem. Eur. J. 2018, 24, 19200-19207.
[122] Wang, R.; Wang, X.; Zhan, Y.; Xu, Z.; Xu, Z.; Feng, X.; Li, S.; Xu, H. A dual network hydrogel sunscreen based on poly-gamma-glutamic acid/tannic acid demonstrates excellent anti-uv, self-recovery, and skin-integration capacities. ACS Appl. Mater. Interfaces 2019, 11, 37502-37512.
[123] Hu, X.; Zhou, J.; Daniel, W. F. M.; Vatankhah-Varnoosfaderani, M.; Dobrynin, A. V.; Sheiko, S. S. Dynamics of dual networks: strain rate and temperature effects in hydrogels with reversible H-bonds. Macromolecules 2017, 50, 652-659.
[124] Wen, J.; Pan, M.; Yuan, J.; Wang, J.; Zhu, L.; Jia, Z.; Song, S. Facile fabrication of dual-crosslinked single network heterostructural polyurethane hydrogels with superior mechanical and fluorescent performance. React. Funct. Polym. 2020, 146, 104433.
[125] Alemán, J. V.; Chadwick, A. V.; He, J.; Hess, M.; Horie, K.; Jones, R. G.; Kratochvíl, P.; Meisel, I.; Mita, I.; Moad, G.; Penczek, S.; Stepto, R. F. T. Definitions of terms relating to the structure and processing of sols, gels, networks, and inorganic-organic hybrid materials. IUPAC Recommendations. Pure Appl. Chem. 2007, 79, 1801-1829.

[126] James, J.; Thomas, G. V.; Akhina, H.; Thomas, S.; Micro- and nano-structured interpenetrating polymer networks: state of the art, new challenges and opportunities. In Micro- and nano-structured interpenetrating polymer networks: from design to applications: Thomas, S.; Grande, D.; Cvelbar, U.; Raju, K. V. S. N.; Narayan, R.; Thomas, S. P. Ed.; Wiley, 2016, pp 1-27.
[127] Sperling, L. H. Interpenetrating polymer networks and related materials, Plenum Press, New York, 1981, pp 1-30.
[128] Klempner, D.; Sperling, L. H.; Utracki, L. A. Interpenetrating polymer networks, American Chemical Society, Washington DC, 1994, pp. 3-39.
[129] Wu, X.; He, G.; Yan, X.; Li, X.; Xiao, W.; Jiang, X. Miscibility, morphology, and phase behavior of IPNs. In Micro- and nano-structured interpenetrating polymer networks: from design to applications: Thomas, S.; Grande, D.; Cvelbar, U.; Raju, K. V. S. N.; Narayan, R.; Thomas, S. P. Ed.; Wiley, 2016, pp 29-68.
[130] Dhand, A. P.; Galarraga, J. H.; Burdick, J. A. Enhancing biopolymer hydrogel functionality through interpenetrating networks. Trends. Biotechnol. 2021, 39, 519-538.
[131] Silverstein, M. S. Interpenetrating polymer networks: so happy together? Polymer 2020, 207, 122929.
[132] Mathew, A.P. Interpenetrating polymer networks: processing, properties and applications. In Advances in elastomers I. Ochsner, A.; Silva, L. F. M.; Altenbach, H. Ed.; Springer, Berlin, pp 283-301.
[133] Gong, J. P.; Katsuyama, Y.; Kurokawa, T.; Osada, Y. Double-network hydrogels with extremely high mechanical strength. Adv. Mater. 2003, 15, 1155-1158.
[134] Chen, Q.; Chen, H.; Zhu, L.; Zheng, J. Fundamentals of double network hydrogels. J. Mater. Chem. B, 2015, 3, 3654-3676.
[135] Gong, J. P. Why are double network hydrogels so tough? Soft Matter 2010, 6, 2583-2590.
[136] Gong, J. P. Materials both tough and soft. Science 2014, 344, 161-162.
[137] Chen, Q.; Chen, H.; Zhu, L.; Zheng J. Engineering of tough double network hydrogels. Macromol. Chem. Phys. 2016, 217, 1022-1036.
[138] Yang, J.; Li, Y.; Zhu, L.; Qin, G.; Chen, Q. Double network hydrogels with controlled shape deformation: a mini review. J. Polym. Sci., Part B: Polym. Phys. 2018, 56, 1351-1362.
[139] Xu, X.; Jerca, V. V.; Hoogenboom, R. Bioinspired double network hydrogels: from covalent double network hydrogels via hybrid double network hydrogels to physical double network hydrogels. Mater. Horiz. 2021, doi: 10.1039/d0mh01514h.
[140] Henderson, K. J.; Zhou, T. C.; Otim, K. J.; Shull, K. R. Ionically cross-linked triblock copolymer hydrogels with high strength. Macromolecules 2010, 43, 6193-6201.
[141] Zhang, Q.; Niu, S.; Wang, L.; Lopez, J.; Chen, S.; Cai, Y.; Du, R.; Liu, Y.; Lai, J. C.; Liu, L.; Li, C. H.; Yan, X.; Liu, C.; Tok, J. B.; Jia, X.; Bao, Z. An elastic autonomous self-healing capacitive sensor based on a dynamic dual crosslinked chemical system. Adv. Mater. 2018, 1801435.
[142] Peng, W. L.; Zhang, Z. P.; Rong, M. Z.; Zhang, M. Q. Reversibly interlocked macromolecule networks with enhanced mechanical properties and wide pH range of underwater self-healability. ACS Appl. Mater. Interfaces 2020, 12, 27614-27624.

[143] Danielsen, S. P. O.; Beech, H. K.; Wang, S.; El-Zaatari, B. M.; Wang, X.; Sapir, L.; Ouchi, T.; Wang, Z.; Johnson, P. N.; Hu, Y.; Lundberg, D. J.; Stoychev, G.; Craig, S. L.; Johnson, J. A.; Kalow, J. A.; Olsen, B. D.; Rubinstein, M. Molecular characterization of polymer networks. Chem. Rev. 2021, 121, 8, 5042-5092.

[144] Tang, S.; Richardson, B. M.; Anseth, K. S. Dynamic covalent hydrogels as biomaterials to mimic the viscoelasticity of soft tissues. Prog. Mater Sci. 2020, doi: 10.1016/j.pmatsci.2020.100738.

[145] Sathaye, S.; Mbi, A.; Sonmez, C.; Chen, Y.; Blair, D. L.; Schneider, J. P.; Pochan, D. J. Rheology of peptide- and protein-based physical hydrogels: are everyday measurements just scratching the surface? Wiley Interdiscip. Rev.: Nanomed. Nanobiotechnol. 2015, 7, 34-68.

[146] Mezger T. G. The rheology handbook, 4th Edn. Vincentz, Hannover, 2014.

[147] Yan, C.; Pochan, D. J. Rheological properties of peptide-based hydrogels for biomedical and other applications. Chem. Soc. Rev. 2010, 39, 3528-3540.

[148] Chopin-Doroteo, M.; Mandujano-Tinoco, E. A.; Krotzsch, E. Tailoring of the rheological properties of bioinks to improve bioprinting and bioassembly for tissue replacement. Biochim. Biophys. Acta-Gen. Subj. 2021, 1865, 129782.

[149] Boufas, S.; Benhamza, M. E. H.; Ben Seghir, B.; Hadria, F. Synthesis and characterization of chitosan/carrageenan/hydroxyethyl cellulose blended gels. Asian J. Research Chem. 2020, 13, 209-215.

[150] Czarnecki, S.; Rossow, T.; Seiffert, S. Hybrid polymer-network hydrogels with tunable mechanical response. Polymers 2016, 8, 82.

[151] Dawn, A.; Kumari, H. Low molecular weight supramolecular gels under shear: rheology as the tool for elucidating structure-function correlation. Chem. Eur. J. 2018, 24,762-776.

[152] Shi, W. H.; Pathiranage, T. M. S. K.; Marciel, A. B. Rheological properties of engineered protein polymer networks. MRS Bull. 2020, 45, 1048-1054.

[153] Rossow, T.; Hackelbusch, S.; Van Assenbergh, P.; Seiffert, S. A modular construction kit for supramolecular polymer gels. Polym. Chem. 2013, 4, 2515-2527.

[154] Hofmeier, H.; El-Ghayoury, A.; Schubert, U. S. Combination of supramolecular cross-linking with covalent cross-linking through epoxide ring-opening including gel studies. e-Polymers, 2003, 053, 1-15.

[155] Schubert, U.; Hofmeier, H.; Newkome, G. R. Modern terpyridine chemistry; Wiley-VCH: Weinheim, Germany, 2006.

[156] Shunmugam, R.; Gabriel, G. J.; Aamer, K. A.; Tew, G. N. Metal-ligand-containing polymers: terpyridine as the supramolecular unit. Macromol. Rapid Commun. 2010, 31,784-793.

[157] Schubert, U. S.; Winter, A.; Newkome, G. R. Terpyridine-based materials. Wiley-VCH: Weinheim, 2011.

[158] Brassinne, J.; Fustin, C.-A.; Gohy, J.-F. Polymer gels constructed through metal-ligand coordination. J. Inorg. Organomet. Polym. 2013, 23, 24-40.

[159] Kimura, M.; Nakagawa, Y.; Adachi, N.; Tatewaki, Y.; Fukawa, T.; Shirai, H. Metallosupramolecular gels made of four-armed poly-(ethylene glycol)s having terpyridine termini. Chem. Lett. 2009, 38, 382-383.

[160] Asoh, T. -A.; Yoshitake, H.; Takano, Y.; Kikuchi, A. Fabrication of self-healable hydrogels through sol-gel transition in metallo-supramolecular aqueous solution by aeration. Macromol. Chem. Phys. 2013, 214, 2534-2539.

[161] Rossow, T.; Habicht, A.; Seiffert, S. Relaxation and dynamics in transient polymer model networks. Macromolecules 2014, 47, 6473-6482.
[162] Rossow, T.; Seiffert, S. Supramolecular polymer gels with potential model-network structure. Polym. Chem. 2014, 5, 3018-3029.
[163] Tang, S.; Habicht, A.; Li, S.; Seiffert, S.; Olsen, B. D. Self-diffusion of associating star-shaped polymers. Macromolecules 2016, 49, 5599-5608.
[164] Habicht, A.; Czarnecki, S.; Rossow, T.; Seiffert, S. Connectivity defects enhance chain dynamics in supramolecular polymer model-network gels. J. Polym. Sci. Part B: Polym. Phys. 2017, 55, 19-29.
[165] Schmolke, W.; Ahmadi, M.; Seiffert, S. Enhancement of metallo-supramolecular dissociation kinetics in telechelic terpyridine-capped poly(ethylene glycol) assemblies in the semi-dilute regime. Phys. Chem. Chem. Phys. 2019, 21, 19623-19638.
[166] Wang, R.; Geven, M.; Dijkstra, P. J.; Martens, P.; Karperien, M. Hydrogels by supramolecular crosslinking of terpyridine end group functionalized 8-arm poly(ethylene glycol). Soft Matter 2014, 10,7328-7336.
[167] Wang, R.; Both, S. K.; Geven, M.; Calucci, L.; Forte, C.; Dijkstra, P. J.; Karperien, M. Kinetically stable metal ligand charge transfer complexes as crosslinks in nanogels/hydrogels: physical properties and cytotoxicity. Acta Biomater. 2014, 26, 136-144.
[168] Creusen, G.; Roshanasan, A.; Garcia Lopez, J.; Peneva, K.; Walther, A. Bottom-up design of model network elastomers and hydrogels from precise star polymers. Polym. Chem. 2019, 10, 3740-3750.
[169] Jochum, F. D.; Brassinne, J.; Fustin, C.-A.; Gohy, J.-F. Metallo-supramolecular hydrogels based on copolymers bearing terpyridine side-chain ligands. Soft Matter 2013, 9, 2314-2320.
[170] Brassinne, J.; Jochum, F.; Fustin, C.-A.; Gohy, J.-F. Revealing the supramolecular nature of side-chain terpyridine-functionalized polymer networks. Int. J. Mol. Sci. 2015, 16, 990-1007.
[171] Xu, X.; Jerca, F. A.; Jerca, V. V.; Hoogenboom, R. Self-healing and moldable poly(2-isopropenyl-2-oxazoline) supramolecular hydrogels based on a transient metal coordination network. Macromolecules 2020, 53, 6566-6575.
[172] Es Sayed, J.; Meyer, C.; Sanson, N.; Perrin, P. Oxidation-responsive emulsions stabilized by cleavable metallo-supramolecular cross-linked microgels. ACS Macro. Lett. 2020, 9, 1040-1045.
[173] Xin, Y.; Yuan, J. Schiff's base as a stimuli-responsive linker in polymer chemistry. Polym. Chem. 2012, 3, 3045-3055.
[174] Apostolides, D. E.; Patrickios, C. S. Dynamic covalent polymer hydrogels and organogels crosslinked through acylhydrazone bonds: synthesis, characterization and applications. Polym. Int. 2018, 67, 627-649.
[175] Xu, J.; Liu, Y.; Hsu, S. H. Hydrogels based on Schiff base linkages for biomedical applications. Molecules 2019, 24, 3005.
[176] Xu, Y.; Li, Y.; Chen, Q.; Fu, L.; Tao, L.; Wei, Y. Injectable and self-healing chitosan hydrogel based on imine bonds: design and therapeutic applications. Int. J. Mol. Sci. 2018, 19, 2198.
[177] Zhang, Z.; He, C.; Chen, X. Hydrogels based on pH-responsive reversible carbon-nitrogen double-bond linkages for biomedical applications. Mater. Chem. Front. 2018, 2, 1765-1778.

[178] Antony, R.; Arun, T.; Manickam, S. T. D. A review on applications of chitosan-based Schiff bases. Int. J. Biol. Macromol. 2019, 129, 615-633.
[179] Kilic R.; Sanyal A. Self-healing hydrogels based on reversible covalent linkages: a survey of dynamic chemical bonds in network formation. In Self-healing and self-recovering hydrogels. Creton C.; Okay O. Ed; Springer, Cham. Adv. Polym. Sci. 2020, 285. pp 243-294.
[180] Zhang, Y.; Tao, L.; Li, S.; Wei, Y. Synthesis of multiresponsive and dynamic chitosan-based hydrogels for controlled release of bioactive molecules. Biomacromolecules 2011, 12, 2894-2901.
[181] Yang, X.; Wang, B.; Sha, D.; Liu, Y.; Xu, J.; Shi, K.; Yu, C.; Ji, X. Injectable and antibacterial ε-poly(l-lysine)-modified poly(vinyl alcohol)/chitosan/AgNPs hydrogels as wound healing dressings. Polymer 2021, 212, 123155.
[182] Qu, J.; Zhao, X.; Liang, Y.; Xu, Y.; Ma, P. X.; Guo, B. Degradable conductive injectable hydrogels as novel antibacterial, anti-oxidant wound dressings for wound healing. Chem. Eng. J. 2019, 362, 548-560.
[183] Vahedi, M.; Shokrolahi, F.; Barzin, J.; Shokrollahi, P.; Taghiyar, L.; Ashtiani, M. K. Amylopectin multiple aldehyde crosslinked hydrogel as an injectable and self-healing cell carrier for bone tissue engineering. Macromol. Mater. Eng. 2020, 305, 2000045.
[184] Li, K.; Wang, J.; Li, P.; Fan, Y. Ternary hydrogels with tunable mechanical and self-healing properties based on the synergistic effects of multiple dynamic bonds. J. Mater. Chem. B 2020, 8, 4660-4671.
[185] Du, S.; Chen, X.; Chen, X.; Li, S.; Yuan, G.; Zhou, T.; Li, J.; Jia, Y.; Xiong, D.; Tan, H. Covalent chitosan-cellulose hydrogels via Schiff-base reaction containing macromolecular microgels for pH-sensitive drug delivery and wound dressing. Macromol. Chem. Phys. 2019, 220, 1900399.
[186] Liang, Y.; Zhao, X.; Ma, P. X.; Guo, B.; Du. Y.; Han, X. pH-Responsive injectable hydrogels with mucosal adhesiveness based on chitosan-grafted-dihydrocaffeic acid and oxidized pullulan for localized drug delivery. J. Colloid Interface Sci. 2019, 536, 224-234.
[187] Yu, R.; Zhang, Y.; Barboiu, M.; Maumus, M.; Noel, D.; Jorgensen, C.; Li, S. Biobased pH-responsive and self-healing hydrogels prepared from o-carboxymethyl chitosan and a 3-dimensional dynamer as cartilage engineering scaffold. Carbohydr. Polym. 2020, 244, 116471.
[188] Li, G.; Jiang, Y.; Li, M.; Zhang, W.; Li, Q.; Tang, K. Investigation on the tunable effect of oxidized konjac glucomannan with different molecular weight on gelatin-based composite hydrogels. Int. J. Biol. Macromol. 2021, 168, 233-241.
[189] Pandit, A. H.; Mazumdar, N.; Imtiyaz, K.; Alam Rizvi, M. M.; Ahmad, S. Self-healing and injectable hydrogels for anticancer drug delivery: A study with multialdehyde gum arabic and succinic anhydride chitosan. ACS Appl. Bio. Mater. 2020, 3, 8460-8470.
[190] Fan, M.; Ma, Y.; Tan, H.; Jia, Y.; Zou, S.; Guo, S.; Zhao, M.; Huang, H.; Ling, Z.; Chen, Y.; Hu, X. Covalent and injectable chitosan-chondroitin sulfate hydrogels embedded with chitosan microspheres for drug delivery and tissue engineering. 2017, 71, 67-74.
[191] Zhang, Z.; Wang, X.; Wang, Y.; Hao, J. Rapid-forming and self-healing agarose-based hydrogels for tissue adhesives and potential wound dressings. Biomacromolecules 2018, 19, 980-988.

[192] Ding, C.; Tian, M.; Feng, R.; Dang, Y.; Zhang, M. Novel self-healing hydrogel with injectable, pH-responsive, strain-sensitive, promoting wound-healing, and hemostatic properties based on collagen and chitosan. ACS Biomater. Sci. Eng. 2020, 6, 3855-3867.
[193] Tian, Y.; Pang, L.; Zhang, R.; Xu, T.; Wang, S.; Yu, B.; Gao, L.; Cong, H.; Shen, Y. Poly-tetrahydropyrimidine antibacterial hydrogel with injectability and self-healing ability for curing the purulent subcutaneous infection. ACS Appl. Mater. Interfaces 2020, 12, 50236-50247.
[194] Wang, C.; Zhao, N.; Yuan, W. NIR/Thermoresponsive injectable self-healing hydrogels containing polydopamine nanoparticles for efficient synergistic cancer thermochemotherapy. ACS Appl. Mater. Interfaces 2020, 12, 9118-9131.
[195] Deng G.; Tang C.; Li F.; Jiang, H.; Chen, Y. Covalent cross-linked polymer gels with reversible sol-gel transition and self-healing properties. Macromolecules 2010, 43, 1191-1194.
[196] Wei, Z.; Yang, J. H.; Zhou, J.; Xu, F.; Zrinyi, M.; Dussault, P. H.; Osada, Y.; Chen, Y. M. Self-healing gels based on constitutional dynamic chemistry and their potential applications. Chem. Soc. Rev. 2014, 43, 8114-8131.
[197] Chakma, P.; Konkolewicz, D. Dynamic covalent bonds in polymeric materials. Angew. Chem. Int. Ed. 2019, 58, 2-16.
[198] Alves, M. H.; Young, C. J.; Bozzetto, K.; Poole-Warren, L. A.; Martens, P. J. Degradable, click poly(vinyl alcohol) hydrogels: characterization of degradation and cellular compatibility. Biomed. Mater. 2012, 7, 1-11.
[199] Patenaude, M.; Hoare, T. Injectable, Degradable thermoresponsive poly(N-isopropylacrylamide) hydrogels. ACS Macro Lett. 2012, 1, 409-413.
[200] Patenaude, M.; Campbell, S.; Kinio, D.; Hoare, T. Tuning gelation time and morphology of injectable hydrogels using ketone-hydrazide cross-linking. Biomacromolecules 2014, 15, 781-790.
[201] Whitaker, D. E.; Mahon, C. S.; Fulton, D. A. Thermoresponsive dynamic covalent single-chain polymer nanoparticles reversibly transform into a hydrogel. Angew. Chem. Int. Ed. 2013, 52, 956-959.
[202] McKinnon, D. D.; Domaille, D. W.; Brown, T. E.; Kyburz, K. A.; Kiyotake, E.; Cha, J. N.; Anseth, K. S. Measuring cellular forces using bis-aliphatic hydrazone crosslinked stress-relaxing hydrogels. Soft Matter 2014, 10, 9230-9236.
[203] McKinnon, D. D.; Domaille, D. W.; Cha, J. N.; Anseth, K. S. Biophysically defined and cytocompatible covalently adaptable networks as viscoelastic 3D cell culture systems. Adv. Mater. 2014, 26, 865-872.
[204] McKinnon, Daniel D.; Domaille, Dylan W.; Cha, Jennifer N.; Anseth, Kristi S. Bis-aliphatic hydrazone-linked hydrogels form most rapidly at physiological pH: identifying the origin of hydrogel properties with small molecule kinetic studies. Chem. Mater. 2014, 26, 2382-2387.
[205] Smeets, N. M.; Bakaic, E.; Patenaude, M.; Hoare, T. Injectable and tunable poly(ethylene glycol) analogue hydrogels based on poly(oligoethylene glycol methacrylate). Chem. Commun. 2014, 50, 3306-3309.
[206] Smeets, N. M.; Bakaic, E.; Patenaude, M.; Hoare, T. Injectable poly(oligoethylene glycol methacrylate)-based hydrogels with tunable phase transition behaviours: physicochemical and biological responses. Acta Biomater. 2014, 10, 4143-4155.

[207] Smeets, N. M. B.; Bakaic, E.; Yavitt, F. M.; Yang, F.-C.; Rheinstädter, M. C.; Hoare, T. Probing the internal morphology of injectable poly(oligoethylene glycol methacrylate) hydrogels by light and small-angle neutron scattering. Macromolecules 2014, 47, 6017-6027.
[208] Boehnke, N.; Cam, C.; Bat, E.; Segura, T.; Maynard, H. D. Imine hydrogels with tunable degradability for tissue engineering. Biomacromolecules 2015, 16, 2101-2108.
[209] Grover, G. N.; Lam, J.; Nguyen, T. H.; Segura, T.; Maynard, H. D. Biocompatible hydrogels by oxime Click chemistry. Biomacromolecules 2012, 13, 3013-3017.
[210] Grover, G. N.; Braden, R. L.; Christman, K. L. Oxime cross linked injectable hydrogels for catheter delivery. Adv. Mater. 2013, 25, 2937-2942.
[211] Deng, G.; Ma, Q.; Yu, H.; Zhang, Y.; Yan, Z.; Liu, F.; Liu, C.; Jiang, H.; Chen, Y. Macroscopic organohydrogel hybrid from rapid adhesion between dynamic covalent hydrogel and organogel. ACS Macro Lett. 2015, 4, 467-471.
[212] Li, L.; Gu, J.; Zhang, J.; Xie, Z.; Lu, Y.; Shen, L.; Dong, Q.; Wang, Y. ACS Appl. Mater. Interfaces 2015, 7, 8033-8040.
[213] Mukherjee, S.; Hill, M. R.; Sumerlin, B. S. Self-healing hydrogels containing reversible oxime crosslinks. Soft Matter 2015, 11, 6152-6161.
[214] Chang, R.; Wang, X.; Li, X.; An, H.; Qin, J. Self-activated healable hydrogels with reversible temperature responsiveness. ACS Appl. Mater. Interfaces 2016, 8, 25544-25551.
[215] Urosev, I.; Bakaic, E.; Alsop, R. J. Rheinstädter, M. C. Hoare, T. Tuning the properties of injectable poly(oligoethylene glycol methacrylate) hydrogels by controlling precursor polymer molecular weight. J. Mater. Chem. B 2016, 4, 6541-6551.
[216] An, H.; Li, X.; Fu, X.; Hu, J.; Lang, X.; Liu, X.; Wang, Y.; Wang, H.; Chang, R.; Qin, J. Self-healable hydrogels with NaHCO3 degradability and a reversible gel-sol-gel transition from phenolic ester containing polymers. RSC Adv. 2017, 7, 31212-31220.
[217] Chang, R.; An, H.; Li, X.; Zhou, R.; Qin, J.; Tian, Y.; Deng, K. Self-healable polymer gels with multi-responsiveness of gel-sol-gel transition and degradability. Polym. Chem. 2017, 8, 1263-1271.
[218] Apostolides, D. E.; Sakai, T.; Patrickios, C. S. Dynamic covalent star poly(ethylene glycol) model hydrogels: A new platform for mechanically robust, multifunctional materials. Macromolecules 2017, 50, 2155-2164.
[219] Guo, Z.; Ma, W.; Gu, H.; Feng, Y.; He, Z.; Chen, Q.; Mao, X.; Zhang, J.; Zheng, L. pH-Switchable and self-healable hydrogels based on ketone type acylhydrazone dynamic covalent bonds. Soft Matter 2017, 13, 7371-7380.
[220] Wang, X.; Bian, G.; Zhang, M.; Chang, L.; Li, Z.; Li, X.; An, H.; Qin, J.; Chang, R.; Wang, H. Self-healable hydrogels with cross-linking induced thermo-responsiveness and multi-triggered gel-sol-gel transition. Polym. Chem. 2017, 8, 2872-2880.
[221] Wang, X.; Chang, L.; Hu, J.; Lang, X.; Fu, X.; An, H.; Wang, Y.; Wang, H.; Qin, J. Self-healable hydrogels with crosslinking induced thermo-responsiveness and regulated properties from water soluble polymer. Polymer 2017, 131, 202-208.

[222] Sharma, P. K.; Singh, Y. Glyoxylic hydrazone linkage-based PEG hydrogels for covalent entrapment and controlled delivery of doxorubicin. Biomacromolecules 2019, 20, 2174-2184.
[223] An, H.; Xu, K.; Chang, L.; Wang, Y.; Qin, J.; Li, W. Thermo-responsive self-healable hydrogels with extremely mild base degradability and bio-compatibility. Polymer 2018, 147, 38-47.
[224] Zhao, H.; An, H.; Xi, B.; Yang, Y.; Qin, J.; Wang, Y.; He, Y.; Wang, X. Self-healing hydrogels with both LCST and UCST through cross-linking induced thermo-response. Polymers 2019, 11, 490.
[225] Hou, F.; Xi, B.; Wang, X.; Yang, Y.; Zhao, H.; Li, W.; Qin, J.; He, Y. Self-healing hydrogel with cross-linking induced thermo-response regulated light emission property. Coll. Surf. B Biointerfaces 2019, 183, 110441.
[226] Wang, X.; Xu, K.; Yao, H.; Chang, L.; Wang, Y.; Li, W.; Zhao, Y.; Qin, J. Temperature-regulated aggregation-induced emissive self-healable hydrogels for controlled drug delivery. Poly. Chem. 2018, 9, 5002-5013.
[227] Wang, X.; Chang, L.; Lang, X.; An, H.; Wang, Y.; Li, W.; Qin, J. Cross-linking induced thermo-responsive self-healable hydrogels with temperature regulated light emission property. J. Polym. Res. 2019, 26, 115.
[228] Shen, J.; Wang, X.; An, H.; Chang, L.; Wang, Y.; Li, W.; Qin, J. Cross-linking induced thermoresponsive hydrogel with light emitting and self-healing property. J. Polym. Sci. Polym. Chem. 2019, 57, 869-877.
[229] An, H.; Zhu, L. M.; Shen, J. F.; Li, W. J.; Wang, Y.; Qin, J. L. Self-healing PEG-poly(aspartic acid) hydrogel with rapid shape recovery and drug release. Colloids Surf. B 2020, 185, 110601.
[230] Richardson, B. M.; Walker, C. J.; Macdougall, L. J.; Hoye, J. W.; Randolph, M. A.; Bryant, S. J.; Anseth, K. S. Viscoelasticity of hydrazone crosslinked poly(ethylene glycol) hydrogels directs chondrocyte morphology during mechanical deformation. Biomater. Sci. 2020, 8, 3804-3811.
[231] Bakaic, E.; Smeets, N. M. B.; Barrigar, O.; Alsop, R.; Rheinstädter, M. C.; Hoare, T. pH-Ionizable in situ gelling poly(oligo ethylene glycol methacrylate)-based hydrogels: the role of internal network structures in controlling macroscopic properties. 2017, 50, 7687-7698.
[232] Bakaic, E.; Smeets, N. M. B.; Badv, M.; Dodd, M.; Barrigar, O.; Siebers, E.; Lawlor, M.; Sheardown, H.; Hoare, T. Injectable and degradable poly(oligoethylene glycol methacrylate) hydrogels with tunable charge densities as adhesive peptide-free cell scaffolds. 2018, 4, 3713-3725.
[233] An, H.; Yang, Y.; Bo, Y.; Ma, X.; Wang, Y.; Liu, L.; Wang, H.; He, Y.; Qin, J. Fabrication of self-healing hydrogel from quaternized N-[3(dimethylamino)propyl]methacrylamide copolymer for antimicrobial and drug release applications. J. Biomed. Mater. Res. A 2021, 109, 42-53.
[234] Wu, M.; Chen, J.; Huang, W.; Yan, B.; Peng, Q.; Liu, J.; Chen, L.; Zeng, H. Injectable and self-healing nanocomposite hydrogels with ultrasensitive pH-responsiveness and tunable mechanical properties: Implications for controlled drug delivery. 2020, 21, 2409-2420.
[235] Chau, M.; De France, K. J.; Kopera, B.; Machado, V. R.; Rosenfeldt, S.; Reyes, L.; Chan, K. J. W.; Förster, S.; Cranston, E. D.; Hoare, T.; Kumacheva, E. Composite hydrogels with tunable anisotropic morphologies and mechanical properties. Chem. Mater. 2016, 28, 3406-3415.

[236] Azagarsamy, M. A.; Marozas, I. A.; Spaans, S.; Anseth, K. S. Photoregulated hydrazone-based hydrogel formation for biochemically patterning 3D cellular microenvironments. ACS Macro Lett. 2016, 5, 19-23.
[237] Farahani, P. E.; Adelmund, S. M.; Shadish, J. A.; DeForest, C. A. Photomediated oxime ligation as a bioorthogonal tool for spatiotemporally-controlled hydrogel formation and modification. J. Mater. Chem. B 2017, 5, 4435-4442.
[238] Truong, V. X.; Barner-Kowollik, C. Red-light driven photocatalytic oxime ligation for bioorthogonal hydrogel design. ACS Macro Lett. 2021, 10, 78-83.
[239] Vetrík, M.; Přádný, M.; Hrubý, M.; Michálek, Hydrazone-based hydrogel hydrolytically degradable in acidic environment. J. Polym. Degrad. Stab. 2011, 96, 756-759.
[240] Zhou, H.; Yang, Y.; Xu, G.; Chen, W.; Zhang, W.; Wang, Q.; Zheng, Z.; Ding, X. Ru(II)(tpy)2-functionalized hydrogels: Synthesis, reversible responsiveness, and coupling with the belousov-zhabotinsky reaction. J. Polym. Sci. Part A: Polym. Chem. 2015, 53, 2214-2222.
[241] Ahmadi, M.; Löser, L.; Fischer, K.; Saalwächter, K.; Seiffert, S. Connectivity defects and collective assemblies in model metallo-supramolecular dual-network hydrogels. Macromol. Chem. Phys. 2020, 221, 1900400.
[242] Xu, X.; Jerca, F. A.; Jerca, V. V.; Hoogenboom, R. Covalent poly(2-isopropenyl-2-oxazoline) hydrogels with ultrahigh mechanical strength and toughness through secondary terpyridine metal-coordination crosslinks. Adv. Funct. Mater. 2019, 29, 1904886.
[243] Es Sayed, J.; Lorthioir, C.; Banet, P.; Perrin, P.; Sanson, N. Reversible assembly of microgels by metallo-supramolecular chemistry. Angew.Chem. Int. Ed. 2020, 59, 7042-7048.
[244] Hackelbusch, S.; Rossow, T.; Becker, H.; Seiffert, S. Multiresponsive polymer hydrogels by orthogonal supramolecular chain cross-linking. Macromolecules 2014, 47, 4028-4036.
[245] Chiper, M.; Hoeppener, S.; Schubert, U. S.; Fustin, C.-A.; Gohy, J.-F. Self-assembly behavior of bis(terpyridine) and metallo-bis(terpyridine) pluronics in dilute aqueous solutions. Macromol. Chem. Phys. 2010, 211, 2323-2330.
[246] Bharatiya, B.; Fustin, C.-A.; Gohy, J.-F. Supramolecular aqueous gels based on terpyridine-modified pluronics. Macromol. Chem. Phys. 2012, 213, 2253-2260.
[247] Piogé, S.; Fustin, C. A.; Gohy, J. F. Temperature-responsive aqueous micelles from terpyridine end-capped poly(N-isopropylacrylamide)-block-polystyrene diblock copolymers. Macromol. Rapid Commun. 2012, 33, 534-539.
[248] Brassinne, J.; Stevens, A. M.; Van Ruymbeke, E.; Gohy, J.-F.; Fustin, C.-A. Hydrogels with dual relaxation and two-step gel-sol transition from heterotelechelic polymers. Macromolecules 2013, 46, 9134-9143.
[249] Brassinne, J.; Bourgeois, J.-P.; Fustin, C.-A.; Gohy, J.-F. Thermo-responsive properties of metallo-supramolecular block copolymer micellar hydrogels. Soft Matter 2014, 10, 3086-3092.
[250] Brassinne, J.; Gohy, J.-F.; Fustin, C.-A. Controlling the cross-linking density of supramolecular hydrogels formed by heterotelechelic associating copolymers. Macromolecules 2014, 47, 4514-4524.

[251] Brassinne, J.; Zhuge, F.; Fustin, C. A.; Gohy, J. F. Precise control over the rheological behavior of associating stimuli-responsive block copolymer gels. Gels. 2015, 1, 235-255.
[252] Brassinne, J.; Gohy, J.-F.; Fustin, C.-A. Orthogonal control of the dynamics of supramolecular gels from heterotelechelic associating polymers. ACS Macro Lett. 2016, 5, 1364-1368.
[253] Brassinne, J.; Fustin, C.-A.; Gohy, J.-F. Control over the assembly and rheology of supramolecular networks via multi-responsive double hydrophilic copolymers. Polym. Chem. 2017, 8, 1527-1539.
[254] Le Bohec, M.; Banère, M.; Piogé, S.; Pascual, S.; Benyahia, L.; Fontaine, L. Sol-gel reversible metallo-supramolecular hydrogels based on a thermoresponsive double hydrophilic block copolymer. Polym. Chem. 2016, 7, 6834-6842.
[255] Gutierres, A.; Pascual, S.; Fontaine, L.; Piogé, S.; Benyahia, L. The effect of metal ions on the viscoelastic properties of thermosensitive sol-to-gel reversible metallo-supramolecular hydrogels. Polym. Chem. 2018, 9, 2494-2504.
[256] Yuan, L.; Wu, Y.; Gu, Q. S.; El-Hamshary, H.; El-Newehy, M.; Mo, X. Injectable photo crosslinked enhanced double-network hydrogels from modified sodium alginate and gelatin. Int. J. Biol. Macromol. 2017, 96, 569-577.
[257] Wang, L.; Yang, K.; Li, X.; Zhang, X.; Zhang, D.; Wang, L. N.; Lee, C. S. A double-crosslinked self-healing antibacterial hydrogel with enhanced mechanical performance for wound treatment. Acta Biomater. 2021, 124, 139-152.
[258] Rodriguez-Docampo, Z.; Otto, S. Orthogonal or simultaneous use of disulfide and hydrazone exchange in dynamic covalent chemistry in aqueous solution. Chem. Commun. 2008, 5301-5303.
[259] Zhang, Y.; Li, X.; Zhong, N.; Huang, Y.; He, K.; Ye, X. Injectable in situ dual-crosslinking hyaluronic acid and sodium alginate based hydrogels for drug release. J. Biomater. Sci. Polym. Ed. 2019, 30, 995-1007.
[260] Zhang, Y.; Ding, Z.; Liu, Y.; Zhang, Y.; Jiang, S. White-light-emitting hydrogels with self-healing properties and adjustable emission colors. J. Colloid Interface Sci. 2021, 582, 825-833.
[261] Wang, Y.; Xiao, G.; Peng, Y.; Chen, L.; Fu, S. Effects of cellulose nanofibrils on dialdehyde carboxymethyl cellulose based dual responsive self-healing hydrogel. Cellulose 2019, 26, 8813-8827.
[262] Wang, L.; Zhou, W.; Wang, Q.; Xu, C.; Tang, Q.; Yang, H. An injectable, dual responsive, and self-healing hydrogel based on oxidized sodium alginate and hydrazide-modified poly(ethyleneglycol). Molecules 2018, 23, 546.
[263] Li, S.; Pei, M.; Wan, T.; Yang, H.; Gu, S.; Tao, Y.; Liu, X.; Zhou, Y.; Xu, W.; Xiao, P. Self-healing hyaluronic acid hydrogels based on dynamic Schiff base linkages as biomaterials. Carbohydr. Polym. 2020, 250, 116922.
[264] Li, S.; Wang, J.; Song, L.; Zhou, Y.; Zhao, J.; Hou, X.; Yuan, X. Injectable PAMAM/ODex double-crosslinked hydrogels with high mechanical strength. 2017, 12, 015012.
[265] Balakrishnan, B.; Jayakrishnan, A. Self-cross-linking biopolymers as injectable in situ forming biodegradable scaffolds. Biomaterials 2005, 26, 3941-3951.

[266] Balakrishnan, B.; Mohanty, M.; Umashankar, P. R.; Jayakrishnan, A. Evaluation of an in situ forming hydrogel wound dressing based on oxidized alginate and gelatin. Biomaterials 2005, 26, 6335-6342.
[267] Balakrishnan, B.; Joshi, N.; Jayakrishnan, A.; Banerjee, R. Self-crosslinked oxidized alginate/gelatin hydrogel as injectable, adhesive biomimetic scaffolds for cartilage regeneration. Acta Biomater. 2014, 10, 3650-3663.
[268] Pettignano, A.; Häring, M.; Bernardi, L.; Tanchoux, N.; Quignard, F.; Díaz Díaz, D. Self-healing alginate-gelatin biohydrogels based on dynamic covalent chemistry: elucidation of key parameters. Mater. Chem. Front. 2017, 1, 73-79.
[269] Li, J.; Hu, W.; Zhang, Y.; Tan, H.; Yan, X.; Zhao, L.; Liang, H. pH and glucose dually responsive injectable hydrogel prepared by in situ crosslinking of phenylboronic modified chitosan and oxidized dextran. J. Polym. Sci. Part A: Polym. Chem. 2015, 53, 1235-1244.
[270] Zhao, L.; Niu, L.; Liang, H.; Tan, H.; Liu, C.; Zhu, F. pH and glucose dual-responsive injectable hydrogels with insulin and fibroblasts as bioactive dressings for diabetic wound healing. ACS Appl. Mater. Interfaces 2017, 9, 37563-37574.
[271] Li, Y.; Yang, L.; Zeng, Y.; Wu, Y.; Wei, Y.; Tao, L. Self-healing hydrogel with a double dynamic network comprising imine and borate ester linkages. Chem. Mater. 2019, 31, 15, 5576-5583.
[272] Liu, Y.; Liu, Y.; Wang, Q.; Han, Y.; Chen, H.; Tan, Y. Doubly dynamic hydrogel formed by combining boronate ester and acylhydrazone bonds. Polymers 2020, 12, 487.
[273] Zhao, J.; Diaz-Dussan, D.; Wu, M.; Peng, Y. Y.; Wang, J.; Zeng, H.; Duan, W.; Kong, L.; Hao, X.; Narain, R. Dual-cross-linked network hydrogels with multiresponsive, self-healing, and shear strengthening properties. Biomacromolecules 2021, 22, 2, 800-810.
[274] Li, S.; Yi, J.; Yu, X.; Shi, H.; Zhu, J.; Wang, L. Preparation and characterization of acid resistant double cross-linked hydrogel for potential biomedical applications. ACS Biomater. Sci. Eng. 2018, 4, 872-883.
[275] Hu, C.; Long, L.; Cao, J.; Zhang, S.; Wang, Y. Dual-crosslinked mussel-inspired smart hydrogels with enhanced antibacterial and angiogenic properties for chronic infected diabetic wound treatment via pH-responsive quick cargo release. Chem. Eng. J. 2021, 411, 128564.
[276] Teng, L.; Chen, Y.; Jia, Y. G.; Ren, L. Supramolecular and dynamic covalent hydrogel scaffolds: from gelation chemistry to enhanced cell retention and cartilage regeneration. J. Mater. Chem. B, 2019, 7, 6705-6736.
[277] Xu, C.; Zhan, W.; Tang, X.; Mo, F.; Fu, L.; Lin, B. Self-healing chitosan/vanillin hydrogels based on Schiff-base bond/hydrogen bond hybrid linkages. Polym. Test. 2018, 66, 155-163.
[278] Xu, H.; Zhang, L.; Cai, J. Injectable, self-healing, β-chitin-based hydrogels with excellent cytocompatibility, antibacterial activity, and potential as drug/cell carriers. ACS Appl. Bio Mater. 2019, 2, 196-204.
[279] Jiang, Z.; Diggle, B.; Shackleford, I. C. G.; Connal, L. A. Tough, self-healing hydrogels capable of ultrafast shape changing. Adv. Mater. 2019, 1904956.
[280] Qiao, L.; Liu, C.; Liu, C.; Yang, L.; Zhang, M.; Liu, W.; Wang, J.; Jian, X. Self-healing alginate hydrogel based on dynamic acylhydrazone and multiple hydrogen bonds. J. Mater. Sci. 2019, 54, 8814-8828.
[281] Guo, Z.; Gu, H.; He, Y.; Zhang, Y.; Xu, W.; Zhang, J.; Liu, Y.; Xiong, L.; Chen, A.; Feng, Y. Dual dynamic bonds enable biocompatible and tough

hydrogels with fast self-recoverable, self-healable and injectable properties. Chem. Eng. J. 2020, 388, 124282.
[282] Wang, D.; Xia, Y.; Zhang, D.; Sun, X.; Chen, X.; Oliver, S.; Shi, S.; Lei, L. Hydrogen-bonding reinforced injectable hydrogels: application as a thermo-triggered drug controlled-release system. ACS Appl. Polym. Mater. 2020, 2, 1587-1596.
[283] Nadgorny, M.; Collins, J.; Xiao, Z. Y.; Scales, P. J.; Connal, L. A. 3D-printing of dynamic self-healing cryogels with tuneable properties. Polym. Chem. 2018, 9, 1684-1692.
[284] Qu, J.; Zhao, X.; Liang, Y.; Zhang, T.; Ma, P. X.; Guo, B. Antibacterial adhesive injectable hydrogels with rapid self-healing, extensibility and compressibility as wound dressing for joints skin wound healing. Biomaterials 2018, 183, 185-199.
[285] Li, Z.; Zhou, F.; Li, Z.; Lin, S.; Chen, L.; Liu, L.; Chen, Y. Hydrogel cross-linked with dynamic covalent bonding and micellization for promoting burn wound healing. ACS Appl. Mater. Interfaces 2018, 10, 25194-25202.
[286] Liu, J.; Zhang, X,; Chen, X.; Qu, L.; Zhang, L.; Li, W.; Zhang, A. Stimuli-responsive dendronized polymeric hydrogels through Schiff-base chemistry showing remarkable topological effects. Polym. Chem. 2018, 9, 378-387.
[287] Li, H.; Liu, F.; Li, Z.; Wang, S.; Jin, R.; Liu, C.; Chen, Y. Fingerprintable hydrogel from dual reversible cross-linking networks with different relaxation times. ACS Appl. Mater. Interfaces 2019, 11, 17925-17930.
[288] Marin, L.; Moraru, S.; Popescu, M. C.; Nicolescu, A.; Zgardan, C.; Simionescu, B. C.; Barboiu, M. Out-of-water constitutional self-organization of chitosan-cinnamaldehyde dynagels. Chem. Eur. J. 2014, 20, 4814-4821.
[289] Iftime, M. M.; Morariu, S.; Marin, L. Salicyl-imine-chitosan hydrogels: Supramolecular architecturing as a crosslinking method toward multifunctional hydrogels. Carbohydr. Polym. 2017, 165, 39-50.
[290] Yeo, Y. H.; Park, W. H. Dual-crosslinked, self-healing and thermo-responsive methylcellulose/chitosan oligomer copolymer hydrogels. Carbohydr. Polym. 2021, 258, 117705.
[291] Liu, C.; Dong, C.; Liu, S.; Yang, Y.; Zhang, Z. Multiple chiroptical switches and logic circuit based on salicyl iminechitosan hydrogel. Carbohydr. Polym. 2021, 257, 117534.
[292] Zhang, J.; Hou, S.; Chen, Y.; Zhou, J.; Chen, H.; Tan, Y. Dual-cross-linked dynamic hydrogels with cucurbit[8]uril and imine linkages. Soft Matter 2019, 15, 9797-9804.
[293] Janarthanan, G.; Tran, H. N.; Cha, E.; Lee, C.; Das, D.; Noh, I. 3D printable and injectable lactoferrin-loaded carboxymethyl cellulose-glycol chitosan hydrogels for tissue engineering applications. Mat. Sci. Eng. C-Mater. 2020, 113, 111008.
[294] Li, S.; Chen, N.; Li, X.; Li, Y.; Xie, Z.; Ma, Z.; Zhao, J.; Hou, X.; Yuan, X. Bioinspired double-dynamic-bond crosslinked bioadhesive enables post-wound closure care. Adv. Funct. Mater. 2020, 2000130.
[295] Qiao, L.; Liu, C.; Liu, C.; Hu, F.; Li, X.; Wang, C.; Jian, X. Study on new polymer crosslinking agents and their functional hydrogels. Eur. Polym. J. 2020, 134, 109835.
[296] Zhang, X.; Pan, Y.; Li, S.; Xing, L.; Du, S.; Yuan, G.; Li, J.; Zhou, T.; Xiong, D.; Tan, H.; Ling, Z.; Chen, Y.; Hu, X.; Niu, X. Doubly crosslinked

biodegradable hydrogels based on gellan gum and chitosan for drug delivery and wound dressing. Int. J. Biol. Macromol. 2020, 164, 2204-2214.

[297] Song, X.; Wang, X.; Zhang, J.; Shen, S.; Yin, W.; Ye, G.; Wang, L.; Hou, H.; Qiu, X. A tunable self-healing ionic hydrogel with microscopic homogeneous conductivity as a cardiac patch for myocardial infarction repair. Biomaterials 2021, 273, 120811.

[298] Liang, Y.; Li, Z.; Huang, Y.; Yu, R.; Guo, B. Dual-dynamic-bond cross-linked antibacterial adhesive hydrogel sealants with on-demand removability for post-wound-closure and infected wound healing. ACS Nano 2021, doi: 10.1021/acsnano.1c00204

[299] Wang, L.; Deng, F.; Wang, W.; Li, A.; Lu, C.; Chen, H.; Wu, G.; Nan, K.; Li, L. Construction of injectable self-healing macroporous hydrogels via a template-free method for tissue engineering and drug delivery. ACS Appl. Mater. Interfaces 2018, 10, 36721-36732.

[300] Zhou, F.; Hong, Y.; Zhang, X.; Yang, L.; Li, J.; Jiang, D.; Bunpetch, V.; Hu, Y.; Ouyang, H.; Zhang, S. Tough hydrogel with enhanced tissue integration and in situ forming capability for osteochondral defect repair. Appl. Mater. Today 2018, 13, 32-44.

[301] Fu, B; Cheng, B.; Jin, X.; Bao, X.; Wang, Z.; Hu, Q. Chitosan-based double network hydrogels with self-healing and dual-responsive shape memory abilities. J. Appl. Polym. Sci. 2019, 136, 48247.

[302] Zhang, X.; Liu, K.; Liu, J.; Ding, Y.; Li, W.; Zhang, A. Thermoresponsive cryogels from dendronized interpenetrating polymer network showing dual-shape memory. Eur. Polym. J. 2020, 141, 110092.

[303] Wang, L. L.; Highley, C. B.; Yeh, Y. C.; Galarraga, J. H.; Uman, S.; Burdick, J. A. Three-dimensional extrusion bioprinting of single- and double-network hydrogels containing dynamic covalent crosslinks. J. Biomed. Mater. Res. Part A 2018, 106, 865-875.

[304] Ma, X.; Liu, X.; Wang, P.; Wang, X.; Yang, R.; Liu, S.; Ye, Z.; Chi, B. Covalently adaptable hydrogel based on hyaluronic acid and poly(γ-glutamic acid) for potential load-bearing tissue engineering. ACS Appl. Bio Mater. 2020, 3, 4036-4043.

[305] Kheirabadi, M.; Shi, L.; Bagheri, R.; Kabiri, K.; Hilborn, J.; Ossipov, D. A. In situ forming interpenetrating hydrogels of hyaluronic acid hybridized with iron oxide nanoparticles. Biomater. Sci. 2015, 3, 1466-1474.

[306] Wang, Y.; Yu, H.; Yang, H.; Hao, X.; Tang, Q.; Zhang, X. An injectable interpenetrating polymer network hydrogel with tunable mechanical properties and self-healing abilities. Macromol. Chem. Phys. 2017, 218, 1700348.

[307] Cho, I. S.; Ooya, T. Tuned cell attachments by double-network hydrogels consisting of glycol chitosan, carboxylmethyl cellulose and agar bearing robust and self-healing properties. Int. J. Biol. Macromol. 2019, 134, 262-268.

[308] Lei, K.; Li, Z.; Zhu, D.; Sun, C.; Sun, Y.; Yang, C.; Zheng, Z.; Wang, X. Polysaccharide-based recoverable double-network hydrogel with high strength and self-healing properties. J. Mater. Chem. B 2020, 8, 794-802.

[309] Yan, Y.; Li, M.; Yang, D.; Wang, Q.; Liang, F.; Qu, X.; Qiu, D.; Yang, Z. Construction of injectable double-network hydrogels for cell delivery. Biomacromolecules 2017, 18, 2128-2138.

[310] Yang, C.; Han, B.; Cao, C.; Yang, D.; Qu, X.; Wang, X. An injectable double-network hydrogel for the co-culture of vascular endothelial cells and bone

marrow mesenchymal stem cells for simultaneously enhancing vascularization and osteogenesis. J. Mater. Chem. B 2018, 6, 7811-7821.

[311] Zhang, X.; Wang, K.; Hu, J.; Zhang, Y.; Dai, Y.; Xia, F. Role of a high calcium ion content in extending the properties of alginate dual-crosslinked hydrogels. J. Mater. Chem. A 2020, 8, 25390-25401.

[312] Chen, Y.; Zhang, R.; Zheng, B.; Cai, C.; Chen, Z.; Li, H.; Liu, H. A biocompatible, stimuli-responsive, and injectable hydrogel with triple dynamic bonds. Molecules 2020, 25, 3050.

[313] Ding, C.; Yang, Q.; Tian, M.; Guo, C.; Deng, F.; Dang, Y.; Zhang, M. Novel collagen-based hydrogels with injectable, self-healing, wound-healing properties via a dynamic crosslinking interaction. Polym. Int. 2020, 69, 858-866.

[314] Pourjavadi, A.; Tavakolizadeh, M.; Hosseini, S. H.; Rabiee, N.; Bagherzadeh, M. Highly stretchable, self-adhesive, and self-healable double network hydrogel based on alginate/polyacrylamide with tunable mechanical properties. 2020, 58, 2062-2073.

[315] Chen, T.; Chen, Y.; Rehman, H. U.; Chen, Z.; Yang, Z.; Wang, M.; Li, H.; Liu, H. Ultratough, self-healing, and tissue-adhesive hydrogel for wound dressing. ACS Appl. Mater. Interfaces 2018, 10, 33523-33531.

[316] Wang, H.; Zhu, D.; Paul, A.; Cai, L.; Enejder, A.; Yang, F.; Heilshorn, S. C. Covalently adaptable elastin-like protein-hyaluronic acid (ELP-HA) hybrid hydrogels with secondary thermo-responsive crosslinking for injectable stem cell delivery. Adv. Funct. Mater. 2017, 27, 1605609.

Chapter 3

Tunable Interpenetrating Polymer Network Hydrogels

Abstract

This chapter is based on a published paper (Yang H.; Ghiassinejad S.; Van Ruymbeke, E.; Fustin, C. A. Macromolecules 2020, 53, 6956-6967).

A series of tunable interpenetrating polymer network (IPN) hydrogels are designed by the orthogonal incorporation of two distinct types of dynamic bonds, i.e., reversible C=N bonds and metal-ligand coordination bonds. IPN hydrogels are prepared by combining these different types of reversible bonds in order to investigate how the two sub-networks influence each other. To this end, the influence of the crosslinker nature and of the hydrogel preparation protocol on the rheological properties of these IPNs are also studied in details. In particular, we show that the obtained IPN hydrogels exhibit a higher modulus compared to the simple addition of the moduli of the single networks, that we attribute to the entanglements between the two networks. We then study how these IPN hydrogels can disentangle and partially relax if one of the reversible sub-networks is composed of crosslinks with shorter lifetime. Finally, pH is used as a stimulus to affect the dynamics of only one of the sub-network, and the impact of this change on the properties of the IPNs is investigated.

3.1 Introduction

As mentioned in Chapter 2, polymer hydrogels are formed by crosslinked 3D networks that trap large amounts of water[1] and are the material of choice for multiple applications.[2-8] To impart further tunability and adaptiveness to these hydrogels, dynamic covalent bonds (DCBs) and supramolecular interactions have been introduced into polymer networks as crosslinks.[9-13] Particularly, the orthogonal combination of DCB and supramolecular interactions for responsive polymer hydrogels or elastomers has received a rapidly growing attention over the past few years.[14-20] Compared to networks based on a single type of crosslinks, materials combining different crosslinks possess desirable properties such as the ability to respond to multiple (orthogonal) stimuli, fast shape recovery, or good mechanical properties such as high strength, toughness, and fatigue resistance.[17,20]

As the DCB used in this thesis, reversible C=N bonds are one of the most successful DCBs used so far in the preparation of responsive gels.[21-25] The hydrolytic stability of such bonds can be regulated from the less stable but more reversible acylhydrazone bond to the stable but less reversible oxime bond by changing the acylhydrazine for a hydroxylamine to react with the ketone partner.[26] As a result, the dynamics and stability of this type of hydrogels can be tuned.[27] Among supramolecular interactions, the metal-terpyridine coordination bond is most attractive for the fabrication of responsive polymer gels since the bond characteristics (lifetime, strength) can be tuned over several orders of magnitudes simply by changing the metal ions used.[28-33] Therefore, in the present study, we investigate the rheological properties of polymer gels which combine the aforementioned reversible C=N bonds with metal-terpyridine coordination bonds, in order to create very stable – yet reversible – networks thanks to the presence of the DCBs, while keeping some room to tune the material properties, thanks to the metal-ligand interactions.

In general, the combination of several interactions can be done by following either a 'dual-crosslinked network' (DCN) approach, or an 'interpenetrating polymer network' (IPN) approach.[34-37] Unlike the DCN, the IPN allows the combination of the desired properties of each network (e.g. stimuli-responsiveness), and even more, because they may exhibit new properties that are not observed in the component networks alone.[38-44] Most noticeably, IPN hydrogels may show enhanced mechanical properties such as greater toughness, larger extensibility and improved strength due to synergistic interactions between the component networks that transfer the stress and dissipate mechanical energy upon deformation.[34,45,46] Recently, the combination of DCB and supramolecular interactions has been also reported to fabricate responsive IPN hydrogels and elastomers with outstanding mechanical performances.[47-53] For example, Konkolewicz et al[49] synthesized a double dynamic IPN elastomer with superior mechanical (increased stress and strain at break, increased malleability, greater toughness) and self-healing properties based on Diels-Alder adduct and hydrogen bonding. Liang et al[52] prepared highly stretchable IPN hydrogels with the properties of actuation, shape memory, and self-healing capability by using boronic ester bonds and alginate-Ca^{2+} complexation.

In this study, we investigate the rheological properties of reversible IPN hydrogels formed through DCB and metal-ligand supramolecular interactions. In particular, we study how the rheological properties of both networks are combined and modified when these networks are interpenetrated. Since the DCBs (i.e., the acylhydrazone and oxime bonds) have been chosen in order to be very stable, we do not expect to observe a terminal regime. However, the reversibility of the bonds could possibly be observed under large shear and/or in different environmental conditions (e.g. pH or temperature variation). On the other hand, depending on the metal ion selected, the lifetime of the supramolecular junctions can be easily varied. Therefore, the use of a supramolecular network made of labile interactions should allow us to study how the fast association/dissociation dynamics of the

supramolecular network influences the overall response of the IPN hydrogels. Then, by exploiting metal-ligand interactions with long-lifetime, we would like to see how the contribution of both the DCB and supramolecular networks can be distinguished. Finally, the crosslinking density or dynamics of the networks can be modified by varying the pH, which gives us an additional way to vary the relative stability of both networks.

To this end, we have synthesized a series of novel IPN hydrogels which are based on two functionalized hydrophilic copolymers (**Figure 3.1**). The first one bears ketone pendant groups and can be crosslinked by succinic dihydrazide (di-acylhydrazine) or O,O'-(propane-1,3-diyl)bis(hydroxylamine) (bis-hydroxylamine) to form respectively acylhydrazone and oxime bonds. The second copolymer bears terpyridine side groups and can be crosslinked by the addition of transition metal cations (Zn^{2+} and Fe^{2+} were used in this work) to form metal-terpyridine bis-complexes. Of these, the acylhydrazone is more susceptible to hydrolysis compared to the oxime and therefore has a shorter bond lifetime. Similarly, Fe(II)-terpyridine bis-complexes (Fe^{2+}-Tpy) have higher bond energies and longer lifetimes than Zn(II)-terpyridine bis-complexes (Zn^{2+}-Tpy). To distinguish the bonds, in this thesis, the two DCBs are referred to as the less stable acylhydrazone and the stable oxime, and the two metal-terpyridine bis-complexes are referred to as the long lifetime Fe^{2+}-Tpy and the labile Zn^{2+}-Tpy, respectively. Therefore, the obtained IPNs are comprised of a DCB-crosslinked network and of a supramolecularly crosslinked network. As shown in **Figure 3.1**, four IPN hydrogels have thus been obtained by combining these interactions in different ways. First, a stable DCB is combined with a long-lifetime supramolecular interaction (Oxime + Fe^{2+}-Tpy), or with a more dynamic supramolecular interaction (Oxime + Zn^{2+}-Tpy). Secondly, a less stable DCB is combined with the long-lifetime supramolecular interaction (Acylhydrazone + Fe^{2+}-Tpy) or with the more dynamic supramolecular interaction (Acylhydrazone + Zn^{2+}-Tpy).

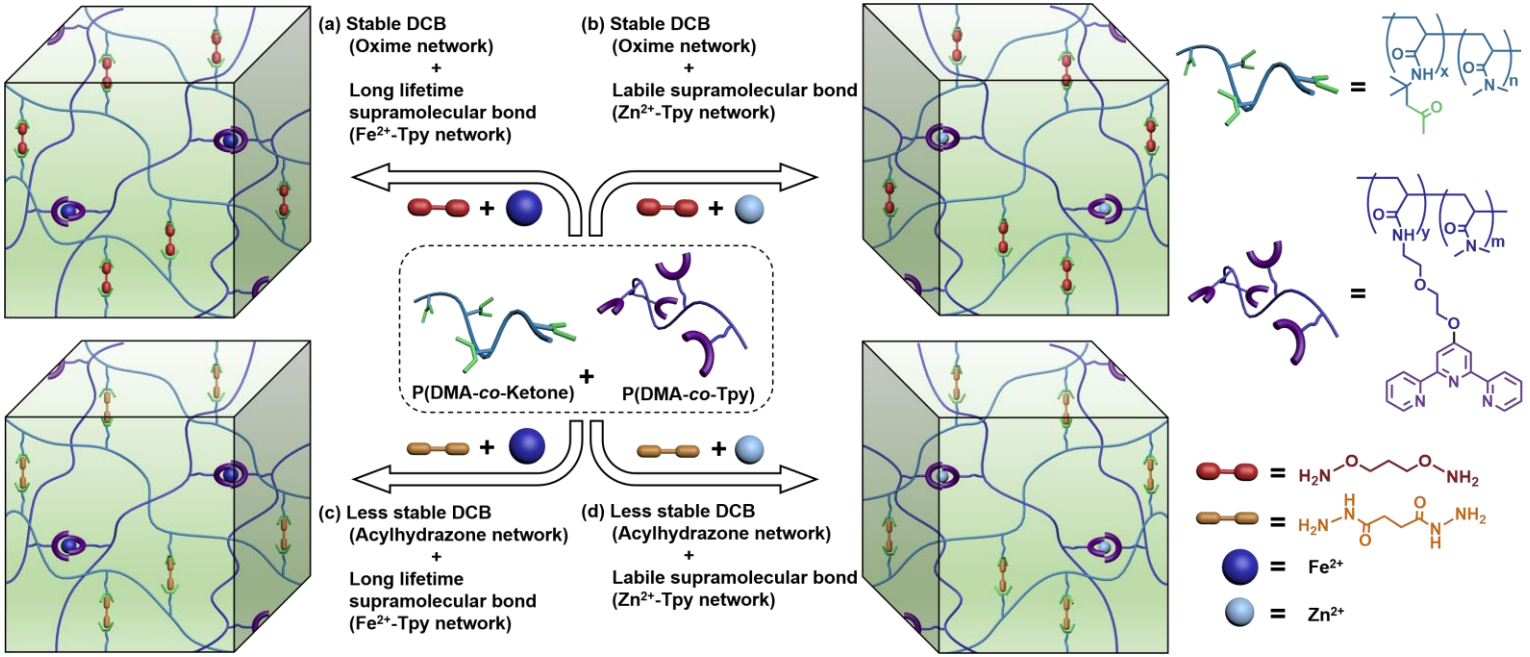

Figure 3.1. Schematic representation of four interpenetrating polymer network (IPN) hydrogels based on different combinations of dynamic covalent bond (DCB) (acylhydrazone or oxime bond) and supramolecular interaction (metal-terpyridine bis-complexes): (a) stable DCB with long-lifetime supramolecular bond (Oxime + Fe^{2+}-Tpy), (b) stable DCB with labile supramolecular bond (Oxime + Zn^{2+}-Tpy), (c) less stable DCB with long-lifetime supramolecular bond (Acylhydrazone + Fe^{2+}-Tpy), and (d) less stable DCB with labile supramolecular bond (Acylhydrazone + Zn^{2+}-Tpy).

3.2 Results and Discussion

3.2.1. Synthesis of hydrophilic functionalized copolymers

Table 3.1. Main characteristics of P(DMA-*co*-Ketone) and P(DMA-*co*-Tpy) copolymers.

Copolymer	Final ratio[a] (mol%)			M_n[b] (g/mol)	M_n[c] (g/mol)	$Đ$[c]	N_f/Chain[d]	
	DMA	Ketone	Tpy				Ketone	Tpy
P(DMA-*co*-Ketone)	96	4	/	40000	56000	1.32	16	/
P(DMA-*co*-Tpy)	98.5	/	1.5	44000	42500	1.73	/	6

[a] Calculated from the ^{1}H NMR spectra. [b] Evaluated by monomer conversion (^{1}H NMR). [c] Determined by SEC (polymethylmethacrylate standards). [d] Average number of functional groups per chain.

We have chosen the hydrophilic biocompatible poly(N,N-dimethyl acrylamide) (PDMA) as the backbone polymer for fabricating the hydrogels. The commercially available comonomer, diacetone acrylamide (DAAM), which contains a ketone group that can react with di-acylhydrazine or bis-hydroxylamine compounds to form acylhydrazone or oxime bonds, was employed to create reversible C=N bond-based networks (**Figure 3.1**). The hydrophilic terpyridine-functionalized monomer (N-(2-(2-([2,2':6',2''-terpyridine]-4'-yloxy)ethoxy)ethyl) acrylamide (TPy-DEG-AM)) was synthesized in two steps from commercially available precursors (see Experimental Section), and can form metal-terpyridine bis-complexes with various strengths and labilities in combination with transition metal ions. The copolymers that will be the precursors of the network were prepared by copolymerizing functionalized monomers, i.e., one bearing a ketone group and the other bearing a terpyridine, with the base monomer of DMA. Reversible addition-fragmentation chain transfer (RAFT)

controlled radical polymerization was used to this aim. Two copolymers: P(DMA-*co*-Ketone) and P(DMA-*co*-Tpy) were obtained in this way and were characterized by NMR and SEC (**Table 3.1**). Due to the poor solubility of terpyridine-functionalized monomer (TPy-DEG-AM) in the polymerization solvent (DMF), the molar dispersity dispersity of the obtained P(DMA-*co*-Tpy) copolymer was rather high as shown in **Table 3.1**.

3.2.2. Preparation of networks

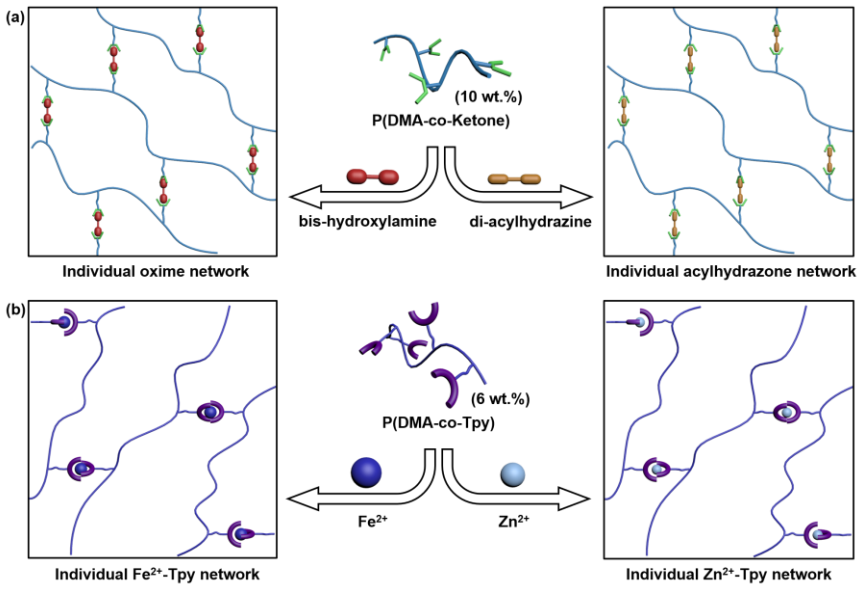

Scheme 3.1. (a) Preparation of individual reversible C=N bonding networks in water from P(DMA-*co*-Ketone) (10 wt.%). (b) Preparation of individual metal-terpyridine bonding networks in water from P(DMA-*co*-Tpy) (6 wt.%).

The P(DMA-*co*-Ketone) copolymer was used as precursor for preparing acylhydrazone/oxime networks, the P(DMA-*co*-Tpy) copolymer was used for the formation of metal-ligand networks. For all the prepared networks, the amount of added crosslinkers (di-acylhydrazines, bis-hydroxylamines or transition metal cations) was

half an equivalent compared to the reaction sites (ketone groups or terpyridine groups) of the copolymers. Three types of networks of increasing complexity were prepared to allow the systematic comparison of their rheological properties and the determination of the respective contributions of the two types of bonds. Individual networks were prepared from each of the above copolymers with corresponding crosslinkers (**Schemes 3.1**). Single networks were prepared from mixed solutions of the two copolymers but crosslinking only one of the copolymers with the appropriate crosslinker (**Scheme 3.2**). Interpenetrating polymer networks were prepared also from mixed solutions of the two copolymers but this time crosslinking both copolymers (**Scheme 3.3**).

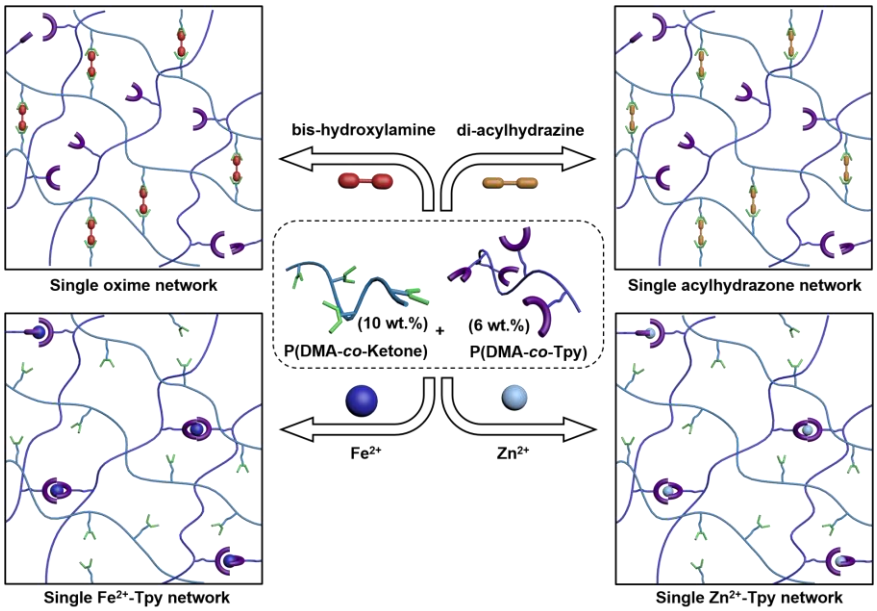

Scheme 3.2. Preparation of single networks in water from mixed copolymers (10+6 wt.%) of P(DMA-*co*-Ketone) (10 wt.%) and P(DMA-*co*-Tpy) (6 wt.%).

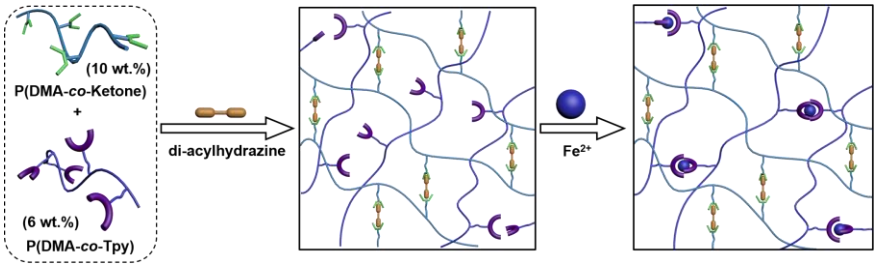

Scheme 3.3. Preparation of interpenetrating polymer network (IPN) hydrogels of 1Acylhydrazone + 2Fe^{2+}-Tpy. The di-acylhydrazine is added firstly to form an acylhydrazone crosslinked 1st network, followed by adding Fe^{2+} to get the 2nd network.

Formation of individual networks from each of the two above copolymers has been first investigated in deionized water (pH: 6~7). We found that the P(DMA-*co*-Ketone) copolymer reacts with the di-acylhydrazine crosslinker to form acylhydrazone hydrogels after 1 day, and with bis-hydroxylamine crosslinker to form oxime hydrogels after 9 hours at a copolymer concentration of 10 wt.%. At lower concentrations, P(DMA-*co*-Ketone) cannot form gels with these crosslinkers even after 1 month of reaction. The P(DMA-*co*-Tpy) copolymer is crosslinked by Fe^{2+} ions in a few minutes via the formation of Fe^{2+}-terpyridine bis-complexes (Fe^{2+}-Tpy) at a minimum copolymer concentration of 6 wt.%. Therefore, concentrations of 10 wt.% for the P(DMA-*co*-Ketone) copolymer and of 6 wt.% for P(DMA-*co*-Tpy) have been adopted in this work for network preparation.

The IPN hydrogels were prepared by adding di-acylhydrazine or bis-hydroxylamine and metal ions (Zn^{2+} or Fe^{2+}) to solutions of mixed copolymers; 10 wt.% of P(DMA-*co*-Ketone) and 6 wt.% of P(DMA-*co*-Tpy) to reach a total polymer concentration of 10+6 wt.% as for the single networks. The influence of the addition sequence of crosslinkers, i.e., inducing first the DCB formation and then the metal-ligand bonds or the reverse, on the rheological properties of the obtained IPNs was studied. In each case, a 24 h waiting time was applied before adding the second crosslinker.

The apparent mechanical properties observed by touching the hydrogels with tweezers revealed that the individual and single networks of acylhydrazone, and the IPN of acylhydrazone + Zn^{2+}-Tpy were soft, slightly sticky hydrogels, whereas the individual and single networks, and IPNs based on oxime and Fe^{2+}-Tpy were all stiff, non-stick hydrogels.

3.2.3. Rheological characterization

Oscillatory shear rheology was used as the main characterization method to investigate the dynamic mechanical properties of all networks under shear. The dynamic covalent bonds generally exhibit higher bond dissociation energies and slower dynamics than supramolecular interactions.[12,17] In our case, the order of rate constants for the formation of crosslinks between two chains is approximatively acylhydrazone < oxime < Zn^{2+}-Tpy < Fe^{2+}-Tpy at 25 °C in water (pH~7).[54-58] Therefore, we first measured the oscillatory shear rheological behavior of the individual acylhydrazone hydrogel, i.e., the slowest forming network according to the above data, at different aging times to determine the best preparation time to achieve stable and reproducible frequency sweeps. Amplitude sweep measurements were also performed to determine the limit of the linear regime of deformation. As depicted in **Figure 3.2**, the rheological behavior of individual acylhydrazone hydrogels did not change significantly after two days of aging, indicating that a stable state has been reached. Based on these results, all following rheology measurements on all hydrogels have been executed after two days of aging time at room temperature.

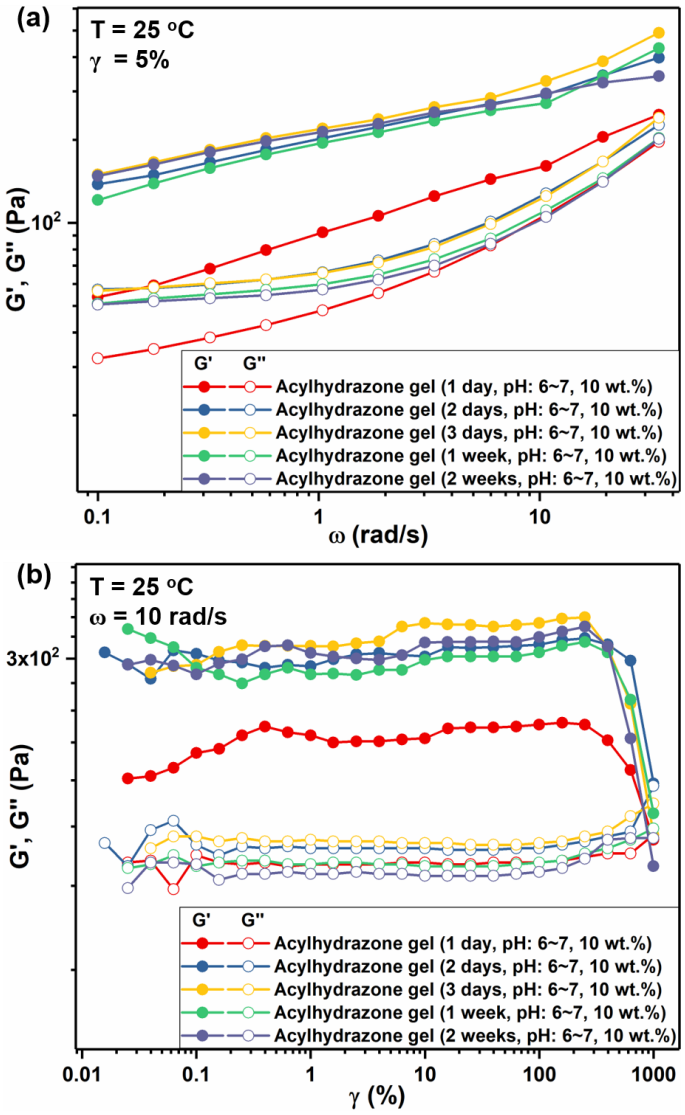

Figure 3.2. Oscillatory frequency sweeps (a) and strain sweeps (b) on individual acylhydrazone network hydrogel at different aging time.

The dynamic viscoelastic behaviors of individual networks of oxime, acylhydrazone, Fe^{2+}-Tpy, and Zn^{2+}-Tpy were measured by oscillatory frequency sweeps (**Figure 3.3**). For these four samples, the storage moduli (*G'*) are always higher than their pure copolymer solutions indicating the formation of crosslinks after two days of aging.

The ^{1}H NMR characterizations (**Figure 3.4**) also proved the formation of oxime and acylhydrazone crosslinks.

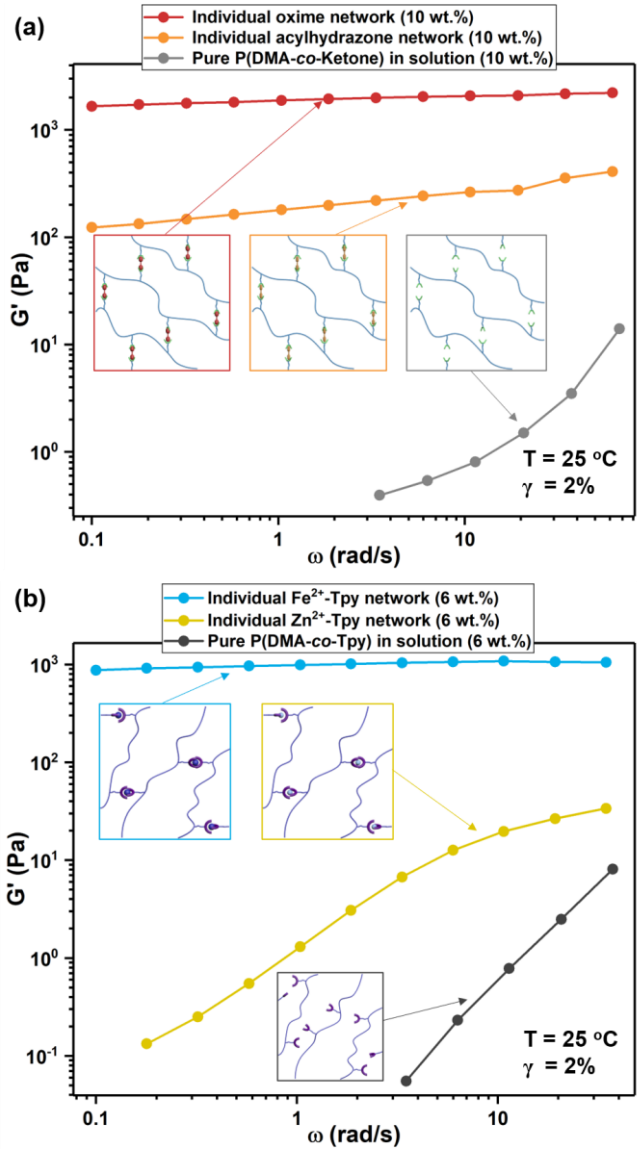

Figure 3.3. Oscillatory frequency sweeps on individual networks based on (a) acylhydrazone and oxime, and on (b) Fe^{2+}-Tpy and Zn^{2+}-Tpy, compared to their respective polymer solution of P(DMA-*co*-Ketone) and P(DMA-*co*-Tpy).

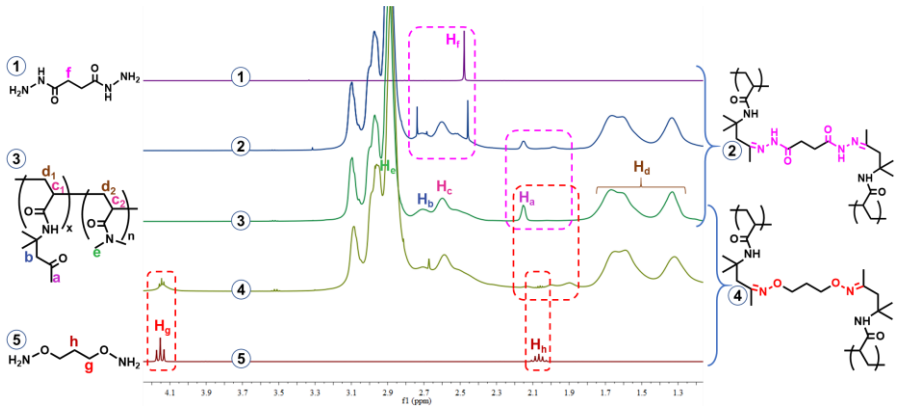

Figure 3.4. ^{1}H NMR spectra of P(DMA-*co*-Ketone) **3**, di-acylhydrazine **1**, bis-hydroxylamine **5**, acylhydrazone network **2** and oxime network **4** in D_2O.

The characterizations of purified P(DMA-*co*-Ketone), di-acylhydrazine, bis-hydroxylamine, and the formed acylhydrazone network and oxime network (2 days of aging) were performed by ^{1}H NMR in D_2O at same group concentration. As shown in **Figure 3.4**, the peak position of methyl protons adjacent to the carbonyl group of the ketone unit (signal a) has shifted from 2.15 ppm to 1.99 ppm for acylhydrazone network and to 1.90 ppm for oxime network, suggesting the formation of both individual networks. For the acylhydrazone, the signal around 2,15 ppm is still visible after crosslinking, showing incomplete reaction in agreement with the rheology results.

The storage moduli of the acylhydrazone, oxime, and Fe^{2+}-Tpy samples are almost constant over the whole experimental frequency window, showing that stable gels have been formed. Their values, which are close to 1 kPa for oxime and Fe^{2+}-Tpy, and to 200 Pa for acylhydrazone, can be compared to the values found if we assume that all the functional groups lead to the creation of effective intermolecular crosslinks, i.e., $G_N^0 = \frac{c\rho_0 RT}{M_{XX}}(1-\varphi_{dangling})$, where ρ_0 is the density of PDMA in the melt state (approximated as 1 g/cm^3), c is the sample concentration, M_{xx} is the average molar mass between two sticky groups (estimated to be 2.5 kg/mol for P(DMA-*co*-Ketone) and 7.3 kg/mol for

P(DMA-*co*-Tpy), see **Table 3.1**) and $\varphi_{dangling}$ is the weight fraction of dangling ends, which do not participate to the network elasticity, and can be approximated as equal to $2M_{xx}/M_w$. In such a case, the plateau moduli G_N^0 of the P(DMA-*co*-Ketone) and the P(DMA-*co*-Tpy) samples should be roughly equal to 89 kPa and 16 kPa, respectively, which is much higher than the values found experimentally. This result suggests the presence of a large number of unreacted groups, as well as the presence of internal loops due to intramolecular crosslinks that do not contribute to the sample elasticity, especially in the case of the acylhydrazone network. The higher level of the plateau modulus of the oxime network is due to a higher crosslinking density of oxime hydrogels, consistent with the greater equilibrium constant and the greater intrinsic hydrolytic stability of oximes compared to acylhydrazones. Given the high equilibrium constants (K_{eq}) of acylhydrazone (10^4~10^6 M^{-1}), oxime (> 10^8 M^{-1}), Zn^{2+}-Tpy ($10^{5.2}$ M^{-1}), and Fe^{2+}-Tpy ($10^{13.8}$ M^{-1}) (values of Zn^{2+}-Tpy and Fe^{2+}-Tpy are the $K_{eq,2}$ equilibrium constants for the formation of bis-complexes),[31, 58] it is reasonable to assume that all bonds that can be formed are in their associated state, and that taking into account K_{eq} to correct for G_N^0 would have a negligible effect.

On the other hand, the relatively higher level of the rubbery plateau observed for the Fe^{2+}-Tpy system (compared to the value found in case of the perfect network) demonstrates its larger capability to create intermolecular junctions. This can be due to both the high association constant of Fe^{2+}-terpyridine bis-complexes[54] and the fact that the molecular strands between two sticky groups are longer, which reduces the probability of creating internal loops. Only the system based on Zn^{2+}-Tpy associations is able to flow within the experimental frequency window. This is attributed to the lower equilibrium constant and high lability of Zn^{2+}-terpyridine bis-complexes,[54] which largely reduce the lifetime of the supramolecular network.[28] Moreover, at high frequency, a power-law of ½ is found for $G'(\omega)$, indicating that before the terminal regime, the relaxation of this material is well described by a (Constraint Release) Rouse process.

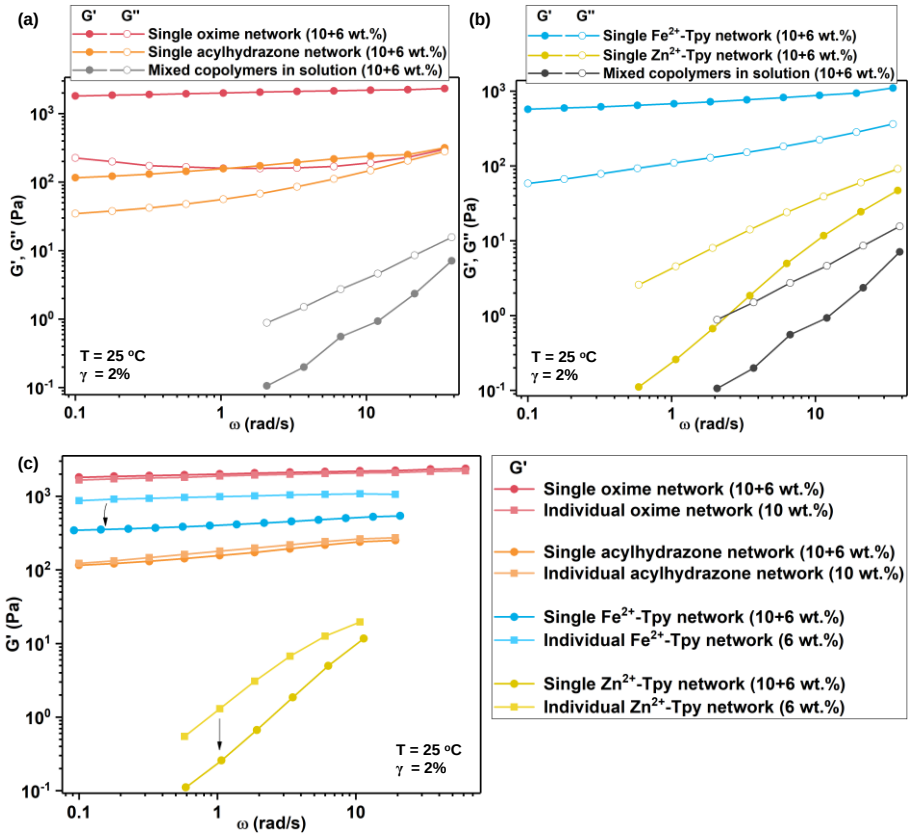

Figure 3.5. Oscillatory frequency sweeps on single networks based on (a) acylhydrazone and oxime; and (b) on Fe^{2+}-Tpy and Zn^{2+}-Tpy from the mixed copolymer solution of P(DMA-*co*-Ketone) and P(DMA-*co*-Tpy). (c) Comparison of the dynamic mechanical properties of individual and single networks of oxime, acylhydrazone, Fe^{2+}-Tpy and Zn^{2+}-Tpy.

Next, the possible influence of free chains (non-crosslinked) of the other copolymer type on the network properties is investigated, as shown in **Figures 3.5a and 3.5b**. These single networks contain 10 wt% of P(DMA-*co*-Ketone) and 6 wt% of P(DMA-*co*-Tpy), and only one type of crosslinker. **Figure 3.5c** compares their storage moduli to the ones of their individual networks. It is seen that the viscoelastic response of the acylhydrazone and oxime samples is not influenced by the presence of P(DMA-*co*-Tpy) chains, which suggests that there is no interaction between P(DMA-*co*-Ketone) and P(DMA-*co*-Tpy) chains

when the P(DMA-*co*-Ketone) copolymer is crosslinked in the presence of the other copolymer type. This also highlights the fact that the unassociated chains (or dangling ends) are relaxing very fast compared to the lifetime of the associated dynamic covalent interactions, and do not contribute to the sample elasticity in the frequency window measured experimentally.

In the case of the supramolecular networks (Fe^{2+}-Tpy and Zn^{2+}-Tpy), the comparison between the dynamic mechanical properties of their single and individual supramolecular networks shows that mixing the two copolymers slightly reduces the level of the elastic modulus. The reason behind this could be a "screening effect" induced by the presence of a large amount of non-active P(DMA-*co*-Ketone) copolymer compared to the P(DMA-*co*-Tpy) copolymer (10% vs. 6%), slightly reducing the proportion of associated stickers or promoting the formation of internal loops and therefore affecting the, already low, crosslinking density of Fe^{2+}-Tpy and Zn^{2+}-Tpy.

Knowing the dynamics of the single networks, we can now investigate the viscoelastic properties of the four IPN hydrogels, which are presented in **Figure 3.6**. There are several points to highlight here. First, as for the single networks, the frequency dependence of the storage modulus of most of the IPNs is very limited, showing only a weak decrease with decreasing frequency, indicating that stable gels have been formed. As expected, the storage modulus measured at 10 rad/s, G' (ω=10 rad/s), is larger for the IPN containing the more stable bonds, i.e., 1Fe^{2+}-Tpy + 2Oxime, with G' (ω=10 rad/s) = 5780 Pa. The modulus then takes lower value for the IPNs 1Zn^{2+}-Tpy + 2Oxime (3980 Pa) and 1Fe^{2+}-Tpy + 2Acylhydrazone (2070 Pa), and becomes very small for the IPN 1Zn^{2+}-Tpy + 2Acylhydrazone (530 Pa). The latter value is not representative of the plateau modulus since it is taken in the flow regime of the sample. Furthermore, it is observed that the addition order of the two crosslinkers has a slight influence on the dynamic mechanical properties of the IPNs. For the systems with at least one long-lifetime crosslink type, i.e., Fe^{2+}-Tpy + Oxime, Zn^{2+}-Tpy

+ Oxime, and Fe^{2+}-Tpy + Acylhydrazone (**Figures 3.6b**, **3.6c**, and **3.6d**), adding first the metal ions (Zn^{2+}, Fe^{2+}) to build the supramolecular network, followed by the addition of di-acylhydrazine/bis-hydroxylamine to create the second network yields IPNs with slightly higher moduli. This could come from the greater chain mobility of the P(DMA-*co*-Ketone) copolymer inside the more sparsely crosslinked supramolecular first network, compared to the reverse crosslinking order where the denser DCB network is formed first, allowing a slightly easier and more efficient formation of the second network. On the other hand, the less stable DCB with labile metal-ligand bond (Acylhydrazone + Zn^{2+}-Tpy) system shows the opposite behavior, the dynamic moduli of the IPN being higher when the acylhydrazone crosslinks are formed before the Zn^{2+}-Tpy crosslinks (**Figure 3.6e**). This could be explained by the fact that the viscoelastic response of the IPN in which Zn^{2+}-Tpy crosslinks are formed first does not easily reach its equilibrium state, as confirmed by **Figure 3.7**, which shows that the moduli of this IPN reach the same level as for the other one after one month of aging.

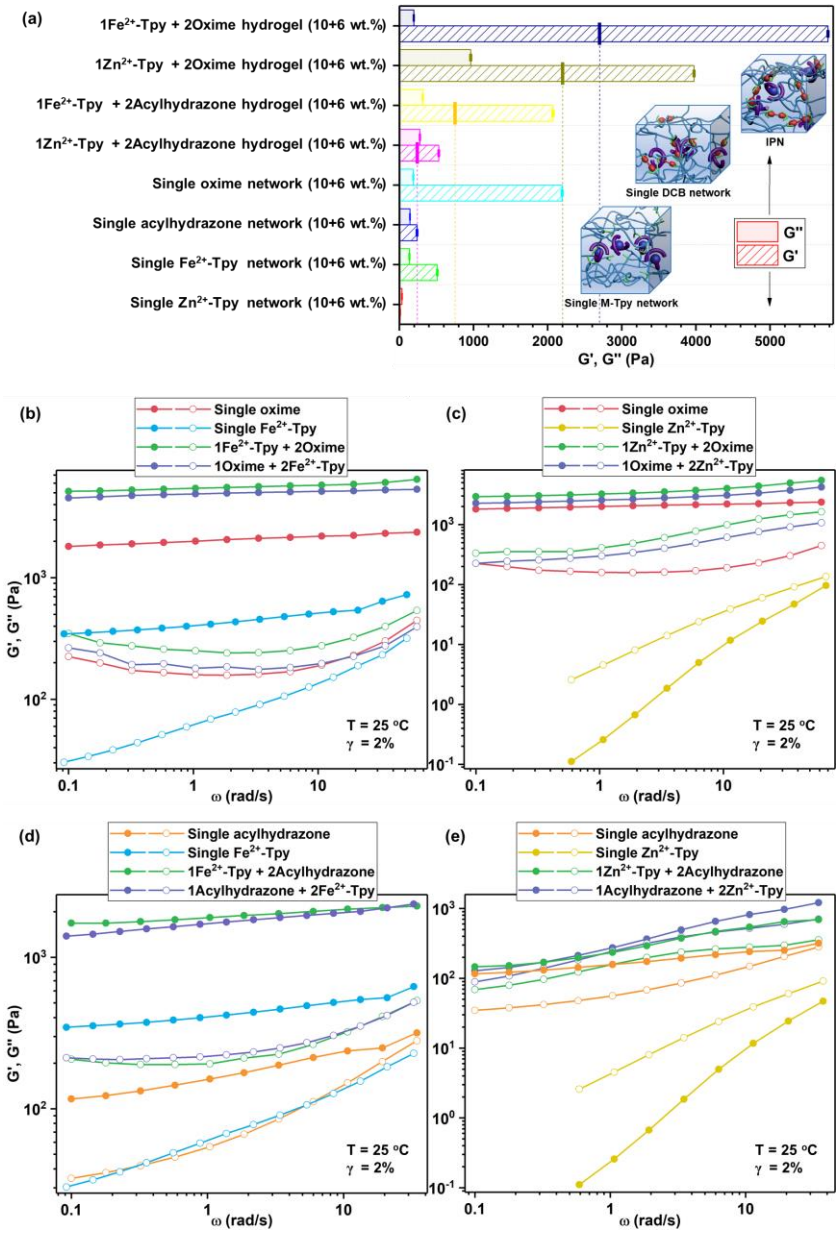

Figure 3.6. (a) Summary of the dynamic moduli values for the different IPN hydrogels and the corresponding single networks. The values were obtained from the frequency sweeps at a frequency of 10 rad/s. The vertical lines on the *G′* bar of the four IPN hydrogels represent the sum of the *G′* of the corresponding single networks. (b-e) Oscillatory frequency sweeps on the IPN hydrogels and their corresponding single networks (*G′*: filled symbols, *G″*: open symbols). The numbers 1 and 2 in the sample names refer to the addition sequence of the crosslinkers.

An interesting point to observe on **Figure 3.6** is the fact that the storage modulus of each IPN hydrogel is higher than the sum of their single network hydrogels. For example, the sum of the storage modulus of the single Fe^{2+}-Tpy hydrogel (510 Pa) and oxime hydrogel (2190 Pa) is only equal to 2710 Pa, which is much lower than the corresponding IPN hydrogel (5780 Pa). These results indicate a synergetic behavior between the two interpenetrating networks which stiffens the IPN hydrogels beyond the simple sum of the moduli (**Figure 3.6a**). This enhanced modulus of IPN hydrogels most probably arises from the fact that part of the entanglements created between the P(DMA-*co*-Ketone) and P(DMA-*co*-Tpy) chains due to the two crosslinked networks can now be trapped between associated stickers, and therefore act as additional physical interactions governed by the dynamics of the stickers. Thus, the IPN elasticity is not only due to the associated reversible junctions, but also to the possible interactions between the chains.

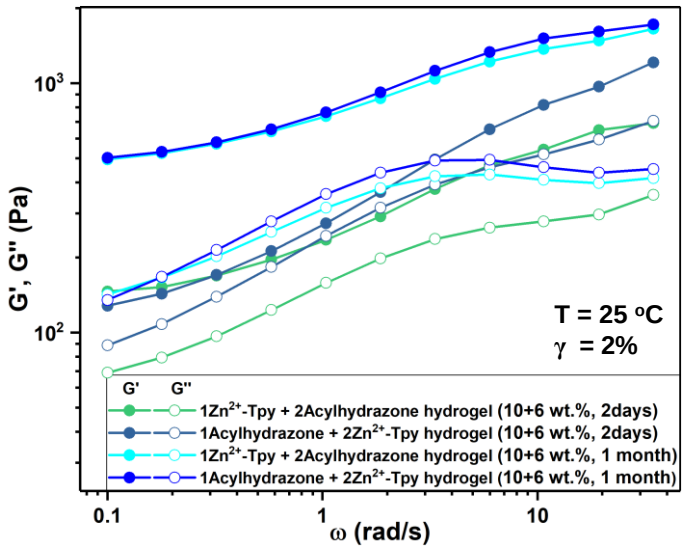

Figure 3.7. Oscillatory frequency sweeps on IPN hydrogels of Zn^{2+}-Tpy + Acylhydrazone from two different preparation protocols at aging time of 2 days and 1 month, respectively.

While the influence of blending two networks on the sample elasticity is clearly observed in **Figure 3.6a**, it is also important to investigate how it influences the relaxation dynamics of the IPN. To this end, we focus on the IPN containing Zn^{2+}-Tpy junctions since the relaxation of the complexes is fast enough to be measured under the conditions used here. The Zn^{2+}-Tpy + Acylhydrazone IPN shows the strongest frequency dependence since it is made of the two weakest bonds (**Figure 3.6e**). The decrease of *G'* with frequency for this IPN is proportionally more pronounced than for the acylhydrazone single network, showing that this decrease is mainly due to the relaxation of the Zn^{2+}-Tpy network, which allows in turn the release of both the supramolecular network elasticity and the interactions between the two networks. As shown in **Figure 3.8**, we also observe that the relaxation of the Zn^{2+}-Tpy network within this IPN starts at a time similar to the relaxation time of the single Zn^{2+}-Tpy network. However, much longer time is required before the contribution of the Zn^{2+}-Tpy network fully vanishes and the IPN reaches the modulus of the acylhydrazone single network. In the transition zone between these two times, a characteristic slope of -1/2 is observed in the storage modulus, indicating a Rouse relaxation. This result can be understood as follows: the IPN elasticity mostly arises from the interactions between the two networks. With time, since the Zn^{2+}-Tpy complexes of the supramolecular network continuously dissociate and associate, the molecular segments located between two DCBs of the acylhydrazone network are able to explore their surrounding, but only at the rhythm of the relaxation (or association/dissociation dynamics) of the supramolecular bonds (see **Figure 3.8b**). Therefore, this slow (and partial) relaxation of the acylhydrazone network segments is well described by a sticky Rouse process:[59,60]

$$G(t) = G_N^0 \phi(t) + G_N^0 \sum_{p=1}^{N_{Zn-Tpy}} \exp\left(\frac{-p^2 t}{\tau_{Zn-Tpy} N_{Zn-Tpy}^{\ 2}}\right) \qquad (3.1)$$

where G_N^0 is the plateau modulus of the acylhydrazone network, $\phi(t)$ is the fraction of the acylhydrazone network which is not relaxed at time t, $N_{\text{Zn-Tpy}}$ is the number of interactions between the acylhydrazone and Zn^{2+}-Tpy networks located between two associated DCBs, and $\tau_{\text{Zn-Tpy}}$ is the average lifetime of the Zn^{2+}-Tpy network. This model is tested in **Figure 3.8a**, in which we consider that $\tau_{\text{Zn-Tpy}}$=0.012s (as determined by approximating the viscoelastic response of the single network by a single Maxwell mode), G_N^0= 300 Pa (as observed experimentally), and considering a stretched exponential function to approximate the relaxation function $\phi(t)$ of the single acylhydrazone network (green curve), $\phi(t) = 0.5 + 0.5\ exp(-t^{0.5}/0.45)$.

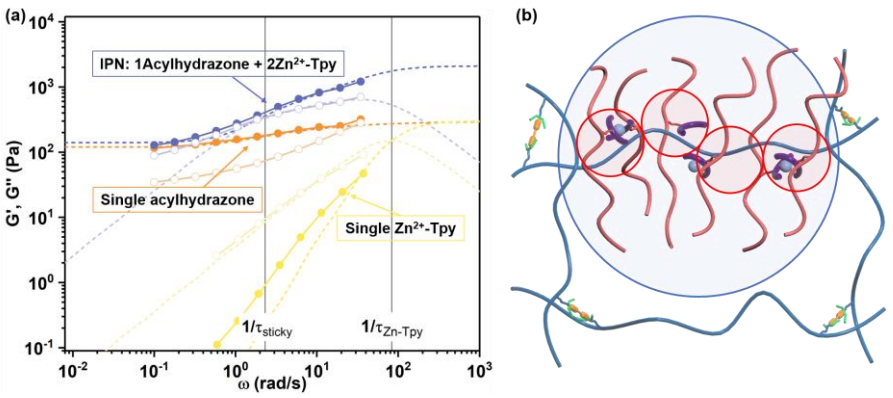

Figure 3.8. (a) Experimental (symbols) and theoretical (dashed curves) storage (full symbols) and loss moduli (empty symbols) of the single Zn^{2+}-Tpy network, the single acylhydrazone network and the 1Acylhydrazone + 2Zn^{2+}-Tpy IPN. (b) Cartoon representing the sticky Rouse relaxation of the molecular segments in the acylhydrazone network (represented in blue). While at very short times, interactions with the Zn^{2+}-Tpy network (in red) prevent the motion of these segments (see the red blobs), at longer times the segments are able to explore a larger surrounding (see the blue blob) and partially relax, at the rhythm of dissociations-associations of the Zn^{2+}-Tpy network.

The only unknown parameter is the number of network-network interactions per segment of the acylhydrazone network, which

determines both the level of the high frequency rubbery plateau of the IPN and the time needed for the influence of the Zn^{2+}-Tpy network to disappear. This number must be fixed to 6 in order to correctly describe the experimental data (**Figure 3.8a**).

These results suggest that the partial relaxation of the long-lifetime network takes place through sticky Rouse relaxation process. This means that the time needed to recover the same elasticity as in the single, long-lifetime, network, τ_{sticky}, is $N_{Zn\text{-}Tpy}^2$ times longer than the lifetime of the short lifetime network.

A short comment should be made here. Usually, sticky Rouse relaxation is observed with dual networks,[61] and not with interpenetrated networks. To be exact, one could argue that the Rouse regime observed in **Figure 3.8a** is not a sticky Rouse process, but rather a Constraint Release Rouse regime, where the molecular segments of the acylhydrazone network partially relax thanks to the disentanglement and relaxation of the Zn^{2+}-Tpy network, as described in ref.[62] However, since the relaxation of the Zn^{2+}-Tpy network is fully governed by the relaxation the supramolecular complexes, it seems appropriate to define this Rouse regime by a sticky Rouse relaxation.

The viscoelastic response of the 1Oxime + 2Zn^{2+}-Tpy IPN can also be modelled based on Equation 1 (**Figure 3.9**). In this case, we consider the same relaxation time $\tau_{Zn\text{-}Tpy}$ as with the 1Acylhydrazone + 2Zn^{2+}-Tpy IPN since the oxime network is diluted in the same short lifetime network. Furthermore, the plateau modulus of the single oxime network is fixed from the experimental data as equal to 2100 Pa, while the function $\phi(t)$ is well approximated by $\phi(t)=1$. The number of interactions per molecular segment between the two networks is, again, determined by best fitting. We find that ($N_{Zn\text{-}tpy}$ = 2) leads to a good agreement between the theoretical and the experimental data (**Figure 3.9**). This lower value is a direct consequence of the fact that the oxime network is much denser than the acylhydrazone network. Therefore, the molecular segments between two associated DCBs are shorter, which limits the number of interactions with the Zn^{2+}-Tpy network.

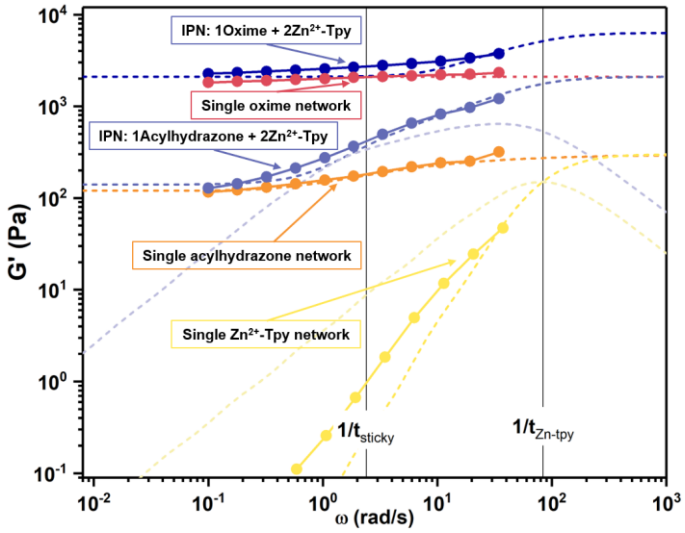

Figure 3.9. Experimental (symbols) and theoretical (dashed curves) storage modulus of: the single Zn^{2+}-Tpy network, the single acylhydrazone network, the 1Acylhydrazone + $2Zn^{2+}$-Tpy IPN, the single oxime network, and the 1Oxime + $2Zn^{2+}$-Tpy IPN.

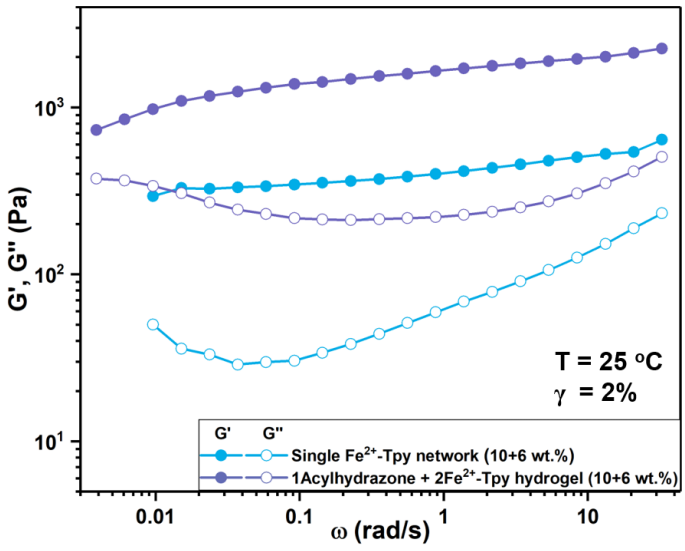

Figure 3.10. Oscillatory frequency sweep on the IPN hydrogel of Fe^{2+}-Tpy + Acylhydrazone and the corresponding Fe^{2+}-Tpy single network.

When Fe^{2+} ions are used instead of Zn^{2+} in the supramolecular network, the lifetime of the complexes becomes too long to easily observe its relaxation. As shown in **Figure 3.10**, the loss modulus of the single Fe^{2+}-Tpy network only starts to increase at a frequency around 0.01 rad/s, which indicates the beginning of the network relaxation. Nevertheless, the data suggest that, similarly to the 1Acylhydrazone + 2Zn^{2+}-Tpy IPN, the partial relaxation 1Acylhydrazone + 2Fe^{2+}-Tpy IPN starts to take place at a time equal to the lifetime of the complexes, followed by a Rouse-like relaxation. This behavior is thus similar to the one with the Zn^{2+}-Tpy complexes, but it is slowed down by around three orders of magnitude.

In order to speed up the partial relaxation of these IPNs, external conditions must be changed. In the following, we investigate the influence of a reduced pH on the dynamics of the IPN hydrogels. Indeed, as mentioned in the introduction, due to the fact that reversible C=N bonds are pH-sensitive[58] and that the protonation of the terpyridine ligand weaken the metal-terpyridine coordination bonds,[63] the IPN hydrogels are expected to have the ability of gel-sol transition by changing the pH of the environment. To study the pH-responsiveness of the prepared IPN hydrogels, HCl (2 M) and triethyl-amine were used as pH regulators. As mentioned above, all IPN hydrogels were prepared from pure water at pH 6~7.

Figure 3.11 presents the rheology data on the four IPNs at different pH. Most IPN hydrogels stay in the gel state even at low pH (**Figure 3.11a**, **3.11b** and **3.11c**), apart from the Acylhydrazone + Zn^{2+}-Tpy IPN, made of the two weakest bonds, which turns into a solution at pH 1~2, showing that both sub-networks have been fully destructured (**Figure 3.11d**). The oxime-based IPN hydrogels (**Figure 3.11a and 3.11b**), and the corresponding individual oxime network (**Figure 3.12a**) are the least affected by the pH change. This difference compared to the acylhydrazone-based systems (**Figure 3.11c and 3.11d**) can be attributed to the higher resistance toward hydrolysis of oxime compared to acylhydrazone bonds.[26,58,64]

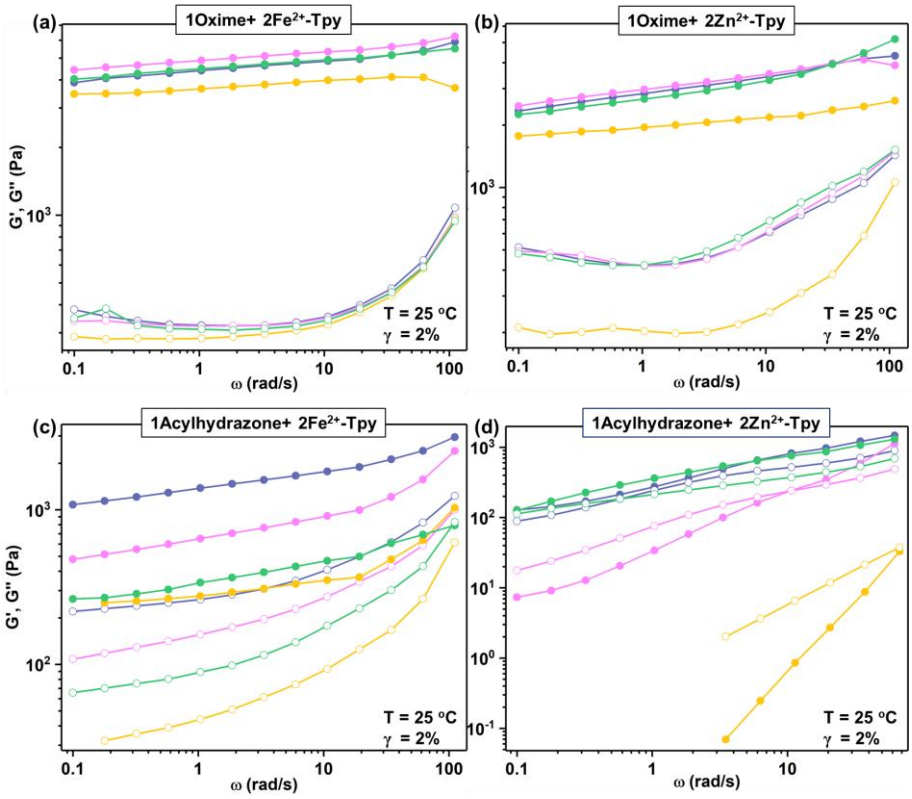

Figure 3.11. pH dependence of the dynamic moduli (G′: filled symbols, G″: empty symbols) of the IPN hydrogels. Blue curves: initial hydrogel at pH 6~7, pink curves: pH 3~4, yellow curves: pH 1~2, green curves: back to pH 6~7.

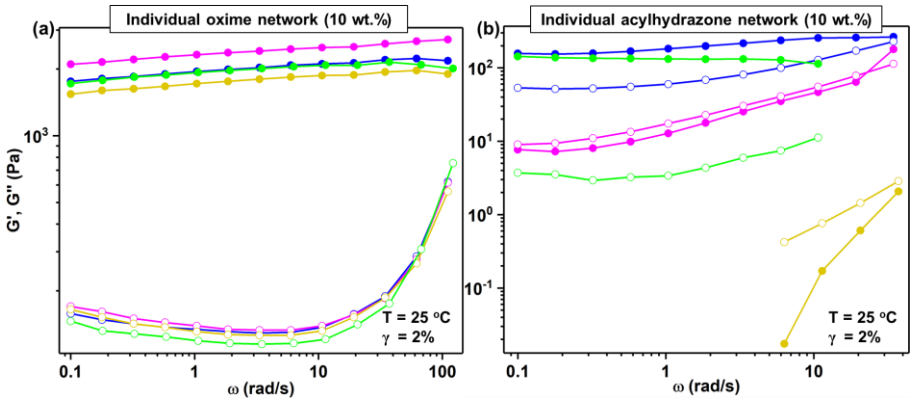

Figure 3.12. pH dependence of the dynamic moduli of individual networks of oxime and acylhydrazone. Blue curves: initial network at pH 6~7, pink curves: pH 3~4, yellow curves: pH 1~2, green curves: back to pH 6~7. Note that the acylhydrazone sample at final pH of 6-7 (green curve, panel b) has most probably not yet reached equilibrium in view of the *G'* evolution at high frequency.

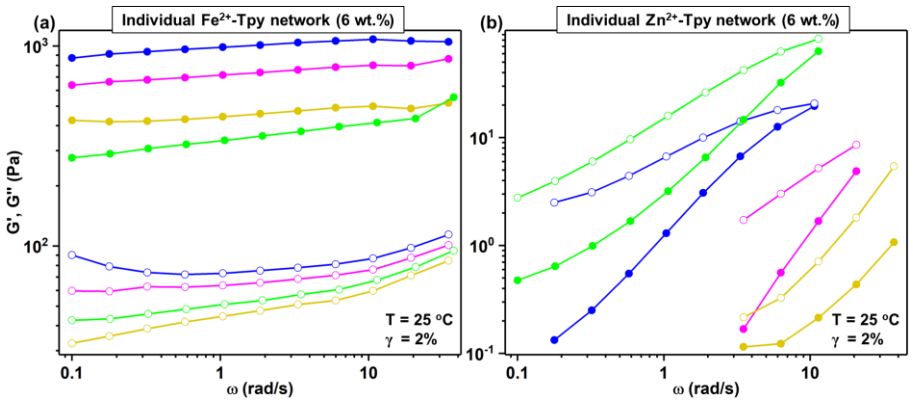

Figure 3.13. pH dependence of the dynamic moduli of individual networks of Fe^{2+}-Tpy and Zn^{2+}-Tpy. Blue curves: initial network at pH 6~7, pink curves: pH 3~4, yellow curves: pH 1~2, green curves: back to pH 6~7.

We also observe that the individual network based on Fe^{2+}-Tpy complexes (**Figure 3.13a**) is more affected by pH than the individual oxime network (**Figure 3.12a**), as can be seen by the drop of modulus by a factor of around 2.5 at pH 1~2, indicating that a lower number of complexes are formed at this pH. However, even at pH 1~2, this sample

still displays a second, low frequency plateau, which can be attributed to the long relaxation time of the supramolecular complexes. The influence of pH is much more important for the 1Acylhydrazone + 2Fe^{2+}-Tpy IPN since low pH completely fluidizes the acylhydazone individual network (**Figure 3.12b**). Therefore, at low pH, the contribution of acylhydrazone to the IPN is only observed at high frequency and vanishes at longer time, at which the IPN behaves similarly as the individual Fe^{2+}-Tpy network, i.e., as if the acylhydrazone network was not present. Playing with the pH is thus a way to promote the reversible dynamics of this IPN, otherwise too stable at neutral pH. In particular, at low pH, it is the DCB network which is relaxing first, not the Fe^{2+}-Tpy supramolecular network as it is the case at neutral pH (see **Figure 3.10**).

For the two other IPNs (**Figure 3.11b and 3.11d**), the association dynamics of the Zn^{2+}-Tpy network is always much faster than the one of both DCB networks. Therefore, at low frequency, the *G'* and *G"* moduli of the Acylhydrazone + Zn^{2+}-Tpy and Oxime + Zn^{2+}-Tpy IPNs are similar to ones of the DCB individual network, showing that the Zn^{2+}-Tpy network is completely destructured and only the acylhydrazone and oxime networks partially remain (**Figure 3.12**).

From **Figure 3.11**, we also note that three out of the four IPN hydrogels show complete recovery when the pH is returned to its original value. Only the Acylhydrazone + Fe^{2+}-Tpy IPN cannot recover its original state. This may be explained by the fact that for this IPN, the supramolecular bonds (Fe^{2+}-Tpy) are more stable than the acylhydrazone bonds, and are thus dominant in the viscoelastic response. Since these bonds are quite sensitive to pH as shown in **Figure 3.13a** for the Fe^{2+}-Tpy individual network, a significant part of these bonds dissociates at low pH, leading to a decrease of the plateau modulus, as observed in **Figure 3.11c**. When the pH is set back to the original value, the Fe^{2+}-Tpy complexes reform rapidly but in a less optimal configuration, yielding a network with a lower degree of

crosslinking. The optimal reorganization of this 'frozen' network is strongly limited due to the low lability of the Fe^{2+}-Tpy complexes.

These results show that the rheological properties of the IPN hydrogels can be finely tuned by changing the pH and that the pH sensitivity and reversibility of the gel-sol transition depends strongly on the combination of interactions used to build the IPNs.

Finally, we study the behavior of the single networks and IPNs under large deformation by performing strain sweeps (**Figure 3.14**). The three single networks (the Zn^{2+}-Tpy sample is not shown since its dynamics is too fast) show a constant elastic modulus over a rather large strain range indicative of an extended linear deformation regime. The limiting strain value (γ_L), marking the end of the linear regime, increases in the order oxime, Fe^{2+}-Tpy, acylhydrazone (**Table 3.2**), following the decrease of crosslinking density in these three networks. At large strain amplitudes, the networks cannot withstand the deformation anymore and the samples break and are expelled from the geometries. Therefore, in order to probe the reversibility of the bonds, measurements were performed from low strain up to the maximum strain amplitude that can be reached without destroying the sample, then from this high strain amplitude down to low strain. In such conditions, all of the single networks fully recover their original state as shown in **Figure 3.15**. The small hysteresis which is observed for the highly sheared samples is attributed to the strain-induced breaking of part of the reversible bonds, the latter being able to reform when the deformation amplitude is reduced.

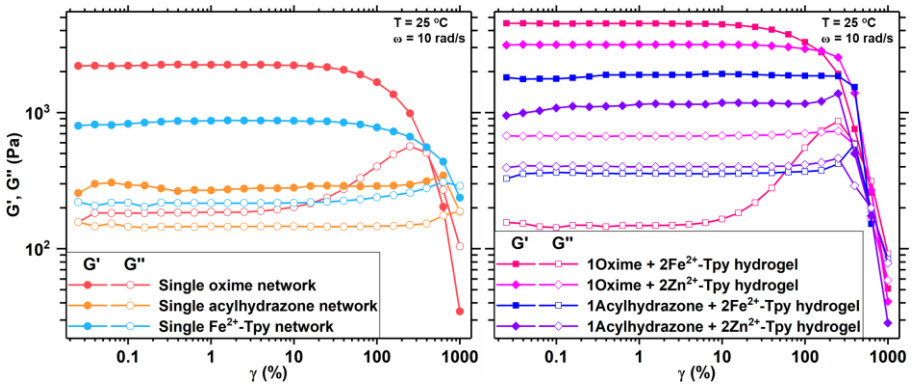

Figure 3.14. Oscillatory strain sweeps performed on the single networks (left) and the four IPN hydrogels (right). The single Zn^{2+}-Tpy sample is not shown because it is completely relaxed under these conditions due to its fast dynamics.

Table 3.2. Strain parameters obtained from Figure 3.14 for single networks and the four IPN hydrogels.

Sample	γ_L [a] (%)	γ_r [b] (%)
Single oxime network (10+6 wt.%)	15	432
Single acylhydrazone network (10+6 wt.%)	150	996
Single Fe^{2+}-Tpy network (10+6 wt.%)	25	845
1Oxime+2Fe^{2+}-Tpy hydrogel (10+6 wt.%)	18	514
1Oxime+2Zn^{2+}-Tpy hydrogel (10+6 wt.%)	42	822
1Acylhydrazone+2Fe^{2+}-Tpy hydrogel (10+6 wt.%)	215	577
1Acylhydrazone+2Zn^{2+}-Tpy hydrogel (10+6 wt.%)	110	576

[a] Obtained from the strain at which the G' starts to decrease/increase in the strain sweeps at a fixed frequency of 10 rad/s. [b] Obtained from the crossover of G' and G'' in the strain sweeps at a fixed frequency of 10 rad/s.

For the single acylhydrazone network, a slight shear thickening effect is observed at high shear amplitude. Such behavior has already been reported in literature for reversible networks and can be attributed to the fact that large shear flow promotes the formation of inter-

molecular associations.[65,66] While other mechanisms could also lead to shear thickening (such as chain stretching), an increase of inter-molecular associations fits our results since when going back from high to low strain amplitude, the storage and loss moduli of this network are slightly higher than initially (**Figure 3.15c and 3.15d**), indicating a better organization of the network. This shear thickening property is observed only for acylhydrazone network, which contains a large amount of non-active crosslinks and/or unreacted groups, and which did not fully reach equilibrium after an aging time of two days (**Figure 3.2 and 3.7**).

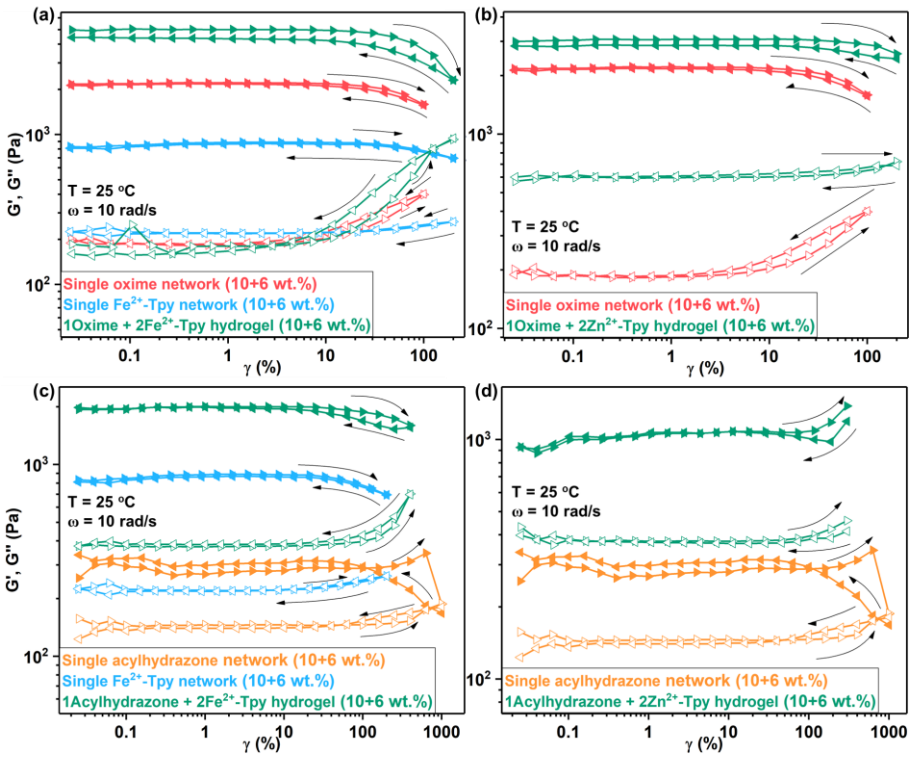

Figure 3.15. Oscillatory reversible strain sweeps performed on the different IPNs and their corresponding single networks: (a) 1Oxime + $2Fe^{2+}$-Tpy I, (b) 1Oxime + $2Zn^{2+}$-Tpy, (c) 1Acylhydrazone + $2Fe^{2+}$-Tpy, (d) 1Acylhydrazone + $2Zn^{2+}$-Tpy.

The four IPNs also show an extended linear regime. As for the single networks, as long as the strain sweep test is stopped before reaching the amplitude at which the samples break, the data measured from low to high to low strain amplitude show a good reversibility (**Figure 3.15**). Again, a hysteresis appears at high strain. The reversible bonds are forced to break under large oscillatory shear in order to allow the sample to follow the deformation, but as soon as the deformation is reduced, the reversible bonds are able to quickly reform. This shows the ability of the networks to self-heal after a large deformation.

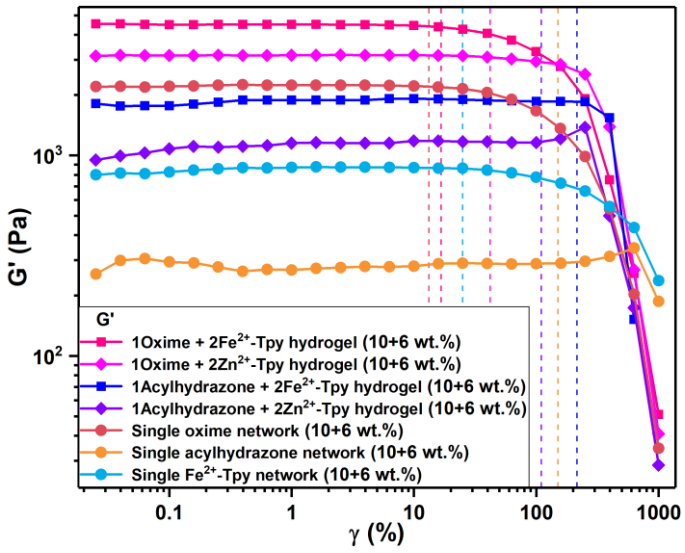

Figure 3.16. Oscillatory strain sweeps performed on four IPN hydrogels and the single networks. The dashed line in the graph shows the position of the limiting strain value (γ_L) for each curve.

Interestingly, the evolution of the limiting strain value (γ_L) between the single networks and the IPNs depends on the considered combination of networks (**Figure 3.16**). In particular, while the stiffest IPN network, built from oxime and Fe^{2+}-Tpy bonds, has a similar γ_L value to the oxime single network (**Table 3.2**), the IPN network containing oxime and the most labile supramolecular bond, Zn^{2+}-Tpy, displays a longer linear regime, corresponding to a larger γ_L value.

Similarly, the linear regime of the IPN network formed from the long-lifetime Fe^{2+}-Tpy complexes and the weak acylhydrazone is longer than the linear regime of the single network formed only from the Fe^{2+}-Tpy complexes. Thus, one can conclude that using IPNs allows a significant increase of storage modulus while conserving, or even improving, the deformability of the materials.

3.3 Conclusion

In this work, we investigated the viscoelastic properties of interpenetrated network hydrogels based on two orthogonal types of reversible bonds; dynamic covalent bonds (DCB) and metal-ligand bonds, with the aim of creating very stable – yet reversible – networks thanks to the presence of the DCBs, while the more tunable metal-ligand interactions can be used to adjust the material properties. In particular, we have studied how the rheological properties of both networks are combined and modified when these networks are interpenetrated. Four IPN hydrogels were thus obtained by combining either a very stable and pH insensitive DCB (oxime) or a slightly less stable and pH sensitive DCB (acylhydrazone), with either a long-lifetime supramolecular interaction (Fe^{2+}-Tpy) or a more dynamic one (Zn^{2+}-Tpy).

The results show that the obtained IPN hydrogels exhibit a higher modulus compared to the simple addition of the moduli of the single networks. We attributed this observation to fact that part of the entanglements between the chains of the two networks are trapped between associated stickers, and therefore act as additional physical interactions governed by the dynamics of the stickers. The study also revealed that the partial relaxation of the IPNs is induced by the relaxation of the supramolecular network and takes place through a sticky Rouse relaxation. We then studied how lowering the pH can be

used as a stimulus to affect the dynamics of the IPNs. In particular, we showed that a low pH strongly influences the stability of the acylhydrazone DCB network. At low pH, the acylhydrazone sub-network relaxes faster than the Fe^{2+}-Tpy supramolecular network, which corresponds to an inversion of the relaxation times of the two sub-networks compared to neutral pH. Finally, we demonstrated that building IPNs allows a significant increase of storage modulus while conserving, or even improving, the deformability of the materials. Combining DCB and metal-ligand bonds seems thus a promising approach toward highly tunable interpenetrated network hydrogels. Their properties under elongation should now be investigated in order to study the role played by the two networks on their extensibility.

3.4 Experimental Section

3.4.1. Reagents and materials

Unless otherwise stated, all the reagents were purchased at the highest purity available and used without further purification. The organic solvents used for synthesis were purified by conventional methods.[67] 4-Chloro-2,2':6',2''-terpyridine was purchased from Acros Organics Co. 2-(2-Aminoethoxy) ethanol and succinic dihydrazide were purchased from TCI Tokyo Chemical Industry Co. Aluminum oxide (activated, basic, Brockmann Grade I, 58 angstroms) was from Alfa Aesar Co. Acryloyl chloride and O,O'-(propane-1,3-diyl)bis(hydroxylamine) dihydrochloride were from Sigma Aldrich Co. N,N-Dimethylacrylamide (DMA) was from Sigma Aldrich Co., Ltd. and was passed through basic alumina immediately prior to use. Diacetone acrylamide (DAAM) was from Alfa Aesar Co. and was recrystallized three times in dichloromethane/*n*-hexane (1/4). 2,2'-Azobis(isobutyronitrile) (AIBN) was recrystallized two times in methanol. S-1-dodecyl-S'-(α,α'-dimethyl-α"-acetic acid) trithiocarbonate (DDMAT) was synthesized following a reported procedure[68] and recrystallized two times in *n*-hexane.

3.4.2. Preparation and characterization of monomers

Synthesis of 2-(2-([2,2':6',2''-terpyridine]-4'-yloxy)ethoxy)ethan-1-amine (TPy-DEG-NH_2).

The TPy-DEG-NH_2 was synthesized following a literature method.[69] 2-(2-aminoethoxy) ethanol (216 mg, 2.05 mmol) and anhydrous KOH (735 mg, 13.1 mmol) were dispersed in 7 mL of dry DMSO. The suspension was stirred at 60 °C for 1 h under argon atmosphere. To this mixture, 4-chloro-2,2':6',2''-terpyridine (500 mg,

1.87 mmol) was subsequently added, and the reaction mixture was heated at 70 ℃ for an additional 24 h. The reaction mixture was then placed under reduced pressure at 60 ℃ to remove most of DMSO. The residue was allowed to cool down to room temperature, and 80 mL of deionized water were added and stirred for 3 h. This aqueous solution was extracted with DCM (3×50 mL). The organic phases were collected and dried with anhydrous Na_2SO_4, and then concentrated under vacuum to get a yellow solid with 74 % yield (0.465 g). ^{1}H NMR (300 MHz, $CDCl_3$, δ): 8.66 (ddd, 2H, J = 2.7, 1.8, 0.9 Hz, CH_{terpy}, $H_{6,6''}$), 8.58 (d, 2H, J = 8.1 Hz, CH_{terpy}, $H_{3,3''}$), 8.04 (s, 2H, CH_{terpy}, $H_{3',5'}$), 7.83 (td, 2H, J = 7.5, 1.8 Hz, CH_{terpy}, $H_{4,4''}$), 7.32 (ddd, 2H, J = 6, 4.8, 1.2 Hz, CH_{terpy}, $H_{5,5''}$), 4.38 (t, 2H, J = 4.65 Hz, CH_2, H_a), 3.89 (t, 2H, J = 4.65 Hz, CH_2, H_d), 3.59 (t, 2H, J = 5.1 Hz, CH_2, H_b), 2.88 (t, 2H, J = 5.1 Hz, CH_2, H_c), 1.77 (s, broad, NH_2). HRMS (ESI-MS) m/z: $[M+H]^+$ calcd for $C_{19}H_{21}N_4O_2$, 337.1665; found, 337.1659.

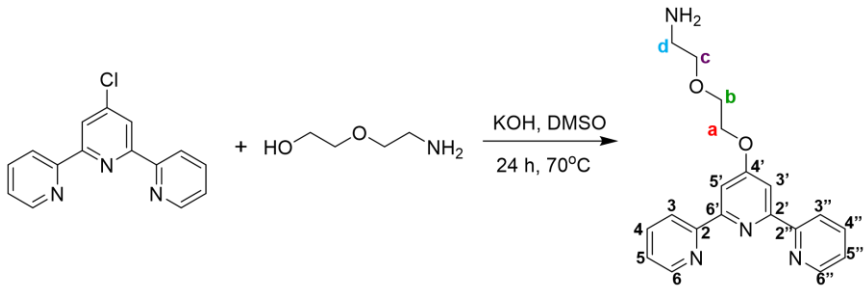

Scheme 3.4. Synthetic route of TPy-DEG-NH_2.

Synthesis of N-(2-(2-([2,2':6',2''-terpyridine]-4'-yloxy)ethoxy) ethyl)acrylamide (TPy-DEG-AM).

TPy-DEG-NH_2 (0.20 g, 0.60 mmol) and dry triethylamine (0.12 g, 1.2 mmol) were dissolved in dry DCM (10 mL) on an ice bath under argon atmosphere. To this solution, a solution of acryloyl chloride (0.11 g, 1.2 mmol) in 5 mL of dry DCM was added dropwise under stirring. After the addition was completed, the reaction mixture was stirred

overnight at room temperature, and then quenched with 15 mL of a saturated solution of Na_2CO_3. The organic fraction was isolated, and the aqueous fraction was extracted with dichloromethane (3×15 mL). The organic phases were recombined and dried with anhydrous Na_2CO_3, and then concentrated under vacuum below 25 °C. The crude product was purified through column chromatography (basic aluminum oxide), eluting with a mixture of ethyl acetate/hexane (gradient from 14% to 80% of ethyl acetate). The pure N-(2-(2-([2,2':6',2''-terpyridin]-4'-yloxy)ethoxy)ethyl)acrylamide (TPy-DEG-AM) was obtained as a white solid with 77 % yield (0.179 g). ^{1}H NMR (300 MHz, $CDCl_3$, δ): 8.69 (ddd, 2H, J = 2.7, 1.8, 0.9 Hz, CH_{terpy}, $H_{6,\,6''}$), 8.63 (d, 2H, J = 7.8 Hz, CH_{terpy}, $H_{3,\,3''}$), 8.10 (s, 2H, CH_{terpy}, $H_{3',\,5'}$), 7.86 (td, 2H, J = 7.5, 1.8 Hz, CH_{terpy}, $H_{4,\,4''}$), 7.35 (ddd, 2H, J = 6, 4.8, 1.2 Hz, CH_{terpy}, $H_{5,\,5''}$), 6.46 (br, 1H; CONH), 6.21 (dd, 1H, J = 16.8, 1.5 Hz, CH_2=CH), 6.01 (dd, 1H, J = 16.8, 10.2 Hz, CH_2=CH), 5.56 (dd, 1 H, J = 10.2, 1.5 Hz, CH_2=CH), 4.43 (m, 2H, CH_2, H_a), 3.90 (m, 2H, CH_2, H_d), 3.68 (t, 2H, J = 4.65 Hz, CH_2, H_b), 3.59 (t, 2H, J = 5.7 Hz, CH_2, H_c). HRMS (ESI-MS) m/z: $[M+H]^+$ calcd for $C_{22}H_{23}N_4O_3$, 391.1770; found, 391.1765.

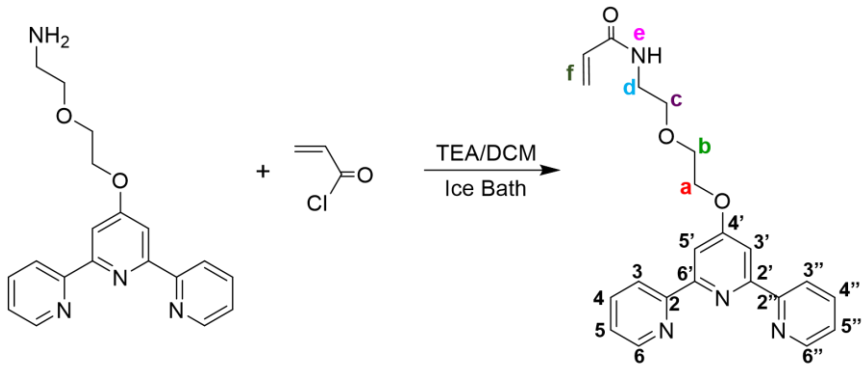

Scheme 3.5. Synthetic route of TPy-DEG-AM.

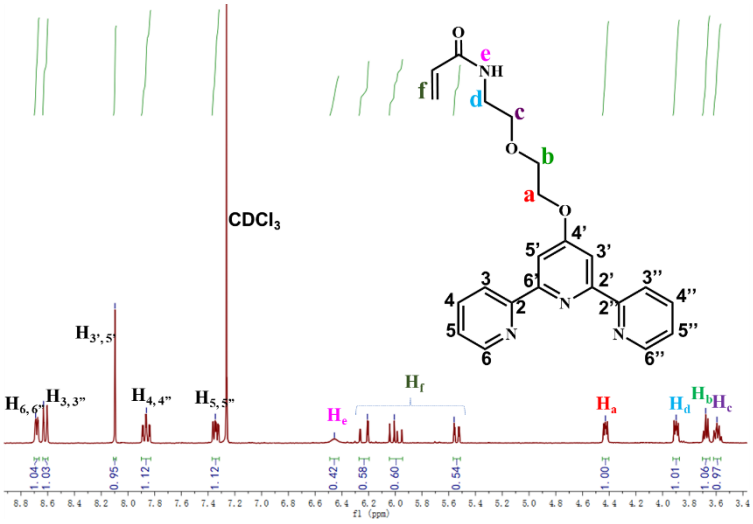

Figure 3.17. ^{1}H NMR spectrum of TPy-DEG-AM.

3.4.3. Preparation and characterization of copolymers

Synthesis of side-chain ketone-functionalized poly(N,N-dimethylacrylamide), P(DMA-*co*-Ketone).

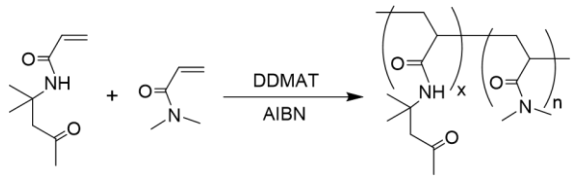

Scheme 3.6. Synthetic route of P(DMA-*co*-Ketone).

AIBN (2.5 mg, 0.015 mmol), DDMAT (36.5 mg, 0.1 mmol), DAAM (389.2 mg, 2.3 mmol) and DMA (5.472 g, 55.2 mmol) were dissolved in 10 mL of dry dioxane in a 50 mL round-bottom Schlenk-flask. The solution was degassed by five freeze-pump-thaw cycles, backfilled with argon, and stirred in a preheated oil bath at 70 °C for 5 h. The polymerization was stopped by opening the flask to air and

placing it in liquid nitrogen. The conversion of monomer was determined to be 78%, by comparing the integral ratio of the vinyl signals to the methylene proton of dioxane on the ^{1}H NMR spectrum. The viscous liquid was diluted with DCM and precipitated three times in 20-times volume excess of diethyl ether, and the polymer was finally dried in a vacuum oven at 40 °C for 24 h. The product was characterized by ^{1}H NMR and GPC.

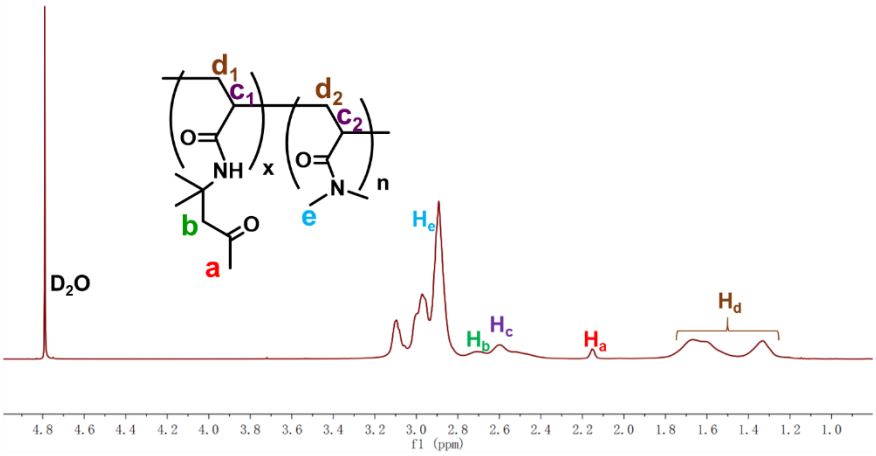

Figure 3.18. ^{1}H NMR spectrum of P(DMA-*co*-Ketone).

Synthesis of side-chain terpyridine-functionalized poly(N,N-dimethylacrylamide), P(DMA-*co*-Tpy).

AIBN (0.6 mg, 0.00375 mmol), DDMAT (9.1 mg, 0.025 mol), TPy-DEG-AM (113.2 mg, 0.29 mmol) and DMA (1.397 g, 14.09 mmol) were dissolved in 4.5 mL of dry DMF and 0.5 mL of dry anisole in a 25 mL round-bottom Schlenk-flask. The solution was degassed by five freeze-pump-thaw cycles, backfilled with argon and stirred in a preheated oil bath at 70 °C for18 h. The polymerization was stopped by opening the flask to air and placing it in liquid nitrogen. The conversion of monomer was determined to be 86% by comparing the integral ratio of the vinyl signal to the methyl proton of anisole on the ^{1}H NMR spectrum. The viscous liquid was diluted with DCM and precipitated

three times in 20-times volume excess diethyl ether, and the polymer was finally dried in a vacuum oven at 40 °C for 24 h. The product was characterized by ^{1}H NMR and GPC.

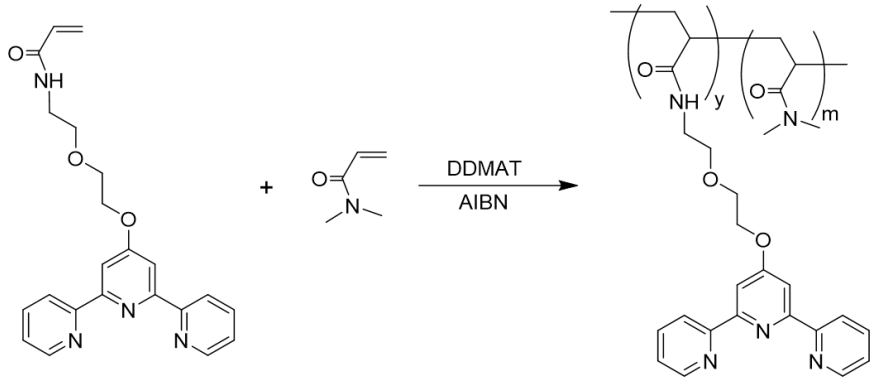

Scheme 3.7. Synthetic route of P(DMA-*co*-Tpy).

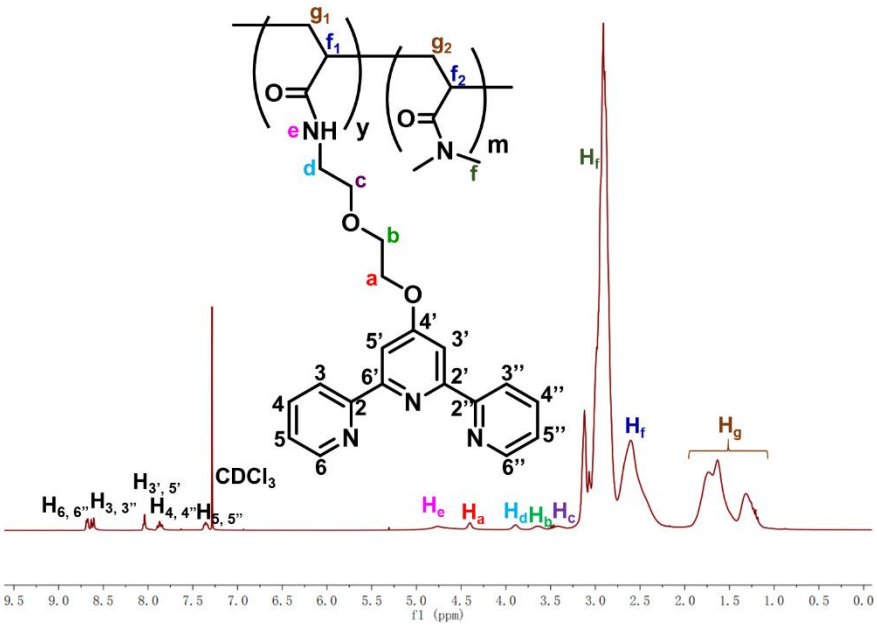

Figure 3.19. ^{1}H NMR spectrum of P(DMA-*co*-Tpy).

3.4.4. Preparation of networks

For all the prepared networks, the amount of added crosslinkers (di-acylhydrazine, bis-hydroxylamines or transition metal cations) was half an equivalent compared to the reactive sites (ketone or terpyridine groups) of the copolymers. The di-acylhydrazine (succinic dihydrazide) or bis-hydroxylamine (O,O'-(propane-1,3-diyl)bis(hydroxylamine) dihydrochloride) was used to react with ketone groups of P(DMA-*co*-Ketone) to build reversible C=N binding network, and the transition metal cations ($FeCl_2$ or $ZnCl_2$) were employed to interact with terpyridine groups of P(DMA-*co*-Tpy) to get metal-terpyridine association bridging network. Aqueous solutions of the four crosslinkers were prepared, and a certain amount was added to the polymer aqueous solutions to obtain the desired amount of crosslinker. The Fe^{2+} solution was dosed with 10 mol.% ascorbic acid to prevent the oxidation of Fe(II) to Fe(III).

Preparation of individual networks.

As shown in **Scheme 3.1**, the individual networks were prepared by first dissolving a given amount of P(DMA-*co*-Ketone) or P(DMA-*co*-Tpy) copolymer in 400 μL of deionized water. The sealed reaction vials were placed at room temperature overnight until the copolymers were dissolved completely and shaken periodically to get homogeneous solutions. To these solutions, 100 μL of a solution containing the appropriate amount of a crosslinker were added dropwise under shaking. After the crosslinker was added, the network was formed upon standing at ambient conditions for 2 days. The final concentration of the P(DMA-*co*-Ketone) in sample is 10 wt.%, and the P(DMA-*co*-Tpy) in sample is 6 wt.%, respectively.

Preparation of single networks.

As shown in **Scheme 3.2**, 500 μL of single networks were prepared at a total copolymer concentration of 10+6 wt.% (10 wt.% of P(DMA-

co-Ketone) and 6 wt.% of P(DMA-*co*-Tpy)). The preparation process is similar to the preparation of the individual networks. The copolymers of P(DMA-*co*-Ketone) and P(DMA-*co*-Tpy) were dissolved in 400 μL of deionized water to get homogeneous solutions, and 100 μL of a solution containing the appropriate amount of a crosslinker were then added. After 2 days of aging, the final single networks were obtained.

Preparation of interpenetrating polymer networks.

As shown in **Scheme 3.3**, in a typical experiment, 0.05 g of the P(DMA-*co*-Ketone) and 0.03 g of the P(DMA-*co*-Tpy) copolymer were mixed together and 300 μL of deionized water were added. The solution was placed at room temperature overnight and shaken periodically until the copolymers were completely dissolved. To this solution, 100 μL of first crosslinker solution were added dropwise under shaking to create the first network. After 24 h, the 100 μL of second crosslinker solution were added dropwise under shaking. The desired IPN hydrogels were obtained at room temperature after 2 days of aging.

3.4.5. Rheological measurements

Rheological measurements were conducted on a rotational rheometer (MCR 301, Anton Paar) equipped with a solvent trap at a reference temperature of 25 °C. The gel samples, in the form of sheets with diameter 8 mm and thickness 0.2~0.4 mm, were set in an 8 mm diameter parallel plate geometry. A 25 mm diameter parallel plate geometry with distance 0.1~0.2 mm was used for solution samples.

In the rheological experiments in this chapter, the testing time for each fresh sample did not exceed 40 min. Although the samples tested were relatively small as described above, the relatively short testing time avoided significant evaporation of water from the samples, and therefore classical solvent trapping measures were sufficient. As shown in **Figure 3.20**, water was added to the grooves of the bottom static

plate, and two Teflon models were also set up as solvent traps to avoid evaporation of the sample during measurement.

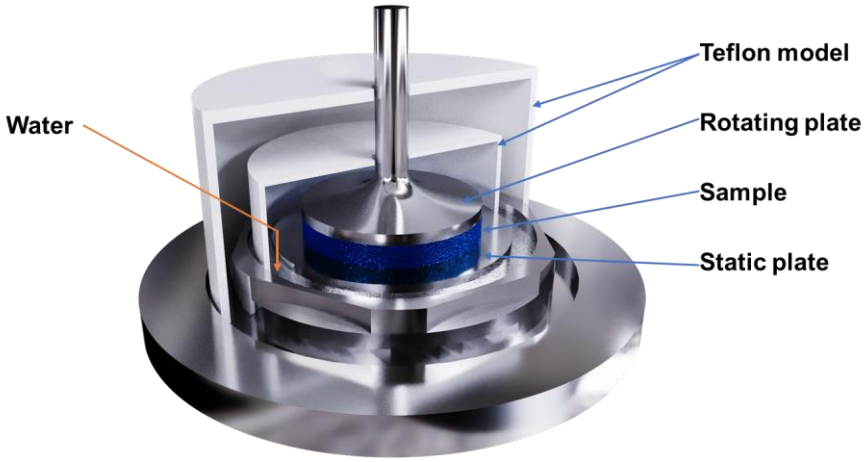

Figure 3.20. Solvent trap installation for rheological measurements in this chapter.

The linear viscoelastic regions of all samples were determined by oscillatory strain sweeps (0.01-1000% strain) performed at a frequency of 10 rad s^{-1}. The dynamic properties of the samples were determined by oscillatory frequency sweep (100-0.1 rad s^{-1}) at 2% strain, which is within the linear viscoelastic region. We estimate an accuracy of 10% on the mearued modulus values.

3.5 Reference

[1] Appel, E. A.; del Barrio, J.; Loh, X. J.; Scherman, O. A. Supramolecular polymeric hydrogels. Chem. Soc. Rev. 2012, 41, 6195-6214.

[2] Ulrich, S. Growing prospects of dynamic covalent chemistry in delivery applications. Acc. Chem. Res. 2019, 52, 510-519.

[3] Saunders, L.; Ma, P. X. Self-healing supramolecular hydrogels for tissue engineering applications. Macromol. Biosci. 2019, 19, No. 1800313.

[4] Heidarian, P.; Kouzani, A. Z.; Kaynak, A.; Paulino, M.; Nasri-Nasrabadi, B. Dynamic hydrogels and polymers as inks for three-dimensional printing. ACS Biomater. Sci. Eng. 2019, 5, 2688-2707.

[5] Li, J.; Geng, L.; Wang, G.; Chu, H.; Wei, H. Self-healable gels for use in wearable devices. Chem. Mater. 2017, 29, 8932-8952.

[6] Shang, J.; Le, X.; Zhang, J.; Chen, T.; Theato, P. Trends in polymeric shape memory hydrogels and hydrogel actuators. Polym. Chem. 2019, 10, 1036-1055.

[7] Guo, Y.; Bae, J.; Zhao, F.; Yu, G. Functional hydrogels for next-generation batteries and supercapacitors. Trends Chem. 2019, 1, 335-348.

[8] Yuk, H.; Lu, B.; Zhao, X. Hydrogel bioelectronics. Chem. Soc. Rev. 2019, 48, 1642-1667.

[9] Voorhaar, L.; Hoogenboom, R. Supramolecular polymer networks: hydrogels and bulk materials. Chem. Soc. Rev. 2016, 45, 4013-4031.

[10] Zou, W.; Dong, J.; Luo, Y.; Zhao, Q.; Xie, T. Dynamic covalent polymer networks: from old chemistry to modern day innovations. Adv. Mater. 2017, 29, 1606100.

[11] Wojtecki, R. J.; Meador, M. A.; Rowan, S. J. Using the dynamic bond to access macroscopically responsive structurally dynamic polymers. Nature Mater. 2011, 10, 14-27.

[12] Chakma, P.; Konkolewicz, D. Dynamic covalent bonds in polymeric materials. Angew. Chem., Int. Ed. 2019, 58, 9682-9695.

[13] Liu, Y.; Lehn, J.-M.; Hirsch, A. K. H. Molecular biodynamers: dynamic covalent analogues of biopolymers. Acc. Chem. Res. 2017, 50, 376-386.

[14] Lu, W.; Le, X.; Zhang, J.; Huang, Y.; Chen, T. Supramolecular shape memory hydrogels: a new bridge between stimuli-responsive polymers and supramolecular chemistry. Chem. Soc. Rev. 2017, 46, 1284-1294.

[15] Jiang, Z.-C.; Xiao, Y.-Y.; Kang, Y.; Pan, M.; Li, B.-J.; Zhang, S. Shape memory polymers based on supramolecular interactions. ACS Appl. Mater. Interfaces 2017, 9, 20276-20293.

[16] Schäfer, S.; Kickelbick G. Double reversible networks: improvement of self-healing in hybrid materials via combination of diels-alder cross-linking and hydrogen bonds. Macromolecules 2018, 51, 6099-6110.

[17] Jiang, Z.; Bhaskaran, A.; Aitken, H. M.; Shackleford, I. C. G.; Connal, L. A. Using synergistic multiple dynamic bonds to construct polymers with engineered properties. Macromol. Rapid Commun. 2019, 40, 1900038.

[18] Zhang, H.; Wu, Y.; Yang, J.; Wang, D.; Yu, P.; Lai, C. T.; Shi, A.-C.; Wang, J.; Cui, S.; Xiang, J.; Zhao, N.; Xu J. Superstretchable dynamic polymer networks. Adv. Mater. 2019, 31,1904029.

[19] Sheiko, S. S.; Dobrynin, A. V. Architectural code for rubber elasticity: from supersoft to superfirm materials. Macromolecules 2019, 52, 7531-7546.
[20] Zhang, C.; Yang, Z.; Duong, N. T.; Li, X.; Nishiyama, Y.; Wu, Q.; Zhang, R.; Sun P. Using dynamic bonds to enhance the mechanical performance: from microscopic molecular interactions to macroscopic properties. Macromolecules 2019, 52, 5014-5025.
[21] Xi, W.; Scott, T. F.; Kloxin, C. J.; Bowman, C. N. Click chemistry in materials science. Adv. Funct. Mater. 2014, 24, 2572-2590.
[22] Zhang, J.-Y.; Zeng, L.-H.; Feng, J. Dynamic covalent gels assembled from small molecules: from discrete gelators to dynamic covalent polymers. Chin. Chem. Lett. 2017, 28, 168-183.
[23] Zhang, J.; Hu, Y.; Li, Y. Dynamic covalent gels. In gel chemistry: interactions, structures and properties. lecture notes in chemistry; Springer: Singapore, 2018; Vol. 96, pp 119-151.
[24] Apostolides, D. E.; Patrickios, C. S. Dynamic covalent polymer hydrogels and organogels crosslinked through acylhydrazone bonds: synthesis, characterization and applications. Polym. Int. 2018, 67, 627-649.
[25] Zhang, Z. P.; Rong, M. Z.; Zhang, M. Q. Polymer engineering based on reversible covalent chemistry: a promising innovative pathway towards new materials and new functionalities. Prog. Polym. Sci. 2018, 80, 39-93.
[26] Sims, M. B.; Patel, K. Y.; Bhatta, M.; Mukherjee, S.; Sumerlin, B. S. Harnessing imine diversity to tune hyperbranched polymer degradation. Macromolecules 2018, 51, 356-363.
[27] Li, L.; Lin, Q.; Tang, M.; Duncan, A. J. E.; Ke, C. Advanced polymer designs for direct-ink-write 3D printing. Chem. Eur. J. 2019, 25,10768-10781.
[28] Shi, L.; Ding, P.; Wang, Y.; Zhang, Y.; Ossipov, D.; Hilborn, J. Self-healing polymeric hydrogel formed by metal-ligand coordination assembly: design, fabrication, and biomedical applications. Macromol. Rapid Commun. 2019, 40, 1800837.
[29] Brassinne, J.; Stevens, A. M.; Van Ruymbeke, E.; Gohy, J. F.; Fustin, C. A. Hydrogels with dual relaxation and two-step gel-sol transition from heterotelechelic polymers. Macromolecules 2013, 46, 9134-9143.
[30] Brassinne, J.; Fustin, C. A.; Gohy, J. F. Control over the assembly and rheology of supramolecular networks via multi-responsive double hydrophilic copolymers. Polym. Chem. 2017, 8, 1527-1539.
[31] Winter, A.; Schubert, U. S. Synthesis and characterization of metallo-supramolecular polymers. Chem. Soc. Rev. 2016, 45, 5311-5357.
[32] Grindy, S. C.; Learsch, R.; Mozhdehi, D.; Cheng, J.; Barrett, D. G.; Guan, Z.; Messersmith, P. B.; Holten-Andersen, N. Control of hierarchical polymer mechanics with bioinspired metal-coordination dynamics. Nature Mater. 2015, 14, 1210-1216.
[33] Wu, H.; Zheng, J.; Kjøniksen, A.-L.; Wang, W.; Zhang, Y.; Ma, J. Metallogels: availability, applicability, and advanceability. Adv. Mater. 2019, 31, 1806204.
[34] Creton, C. 50th Anniversary perspective: networks and gels: soft but dynamic and tough. Macromolecules 2017, 50, 8297-8316.
[35] Narita, T.; Mayumi, K.; Ducouret, G.; Hébraud, P. Viscoelastic properties of poly(vinyl alcohol) hydrogels having permanent and transient cross-links studied by microrheology, classical rheometry, and dynamic light scattering. Macromolecules 2013, 46, 4174-4183.

[36] Ahmadi, M.; Seiffert, S. Thermodynamic control over energy dissipation modes in dual-network hydrogels based on metal-ligand coordination. Soft Matter 2020, 16, 2332-2341.
[37] Liu, Y.; Tang, Z.; Wu, S.; Guo, B. Integrating sacrificial bonds into dynamic covalent networks toward mechanically robust and malleable elastomers. ACS Macro Lett. 2019, 8, 193-199.
[38] Myung, D.; Waters, D.; Wiseman, M.; Duhamel, P.-E.; Noolandi, J.; Ta, C. N.; Frank, C. W. Progress in the development of interpenetrating polymer network hydrogels. Polym. Adv. Technol. 2008, 19, 647-657.
[39] Dragan, E. Design and applications of interpenetrating polymer network hydrogels. A Review. Chem. Eng. J. 2014, 243, 572-590.
[40] Klymenko, A.; Nicolai, T.; Benyahia, L.; Chassenieux, C.; Colombani, O.; Nicol, E. Multiresponsive hydrogels formed by interpenetrated self-assembled polymer networks. Macromolecules 2014, 47, 8386-8393.
[41] Yu, Z.; Zhang, Y.; Gao, Z. J.; Ren, X. Y.; Gao, G. H. Enhancing mechanical strength of hydrogels via IPN structure. J. Appl. Polym. Sci. 2017, 134, 44503.
[42] Kausar, A. Interpenetrating polymer network and nanocomposite IPN of polyurethane/epoxy: a review on fundamentals and advancements. Polym. -Plast. Mater. Technol. 2019, 58, 691-706.
[43] Zhang, B.; Ke, J.; Vakil, J. R.; Cummings, S. C.; Digby, Z. A.; Sparks, J. L.; Ye, Z.; Zanjani, M. B.; Konkolewicz, D. Dual-dynamic interpenetrated networks tuned through macromolecular architecture. Polym. Chem. 2019, 10, 6290-6304.
[44] Yang, J.; Ma, M. G.; Zhang, X. M.; Xu, F. Elucidating dynamics of precoordinated ionic bridges as sacrificial bonds in interpenetrating network hydrogels. Macromolecules 2016, 49, 4340-4348.
[45] Gong, J. P. Why are double network hydrogels so tough? Soft Matter 2010, 6, 2583-2590.
[46] Chen, Q.; Chen, H.; Zhu, L.; Zheng J. Engineering of tough double network hydrogels. Macromol. Chem. Phys. 2016, 217, 1022-1036.
[47] Le, X.; Lu, W.; Zheng, J.; Tong, D.; Zhao, N.; Ma, C.; Xiao, H.; Zhang, J.; Huang, Y.; Chen, T. Stretchable supramolecular hydrogels with triple shape memory effect. Chem. Sci. 2016, 7, 6715-6720.
[48] Xiao, H.; Lu, W.; Le, X. X.; Ma, C. X.; Li, Z. W.; Zheng, J.; Zhang, J. W.; Huang, Y. J.; Chen, T. A multi-responsive hydrogel with a triple shape memory effect based on reversible switches. Chem. Commun. 2016, 52, 13292-13295.
[49] Foster, E. M.; Lensmeyer, E. E.; Zhang, B.; Chakma, P.; Flum, J. A.; Via, J. J.; Sparks, J. L.; Konkolewicz, D. Effect of polymer network architecture, enhancing soft materials using orthogonal dynamic bonds in an interpenetrating network. ACS Macro Lett. 2017, 6, 495-499.
[50] Le, X.; Lu, W.; Xiao, H.; Wang, L.; Ma, C.; Zhang, J.; Huang, Y.; Chen, T. Fe^{3+}-, pH-, Thermoresponsive supramolecular hydrogel with multishape memory effect. ACS Appl. Mater. Interfaces 2017, 9, 9038-9044.
[51] Tang, L.; Wen, L.; Xu, S.; Pi, P.; Wen, X. Ca^{2+}, Redox, and Thermoresponsive supramolecular hydrogel with programmed quadruple shape memory effect. Chem. Commun. 2018, 54, 8084-8087.
[52] Zhang, F.; Xiong, L.; Ai, Y.; Liang, Z.; Liang, Q. Stretchable multiresponsive hydrogel with actuatable, shape memory, and self-healing properties. Adv. Sci. 2018, 5, 1800450.

[53] Wang, M.; Wang, L.; Xu, Y.; Fu, L.; Yang, H. One-pot fabrication of triple shape memory hydrogel based on coordination bond, the dynamic borate ester bonds, and hydrogen bond. Soft Materials 2019, 17, 342-349.
[54] Lewis, R. W.; Malic, N.; Saito, K.; Evans, R. A.; Cameron, N. R. Ultra-high molecular weight linear coordination polymers with terpyridine ligands. Chem. Sci. 2019, 10, 6174-6183.
[55] Dirksen, A.; Dawson, P. E. Rapid oxime and hydrazone ligations with aromatic aldehydes for biomolecular labeling. Bioconjugate Chem. 2008, 19, 2543-2548.
[56] McKinnon, D. D.; Domaille, D. W.; Cha, J. N.; Anseth, K. S. Biophysically defined and cytocompatible covalently adaptable networks as viscoelastic 3d cell culture systems. Adv. Mater. 2014, 26, 865-872.
[57] McKinnon, D. D.; Domaille, D. W.; Cha, J. N.; Anseth, K. S. Bis-aliphatic hydrazone-linked hydrogels form most rapidly at physiological pH: identifying the origin of hydrogel properties with small molecule kinetic studies. Chem. Mater. 2014, 26, 2382-2387.
[58] Kölmel, D. K.; Kool, E. T. Oximes and hydrazones in bioconjugation: mechanism and catalysis. Chem. Rev. 2017, 117, 10358-10376.
[59] Chen, Q.; Tudryn, G. J.; Colby, R. H. Ionomer dynamics and the sticky rouse Model. J. Rheol. 2013, 57, 1441-1462.
[60] Zhang, Z.; Chen, Q.; Colby, R. H. Dynamics of associative polymers. Soft Matter 2018, 14, 2961-2977.
[61] Ahmadi, M.; Hawke, L. G. D.; Goldansaz, H.; van Ruymbeke, E. Dynamics of entangled linear supramolecular chains with sticky side groups: influence of hindered fluctuations. Macromolecules 2015, 48, 7300-7310.
[62] Hawke, L. G. D.; Ahmadi, M.; Goldansaz, H.; van Ruymbeke, E. Viscoelastic properties of linear associating poly(n-butyl acrylate) chains. J. Rheol. 2016, 60, 297-310.
[63] Brassinne, J.; Gohy, J. F.; Fustin, C. A. Orthogonal control of the dynamics of supramolecular gels from heterotelechelic associating polymers. ACS Macro Lett. 2016, 5, 1364-1368.
[64] Kalia J.; Raines, R. T. Hydrolytic stability of hydrazones and oximes. Angew. Chem. Int. Ed. 2008, 47, 7523-7526.
[65] Xu, D.; Hawk, J. L.; Loveless, D. M.; Jeon, S. L.; Craig, S. L. Mechanism of shear thickening in reversibly cross-linked supramolecular polymer networks. Macromolecules 2010, 43, 3556-3565.
[66] Shangguan, Y.; Liu, M.; Luo, G.; Zheng, Q. Shear induced self-thickening of chitosan/β-cyclodextrin compound solution. RSC Adv. 2016, 6, 110367-110374.
[67] Armarego, W. L. F.; Chai, C. L. L. Purification of laboratory chemicals, Butterworth-Heinemann, 2009.
[68] Lai, J. T.; Filla, D.; Shea, R. Functional polymers from novel carboxyl-terminated trithiocarbonates as highly efficient RAFT agents. Macromolecules 2002, 35, 6754-6756.
[69] Burazerovic, S.; Gradinaru, J.; Pierron, J.; Ward, T. R. Hierarchical self-assembly of one-dimensional streptavidin bundles as a collagen mimetic for the biomineralization of calcite. Angew. Chem. Int. Ed. 2007, 46, 5510-5514.

Chapter 4

Comparing the Dynamics of Hydrogels of Different Topologies

Abstract

Dual-crosslinked networks (DCN), interpenetrating polymer networks (IPN) and IPN-derived double networks (DN) are increasingly utilized to fabricate hydrogels with superb mechanical properties. However, the relationship between the microstructures of these networks and the resulting dynamics is rarely compared and little understood. To tackle this shortcoming, this work presents a systematic investigation of the viscoelastic properties of DCN, IPN and DN hydrogels, as well as their corresponding single networks, by oscillatory shear rheology. All the hydrogels are based on the same orthogonal combination of supramolecular interactions: zinc(II)-terpyridine bis-complexes, and reversible covalent bonds: oxime, as crosslinks. The contribution of single crosslinked networks to the modulus and relaxation of DCN, IPN and DN hydrogels is studied in detail. In particular, we show that the modulus of the hydrogels strongly depends on their topology. Elastic modulus nearly 2 times higher for DCN hydrogels, about 3 times for IPN hydrogels and 3.6 times for DN hydrogels, compared to the simple addition of the moduli of their corresponding single networks, have been obtained. The deformability and stability of the hydrogels increased in the order of DCN < IPN < DN. We also study how the relaxation behaviors of DCN, IPN and DN hydrogels is influenced by the dynamics of the corresponding single dynamic networks.

4.1 Introduction

As described in the literature review in Chapter 2, the hydrophilic crosslinked three-dimensional macromolecular networks in hydrogels can extend the range of applications of such soft materials by conferring many special properties on hydrogels such as stimuli-responsiveness, self-healing, stress relaxation, shape memory, etc.[1-8] However, the high water content also brings fragility to the polymer hydrogels, which limits their real-world applications. Aiming to address this shortcoming, two major strategies have been adopted to improve the mechanical properties of polymer hydrogels: introducing a variety of crosslinks and modifying the network topology.[9]

On the facet of crosslinks, dynamic bonds, comprising dynamic covalent bonds (DCBs) and supramolecular interactions, have been widely embedded into polymeric networks, often to study the relationship between the bond strength and kinetics, and the macroscopic rheological and mechanical properties of the materials.[10-14] Compared to the use of a single type of dynamic bonds, the combination of robust and adaptable DCBs with more dynamic supramolecular interactions is a promising strategy for engineering the next generation of smart polymeric materials exhibiting unusual viscoelastic characteristics such as tunable time-dependent mechanical modulus,[15] adjustable stress relaxation,[16] shear-thinning properties,[17] and combining enhanced toughness[18,19] and stimuli-responsiveness[20] with efficient self-healing.[21] As for the network topology of the hydrogels, dual-crosslinked network (DCN), interpenetrating polymer network (IPN), and double network (DN) are highlighted strategies for preparing polymer hydrogels with enhanced mechanical properties.[22-31] The differences and relationships between these three network topologies have been detailed in Chapter 2 and will not be repeated here.

The two above strategies, i.e., adapting network topology and using different types of (dynamic) crosslinks, have also been combined to

further tune the hydrogel properties, and impart them with reversibility and stimuli responsiveness.[32,33] However, the synergetic effects between these two categories of crosslinks on the viscoelastic behaviors of gels are rarely studied in detail, not to mention the interplay with the network architecture. For example, Zhang and coworkers investigated the hierarchical dynamics of boronic ester bonds and quadruple hydrogen bonds in poly(n-butyl acrylate) (PnBA) based DCN elastomers.[34] They showed that boronic ester transesterification can reduce the chain relaxation time compared to a permanently crosslinked PnBA, while the strong quadruple hydrogen bonds can increase the chain relaxation time, compared to the boronic ester crosslinked polymers, due to the topological constraints between quadruple hydrogen bond dimers. The interplay between these two dynamic bonds enables the elastomer to flow on the time scale of seconds.

Herein, we investigate the viscoelastic properties of networks of different topologies: DCN, IPN, and DN, which are crosslinked by the same couple of interactions, i.e., reversible C=N bonds and metal-terpyridine bis-complexes. To have a clear contrast of dynamics, we selected the combination of oxime bonds and zinc(II)-terpyridine bis-complexes (Zn^{2+}-Tpy) for crosslinking. The oxime bond is selected because it is formed by an efficient "click" reaction between a ketone and a hydroxylamine,[35] and because of its weak dynamic character and high hydrolytic stability compared to other C=N bonds (e.g. semicarbazone, acylhydrazone, imine).[36] Oxime-based crosslinks are thus stable under the used conditions, and will preserve the network integrity under shear stress. More importantly, our work in Chapter 3 showed that the networks crosslinked by oxime are frequency independent and behave more like static covalent networks in the used measuring conditions. The Zn^{2+}-Tpy was used to provide dynamic properties to the networks due to its highly kinetically labile character.[37-39] Therefore, the combination of oxime and Zn^{2+}-Tpy allows the hydrogel to be partially disentangled and relaxed by the labile Zn^{2+}-Tpy, while the stable oxime network could still maintain the integrity of the gel sample after the dissociation of the Zn^{2+}-Tpy

network. As we demonstrated in Chapter 3, partial relaxation of the IPN of oxime + Zn^{2+}-Tpy takes place through a sticky Rouse relaxation process. By using the same combination, we will be able to systematically compare and discuss the interplay and possible synergy effects between DCN, IPN and DN topologies, and the contribution of the two types of crosslinks.

To reach this goal, we have synthesized a series of terpyridine (Tpy) and/or ketone functionalized hydrophilic poly(N,N-dimethyl acrylamide) (PDMA) random copolymers by reversible addition-fragmentation chain transfer (RAFT) controlled radical polymerization. We firstly obtained five "short-chain" (M_n approximately 50 kDa) copolymers that can be crosslinked with Zn^{2+}, to form zinc (II)-terpyridine bis-complexes, and/or with bis-hydroxylamine to form oxime bonds. With the two types of crosslinks and these copolymers, we thus successfully obtained a DCN and two IPN hydrogels as described in **Figure 4.1**. In addition, one of the above Tpy-functionalized copolymers with two other long-chain (M_n approximately 150 kDa and 250 kDa) copolymers bearing ketone groups were employed for preparing two DN hydrogels (**Figure 4.1**). The single networks of DCN, IPN1, IPN2, DN1 and DN2 were also prepared in the same polymer compositions and concentrations but only crosslinked by one type of bond. We measured the rheological behaviors of the prepared DCN, IPN and DN hydrogels as well as their corresponding single networks to determine the respective contributions of two single networks (Zn^{2+}-Tpy and oxime crosslinked) and the effect of network topology on the viscoelastic properties.

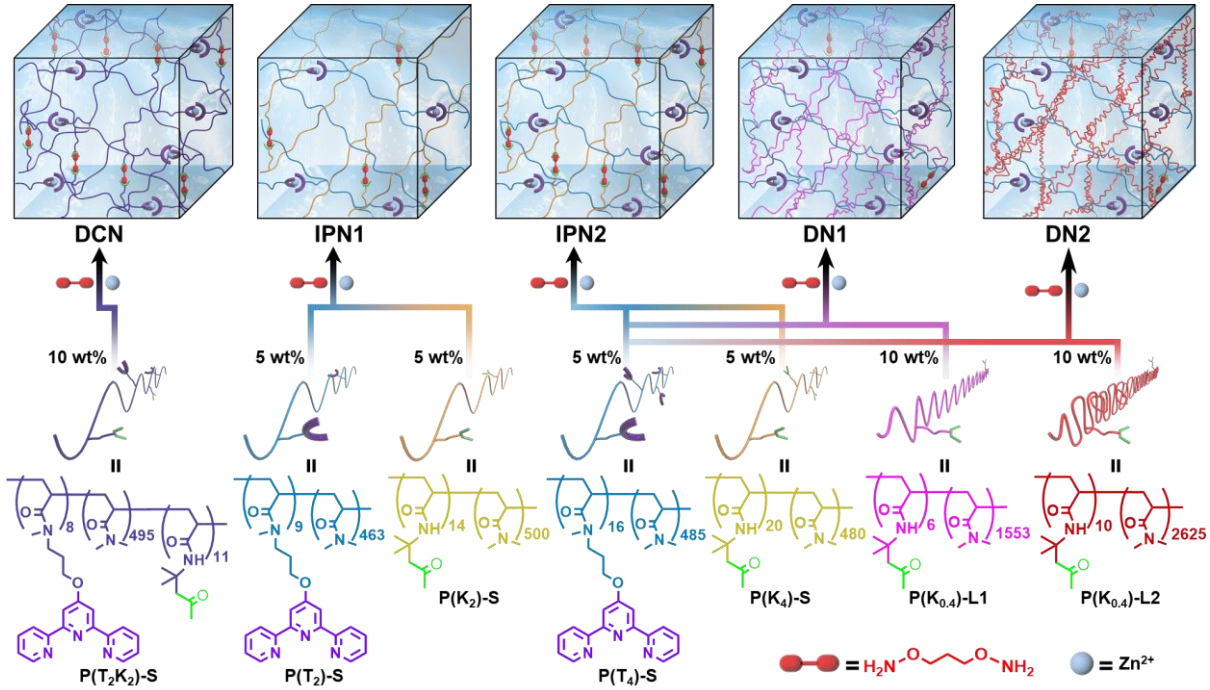

Figure 4.1. Schematic representation of dual-crosslinked network (DCN), interpenetrating polymer network (IPN), and double network (DN) hydrogels prepared by crosslinking various copolymers bearing ketone and/or terpyridine groups by formation of oxime bonds and zinc(II)-terpyridine bis-complexes (Zn^{2+}-Tpy).

4.2 Results and Discussion

4.2.1. Synthesis of hydrophilic functionalized copolymers

The building blocks of the different hydrogels are water-soluble functionalized copolymers with determined molar masses that were prepared by RAFT polymerization. N,N-dimethyl acrylamide (DMA) was selected as the base monomer for constituting the hydrophilic backbone of the copolymers. The commercially available diacetone acrylamide (DAAM) monomer was used to create oxime-based crosslinks owning to the reaction between ketone group of DAAM and the hydroxylamine group of O,O'-(propane-1,3-diyl)bis(hydroxylamine). In Chapter 3, we synthesized TPy-DEG-AM as a terpyridine functionalized monomer for copolymerization with DMA. However, the low solubility of TPy-DEG-AM in polymerization solvents such as 1,4-dioxane, makes it difficult to synthesize terpyridine functionalized copolymers with low molar mass dispersity. Thus, well-defined copolymers with both ketone and Tpy groups attached to the same PDMA chain were not obtained from TPy-DEG-AM. In order to improve the solubility of Tpy monomer and thus to obtain copolymers with homogeneous dispersion of Tpy units in the chain, we have newly synthesized the N-(3-([2,2':6',2''-terpyridin]-4'-yloxy)propyl)-N-methylacrylamide (TPy-AM) (see Experimental Section) monomer, whose structure without hydrogen on the amide group facilitates the solubility of the monomer in 1,4-dioxane. The TPy-AM served as handles for the formation of zinc(II)-terpyridine bis-complexes (Zn^{2+}-Tpy) crosslinks. Since all three monomers are of the acrylamide family, we can assume that they will be randomly incorporated into the different copolymers.

Table 4.1. Main characteristics of hydrophilic functionalized copolymers.

Copolymer	Final ratio[a] (mol%)			M_n[b] (g/mol)	M_n[c] (g/mol)	$Đ$[c]	N_f/Chain[d]	
	Tpy	Ketone	DMA				Tpy	Ketone
P(T_2K_2)-S	1.6	2.2	96.2	54100	53700	1.37	8	11
P(T_2)-S	1.9	/	98.1	49200	46400	1.35	9	/
P(K_2)-S	/	2.8	97.2	52100	53600	1.23	/	14
P(T_4)-S	3.2	/	96.8	54100	53200	1.36	16	/
P(K_4)-S	/	4.0	96.0	51000	58300	1.34	/	20
P($K_{0.4}$)-L1	/	0.4	99.6	155000	119000	1.37	/	6
P($K_{0.4}$)-L2	/	0.4	99.6	262000	171000	1.58	/	10

[a] Calculated from the ^{1}H NMR spectra. [b] Evaluated by monomer conversion (^{1}H NMR). [c] Determined by SEC (polymethylmethacrylate standards). [d] Average number of functional groups per chain.

Seven copolymers were thus obtained by varying ratios of functionalized monomers, and will be combined differently to yield the desired hydrogels of varying topology. Among the copolymers, the short-chain PDMA copolymer with ~2% terpyridine and ~2% ketone with an approximate molecular weight of ~50 kDa and is named as P(T_2K_2)-S; the short-chain PDMA copolymer with ~2% terpyridine with an approximate molecular weight of ~50 kDa and is named as P(T_2)-S; the short-chain PDMA copolymer with ~2% ketone with an approximate molecular weight of ~50 kDa and is named as P(K_2)-S; the short-chain PDMA copolymer with ~4% terpyridine with an approximate molecular weight of ~50 kDa and is named as P(T_4)-S; the short-chain PDMA copolymer with ~4% ketone with an approximate molecular weight of ~50 kDa and is named as P(K_4)-S; the long-chain PDMA copolymer with ~0.4% ketone with an approximate molecular weight of ~150 kDa and is named as P($K_{0.4}$)-L1; the long-chain PDMA

copolymer with ~0.4% ketone with an approximate molecular weight of ~250 kDa and is named as P($K_{0.4}$)-L2. All copolymers were characterized by ^{1}H NMR spectroscopy (see Supporting Information) and Size-Exclusion Chromatography (SEC) (**Table 4.1**).

4.2.2. Preparation of networks

For all the prepared networks, the amount of added crosslinkers (Zn^{2+} or bis-hydroxylamine) was half an equivalent compared to the reaction sites (terpyridine groups or ketone groups) of the corresponding functional copolymers unless otherwise stated. To enable comparisons between the different topological systems shown in **Figure 4.1**, the polymer concentration used is such that at least one of the crosslinks (Zn^{2+}-Tpy or oxime) in a system can lead to the formation of a hydrogel, i.e. the polymer concentration used for at least one type of the crosslinks is slightly higher than the minimum gelation concentration. Five "short-chain" copolymers with a M_n approximately 50 kg/mol were utilized for synthesizing DCN and two IPN hydrogels as well as their single networks.

Specifically, the copolymer P(T_2K_2)-S was used as precursor for preparing a DCN hydrogel and the corresponding single-crosslinked networks, i.e., networks crosslinked by only one type of bond (Zn^{2+}-Tpy or oxime) at 10 wt.% polymer concentration (**Scheme 4.1**). The molar amounts of the added crosslinkers of Zn^{2+} or bis-hydroxylamine correspond to half of the Tpy or ketone groups on the P(T_2K_2)-S chain, respectively.

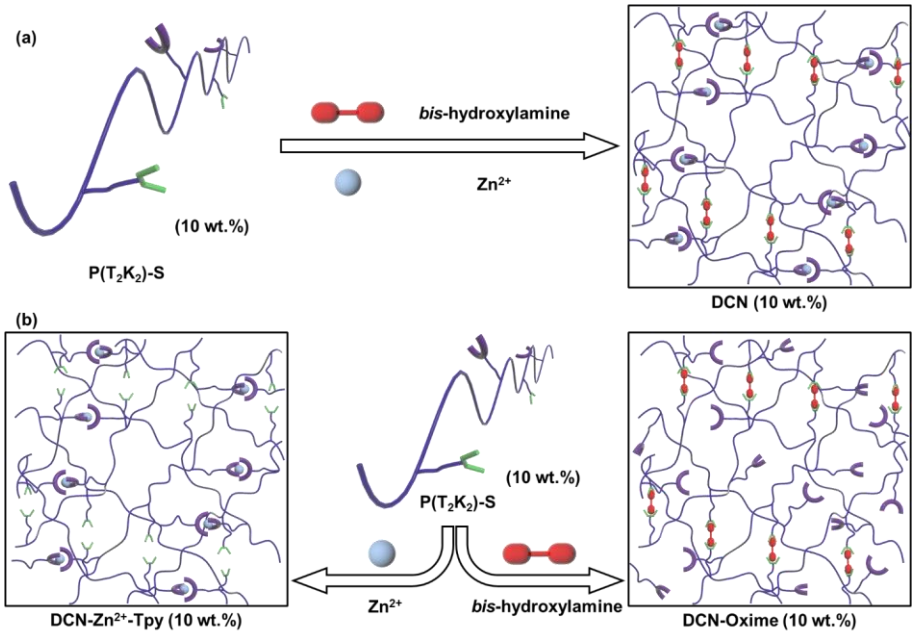

Scheme 4.1. Preparation of (a) DCN hydrogel as well as (b) its two single networks of DCN-Zn^{2+}-Tpy or DCN-Oxime from $P(T_2K_2)$-S (10 wt.%).

Three IPN hydrogels were then prepared by mixing two copolymers, one bearing ketone groups, and the other one bearing terpyridine groups. Two IPN1 hydrogels were obtained from the approximately 2% terpyridine-functionalized $P(T_2)$-S with 2% ketone-functionalized $P(K_2)$-S copolymers (**Schemes 4.2a** and **4.3a**). The first IPN1 was prepared at 10 wt.% total concentration (5 wt.% of each copolymer), and the second IPN1 at 20 wt.% total concentration. The IPN1 hydrogels have similar strand length between the same type of crosslinks as the DCN hydrogel (as illustrated in **Figure 4.1**). IPN2 hydrogel was prepared from the same kind of copolymers but bearing approximately 4 mol% of functional groups ($P(T_4)$-S and $P(K_4)$-S) (**Scheme 4.4a**) to reach a comparable crosslinker concentrations at the same total polymer concentration as the DCN hydrogel (10 wt.%). The corresponding single networks were also prepared from the mixed solutions of the two copolymers but only one of the copolymers was crosslinked with the appropriate crosslinker (**Schemes 4.2b**, **4.3b**, and

4.4b). Accordingly, the molar amounts of the added crosslinkers of Zn^{2+} or bis-hydroxylamine were half of the Tpy on the $P(T_2)$-S/$P(T_4)$-S chain or half of the ketone groups on the $P(K_2)$-S/$P(K_4)$-S chain, respectively.

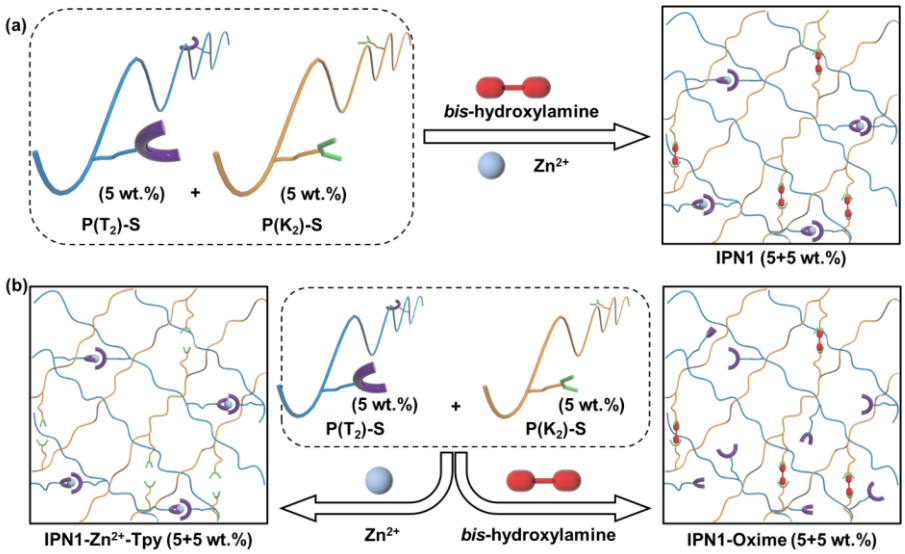

Scheme 4.2. Preparation of (a) IPN1 hydrogel as well as (b) its two single networks of IPN1-Zn^{2+}-Tpy or IPN1-Oxime, by mixing equal concentration (5 wt.%) of the $P(T_2)$-S with $P(K_2)$-S copolymers, leading to a total polymer concentration of 10 wt.%.

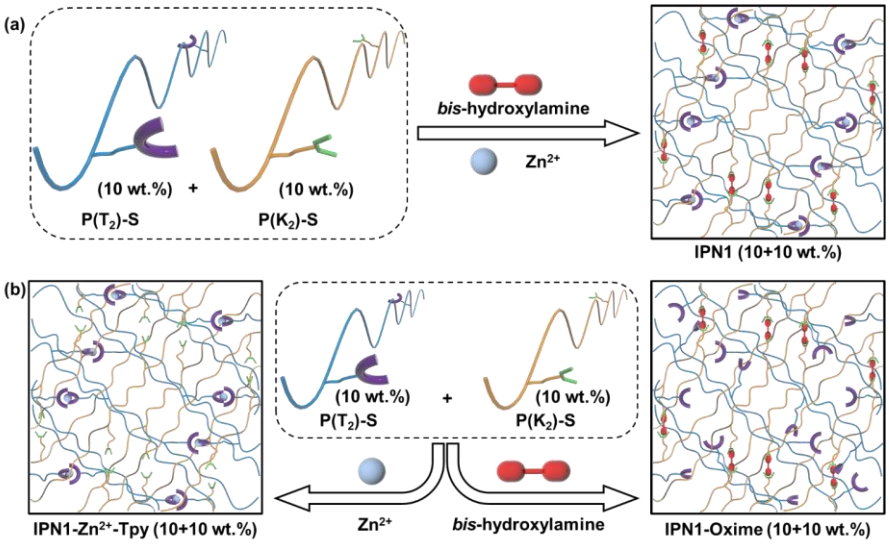

Scheme 4.3. Preparation of (a) IPN1 hydrogel as well as (b) its two single networks of IPN1-Zn^{2+}-Tpy or IPN1-Oxime, by mixing equal concentration (10 wt.%) of the $P(T_2)$-S with $P(K_2)$-S copolymers, leading to a total polymer concentration of 20 wt.%.

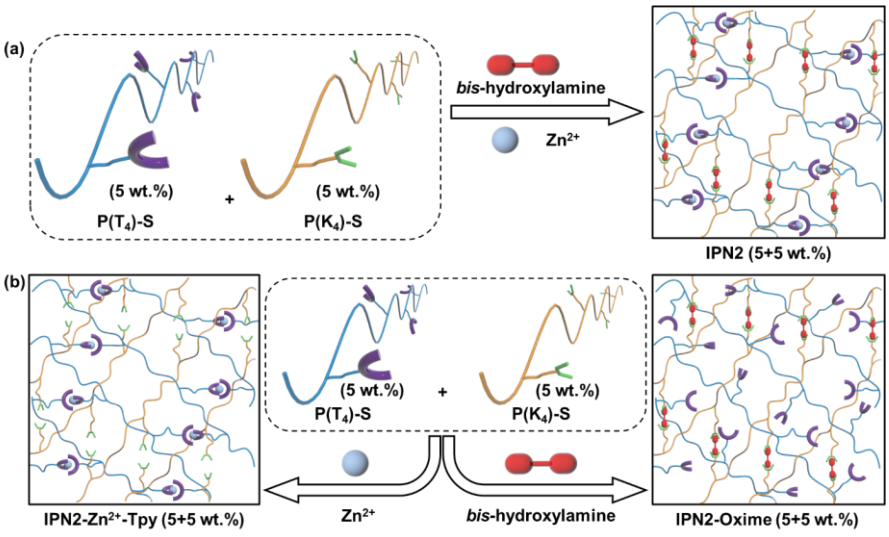

Scheme 4.4. Preparation of (a) IPN2 hydrogel as well as (b) its two single networks of IPN2-Zn^{2+}-Tpy or IPN2-Oxime, by mixing equal concentration (5 wt.%) of the $P(T_4)$-S with $P(K_4)$-S copolymers, leading to a total polymer concentration of 10 wt.%.

Moreover, two DN hydrogels were prepared from the short-chain P(T_4)-S and the long-chain ~0.4 mol% ketone-functionalized copolymers (P($K_{0.4}$)-L1 and P($K_{0.4}$)-L2). P($K_{0.4}$)-L1, with a M_n of approximately 150 kg/mol, was used for DN1 (**Scheme 4.5a**), and P($K_{0.4}$)-L2, with a M_n of approximately 250 kg/mol, was used for DN2 (**Scheme 4.6a**). In these DN hydrogels, the highly crosslinked and labile Zn^{2+}-Tpy network serves as the first (sacrificial) network, while the sparsely crosslinked and stable oxime network acts as the second network. The comparison of these two DNs will allow us to understand the impact of the length of the copolymer forming the second network on the viscoelastic behaviors of DN hydrogels since the networks are built directly from polymers instead of monomers.[40] As for the DNs, the corresponding single networks were also prepared by crosslinking only one copolymer of the mixture (**Schemes 4.5b** and **4.6b**). Similar to the IPN systems, the molar amounts of the added crosslinkers of Zn^{2+} or bis-hydroxylamine were calculated from half of the Tpy on the P(T_4)-S chain or half of the ketone groups on the P($K_{0.4}$)-L1/P($K_{0.4}$)-L2 chain, respectively.

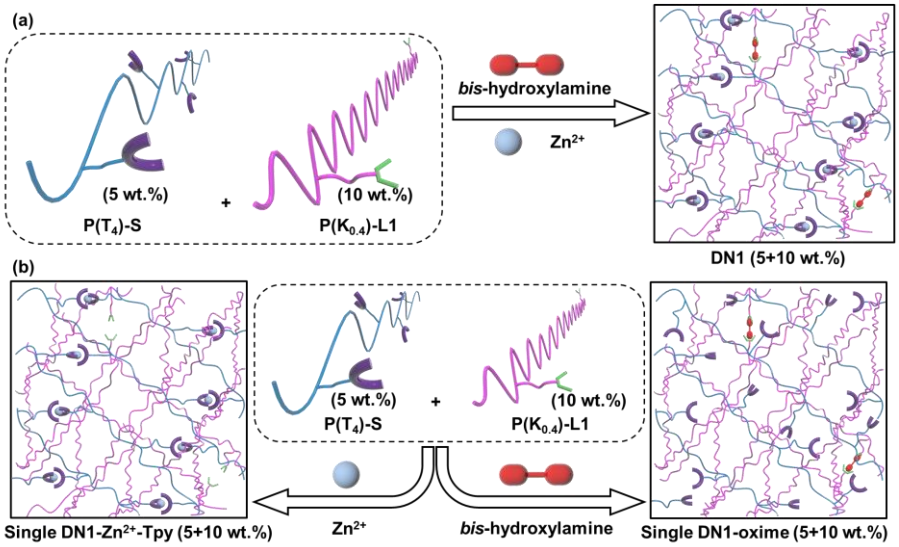

Scheme 4.5. Preparation of (a) DN1 hydrogel as well as (b) its two single networks of DN1-Zn^{2+}-Tpy or DN1-Oxime by mixing 5 wt.% of $P(T_4)$-S copolymer with 10 wt.% of $P(K_{0.4})$-L1 copolymer, leading to a total polymer concentration of 15 wt.%.

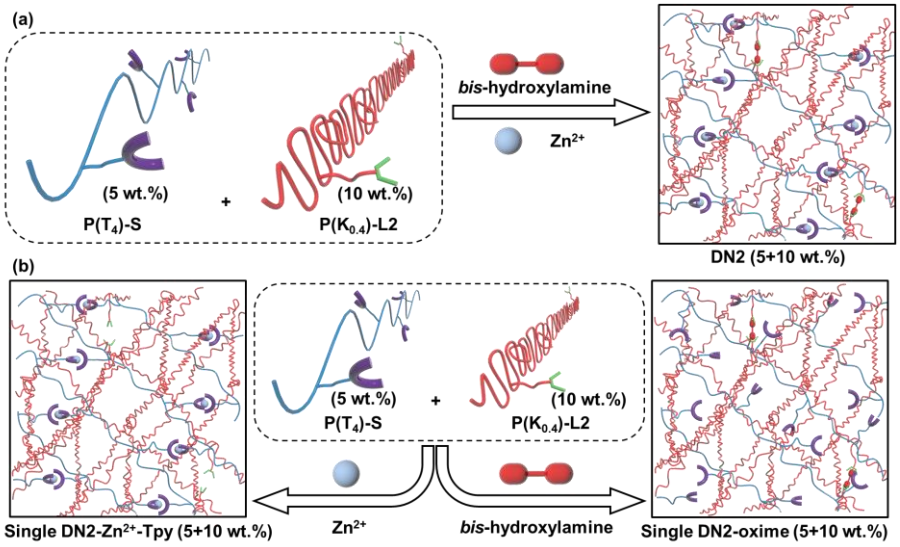

Scheme 4.6. Preparation of (a) DN2 hydrogel as well as (b) its two single networks of DN2-Zn^{2+}-Tpy or DN2-Oxime, by mixing 5 wt.% of $P(T_4)$-S copolymer with 10 wt.% of $P(K_{0.4})$-L2 copolymer, leading to a total polymer concentration of 15 wt.%.

To promote all crosslinking reactions and get stable and reproducible networks, an aging time of 2 days at 55 ℃ was applied, followed by a slow cooling down to room temperature for another 2 days, for all networks, after the needed crosslinkers were added. By using such aging procedures, gelation behaviors of DCN, IPN1, IPN2, DN1 and DN2 as well as of their single networks have been tested and confirmed by the tube inversion method, the results are illustrated in **Figure 4.2**. Among these, 5 wt.% P(K_2)-S in IPN1-Oxime (5+5 wt.%), 5 wt.% P(T_4)-S in IPN2-Zn^{2+}-Tpy (5+5 wt.%), and 10 wt.% P($K_{0.4}$)-L1 in DN1-Oxime (5+10 wt.%) were the minimum polymer concentration for gelation. As shown in **Figure 4.2b**, the IPN1-Zn^{2+}-Tpy (5+5 wt.%) was not a gel, hence the polymer composition of 10+10 wt.% was also used to prepare IPN1 and its two single networks (**Figure 4.2c**) to ensure that they were all in the gel state. The other single networks have polymer concentrations higher than their minimum gelation concentrations. As a result, a total of six major systems will be used for discussion, namely, DCN hydrogel and its two single networks at 10 wt.% (**Schemes 4.1**), IPN1 hydrogel and its two single networks at 5+5 wt.% (**Schemes 4.2**), IPN1 hydrogel and its two single networks at 10+10 wt.% (**Schemes 4.3**), IPN2 hydrogel and its two single networks at 5+5 wt.% (**Schemes 4.4**), DN1 hydrogel and its two single networks at 10+10 wt.% (**Schemes 4.5**), and DN2 hydrogel and its two single networks at 10+10 wt.% (**Schemes 4.6**). The concentration in parentheses for each sample name indicates the concentration of the copolymer components. The apparent mechanical properties observed by touching the hydrogels with tweezers revealed that DCN and its two single networks (**Figure 4.2a**) were stiff hydrogels; single networks of IPN1-Oxime (5+5 wt.%), IPN2-Oxime (5+5 wt.%), DN1-Oxime (5+10 wt.%), and DN2-Oxime (5+10 wt.%) (**Figures 4.2b**, **4.2d**, **4.2e**, **and 4.2f**) were were soft and sticky hydrogels; single networks of IPN1-Zn^{2+}-Tpy (10+10 wt.%), IPN2-Zn^{2+}-Tpy (5+5 wt.%), DN1-Zn^{2+}-Tpy (5+10 wt.%), and DN2-Zn^{2+}-Tpy (5+10 wt.%) (**Figures 4.2c**, **4.2d**, **4.2e**, **and 4.2f**) were were soft and non-sticky hydrogels; both oxime and Zn^{2+}-Tpy crosslinked IPN1 and IPN2 (**Figures 4.2b**, **4.2c**, **and 4.2d**)

were stiff hydrogels; the DN1 and DN2 (**Figures 4.2e and 4.2f**) were tough hydrogels.

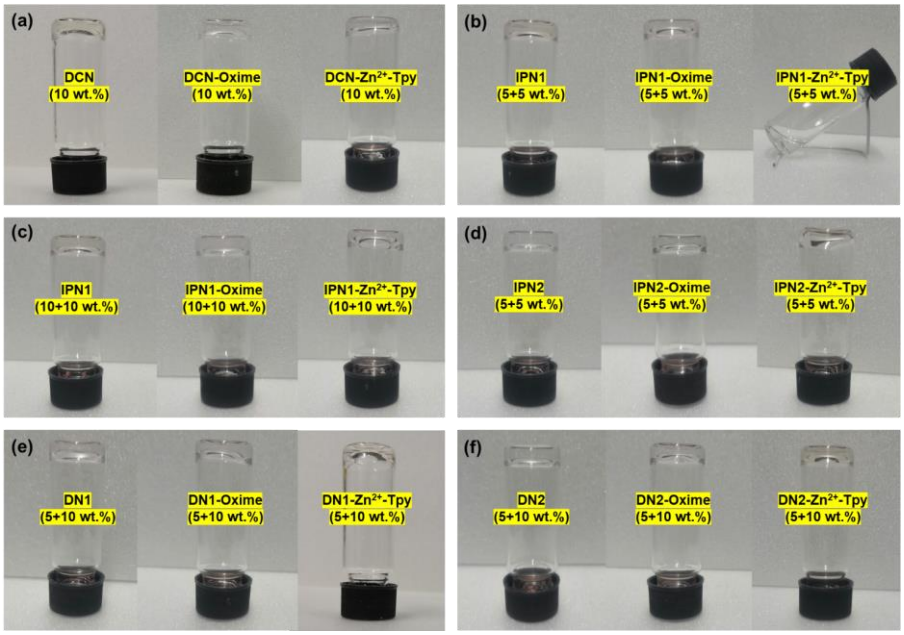

Figure 4.2. Optical images of: (a) DCN (10 wt.%), (b) IPN1 (5+5 wt.%), (c) IPN1 (10+10 wt.%), (d) IPN2 (5+5 wt.%), (e) DN1 (5+10 wt.%), (f) DN2 (5+10 wt.%) hydrogels and their single networks.

It can be seen that the above single networks were prepared in the presence of another sticker type or another non-crosslinked copolymer, which may affect the effective interchain crosslinking.[15] As shown in the parameters in **Table 4.1**, the short-chain P(T_4)-S and P(K_4)-S have very comparable chain lengths and functionalization ratios, and contain only one type of stickers on the polymer chains. Comparing the rheological behavior of the two individual networks consisting of P(T_4)-S crosslinked by Zn^{2+}-Tpy or P(K_4)-S crosslinked by oxime linkages, respectively, in the absence of the other copolymer, is interesting to determine the effects of the two crosslink types on the overall gel. For this purpose, we prepared an individual Zn^{2+}-Tpy network (10 wt.%) from pure P(T_4)-S and an individual oxime network

(10 wt.%) from pure P(K_4)-S (**Scheme 4.7**). Since P(T_4)-S is actually a little less functionalized than P(K_4)-S (see **Table 4.1**), the added crosslinker concentrations for both Zn^{2+}-Tpy and oxime bonds were calculated based on the concentration of the P(T_4)-S reaction sites to ensure the same maximum crosslinking in the two individual networks for comparison purposes. Accordingly, the amount of added bis-hydroxylamine is slightly less than the half of ketone concentration on P(K_4)-S, yet it avoids the creation of ineffective reactions, which could result from an excess of crosslinkers.

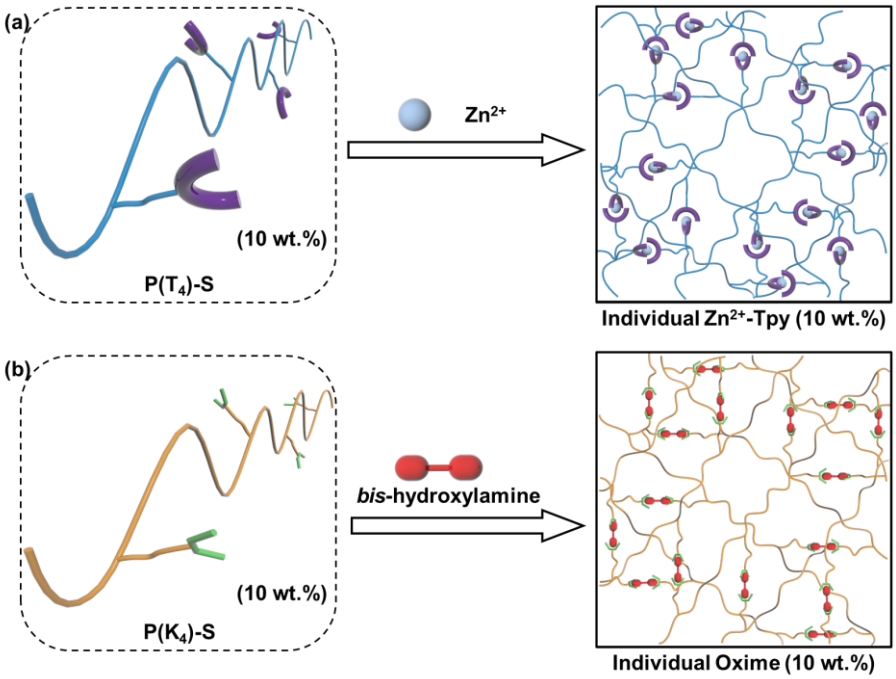

Scheme 4.7. Preparation of the individual Zn^{2+}-Tpy network from 10 wt.% pure P(T_4)-S and of the individual oxime network from 10 wt.% pure P(K_4)-S.

4.2.3. Rheological characterization

To investigate the contribution of the two types of crosslinks to the dynamics (viscoelasticity) of the hydrogels of different topologies and

of the corresponding single networks, oscillatory shear rheology in the linear viscoelastic (LVE) regime was used as the main characterization tool. As mentioned above, an aging protocol of 4 days (2 days at 55 °C followed by a slow cooling down to room temperature for another 2 days) was applied during the hydrogel preparation to obtain reproducible results. As shown in **Figure 4.3a**, the rheological behavior of the single-crosslinked oxime network did not change significantly after an additional 4 months of aging, indicating that a stable equilibrium has been reached during the aging protocol of 4 days. This result also suggests that our preparation is sufficient to obtain stable Zn^{2+}-Tpy networks since the formation rate constant of oxime is lower than Zn^{2+}-Tpy at 25 °C in neutral water.[15]

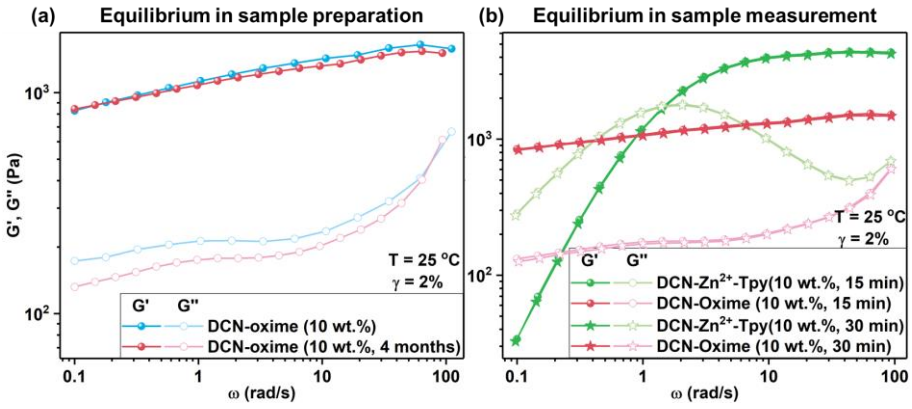

Figure 4.3. (a) Oscillatory frequency sweeps on DCN-Oxime network prepared from procedure aging process (heating at 55 °C for 2 days followed by slowly cooling down to room temperature in 2 days) and additional 4 months of aging at room temperature. (b) Oscillation frequency sweeps were performed after loading the samples into the rheometer and allowing them to stand for 15 and 30 minutes, respectively.

In addition, the samples were well-placed between the parallel plates of the rheometer for at least 15 min to equilibrate the samples before any experiments were performed. As can be seen in **Figure 4.3b**, the data from the frequency sweeps performed after 15 and 30 min of

resting for the single oxime and Zn^{2+}-Tpy crosslinked samples are similar. This indicates that 15 min of standing prior to testing is sufficient to allow the samples to reach reproducible conditions.

4.2.3.1. Single Zn^{2+}-Tpy or oxime crosslinked networks (main systems)

Oscillatory frequency sweeps were first measured on the single networks (systems in presence of only one type of crosslinkers) to evaluate and compare their dynamic properties. The curves of the storage modulus (G') and loss modulus (G") were thus obtained by the frequency sweeps from high to low frequency. Since the frequency sweeps from 100 rad/s to 0.01 rad/s took several hours, slight solvent evaporation was observed at the end of the tests (i.e. near 0.01 rad/s in the frequency sweep curve) for the samples with the single Zn^{2+}-Tpy networks, despite the rheometer being equipped with a solvent trap device. This solvent evaporation phenomenon was less apparent in the single oxime networks and the orthogonal crosslinking hydrogel systems.

The curves of G' and G" versus frequency for the single Zn^{2+}-Tpy networks of the six systems are shown in **Figure 4.4a**. As mentioned already, the IPN1-Zn^{2+}-Tpy (5+5 wt.%) did not result in a gel, in other words the IPN1-Zn^{2+}-Tpy failed to form an effective network at a concentration of 5+5 wt.%. Disregarding the behaviors at low frequency region, as a result, all single Zn^{2+}-Tpy networks except the IPN1-Zn^{2+}-Tpy (5+5 wt.%) showed similar dynamic modulus curves with frequency (**Figure 4.4a**). As shown in **Figure 4.4b**, frequency sweeps performed on three fresh DCN-Zn^{2+}-Tpy single network samples showed a non-reproducible low frequency behavior in G', suggesting that the observed low frequency behaviors of single Zn^{2+}-Tpy networks may be due to variable evaporation of water from the samples. Since the chains are unentangled, it is expected that the elastic plateau observed in the rheological data comes from the molecular segments trapped between two Zn^{2+}-Tpy complexes, and that chains

bearing the Tpy groups along their backbone relax according to a sticky Rouse process. [41] It should therefore be possible to rationalize the data based on this model and considering only crosslinked chains (i.e., assuming negligible contributions from non-crosslinked chains).

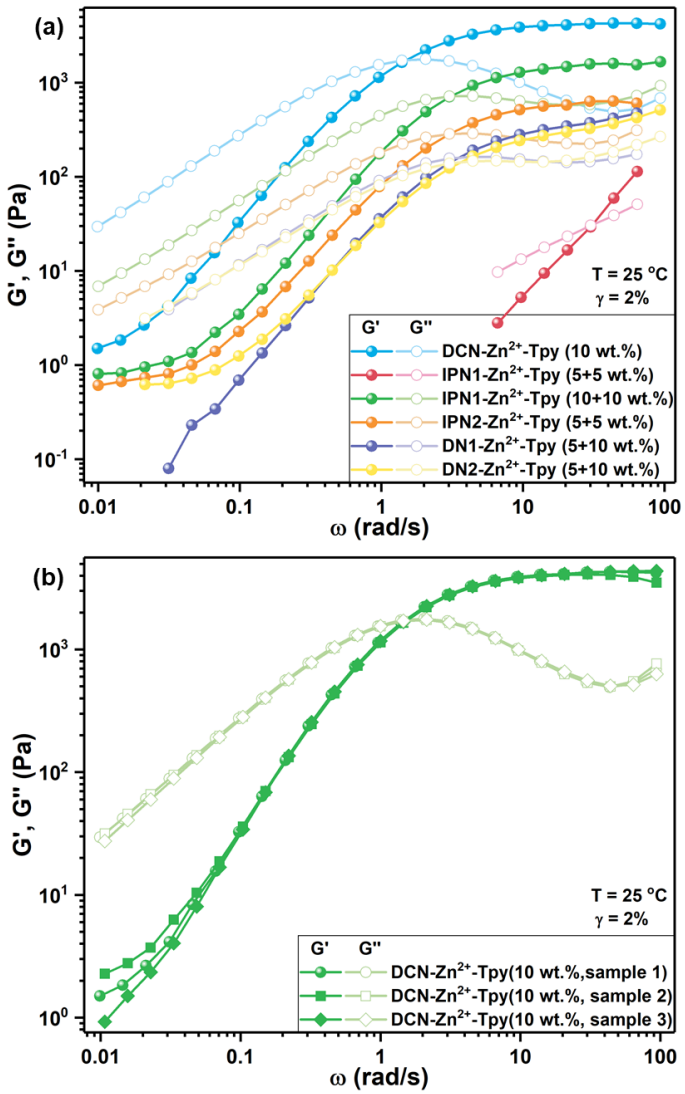

Figure 4.4. (a) Comparison of oscillatory frequency sweeps on single Zn^{2+}-Tpy networks of the six systems. (b) Frequency sweeps of three DCN-Zn^{2+}-Tpy single network samples.

As can be seen from **Figure 4.4**, the DCN-Zn^{2+}-Tpy (10 wt.%) has the highest moduli in the measured frequency range, suggesting that the DCN topology is more favorable for Zn^{2+}-Tpy to form effective interchain linkages and increase the crosslinking density compared to IPN or DN at a comparable crosslinking sites concentration (**Table 4.2**). As can be seen from the network compositions shown in **Table 4.2**, the IPN1-Zn^{2+}-Tpy (10+10 wt.%) has a higher polymer concentration and crosslinker concentration for the formation of Zn^{2+}-Tpy compared to DCN-Zn^{2+}-Tpy (10 wt.%), yet IPN1-Zn^{2+}-Tpy (10+10 wt.%) exhibits a lower G' in the whole frequency range. A possible explanation for this might be a "screening effect" present in the IPN derived single networks that is induced by the presence of the non-crosslinked copolymer.[15] This effect could reduce the possibility for terpyridine groups to explore their surroundings to find a partner to create effective crosslinks. In the IPN2-Zn^{2+}-Tpy (5+5 wt.%), DN1-Zn^{2+}-Tpy (5+10 wt.%), and DN2-Zn^{2+}-Tpy (5+10 wt.%), a 5 wt.% P(T_4)-S was used to form the Zn^{2+}-Tpy crosslinks, which means that the polymer and crosslinker concentrations used to form the single Zn^{2+}-Tpy networks are the same for the three systems. However, the G' values of the two DN systems are lower than the IPN system over the whole frequency range, indicating that the addition of more free chains in the surroundings reduce further the crosslinking of the Zn^{2+}-Tpy network, providing further evidence that the presence of non-crosslinked polymers does have a "screening effect" on network formation. These results indicate that the single Zn^{2+}-Tpy networks of IPN and DN systems with similar polymer and crosslinker concentrations have lower elastic modulus than DCN systems due to the "screening effect" caused by the presence of non-crosslinked polymers in the IPN and DN systems, which suggests that DCN topology may be more favorable for the formation of stiffer hydrogels.

In addition, the rubbery elastic plateau (G'_p) values[42, 43] of the single Zn^{2+}-Tpy networks can also be obtained from the G' at high-frequency region of the frequency sweeps, and are summarized in **Table 4.2**. This plateau modulus is generally attributed to the

contributions of trapped entanglements and crosslinks.[37] For all single Zn^{2+}-Tpy networks, the copolymer concentrations and the average molar mass between two stickers (M_{xx}) are rather low (**Table 4.2**), the contribution of trapped entanglements may thus be considered as negligible. If we assume that all the functional groups of the copolymers are effectively crosslinked in the single networks, the theoretical elastic plateau moduli G_N^0 can be calculated by using the equation as follows[15]:

$$G_N^0 = \frac{c\rho_0 RT}{M_{XX}}\left(1 - \varphi_{dangling}\right) \quad (4.1)$$

where ρ_0 is the density of PDMA in the melt state (approximated as 1 g/cm^3), c is the sample concentration, M_{xx} is the average molar mass between two sticky groups and $\varphi_{dangling}$ is the weight fraction of dangling ends, which, if they do not participate to the network elastic modulus, can be approximated as equal to $2M_{xx}/M_w$, R is the universal gas constant; T is the temperature. Due to the high equilibrium constants of oxime and Zn^{2+}-Tpy (see Chapter 3), all the bonds that can be formed may be considered to be in the associated state, and therefore the effect of the equilibrium constants on G_N^0 was not taken into account.

In the single Zn^{2+}-Tpy networks, the crosslinking efficiency (or probability of the activated sticker to form effective interchain crosslinks) can be roughly estimated by the ratio of the experimental elastic plateau G'_p to the theoretical elastic plateau moduli G_N^0 determined from the synthesis parameters. It should be noted that the role of the dangling ends of the polymer chains in the network was not considered in the calculation of G_N^0. Besides, some other factors such as chain length, polymer and sticker concentration, unreacted sites, and intrachain crosslinking inducing internal loops can also affect the value of the plateau modulus.[37, 44] Therefore, the calculated values of crosslinking efficiency are not precise, but they can be used to roughly

compare the tendency of forming the effective Zn^{2+}-Tpy network between these systems.

Table 4.2. Compositions, experimental and theoretical elastic plateau moduli of different single Zn^{2+}-Tpy networks.

Sample	Copolymer[a]	[C][b] (mmol/L)	M_{xx}[c] (g/mol)	G'_p[d] (Pa)	G_N^0 (Pa)	E_c[e] (%)
DCN-Zn^{2+}-Tpy (10 wt.%)	$P(T_2K_2)$-S (10 wt.%)	7.6	6700	4300	30300	14
IPN1-Zn^{2+}-Tpy (5+5 wt.%)	$P(T_2)$-S (5 wt.%)	4.6	5400	/	19200	/
IPN1-Zn^{2+}-Tpy (10+10 wt.%)	$P(T_2)$-S (10 wt.%)	9.2	5400	1560	38400	4.1
IPN2-Zn^{2+}-Tpy (5+5 wt.%)	$P(T_4)$-S (5 wt.%)	7.4	3300	630	34100	1.8
DN1-Zn^{2+}-Tpy (5+10 wt.%)	$P(T_4)$-S (5 wt.%)	7.4	3300	370	34100	1.1
DN2-Zn^{2+}-Tpy (5+10 wt.%)	$P(T_4)$-S (5 wt.%)	7.4	3300	320	34100	0.94

[a] Copolymer used for Zn^{2+}-Tpy crosslinks. [b] Concentration of added crosslinker (Zn^{2+}) is half of the Tpy concentration. [c] Average molar mass between Tpy groups on the corresponding copolymer. [d] Obtained from the plateau value of G' in the high-frequency domain of the frequency sweeps. [e] The crosslinking efficiency (E_c) is calculated by G'_p/G_N^0.

As shown in **Table 4.2**, the crosslinking efficiency of Zn^{2+}-Tpy is remarkably high in the DCN system compared to IPN and DN systems. This may be due to the fact that the non-crosslinked ketone copolymers in the IPN and DN systems severely prevent the formation of effective interchain Zn^{2+}-Tpy linkages when only Zn^{2+} is added, while DCN showed relatively higher crosslinking efficiency because of the absence of such "screening effect". Since the DN1 and DN2 systems have twice as much non-crosslinked ketone copolymer as the IPN2 system, as a negative consequence of this "screening effect", the crosslinking efficiency of Zn^{2+}-Tpy in DN1 and DN2 is significantly lower than that of the IPN2 system even though all these three systems contain the same

concentration of Tpy copolymer and of Zn^{2+}. The estimated entanglement molar mass (M_e) of the linear PDMA melt is 11 kg/mol (see Experimental Section), which means that the minimum molar mass of PDMA copolymer to produce entanglement in an aqueous solution at 10 wt.% concentration is approximately 110 kg/mol, and the critical entanglement molar mass is $2M_e$ = 220 kg/mol. This means that the 10 wt.% long-chain copolymer of P($K_{0.4}$)-L1 (Mn: 155 kg/mol) in DN1 and P($K_{0.4}$)-L2 (Mn: 262 kg/mol) in DN2 are mostly unentangled, however we cannot exclude the possibility that few entanglements are trapped between the supramolecular crosslinks, which also contribute to the elastic modulus. On the other hand, the probability to have entanglements in the 5 wt.% P(T_4)-S formed Zn^{2+}-Tpy network is much lower in both DN1 and DN2 than IPN2. Besides the "screening effect" of more non-crosslinked polymers, the reduced crosslinking efficiency of Zn^{2+}-Tpy in the DN1 and DN2 systems confirms that the non-crosslinked long-chain polymers provide an almost negligible contribution to the crosslinking density by entanglements. It can be seen that the crosslinking efficiency of Zn^{2+}-Tpy in different network topology systems is strongly influenced by the non-crosslinked polymer. This effect directly leads to higher moduli of the single Zn^{2+}-Tpy crosslinked DCN hydrogels than IPN and DN.

Furthermore, oscillatory frequency sweeps provide information on the bulk relaxation of materials and on the time scale of the material deformation, which are related to the formation, cleavage, and reformation of dynamic crosslinks.[45] As shown in **Figure 4.4**, all single Zn^{2+}-Tpy networks exhibit terminal relaxation as shown by the G'-G" crossover. This relaxation process denotes the onset of macroscopic flow of Zn^{2+}-Tpy networks, mainly caused by the dissociation of zinc(II)-terpyridine bis-complexes due to their rather low equilibrium constant and high lability.[9] The accessible relaxation times (τ) of these single networks obtained from the cross-over points of G' and G" are presented in **Table 4.3.**

Table 4.3. Relaxation times of single Zn^{2+}-Tpy networks.

Sample	Copolymer[a]	[Tpy][b] (mmol/L)	τ^c (s)
DCN-Zn^{2+}-Tpy (10 wt.%)	$P(T_2K_2)$-S (10 wt.%)	7.6	0.67
IPN1-Zn^{2+}-Tpy (5+5 wt.%)	$P(T_2)$-S (5 wt.%)	4.6	0.03
IPN1-Zn^{2+}-Tpy (10+10 wt.%)	$P(T_2)$-S (10 wt.%)	9.2	0.32
IPN2-Zn^{2+}-Tpy (5+5 wt.%)	$P(T_4)$-S (5 wt.%)	7.4	0.33
DN1-Zn^{2+}-Tpy (5+10 wt.%)	$P(T_4)$-S (5 wt.%)	7.4	0.28
DN2-Zn^{2+}-Tpy (5+10 wt.%)	$P(T_4)$-S (5 wt.%)	7.4	0.27

[a] Copolymer used for Zn^{2+}-Tpy crosslinks. [b] Concentration of added crosslinker (Zn^{2+}) is half of the Tpy concentration. [c] The relaxation time is calculated by: $\tau = 1/\omega_c$, where ω_c is the frequency at the cross-over of G' and G" in the frequency sweeps.

As shown in **Table 4.3**, the single DCN-Zn^{2+}-Tpy (10 wt.%) network has the longest relaxation time (0.67 s) among all single networks. This result can be attributed to the higher crosslinking density of active Zn^{2+}-Tpy in the DCN system, and thus to a longer sticky relaxation time, the latter being proportional to the square of the number of active stickers.[46] Since the IPN1-Zn^{2+}-Tpy (5+5 wt.%) did not result in a gel network, this system shows the minimum relaxation time. The relaxation times of single networks of IPN1-Zn^{2+}-Tpy (10+10 wt.%), IPN2-Zn^{2+}-Tpy (5+5 wt.%), DN1-Zn^{2+}-Tpy (5+10 wt.%), and DN2-Zn^{2+}-Tpy (5+10 wt.%) are similar probably because the crosslinker concentrations of these systems are very comparable (**Table 4.3**). The 10 wt.% $P(T_2)$-S used to form IPN1-Zn^{2+}-Tpy (10+10 wt.%) and the 5 wt.% $P(T_4)$-S used to form IPN2-Zn^{2+}-Tpy (5+5 wt.%) have about the same sticker concentrations, and the relaxation time of both systems are essentially equivalent despite the fact that M_{xx} and concentration of the two copolymers are different (**Table 4.2**). The relaxation times of the

two DN systems are slightly shorter compared to IPN2, indicating that the concentration of non-crosslinked polymer would slightly affect the relaxation behavior of Zn^{2+}-Tpy in the interpenetrated networks. As discussed above, the longer relaxation time of Zn^{2+}-Tpy in DCN than in IPN and DN results from the very high crosslinking density of DCN. In the IPN and DN systems, with Tpy copolymer concentrations sufficient to form Zn^{2+}-Tpy gels, the relaxation behaviors of the hydrogels are mainly influenced by the Zn^{2+} concentration and, to a lesser extent, by the non-crosslinked polymer concentration.

The frequency sweeps on single oxime networks of the six systems were then measured and the curves are shown in **Figure 4.5**. As expected, all single oxime networks are stable hydrogels as G' is mostly independent of the frequency and is larger than G", showing a purely elastic response over the whole experimental frequency window. **Table 4.4** also presents the experimental plateau moduli (G'_p) and the theoretical plateau moduli (G_N^0) calculated by Equation 4.1 for single oxime networks.

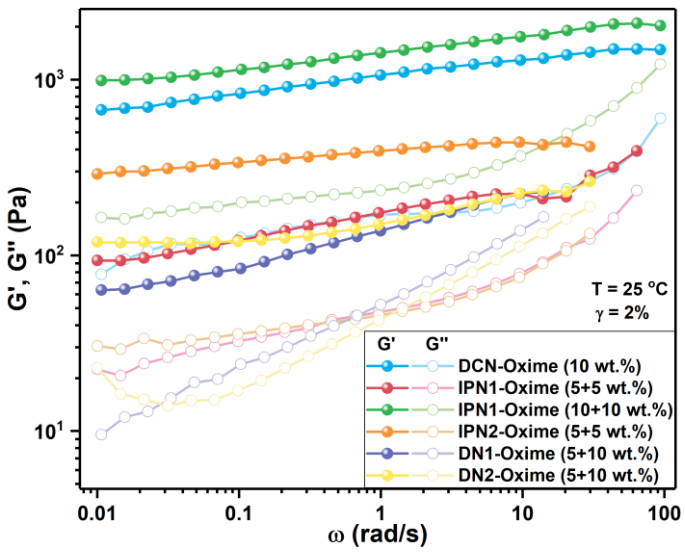

Figure 4.5. Comparison of oscillatory frequency sweeps of single oxime networks for the six systems.

Table 4.4. Compositions, experimental and theoretical elastic plateau moduli of single oxime networks.

Sample	Copolymer[a]	[C][b] (mmol/L)	M_{xx}[c] (g/mol)	G'_p[d] (Pa)	G_N^0 (Pa)	E_c[e] (%)
DCN-Oxime (10 wt.%)	P(T_2K_2)-S (10 wt.%)	10.2	4900	1490	43800	3.4
IPN1-Oxime (5+5 wt.%)	P(K_2)-S (5 wt.%)	6.9	3700	220	29600	0.76
IPN1-Oxime (10+10 wt.%)	P(K_2)-S (10 wt.%)	13.8	3700	2080	59200	3.5
IPN2-Oxime (5+5 wt.%)	P(K_4)-S (5 wt.%)	9.8	2500	440	45900	0.96
DN1-Oxime (5+10 wt.%)	P($K_{0.4}$)-L1 (10 wt.%)	2.0	25800	230	7200	3.2
DN2-Oxime (5+10 wt.%)	P($K_{0.4}$)-L2 (10 wt.%)	2.0	26200	230	8200	2.9

[a] Copolymer used for oxime crosslinks. [b] Concentration of added crosslinker (bis-hydroxylamine) is half of the ketone concentration. [c] Average molar mass between ketone groups on the corresponding copolymer. [d] Obtained from the plateau value of G' in the high-frequency domain of the frequency sweeps. [e] The crosslinking efficiency (E_c) is calculated by G'_p/G_N^0.

It is obvious from **Table 4.4** that when the polymer concentration of the IPN1-Oxime system increases from 5 to 10 wt.%, the corresponding rubbery plateau value G'_p increases about 10 times, which is larger than expected if we only consider the influence of concentration on the level of the elastic plateau, while keeping constant the probability of association of a sticker. Indeed, in this last case, increasing the concentration by a factor 2 should lead to a rubbery plateau only 2 times higher. This suggests that, for the lower concentration, the network is at the limit of the gel formation, which is also supported by the fact that as described previously, 5 wt.% P(K_2)-S in IPN1-Oxime (5+5 wt.%) was the minimum concentration for the formation of the oxime gel network. This result indicates that the oxime network is very sensitive to the polymer concentration. It appears that low concentrations might not favor the formation of oxime bonds or

effective interchain linkages. This may be due to the fact that, unlike the Zn^{2+}-Tpy bis-complexes where the Zn^{2+} ions can directly contact two Tpy entities to form interchain crosslinks, the bis-hydroxylamine crosslinker used to build the oxime network has to form two oxime bonds to lead to an effective interchain linkage by the reaction of its two hydroxylamine sites with two ketone groups on different polymer chains. In other words, the steric hindrances effect of the crosslinker used for oxime bonds may have reduced the amount of effective interchain linkages.

Comparing the compositions of DCN-Oxime (10 wt.%) and IPN2-Oxime (5+5 wt.%), it can be seen that both systems have the same total polymer concentration and very similar concentration of ketone groups (**Table 4.4**). However, the G'_p value of DCN-Oxime is more than three times higher than that of IPN2-Oxime, and the crosslinking efficiency of oxime in DCN-Oxime is much higher than that in IPN2-Oxime. Again, this can be attributed to the screening effect caused by the presence of the non-crosslinked polymers in IPN2-Oxime (half the total polymer amount) reducing the quantities of oximes forming effective interchain crosslinks in this system. This means that DCN also leads to the formation of more effective oxime linkages compared to IPN topology, resulting in a stiffer DCN hydrogel than IPN.

For the single oxime networks of DN1 and DN2, the G'_p plateau values are very low, which may be due to the fact that the long-chain of $P(K_{0.4})$-L1 and $P(K_{0.4})$-L2 copolymers are sparsely ketone-functionalized and thus with a very low oxime crosslinking density. Moreover, it is noticed that the crosslinking efficiency of the DN1-Oxime (5+10 wt.%) and DN2-Oxime (5+10 wt.%) are higher than IPN1-Oxime (5+5 wt.%) and IPN2-Oxime (5+5 wt.%), even though their ketone concentrations are much lower than the latter two. In addition to the difference in the concentration of crosslinking sites, the biggest difference between the DN1 and DN2 systems compared to the IPN1 and IPN2 systems is the fact that the copolymers used to build the oxime networks in the DN systems have much longer chains than in

IPN1 and IPN2 (~150 and ~250 kg/mol vs ~50 kg/mol). The previous discussion on the single Zn^{2+}-Tpy networks in DN1 and DN2 mentioned that the non-crosslinked long-chain ketone copolymers did not significantly contribute to the modulus, therefore the high crosslinking efficiency of oxime in the two DN systems may be due to the local entanglements produced by the formation of oxime bonds in the long-chain polymers. These possible entanglements as additional crosslinks in practice improve the moduli of the single oxime hydrogels thus making the calculated crosslinking efficiency seemingly higher.

4.2.3.2. Individual Zn^{2+}-Tpy and oxime networks

Furthermore, comparing the data in **Table 4.2** and **Table 4.4**, we note that, in the DCN system, the rubbery plateau G'_p of single Zn^{2+}-Tpy network (4300 Pa) is still much higher than that of single oxime network (1490 Pa) even without the screening effect caused by the non-crosslinked copolymers. However, contrary to permanently chemically crosslinked networks, the G'_p value of dynamic networks is not simply depending on the crosslinking density, controlled by the thermodynamics of dynamic bonds, but is also highly influenced by the kinetics of dynamic bonds.[18,47-49] Therefore, the difference in elastic plateau between Zn^{2+}-Tpy and oxime networks can be explained by the different kinetic and thermodynamic contributions of the two types of crosslinks. To quantify the respective contribution of Zn^{2+}-Tpy and oxime to the oscillatory mechanical properties of the networks without the influence of other copolymers and un-reactive groups, we prepared an individual Zn^{2+}-Tpy network from pure $P(T_4)$-S and an individual oxime network from pure $P(K_4)$-S (**Scheme 4.7**). The rheological behaviors of these two networks were measured and are presented in **Figure 4.6** and **Table 4.5**.

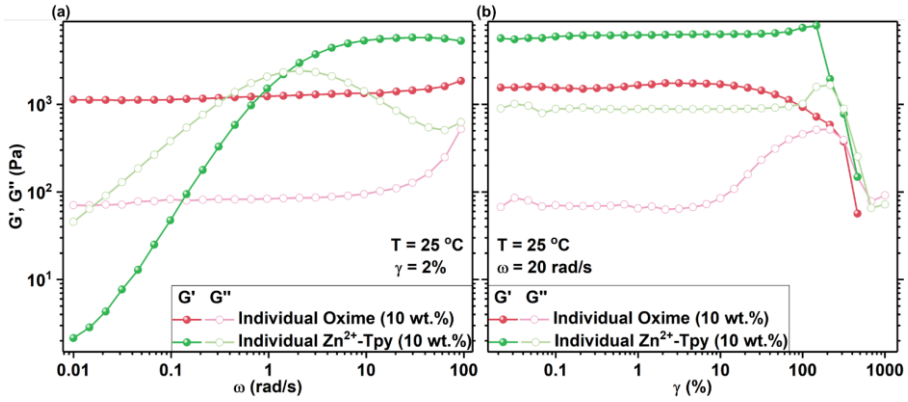

Figure 4.6. Oscillatory frequency sweeps (a) and strain sweeps (b) performed on the individual Zn^{2+}-Tpy network and individual oxime network at a same total polymer concentration and same crosslinker concentration.

Table 4.5. Network parameters of the Zn^{2+}-Tpy and oxime individual networks.

Sample	Copolymer[a]	[C][b]		G'_p[c] (Pa)	γ_L[d] (%)	γ_r[e] (%)
		[Zn^{2+}]	[bis-hydroxylamine]			
Individual Zn^{2+}-Tpy (10 wt.%)	P(T_4)-S (10 wt.%)	14.8	/	5770	46	264
Individual oxime (10 wt.%)	P(K_4)-S (10 wt.%)	/	14.8	1500	10	284

[a] Copolymer used for oxime or Zn^{2+}-Tpy crosslinks. [b] Concentration of added crosslinker (Zn^{2+}, or bis-hydroxylamine) is calculated by half of the Tpy concentration. [c] Obtained from the plateau value of G' in the high-frequency domain of the frequency sweeps. [d] Obtained from the strain at which the G' starts to decrease/increase in the strain sweeps at a fixed frequency of 20 rad/s. [e] Obtained from the crossover of G' and G" in the strain sweeps at a fixed frequency of 20 rad/s.

As shown in **Figure 4.6a**, the individual Zn^{2+}-Tpy network shows a relaxation process, as the single Zn^{2+} networks, due to the finite lifetime of the Zn^{2+}-Tpy bis-complexes, as evidenced by the cross-over of G' and G" in the frequency. The individual oxime network exhibits

robust solid-like behavior over the entire frequency range, similar to the single networks described previously. Interestingly, the G'_p of the individual Zn^{2+}-Tpy network (5770 Pa) is almost four times as high as the individual oxime network (1500) (**Table 4.5**). This suggests that Zn^{2+}-Tpy bis-complexes are more favorable to the formation of high crosslinking density networks than oxime bonds.[11, 50] In addition, as discussed previously, the different steric hindrances of the crosslinkers used to construct the interchain Zn^{2+}-Tpy and oxime crosslinks also suggest that the Zn^{2+}-Tpy network is more homogeneous than the oxime network.

In addition, strain sweeps were performed on both individual networks (**Figure 4.6b**). The limiting strain (γ_L) used to define the limit of the linear viscoelastic (LVE) range, as well as the rupture strain (γ_r) at the critical G'-G'' crossover point that marked the transition of the gel from a solid-like to a liquid-like state, are listed in **Table 4.5**. It is observed that the γ_L of the individual Zn^{2+}-Tpy network (46%) is higher than the individual oxime network (10%). indicating that the Zn^{2+}-Tpy network shows a more extended linear viscoelastic regime compared to the oxime network. This may be due to the fact that the dynamic exchange of Zn^{2+}-Tpy allows the crosslinks to behave as elastic connections compared to the rigid oxime linkages,[39] thus allowing the network to adapt to the applied strain and exhibit a larger linear viscoelastic region. Besides, the γ_r of the individual oxime network (284%) is slightly higher than the individual Zn^{2+}-Tpy network (264%), suggesting that the oxime bonds allow the network to withstand greater deformation compared to Zn^{2+}-Tpy due to the higher bond strength of oxime than Zn^{2+}-Tpy bis-complexes. These results indicate that the Zn^{2+}-Tpy network can better adapt to applied stresses. In other words, the Zn^{2+}-Tpy bis-complexes are more effective in distributing stress than oxime bonds, while the oxime network is able to better resist to a deformation.

Based on the above discussion about the single Zn^{2+}-Tpy networks, the single oxime networks and the two individual networks, the

contribution of the two crosslinks, Zn^{2+}-Tpy and oxime, to the mechanical properties of hydrogels can be briefly summarized here. The labile Zn^{2+}-Tpy allows for network relaxation behavior over the observed time scales, while the stable oxime allows the network to maintain a solid-like behavior over longer time scales. The faster kinetics and more homogeneous Zn^{2+}-Tpy crosslinks in the network impart a higher plateau modulus to the hydrogel and therefore dominate the stiffness of the hydrogel over a short timescale. The dynamic adaptability of Zn^{2+}-Tpy allows the network to extend the LVE region, while the stable oxime bonds help the hydrogel to resist greater stress-induced deformation. Therefore, differences in the dynamic and oscillatory mechanical properties of both Zn^{2+}-Tpy and oxime crosslinked DCN, IPN and DN hydrogels may depend on the difference in how Zn^{2+}-Tpy and oxime crosslinking can contribute in these different topologies.

4.2.3.3. Both Zn^{2+}-Tpy and oxime crosslinked hydrogels (main systems)

Figure 4.7 provides the results of frequency sweeps of the six systems related to both Zn^{2+}-Tpy and oxime crosslinked DCN, IPN and DN hydrogels. Apparently, these six hydrogels of varying topology exhibit the typical frequency-dependent viscoelastic solid behavior of a network crosslinked by both chemical and physical bonds.[51] Two plateaus of G' are observed, one in the high-frequency region attributed to Zn^{2+}-Tpy and oxime crosslinks, and the other in the low-frequency to only oxime crosslinks because of the total dissociation of Zn^{2+}-Tpy.[42] In addition, a characteristic slope of -0,5 is observed for the storage modulus in the transition region between the high-frequency and the low-frequency plateaus, indicating that the partial relaxation of DCN, IPN and DN hydrogels can be described by a sticky Rouse process.[15]

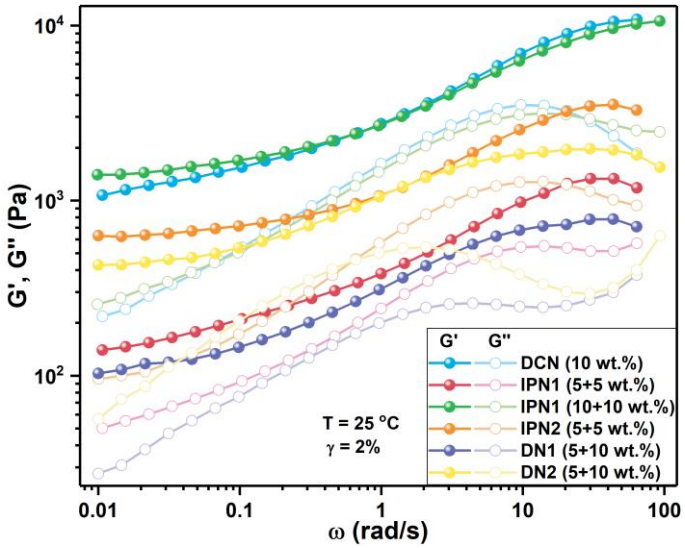

Figure 4.7. Oscillatory frequency sweeps on both Zn^{2+}-Tpy and oxime crosslinked hydrogels of varying topology.

The G'_p values of all DCN, IPN and DN hydrogels are summarized in **Table 4.6**. The concentration of polymers and crosslinkers for IPN1 (10+10 wt.%) is the highest among all systems, and accordingly both Zn^{2+}-Tpy and oxime crosslinked networks have the highest crosslinking density. Therefore, this hydrogel shows a high elastic plateau modulus (10600 Pa). With reference to the schematic structure shown in **Figure 4.1**, and M_{xx} values in **Tables 4.2** and **4.4**, it can be seen that the theoretical length of strands between the same types of crosslinks in the DCN and IPN1 systems are comparable, i.e., the mesh size between the same types of crosslinks should be similar. However, the G'_p value of DCN (10 wt.%) (10800 Pa) is comparable to that of IPN1 (10+10 wt.%), yet about 8 times higher than that of IPN1 (5+5 wt.%) (1330 Pa). These results suggest that the modulus values of DCN and IPN hydrogels might not be related to the strand length between the same type of crosslinks. In addition, the G'_p value of IPN2 (5+5 wt.%) (3530 Pa) is approximately 3 times lower than that of DCN, even though both systems have the same total polymer concentration and comparable crosslinker concentrations (**Table 4.6**). This suggests that the presence

of another polymer in the IPN system, even after it formed a crosslinked network, could still cause a "screening effect" on the other crosslinking reaction, resulting in a lower elastic modulus for the IPN2 hydrogel than for the DCN. The above discussion suggests that the main reason for the difference in mechanical stiffness between DCN and IPN hydrogels is the different effect of the two topologies on the formation of effective crosslinks, and not much the strand length between the same type of crosslinks, polymer concentration or crosslinker concentration.

Table 4.6. Compositions, experimental plateau moduli of hydrogels of different topology crosslinked by both Zn^{2+}-Tpy and oxime.

Sample	Copolymer[a]	[C][b]		G'_p[c] (Pa)
		[Zn^{2+}]	[bis-hydroxylamine]	
DCN (10 wt.%)	$P(T_2K_2)$-S (10 wt.%)	7.6	10.2	10800
IPN1 (5+5 wt.%)	$P(T_2)$-S (5 wt.%) + $P(K_2)$-S (5 wt.%)	4.6	6.9	1330
IPN1 (10+10 wt.%)	$P(T_2)$-S (10 wt.%) + $P(K_2)$-S (10 wt.%)	9.2	13.8	10600
IPN2 (5+5 wt.%)	$P(T_4)$-S (5 wt.%) + $P(K_4)$-S (5 wt.%)	7.4	9.8	3530
DN1 (5+10 wt.%)	$P(T_4)$-S (5 wt.%) + $P(K_{0.4})$-L1 (10 wt.%)	7.4	2.0	780
DN2 (5+10 wt.%)	$P(T_4)$-S (5 wt.%) + $P(K_{0.4})$-L2 (10 wt.%)	7.4	2.0	1970

[a] Copolymers used for both Zn^{2+}-Tpy and oxime crosslinks. [b] Concentrations of added crosslinkers (Zn^{2+} and bis-hydroxylamine) are half of the concentrations of corresponding copolymer reaction sites. [c] Obtained from the plateau value of G' in the high-frequency domain of the frequency sweeps.

As shown in **Table 4.6**, the copolymer and crosslinker concentration used to form the Zn^{2+}-Tpy network in IPN2 and the two DN hydrogels are the same. Both DN1 and DN2 were prepared from

the short-chain P(T_4)-S (5 wt.%) for the first network, and a 0.4% ketone-functionalized long-chain copolymer (10 wt.%) for the second network. This allows to compare the DN1 and DN2 systems since they have the same concentration of total polymers and of crosslinkers. The only difference between DN1 and DN2 is the length of the polymer chain of the second network. The DN1 (780 Pa) and DN2 (1970 Pa) hydrogels exhibit a lower G'_p value than IPN2 (3530 Pa) because the concentration of bis-hydroxylamine used for the formation of oxime bonds is about 5 times lower than that in IPN2. However, since the chain length used to form the oxime network in DN2 is larger than that in DN1, the G'_p value of DN2 is about 2.5 times higher than that of DN1, confirming that increasing the length of the long-chain polymer used to form the second network in DN hydrogels indeed improves the mechanical properties of the hydrogels.[52] These results demonstrate that even if there is a "screening effect" in the two interpenetrated networks that mutually affects the inter-network crosslinks, the mechanical properties of the DN hydrogels can still be regulated by adjusting the chain length.

To compare the variation of the elastic modulus in the hydrogels of varying topology with both Zn^{2+}-Tpy and oxime crosslinks to their single crosslinked networks, **Figure 4.8** summarizes the G'_p of the hydrogel systems and their corresponding two single networks. The sum (G'_{sum}) of the G'_p of the corresponding single Zn^{2+}-Tpy and oxime single networks, and the ratio of G'_p/G'_{sum} of each system is also shown in the **Figure 4.8**. Because the single IPN1-Zn^{2+}-Tpy at 5+5 wt.% was a not gel and the plateau was not accessible in the measured frequency range, the IPN1 (5+5 wt.%) system is not shown in the graph. It is clear from **Figure 4.8** that the G'_p of DCN, IPN and DN hydrogels are much higher than the G'_{sum} of their single networks. This indicates that the incorporation of both Zn^{2+}-Tpy and oxime networks in the hydrogels facilitates the formation of more interchain interactions, may be due to the closer proximity of the chains in such topologies.[37] The new creation of trapped entanglements between Zn^{2+}-Tpy and oxime networks, which serve as additional crosslinks, may be considered as

the main factor responsible for the enhanced modulus of the hydrogels.[15]

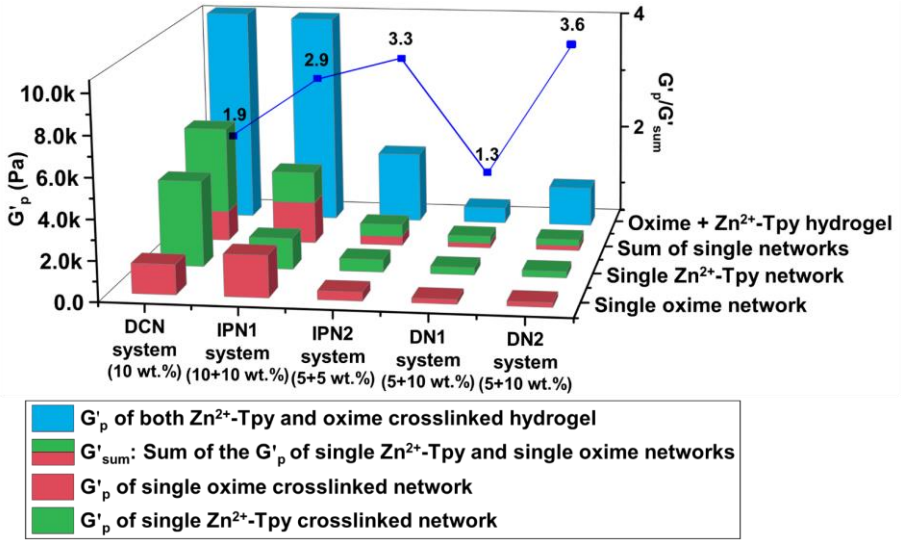

Figure 4.8. Summary of the plateau moduli for the DCN (10 wt.%), IPN1 (10+10 wt.%), IPN2 (5+5 wt.%), DN1 (5+10 wt.%) and DN2 (5+10 wt%) systems including their corresponding single networks. The blue line and the associated numbers are taken from G'_p/G'_{sum} (right axis) of each system.

However, the gain in modulus between the G'_p of the hydrogels and the sum of their two single network moduli varies. For example, the gain in modulus for the DCN (10 wt.%) hydrogel is nearly 2-fold (G'_p/G'_{sum} = 1.9). The gains in modulus for IPN1 (10+10 wt.%) and IPN2 (5+5 wt.%) hydrogels are about 3-fold (G'_p/G'_{sum} of IPN1 is 2.9, G'_p/G'_{sum} of IPN2 is 3.3). The enhanced modulus of DCN hydrogel may be due to the greatly reduced proportion of dangling ends after both Tpy and ketone groups on the $P(T_2K_2)$-S chain are crosslinked. In addition, for DCN networks, a cooperativity effect between the two crosslinks could also explain the higher G'. This is because, unlike IPN and DN, the Tpy and ketone groups in DCN are both on the same polymer chain and the rapid formation of Zn^{2+}-Tpy crosslinks would make the crosslinking of oxime easier or more efficient. For IPN hydrogels, the

synergetic effect between the two interpenetrated networks of Zn^{2+}-Tpy and oxime could also make a contribution to the modulus.[18]

Unlike DCN and IPN hydrogels constructed from short-chain polymers, the mechanical properties of DN hydrogels are strongly dependent on the mesh size and concentration of the two interpenetrated networks.[52] Comparing the G'_p of DN1 and DN2 hydrogels with the G'_{sum} of their single networks could help us to understand the effect of the strand length of the second loosely crosslinked network on the elastic modulus since the only difference between DN1 and DN2 is the M_w of the long chain ketone copolymers (**Table 4.4**). As presented in **Table 4.2**, the G'_p of the single DN1-Zn^{2+}-Tpy is 370 Pa, only slightly higher than that of the single DN2-Zn^{2+}-Tpy (320 Pa). The G'_p of the single DN1-oxime (230 Pa) is almost identical to one of the single DN2-oxime (230 Pa) (**Table 4.4**). Thereby, the G'_{sum} of the single networks of the DN1 system (600 Pa) is almost the same as the DN2 system (550 Pa). The G'_p the of the DN1 hydrogel is 780 Pa, barely 1.3 times higher than the elastic modulus sum of its single networks (**Figure 4.8**), suggesting that the integration of both Zn^{2+}-Tpy and oxime crosslinks can hardly produce more crosslinks such as new trapped entanglements in the DN1 hydrogel because the long-chain P($K_{0.4}$)-L1 copolymer is only about three times longer than the P(T_4)-S copolymer in DN1. Interestingly, the ratio of G'_p/G'_{sum} for the DN2 system reached 3.6, i.e. much higher than for the DN1 system (**Figure 4.8**). Simply replacing the P($K_{0.4}$)-L1 in DN1 with P($K_{0.4}$)-L2 in DN2 to increase the contrast between the chain length of the two copolymers forming the interpenetrated networks from three times to five times has thus a strong impact on the modulus. This result is in agreement with Gong's findings that DN hydrogels with enhanced mechanical properties can be obtained by increasing the length of the second polymer.[40, 52] Compared to DN1, the enhanced elastic modulus in DN2 may mainly come from the formation of more entanglements in DN2. The ($K_{0.4}$)-L2 in DN2 is a long chain, and the motions of this chain are slower than the shorter ($K_{0.4}$)-L1 in DN1. Hence, the formation of crosslinks in DN2 could trap more entanglements between the networks during the

formation of the two interpenetrated networks. Once these trapped entanglements are formed, it is difficult to remove them due to the topological crowding. Consequently, these entanglements serve as new crosslinks and bring a contribution to the enhanced modulus.

Based on the above discussion on the contribution of single Zn^{2+}-Tpy and oxime single networks to the elastic modulus of the corresponding hydrogels, we know that the final modulus depends mainly on the effective crosslinks, which are determined by the kinetics and thermodynamics of Zn^{2+}-Tpy and oxime bonds. Both Zn^{2+}-Tpy and oxime produce more effective crosslinks in the DCN system than in IPN and DN systems due to the presence of non-active copolymers in the latter that induce a "screening effect" on both crosslinks. These differences in effective crosslinking density between the different topologies result in a major elasticity difference between the DCN, IPN and DN hydrogels. As shown in **Figure 4.8** G'_p (DCN) > G'_p (IPN) > G'_p (DN).

Furthermore, by comparing the G'_p/G'_{sum} ratio of DCN, IPN and DN hydrogels, it was demonstrated that the combination of Zn^{2+}-Tpy and oxime yields a modulus enhancement of ~2 times for DCN hydrogel, ~3 times for IPN hydrogel and ~3.6 times for DN hydrogel. In other words, the topological differences between DCN, IPN and DN define the magnitude of potential modulus enhancement (as indicated by the blue curve in **Figure 4.8**).

To further clarify the contributions of the modulus and relaxation of the single networks to the hydrogel properties, the frequency sweeps recorded on each hydrogel and on the corresponding two single networks are shown in **Figure 4.9**.

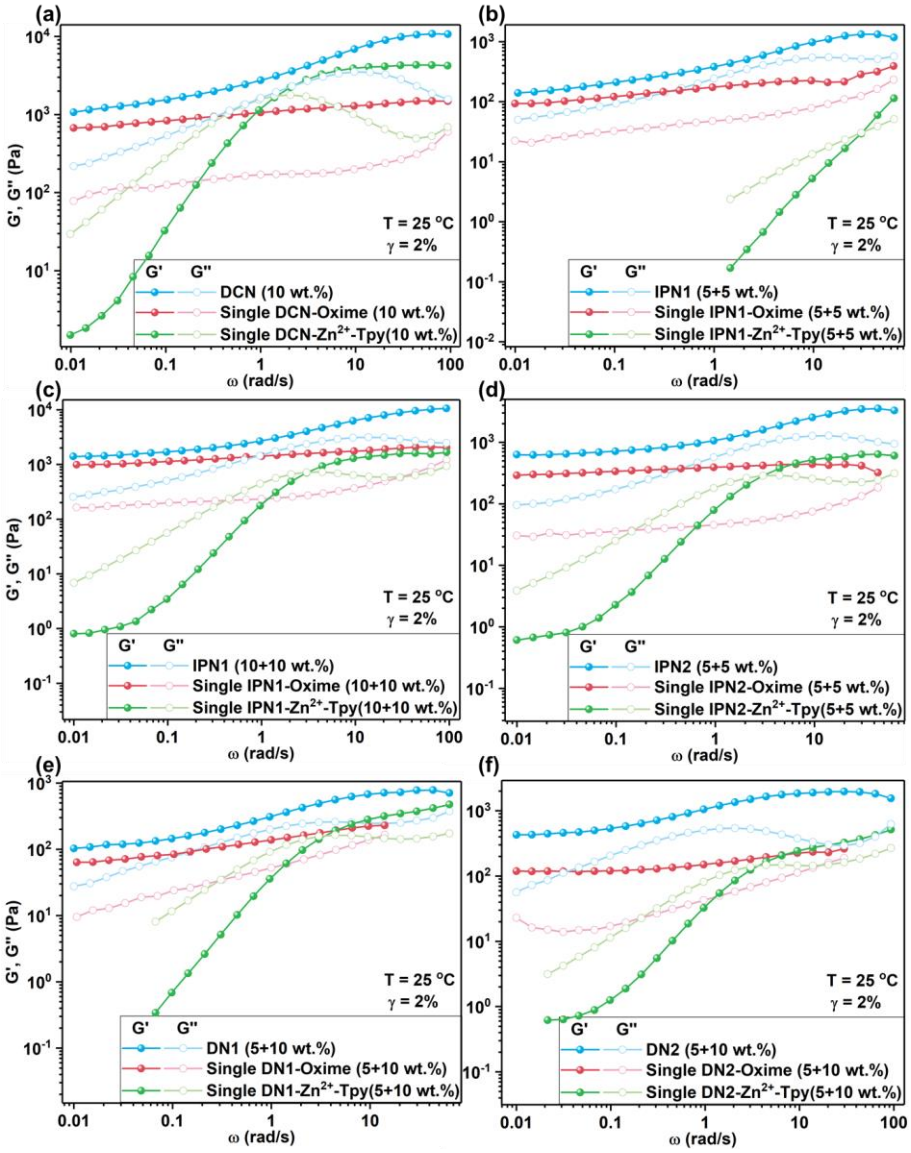

Figure 4.9. Oscillatory frequency sweeps on (a) DCN hydrogel and its single networks at 10 wt.%, (b) IPN1 hydrogel and its single networks at 5+5 wt.%, (c) IPN1 hydrogel and its single networks at 10+10 wt.%, (d) IPN2 hydrogel and its single networks at 5+5 wt.%, (e) DN1 hydrogel and its single networks at 5+10 wt.%, (f) DN2 hydrogel and its single networks at 5+10 wt.%.

The comparison of these six systems shows that the low-frequency plateau modulus of the hydrogels is always higher than that of the

corresponding single oxime network when the Zn^{2+}-Tpy network is fully relaxed in the low-frequency domain. This suggests that the process of DCN, IPN and DN formation can also boost the crosslinking density of the oxime network, which may be due to the topological constraints caused by the rapid formation of the Zn^{2+}-Tpy network that help to bring incompletely crosslinked hydroxylamines and ketones closer to each other.[37]

The difference of storage modulus at 0.01 rad/s between DCN and single DCN-Oxime is 400 Pa (**Figure 4.9a**), while the difference between IPN2 and single IPN2-Oxime is 340 Pa (**Figure 4.9d**), illustrating that the oxime crosslink formation is similar for these two hydrogels since both DCN (10 wt.%) and IPN2 (5+5 wt%) have the same total polymer concentration and approximately the same crosslinker concentrations (**Table 4.6)**. In addition, the difference in the low frequency modulus between the DN hydrogels and their corresponding single oxime network is larger for DN2 than for DN1 (310 Pa for DN2, and 40 Pa for DN1 at 0.01 rad/s) (**Figures 4.9e and 4.9f**). The G'_p of single DN1-oxime and single DN2-oxime are generally the same at high frequency. However, the G' of single DN2-oxime is higher than single DN1-oxime at 0.01 rad/s (**Figures 4.9e and 4.9f**), indicating that the relaxation of the oxime network in DN2 is also slower than in DN1. This may be due to inter-constraints between the oxime network and trapped entanglements in DN2.

The DCN, IPN and DN hydrogels do not reach a terminal relaxation like their single Zn^{2+}-Tpy networks due to the presence of the stable oxime crosslinks that maintain a network structure even at a long-time scale. However, a clear partial relaxation is observed in these hydrogels at a frequency similar to the relaxation frequency of the single Zn^{2+}-Tpy networks, demonstrating that this partial relaxation in DCN, IPN and DN hydrogels is mainly due to the exchange/dissociation kinetics of Zn^{2+}-Tpy crosslinks.[37,42] In fact, the peak in the G" curve represents the maximum energy dissipation,[53] and therefore, the Zn^{2+}-Tpy relaxation in DCN, IPN and DN hydrogels can also be characterized by

the peak of the G"-curve.[34] As shown in **Figure 4.9**, the order of frequencies at the G"-curve peak positions of the six hydrogels typically follows the order of frequencies at the G'-G" crossover points of their corresponding single Zn^{2+}-Tpy networks. This finding suggests that the relaxation behaviors of both Zn^{2+}-Tpy and oxime crosslinked hydrogels are coming from the dynamics of the Zn^{2+}-Tpy crosslinks.

To further probe the contributions of Zn^{2+}-Tpy and oxime crosslinks to the DCN, IPN and DN hydrogel mechanical deformation under strain, we performed amplitude strain sweeps on DCN (10 wt.%), IPN2 (5+5 wt.%) and DN2 (5+10 wt.%) hydrogels as well as on their single networks, since IPN2 and DN2 systems are sharing the same $P(T_4)$-S at 5 wt.%, and they have approximately the same concentrations of Zn^{2+} crosslinkers compared to the DCN (10 wt.%) system (**Table 4.2**). These strain sweeps were carried out at a fixed frequency of 0.2 rad/s, 2 rad/s, and 20 rad/s, corresponding to the different states of the Zn^{2+}-Tpy crosslinks, i.e., after, close to, and before their dissociation, respectively (**Figure 4.4**). These results are shown in **Figures 4.10**, **4.11** and **4.12**, and the limiting strain (γ_L) and rupture strain (γ_r) of DCN (10 wt.%), IPN2 (5+5 wt.%) and DN2 (5+10 wt.%) hydrogels, and of their single networks, at 20 rad/s are summarized in **Table 4.7**.

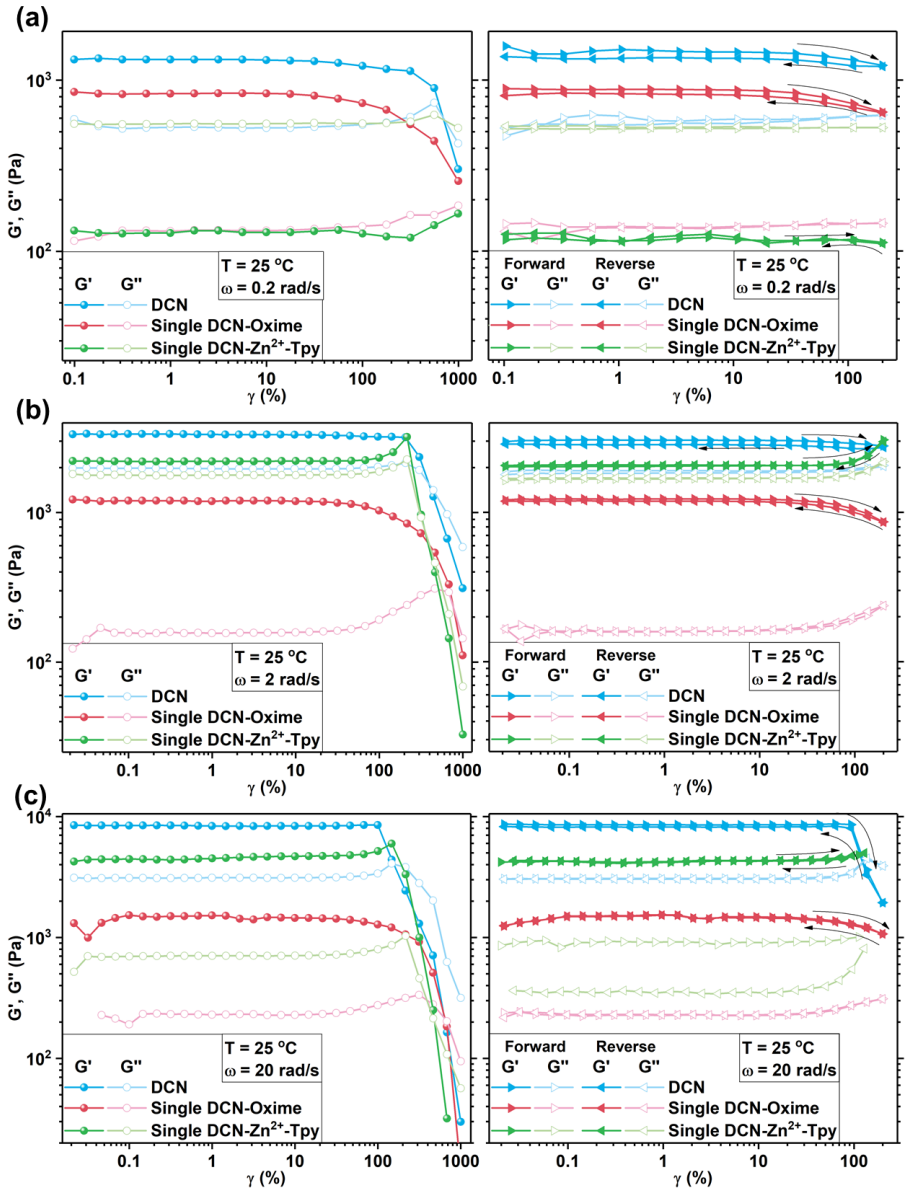

Figure 4.10. Oscillatory strain sweeps performed on the DCN (10 wt.%) hydrogel and its single networks at a fixed frequency of (a) 0.2 rad/s, (b) 2 rad/s, and (c) 20 rad/s. The plots in the right panels are measured from a low strain up to the maximum strain amplitude without destroying the samples, and then from that high strain amplitude down to a low strain.

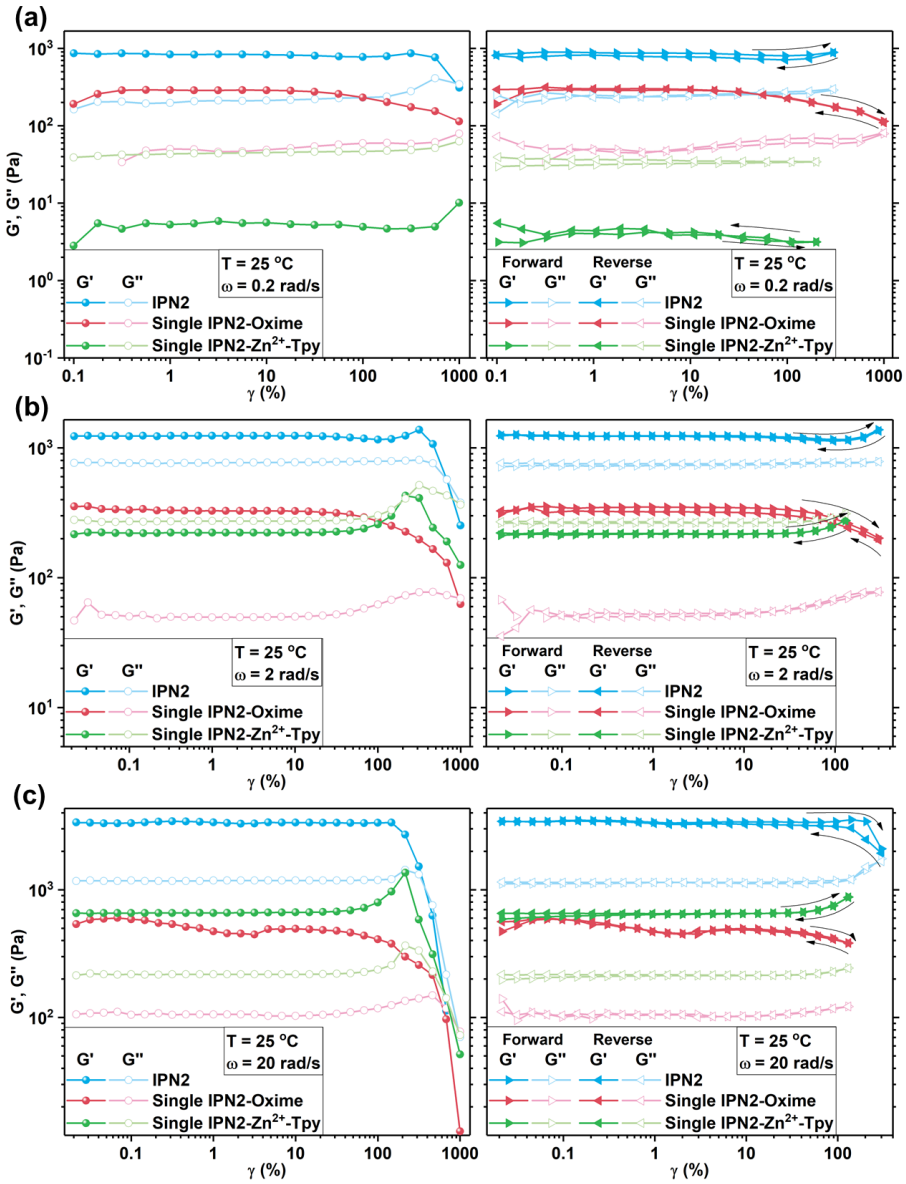

Figure 4.11. Oscillatory strain sweeps performed on the IPN2 (5+5 wt.%) hydrogel and its single networks at a fixed frequency of (a) 0.2 rad/s, (b) 2 rad/s, and (c) 20 rad/s. The plots in the right panels are measured from a low strain up to the maximum strain amplitude without destroying the samples, and then from that high strain amplitude down to a low strain.

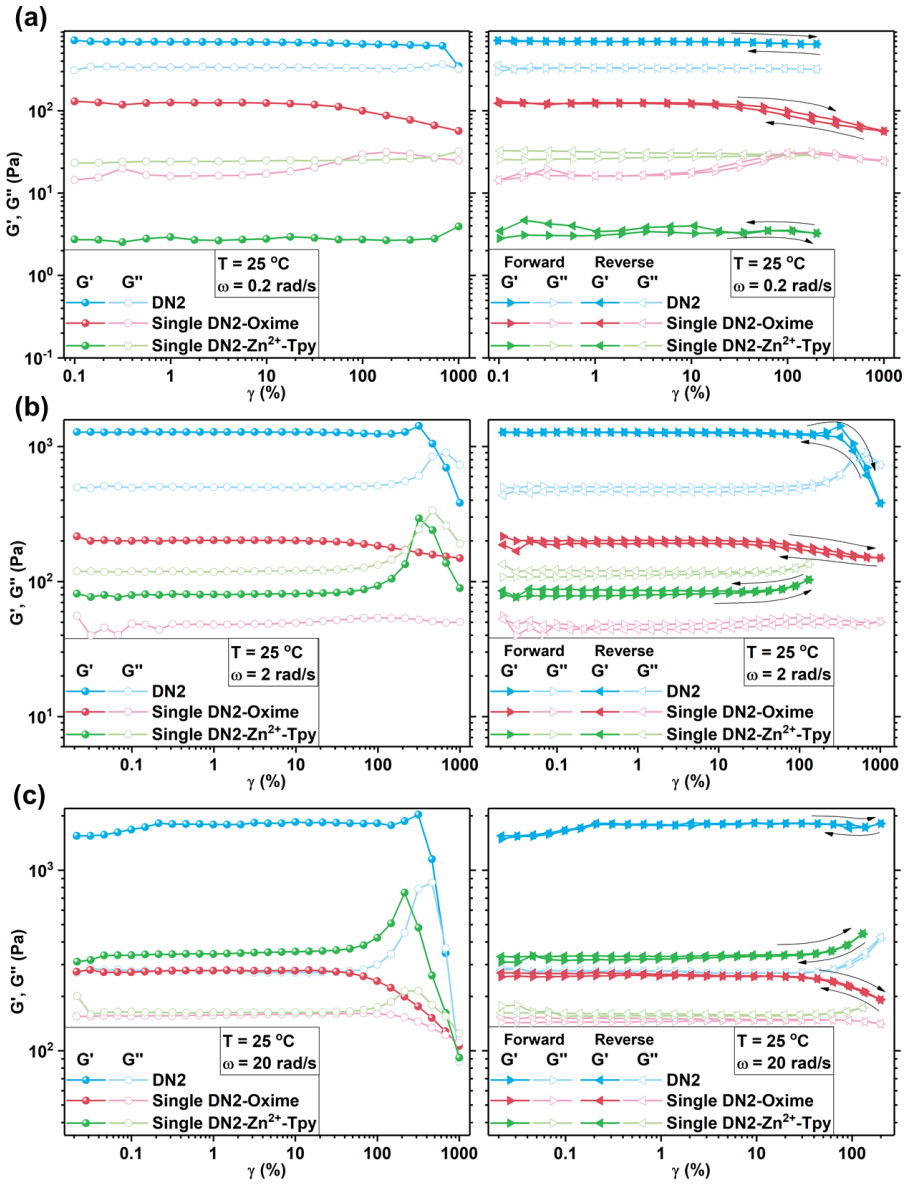

Figure 4.12. Oscillatory strain sweeps performed on the DN2 (5+10 wt.%) hydrogel and its single networks at a fixed frequency of (a) 0.2 rad/s, (b) 2 rad/s, and (c) 20 rad/s. The plots in the right panels are measured from a low strain up to the maximum strain amplitude without destroying the samples, and then from that high strain amplitude down to a low strain.

Table 4.7. Strain parameters for DCN (10 wt.%), IPN2 (5+5 wt.%) and DN2 (5+10 wt.%) hydrogels, and for the corresponding single networks.

Sample	γ_L[a] (%)	γ_r[b] (%)	γ_{Max}[c] (%)
DCN (10 wt.%)	**100**	**155**	**200**
DCN-Zn^{2+}-Tpy (10 wt.%)	70	486	130
DCN-Oxime (10 wt.%)	30	645	200
IPN2 (5+5 wt.%)	**147**	**372**	**300**
IPN2-Zn^{2+}-Tpy (5+5 wt.%)	46	680	130
IPN2-Oxime (5+5 wt.%)	30	596	130
DN2 (5+10 wt.%)	**180**	**635**	**200**
DN2-Zn^{2+}-Tpy (5+10 wt.%)	46	714	130
DN2-Oxime (5+10 wt.%)	30	823	200

[a] Obtained from the strain at which the G' starts to decrease/increase in the strain sweeps at a fixed frequency of 20 rad/s. [b] Obtained from the crossover of G' and G" in the strain sweeps at a fixed frequency of 20 rad/s. [c] Maximum strain applied to the sample for reverse strain sweeps at a fixed frequency of 20 rad/s. Note: γ_{Max} is higher than γ_L to ensure that the applied strain is sufficient to partially break the gel network, but that the high strain is not so high as to extrude the sample from the two parallel plate geometries of the rheometer.

As presented in **Figures 4.10, 4.11** and **4.12**, in all measured strain sweeps, the linear viscoelastic regime of all single Zn^{2+}-Tpy networks is more extended than the one of all single oxime networks, i.e., γ_L (single Zn^{2+}-Tpy network) > γ_L (single oxime network) (**Table 4.7**). This was also observed in Zn^{2+}-Tpy and oxime individual networks (**Figure 4.6**). However, the rupture strain (γ_r) of single oxime networks is always higher than that of single Zn^{2+}-Tpy networks at the same frequencies, by virtue of the higher bond strength of oxime. The stable linear viscoelastic regions of DCN, IPN2 and DN2 hydrogels are longer than those of their corresponding two single networks, while their γ_r values are smaller than those of both single networks. This is because the integration of both Zn^{2+}-Tpy and oxime crosslinks in the hydrogels confers a higher crosslinking density to the hydrogels, maintaining their

elastic modulus over a rather large strain range, but decreasing their abilities to deform.

As shown in **Table 4.7**, the limiting strain of DCN, IPN2 and DN2 hydrogels follows the order: γ_L (DCN, 100%) < γ_L (IPN2, 147%) < γ_L (DN2, 180%), and the rupture strain has the same order, i.e.: γ_r (DCN, 155%) < γ_r (IPN2, 372%) < γ_r (DN2, 635%). This suggests that the stability and deformability follow the order of DCN, IPN and DN hydrogel despite the fact that the combination of Zn^{2+}-Tpy and oxime reduces the deformation capacity compared to their single networks.

At large strain amplitudes, some visual rupture or edge break of the samples may be observed. Therefore, in order to explore the contribution of the two dynamic bonds in the reversibility of the hydrogels, reverse strain-sweep measurements at a fixed frequency of 0.2 rad/s, 2 rad/s, and 20 rad/s were also performed and are illustrated in the right panels of **Figures 4.10, 4.11** and **4.12**. The experiments were conducted by increasing the strain to the maximum strain (γ_{Max}) amplitude that can be reached without expelling the samples from the geometries (**Table 4.7**), and then decreasing the strain amplitude for recovery. Due to the stability and weak dynamics of the oxime bonds, once parts of the network in the sample are disrupted by higher strains, they cannot be quickly recovered to their original state. It can be seen that the G'-curve of the single oxime networks decreases a little after the strain amplitude was lowered in the recovery strain tests compared to the initial strain sweeps from low to high strain. However, this effect is small, suggesting that the oxime network can resist to the large applied deformation. The interesting aspect from these strain sweeps is that all the single Zn^{2+}-Tpy networks show a, sometimes very strong, shear thickening effect at high shear amplitude. However, the G' values generally return close to their initial values when the strain is decreased. This suggests the increased formation of interchain associations under large shear amplitude that could be mainly due to the chain stretching.[54] This may be because, as described in the network preparation, the Zn^{2+}-Tpy network has reached some thermodynamic equilibrium after 4 days

of aging including heating and cooling to room temperature. Increasing the oscillatory strain does not promote the production of more Zn^{2+}-Tpy interchain crosslinks that contribute to the network elasticity. Thus, there is no significant increase in the elastic modulus when the strain is reduced. Importantly, only a small hysteresis was observed in the DCN, IPN2 and DN2 hydrogels after the strain was decreased from the high (before the yield strain) to low amplitude. This reversible recovery is attributed to the reformation of Zn^{2+}-Tpy crosslinks. Therefore, the important point in the reverse strain-sweep experiments is that reversible bonds allow the DCN, IPN and DN hydrogel reformation as soon as the deformation amplitude is reduced. This property could confer the hydrogels self-healing properties that might be of interest for some potential applications.

4.2.3.4. DCN, IPN2 with adjusted crosslinker concentrations for comparisons

Furthermore, in order to compare DCN and IPN hydrogels under the same conditions (same total polymer concentration and same cross-linker concentration), we prepared new DCN and IPN2 hydrogels as DCN-C_1 (10 wt.%) and IPN2-C_1 (5+5 wt.%) (**Table 4.8**). The added concentrations of both Zn^{2+}-Tpy and oxime crosslinker were calculated from the concentration of reaction sites of 5 wt.% P(T_4)-S in IPN2 (5+5 wt.%). Such crosslinker concentration is slightly lower than the concentration of Zn^{2+}-Tpy and oxime of the DCN (10 wt.%) and than the concentration of oxime of the IPN2 (5+5 wt.%) (**Table 4.6**). Thereby, this addition of the same crosslinker concentration will help us to compare the rheological behaviors of both DCN and IPN2 in the same conditions.

Table 4.8. Network parameters of DCN-C_1 and IPN2-C_1 hydrogels.

Sample	Copolymer[a]	[C][b]		G'_p[c] (Pa)	γ_L[d] (%)	γ_r[e] (%)
		[Zn^{2+}]	[bis-hydroxylamine]			
DCN-C_1 (10 wt.%)	$P(T_2K_2)$-S (10 wt.%)	7.4	7.4	9800	68	152
IPN2-C_1 (5+5 wt.%)	$P(T_4)$-S (5 wt.%) + $P(K_4)$-S (5 wt.%)	7.4	7.4	3090	100	372

[a] Copolymers used for both Zn^{2+}-Tpy and oxime crosslinks. [b] Concentration of added crosslinkers (Zn^{2+} or bis-hydroxylamine) is calculated as half of the concentration of 5 wt.% $P(T_4)$-S reaction sites. [c] Obtained from the plateau value of G' in the high-frequency domain of the frequency sweeps. [d] Obtained from the strain at which the G' starts to decrease/increase in the strain sweeps at a fixed frequency of 20 rad/s. [e] Obtained from the crossover of G' and G'' in the strain sweeps at a fixed frequency of 20 rad/s.

As shown in **Figure 4.13a**, the G' and G'' of the DCN-C_1 (10 wt.%) are always much higher than the ones of IPN2-C_1 (5+5 wt.%) in the whole frequency range. The G'_p of DCN-C_1 (9800 Pa) is about 3 times higher than for IPN2-C_1 (3090 Pa) because in the IPN both crosslinks are influenced by the "screening effect", and by the change of kinetics of Zn^{2+}-Tpy as we discussed above. Besides, the relaxation peak ($\omega_{G''}$) in the G''-curve is $\omega_{G''}$ (DCN-C_1) < $\omega_{G''}$ (IPN2-C_1), demonstrating τ (DCN-C_1) > τ (IPN2-C_1) since the DCN has more elastically effective crosslinks than the IPN. From the comparison of their strain sweeps **(Figure 4.13b)**, we obtained the limiting strain value and rupture strain value as shown in **Table 4.8**. The γ_L of DCN-C_1 (68%) is lower than IPN2-C_1 (100%), and the γ_r of DCN-C_1 (152%) is also lower than IPN2-C_1 (372%) due to the higher effective crosslinking density of DCN-C_1 compared to IPN2-C_1. The DCN-C_1 hydrogel has thus a higher elasticity and an increased relaxation time, but less deformation capacity, than the IPN2-C_1 hydrogel.

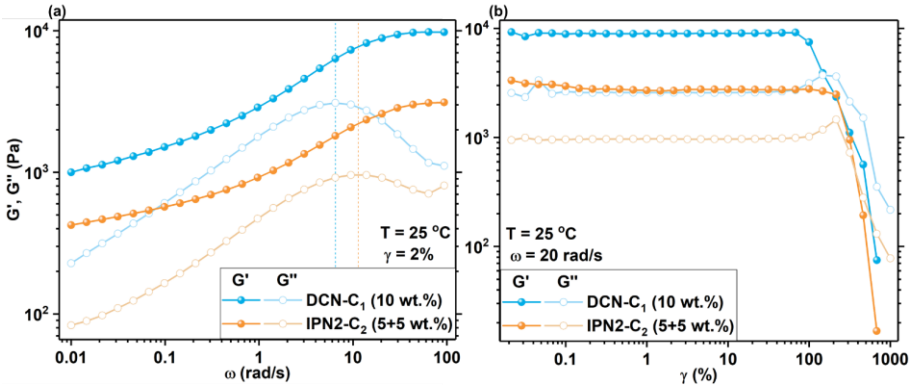

Figure 4.13. Oscillatory frequency sweeps (a) and strain sweeps (b) of the DCN-C_1 (10 wt.%) and IPN2-C_1 (5+5 wt.%) hydrogels at the same total polymer concentration and equal concentration of oxime and Zn^{2+}-Tpy crosslinkers.

We also compared the rheological properties of DCN-C_1 (10 wt.%) and IPN2-C_1 (5+5 wt.%) with the previously prepared Zn^{2+}-Tpy (10 wt.%) and oxime (10 wt.%) individual networks as they all have the same total polymer and crosslinker concentration (**Tables 4.5** and **4.8**). As shown in **Figure 4.14a**, the elastic plateau (G'_p) of DCN-C_1 (9800 Pa) is pretty high, even higher than the sum of the Zn^{2+}-Tpy (5770 Pa) and the oxime (1500 Pa) individual networks, suggesting that the combination of oxime and Zn^{2+}-Tpy crosslinks facilitates the generation of stiffer hydrogels compared to hydrogels created by only a single type of crosslinks. The limiting strain of the DCN-C_1 is between the one of the individual Zn^{2+}-Tpy network and the individual oxime network, suggesting that the deformability and stability of the DCN hydrogel is controlled by both Zn^{2+}-Tpy and oxime crosslinks. The rupture strain of the DCN-C_1 (152%) is lower than the one of both individual Zn^{2+}-Tpy network (264%) and individual oxime network (284%), illustrating that the network-strand flexibility and conformational freedom is reduced in the DCN topology,[42] which further decreases the deformability of hydrogel. This comparison thus indicates that the DCN topology confers a reduced deformability compared to individual oxime and Zn^{2+}-Tpy networks, but confers a higher elastic modulus to the DCN hydrogel.

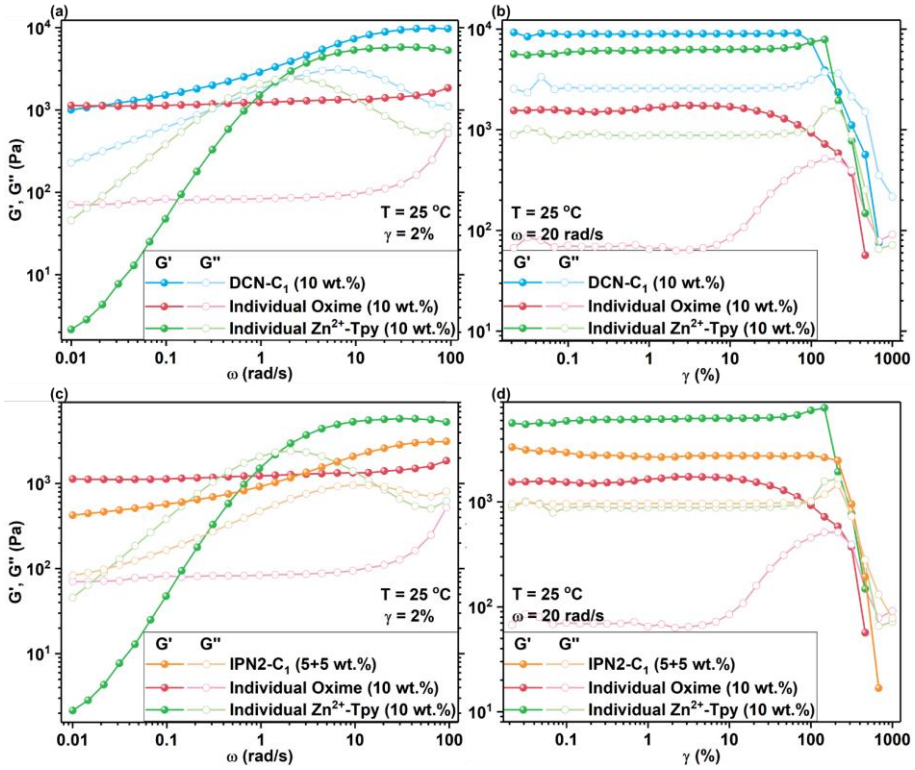

Figure 4.14. Oscillatory frequency sweeps (a) and strain sweeps (b) of DCN-C_1 (10 wt.%) hydrogel, individual Zn^{2+}-Tpy network and individual oxime network, as well as oscillatory frequency sweeps (c) and oscillatory strain sweeps (d) of IPN2-C_1 (5+5 wt.%) hydrogel, individual Zn^{2+}-Tpy network and individual oxime network at the same total polymer and crosslinker concentration.

In addition, comparing the IPN2-C_1 (5+5 wt.%) with the individual Zn^{2+}-Tpy network (10 wt.%) and the individual oxime network (10 wt.%) could also help us to further verify how the "screening effect" influences the Zn^{2+}-Tpy and oxime networks in IPN hydrogels. As shown in **Figure 4.14c**, the G'_p of the IPN2-C_1 (3090 Pa) is lower than that of the individual Zn^{2+}-Tpy network, proving that the formation of the IPN topology reduces the density of interchain Zn^{2+}-Tpy crosslinks and hence reduces the contribution of this type of crosslinks to the elastic modulus because of the "screening effect". However, the G'_p of the IPN2-C_1 is twice higher than that of the individual oxime network, indicating that the presence of Zn^{2+}-Tpy endows the IPN with higher

modulus than pure oxime network despite the "screening effect" existing in the IPN. The limiting strain of IPN2-C_1 is between that of the Zn^{2+}-Tpy and oxime individual networks, and the rupture strain of IPN2-C_1 is higher than both individual networks, suggesting that both Zn^{2+}-Tpy and oxime crosslinks preserve the stability of the IPN hydrogel while the synergetic effects of interpenetrated networks confers larger deformability to the IPN hydrogel compared to pure Zn^{2+}-Tpy and oxime networks.

Table 4.9. Network parameters of DCN-C_2 and IPN2-C_2 hydrogels.

Sample	Copolymer[a]	[C][b]	
		[Zn^{2+}]	[bis-hydroxylamine]
DCN-C_2 (15 wt.%)	P(T_2K_2)-S (15 wt.%)	7.4	2
IPN2-C_2 (5+10 wt.%)	P(T_4)-S (5 wt.%) + P(K_4)-S (10 wt.%)	7.4	2

[a] Copolymers used for both Zn^{2+}-Tpy and oxime crosslinks. [b] Concentrations of added crosslinkers (Zn^{2+} and bis-hydroxylamine) are the same as that of the DN2 hydrogel.

In the end, we prepared DCN-C_2 (15 wt.%) and IPN2-C_2 (5+10 wt.%) (**Table 4.9**) with the same crosslinker concentration as the DN2 hydrogel (**Table 4.6**) to compare the rheological behaviors (**Figure 4.15**) of DCN, IPN and DN. In the case of DCN-C_2 and IPN2-C_2, the Zn^{2+}-Tpy crosslinks are mainly responsible for the network formation, while the oxime crosslinks may not significantly contribute to the network because of the extremely low concentration of oxime (much lower than the critical gelation concentration of oxime in DCN and IPN2). Therefore, the relaxation of DCN-C_2 and IPN2-C_2 generally looks like the one of single Zn^{2+}-Tpy crosslinked networks (**Figure 4.15a**). Because both Zn^{2+}-Tpy and oxime networks in DN2 (15 wt.%) are well crosslinked, DN2 should hence have a higher crosslinking density than both DCN-C_2 (15 wt.%) and IPN2-C_2 (15wt.%). To our

surprise, the limiting strain and rupture strain are following the order: γ_L (DCN-C_2, 46%) < γ_L (IPN2-C_2, 68%) < γ_L (DN2, 215%), and γ_r (DCN-C_2, 450%) < γ_r (IPN2-C_2, 622%) < γ_r (DN2, 635%) (**Figure 4.15b**). This is the same order that we previously observed for DCN and IPN when both Zn^{2+}-Tpy and oxime networks are well crosslinked. This result further confirms that the deformability and stability of the final topological hydrogel increases in the order of DCN, IPN and DN.

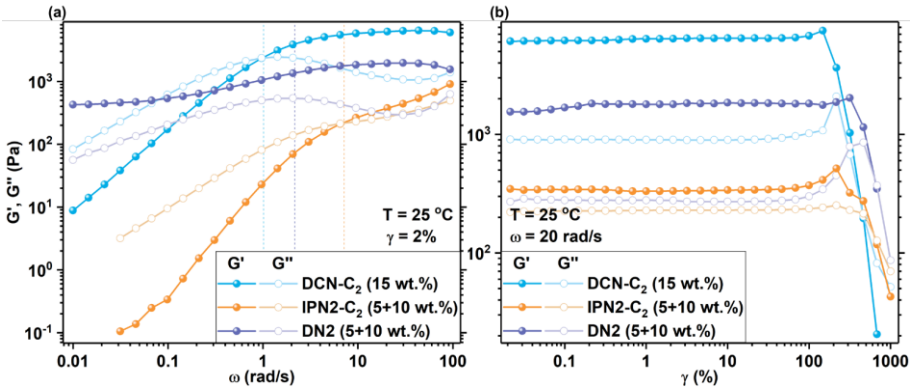

Figure 4.15. Oscillatory frequency sweeps (a) and strain sweeps (b) of the hydrogels of DCN-C_2 (15 wt.%) and IPN2-C_2 (5+10 wt.%) at the same total polymer concentration and the same crosslinker concentration as the DN2 (15 wt.%) hydrogel.

4.3 Conclusion

In this work, we investigated the viscoelastic properties of DCN, IPN and DN hydrogels based on two orthogonal types of reversible bonds: zinc(II)-terpyridine coordination bonds and oxime bonds. We compared the oscillatory mechanical properties and dynamic relaxation behavior of these three hydrogels. Six major systems containing both Zn^{2+}-Tpy and oxime crosslinks, and their corresponding Zn^{2+}-Tpy or

oxime crosslinked single networks, were prepared and measured by oscillatory rheology.

By virtue of the finite lifetime of Zn^{2+}-Tpy and the stability of oxime, the stress relaxation behavior of networks is governed by Zn^{2+}-Tpy crosslinks, while oxime crosslinks maintain the stability of the hydrogels. Compared to oxime linkages, Zn^{2+}-Tpy crosslinks are more efficient in forming networks with higher crosslinking density and more homogeneous, and thus Zn^{2+}-Tpy networks exhibit higher plateau moduli than oxime networks. The dynamic nature of Zn^{2+}-Tpy allows the hydrogel to adapt to the applied oscillatory strain and exhibit an extended linear viscoelastic region, while the stability of the oxime allows the hydrogel to withstand greater rupture strains.

Based on the orthogonal combination of dynamic Zn^{2+}-Tpy and stable oxime, the DCN, IPN and DN hydrogels exhibit similar viscoelastic solid behavior. Due to the differences in the formation of effective crosslinks between Zn^{2+}-Tpy and oxime in DCN, IPN and DN, the relaxation timescales and amplitudes of the hydrogels varied slightly between the different topologies. The Zn^{2+}-Tpy and oxime form more interchain crosslinks in the sub-network of DCN than of IPN or DN, resulting in a higher modulus for the DCN hydrogel than for the DN or IPN hydrogel. Compared to the single crosslinked sub-networks, the topological differences between DCN, IPN and DN result in different magnitudes of potential modulus enhancement for hydrogels crosslinked by both Zn^{2+}-Tpy and oxime. Among them, the elastic moduli of hydrogels with both Zn^{2+}-Tpy and oxime crosslinks show a ~2-fold increase for DCN, ~3-fold for IPN, and ~3.6-fold for DN compared to the sum of the moduli of the respective single networks. The order of deformability and stability of the hydrogels is generally DCN <IPN <DN. In addition, due to the dynamic reversibility of Zn^{2+}-Tpy, DCN, IPN and DN hydrogels show self-healing properties that can be recovered after partial destruction by strain.

4.4 Experimental Section

4.4.1. Reagents and materials

The reagents were purchased from the same suppliers as in Chapter 3 unless otherwise noted. 3-methylamino-1-propanol was purchased from Sigma-Aldrich Co. Reagents and solvents were also purified using the same methods as described in Chapter 3.

4.4.2. Preparation and characterization of monomers

Synthesis of 3-([2,2':6',2''-terpyridine]-4'-yloxy)-N-methylpropan-1-amine.

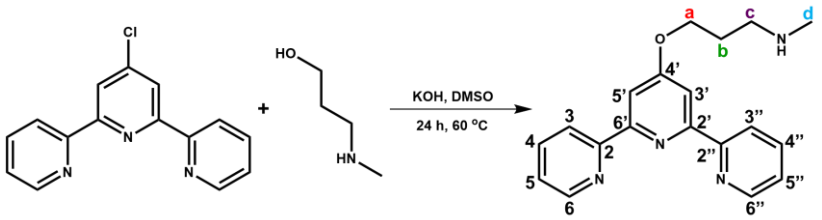

Scheme 4.8. Synthetic route of 3-([2,2':6',2''-terpyridine]-4'-yloxy)-N-methylpropan-1-amine.

3-Methylamino-1-propanol (0.4 g, 4.48 mmol) and anhydrous KOH (1.47 g, 26.15 mmol) were dispersed in dry DMSO (8 mL). The suspension was stirred at 60 ℃ for 1 h under argon atmosphere. To this mixture, a 5 mL solution of 4-chloro-2,2':6',2''-terpyridine (0.556 g, 2.08 mmol) in dry DMSO was added dropwise under stirring. After stirring at 60 ℃ for an additional 24 h, the reaction mixture was poured into deionized water (500 mL). This aqueous solution was extracted with DCM (4×100 mL). The organic phases were recombined and

washed with deionized water (2×100 mL), and then dried with anhydrous Na_2CO_3 and concentrated under vacuum to get a white needlelike crystalline solid (0.65 g, 97%). ^{1}H NMR (300 MHz, $CDCl_3$, δ): 8.68 (ddd, 2H, J = 1.8, 1.2, 0.6 Hz, CH_{terpy}, $H_{6,6''}$), 8.60 (dt, 2H, J = 4.5 Hz, CH_{terpy}, $H_{3,3''}$), 8.01 (s, 2H, CH_{terpy}, $H_{3',5'}$), 7.84 (td, 2H, J = 4.5, 0.9 Hz, CH_{terpy}, $H_{4,4''}$), 7.32 (ddd, 2H, J = 3.6, 3, 0.9 Hz,CH_{terpy}, $H_{5,5''}$), 4.32 (t, 2H, J = 3.75 Hz, CH_2, H_a), 2.83 (t, 2H, J = 4.2 Hz, CH_2, H_c), 2.48 (s, 2H, CH_3, H_d), 2.06 (m, 2H, CH_2, H_b). 1.79 (s, broad, NH).

Synthesis of N-(3-([2,2':6',2''-terpyridine]-4'-yloxy)propyl)-N-methylacrylamide (TPy-AM).

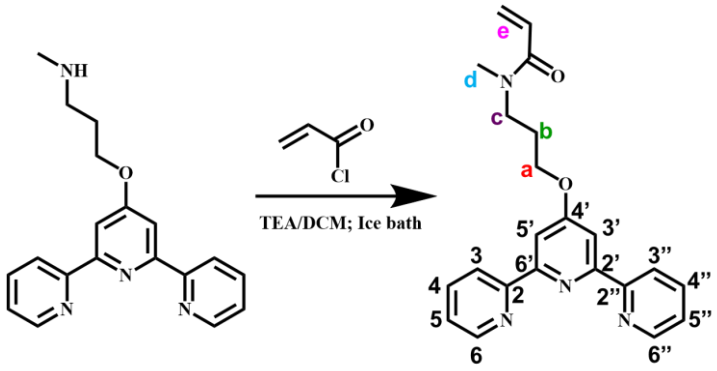

Scheme 4.9. Synthetic route of TPy-AM.

3-([2,2':6',2''-terpyridine]-4'-yloxy)-N-methylpropan-1-amine (638 mg, 1.99 mmol) and freshly dried triethylamine (303 mg, 2.99 mmol) were dissolved in dry DCM (200 mL) on an ice bath under argon atmosphere. To this solution, a solution of acryloyl chloride (360 mg, 3.98 mmol) in 5 mL of dry DCM was added dropwise under stirring. After the addition was completed, the reaction mixture was stirred overnight at room temperature, and then quenched with 100 mL of a saturated solution of Na_2CO_3. The organic fraction was isolated, and the aqueous fraction was extracted with 100 mL of dichloromethane. The organic phases were recombined and washed with deionized water

(3×100 mL), and then dried with anhydrous Na_2CO_3 and concentrated under vacuum below 25 °C. The crude product was purified through column chromatography (basic aluminum oxide), eluting with a mixture of ethyl acetate/hexane (gradient from 15% to 100% of ethyl acetate). The N-(3-([2,2':6',2''-terpyridine]-4'-yloxy)propyl)-N-methylacrylamide (TPy-AM) was obtained as a yellow and viscous oil with 80 % yield (0.6 g). ^{1}H NMR (300 MHz, $CDCl_3$, δ): 8.70 (dd, 2H, J = 2.4, 1.8, 0.9 Hz, CH_{terpy}, $H_{6,6''}$), 8.61 (dd, 2H, J = 7.8, 3.3 Hz, CH_{terpy}, $H_{3,3''}$), 8.02 (s, 2H, CH_{terpy}, $H_{3',5'}$), 7.86 (td, 2H, J = 7.8, 1.8 Hz, CH_{terpy}, $H_{4,4''}$), 7.34 (ddd, 2H, J = 6.3, 4.8, 3.3 Hz, CH_{terpy}, $H_{5,5''}$), 6.60 (dq, 1H, J = 14.4, 10.2 Hz, CH_2=CH), 6.34 (dq, 1H, J = 16.8, 2.1 Hz, CH_2=CH), 5.65 (ddd, 1 H, J = 12.6, 10.5, 2.1 Hz, CH_2=CH), 4.26 (m, 2H, CH_2, H_a), 3.65 (m, 2H, CH_2, H_c), 3.05 (d, 2H, J = 23.7 Hz, CH_3, H_d), 2.16 (m, 2H, CH_2, H_b). HRMS (ESI-MS) m/z: $[M+H]^+$ calcd for $C_{22}H_{23}N_4O_2$, 375.1821 ; found, 375.1815.

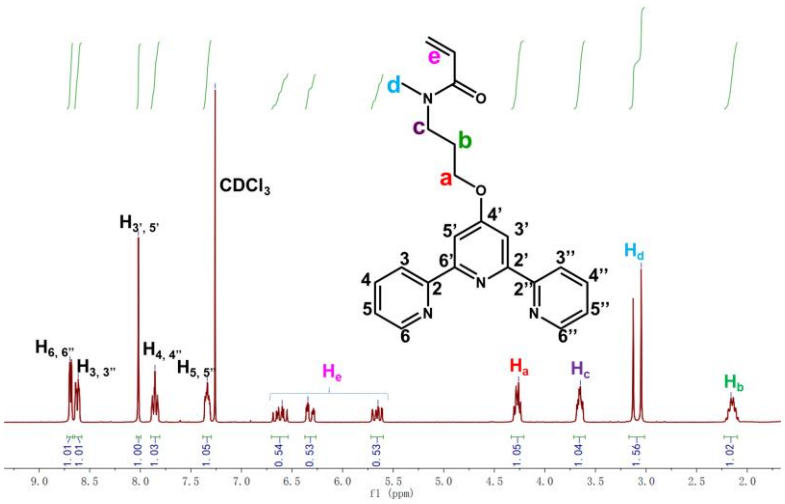

Figure 4.16. ^{1}H NMR spectrum of N-(3-([2,2':6',2''-terpyridine]-4'-yloxy)propyl)-N-methylacrylamide (TPy-AM).

4.4.3. Preparation and characterization of copolymers

Table 4.10. Synthesis recipes for functional copolymers via RAFT.

Copolymer	Feed ratio (mol%)			[AIBN]: [DDMAT]: [monomer]	T (°C)	t (h)	Conversion[a]
	Tpy	Ketone	DMA				
$P(T_2K_2)$-S	2.0	2.0	96.0	1:10:5865	70	12	94%
$P(T_2)$-S	2.0	/	98.0	1:10:5750	70	12	90%
$P(K_2)$-S	/	2.0	98.0	1:10:5830	60	6.5	89%
$P(T_4)$-S	4.0	/	96.0	1:10:5865	70	24	92%
$P(K_4)$-S	/	4.0	96.0	1:10:5830	60	9	94%
$P(K_{0.4})$-L1	/	0.6	99.4	1:10:33000	50	19.5	52%
$P(K_{0.4})$-L2	/	0.6	99.4	1:10:66000	50	16	44%

[a] The conversion of monomer was determined by comparing the integral ratio of the vinyl signals to the methylene proton of dioxane on the ^{1}H NMR spectrum.

Synthesis of short-chain poly(N,N-dimethylacrylamide) copolymers with terpyridine groups.

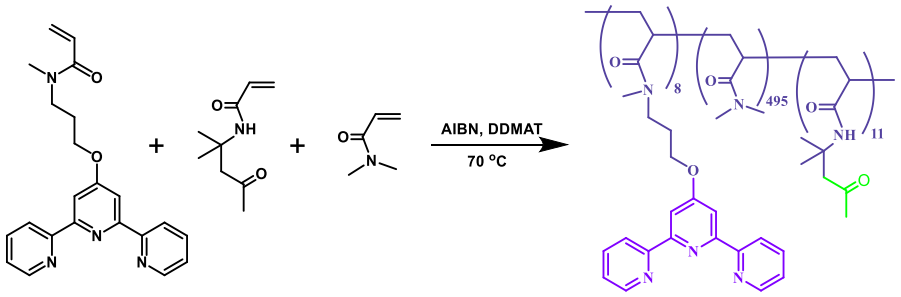

Scheme 4.10. Synthetic route of $P(T_2K_2)$-S.

AIBN (0.7 mg, 0.0045 mmol), DDMAT (16.4 mg, 0.045 mol), TPy-AM (194.5 mg, 0.52 mmol), DAAM (88 mg, 0.52 mmol) and DMA (2.525 g, 25.47 mmol) were dissolved in 8.89 mL of dry dioxane in a 25 mL round-bottom Schlenk-flask. The solution was degassed by five freeze-pump-thaw cycles, backfilled with argon and stirred in a preheated oil bath at 70 °C for 12 h. The polymerization was stopped by opening the flask to air and placing it in liquid nitrogen. The conversion of monomer was determined to be 94% by comparing the integral ratio of the vinyl signals to the methylene proton of dioxane on the ^{1}H NMR spectrum. The viscous liquid was diluted with DCM and precipitated three times in 20-times volume excess diethyl ether, and the polymer was finally dried in a vacuum oven at 40 °C for 24 h. The product was characterized by ^{1}H NMR and SEC.

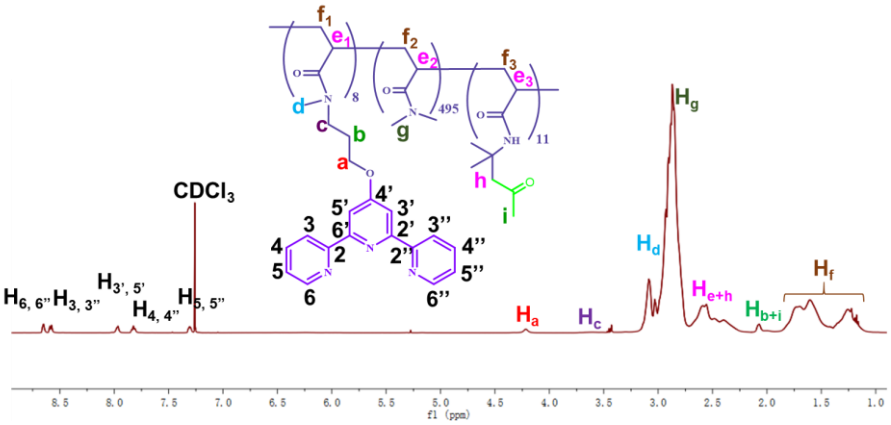

Figure 4.17. ^{1}H NMR spectrum of P(T_2K_2)-S.

The synthesis of ~2% terpyridine-functionalized PDMA (P(T_2)-S) and ~4% terpyridine-functionalized PDMA (P(T_4)-S) with an approximate polymer molecular weight of ~50 kDa was done in the same conditions as the above method with fixed feed ratio of reactants as shown in **Table 4.10**.

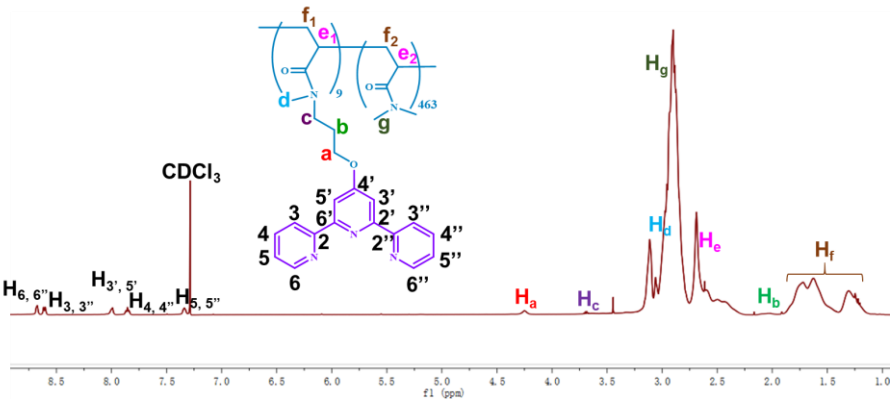

Figure 4.18. ^{1}H NMR spectrum of P(T_2)-S.

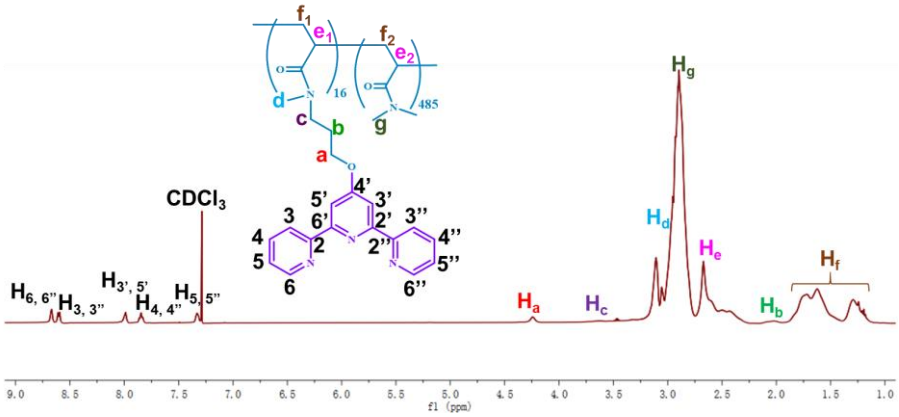

Figure 4.19. ^{1}H NMR spectrum of P(T_4)-S.

Synthesis of short-chain poly(N,N-dimethylacrylamide) copolymer with ketone groups.

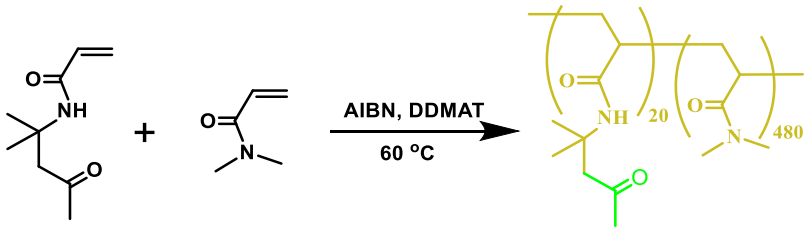

Scheme 4.11. Synthetic route to P(K_4)-S.

The side-chain ~4% ketone-functionalized poly(N,N-dimethylacrylamide) (P(K_4)-S) was synthesized by employing the above method, with some modifications: AIBN (1.5 mg, 0.009 mmol), DDMAT (32.8 mg, 0.09 mmol), DAAM (356.4 mg, 2.106 mmol) and DMA (4.993 g, 50.36 mmol) were dissolved in 10 mL of dry dioxane in a 50 mL round-bottom Schlenk-flask. The solution was degassed by five freeze-pump-thaw cycles, backfilled with argon, and stirred in a preheated oil bath at 60 °C for 9 h. The polymerization was stopped by

opening the flask to air and placing it in liquid nitrogen. The conversion of monomer was determined to be 94%, by comparing the integral ratio of the vinyl signals to the methylene proton of dioxane on the ^{1}H NMR spectrum. The viscous liquid was diluted with DCM and precipitated three times in 20-times volume excess of diethyl ether, and the polymer was finally dried in a vacuum oven at 40 °C for 24 h. The product was characterized by ^{1}H NMR and SEC.

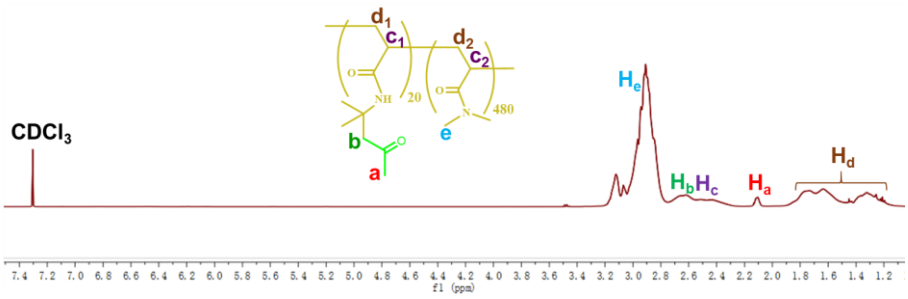

Figure 4.20. ^{1}H NMR spectrum of P(K_4)-S.

The side-chain ~2% ketone-functionalized PDMA (P(K_2)-S) with an approximate polymer molecular weight of ~50 kDa was synthesized by using the same method as the synthesis of P(K_4)-S with fixed feed ratio of reactants.

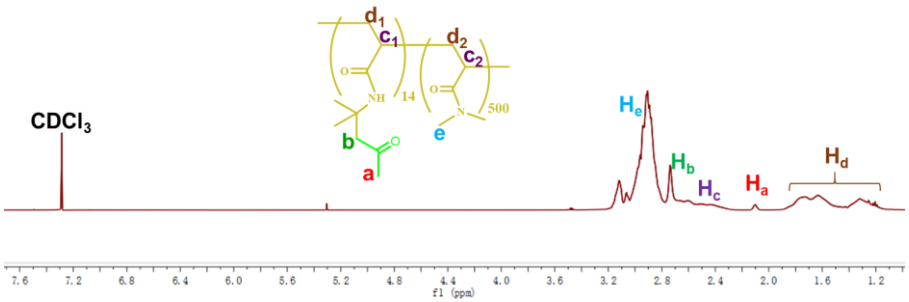

Figure 4.21. ^{1}H NMR spectrum of P(K_2)-S.

Synthesis of long-chain poly(N,N-dimethylacrylamide) copolymer with ~0.4% ketone groups.

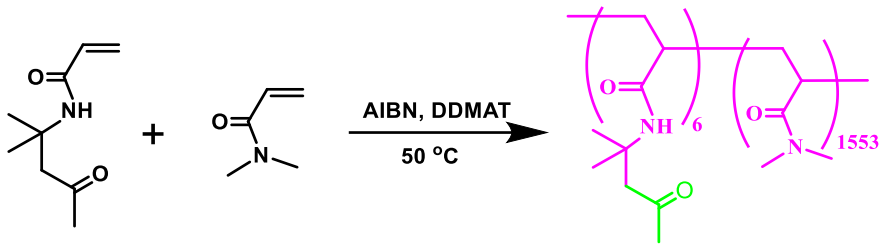

Scheme 4.12. Synthetic route to P($K_{0.4}$)-L1.

AIBN (0.6 mg, 0.0034 mmol), DDMAT (12.4 mg, 0.034 mmol), DAAM (115.1 mg, 0.68 mmol) and DMA (11.055 g, 111.52 mmol) were dissolved in 10 mL of dry dioxane in a 50 mL round-bottom Schlenk-flask. The solution was degassed by five freeze-pump-thaw cycles, backfilled with argon, and stirred in a preheated oil bath at 50 °C for 19.5 h. The polymerization was stopped by opening the flask to air and placing it in liquid nitrogen. The conversion of monomer was determined to be 52%, by comparing the integral ratio of the vinyl signals to the methylene proton of dioxane on the ^{1}H NMR spectrum. The viscous liquid was diluted with DCM and precipitated three times in 40-times volume excess of diethyl ether, and the polymer was finally dried in a vacuum oven at 40 °C for 24 h. The product was characterized by ^{1}H NMR and SEC.

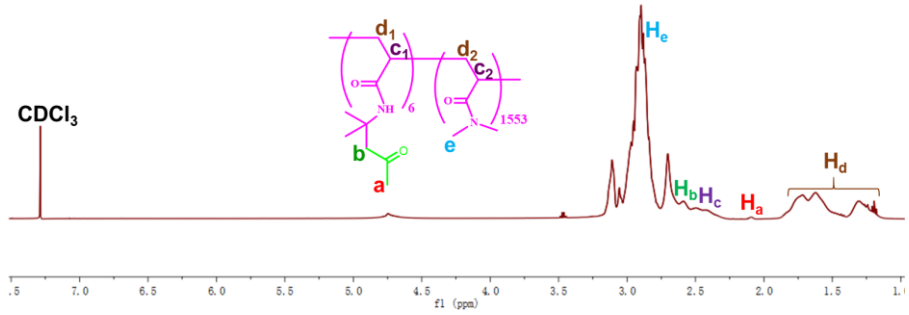

Figure 4.22. ^{1}H NMR spectrum of P($K_{0.4}$)-L1.

By employing the same synthetic method of the P($K_{0.4}$)-L1, another long-chain PDMA copolymer with ~0.4% ketone-functionalized (P($K_{0.4}$)-L2) with an approximate polymer molecular weight of ~250 kDa was obtained.

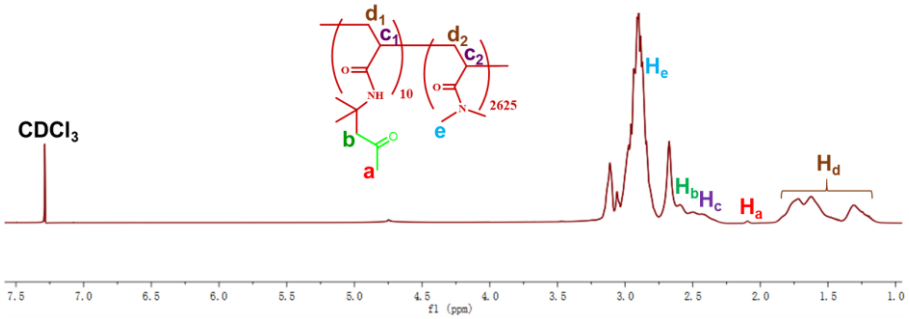

Figure 4.23. ^{1}H NMR spectrum of P($K_{0.4}$)-L2.

4.4.4. Preparation of networks

For either Zn^{2+}-Tpy or oxime network, the stoichiometric amount of added Zn^{2+} or bis-hydroxylamine is half an equivalent compared to the reactive sites (terpyridine or ketone groups) of the corresponding copolymers. The $ZnCl_2$ was employed to associate with terpyridine ligands of P(T_2K_2)-S, P(T_2)-S, or P(T_4)-S, to form zinc(II)-terpyridine bis-complexes (Zn^{2+}-Tpy) bridged network. The bis-hydroxylamine (O,O'-(propane-1,3-diyl)bis(hydroxylamine) dihydrochloride) was used to react with ketone groups of P(T_2K_2)-S, P(K_2)-S, P(K_4)-S, P($K_{0.4}$)-L1, or P($K_{0.4}$)-L2 to construct oxime crosslinked network. Aqueous solutions of the crosslinkers were prepared, and a certain amount was added to the polymer aqueous solutions to obtain the desired amount of crosslinker.

General procedures for hydrogels (or networks) formation: A desired amount of copolymer is dissolved in a set volume of deionized water overnight at 35 °C of the water bath. A known concentration of crosslinkers is then added to the transparent copolymer solutions under shaking, followed by heating at 55 °C for 2 days, and then slowly cooling down to room temperature in 2 days to get homogeneous hydrogels (or networks). Below are some examples that show the differences in the preparation of typical hydrogels (or networks) in this work.

Preparation of dual-crosslinked network (DCN) hydrogels.

In a typical experiment, 0.0250 g P(T_2K_2)-S and 200 μL deionized water were transferred to a clean and dried glass vial. Subsequently, the glass vial was sealed with a rubber septum and placed in a preheated water bath at 35 °C overnight under stirring to obtain a fully transparent and homogeneous solution. Subsequently, 25 μL of a bis-hydroxylamine solution (100 mmol/L) were added dropwise to the previously prepared copolymer solution and vortexed for 1 min, followed by the addition of 25 μL of a $ZnCl_2$ solution (83.2 mmol/L) in

deionized water to the reaction mixture and additionally vortexed for another 1 min. The sealed reaction sample was then placed in a preheated water bath at 55 °C for 2 days of aging and then slowly cooling down to room temperature in 2 days. Ultimately, a transparent dual-crosslinked network (DCN) hydrogel (**Scheme 4.1a**) with a final polymer weight-to-volume fraction of 10 wt.% was obtained.

Preparation of single DCN networks.

Similar to the preparation of DCN hydrogels, 0.0250 g P(T_2K_2)-S were dissolved in 225 μL deionized water to get a transparent and homogeneous copolymer solution. 25 μL of a stock solution containing only a single crosslinker were subsequently added to the previously prepared copolymer solution to reach a final polymer concentration of 10 wt.%. The final reaction mixture was vigorously vortexed for 1 minute and then aged for 2 days at 55 °C and slowly cooled down to room temperature in 2 days. Finally, a homogeneous transparent single network of DCN-Zn^{2+}-Tpy or DCN-Oxime (**Scheme 4.1b**) was observed as a gel as confirmed by the glass vial inversion method.

Preparation of interpenetrating polymer network (IPN) hydrogels.

For the IPN1 (5+5 wt.%) hydrogel (**Scheme 4.2a**), 0.0125 g P(T_2)-S and 0.0125 g P(K_2)-S were first dissolved in 200 μL of deionized water to get a homogeneous solution, followed by the addition of first 25 μL of bis-hydroxylamine solution (69.2 mmol/L), and then of 25 μL of a Zn^{2+} solution (45.8 mmol/L). The solution was vortexed after each crosslinker addition. Finally, the above closed system was submitted to the same aging procedure as described for DCN. By using the same procedures, the IPN1 (10+10 wt.%) hydrogel (**Scheme 4.3a**) was prepared from 10 wt.% P(T_2)-S with 10 wt.% P(K_2)-S, and the IPN2 (5+5 wt.%) hydrogel (**Scheme 4.4a**) was prepared from 5 wt.% P(T_4)-S with 5 wt.% P(K_4)-S.

Preparation of single IPN networks.

The single networks of IPN1 (**Schemes 4.2b** and **4.3b**) were prepared from equal weights of P(T_2)-S with P(K_2)-S. Specifically, IPN1-Zn^{2+}-Tpy and IPN1-Oxime single networks were prepared at a total polymer concentration of 5+5 wt.% from 0.0125 g P(T_2)-S and 0.0125 g P(K_2)-S in 250 μL of deionized water. The preparation process was similar to the preparation of the above single DCN networks: dissolving 0.0250 g of mixed copolymers (0.0125 g P(T_2)-S and 0.0125 g P(K_2)-S) in 225 μL deionized water to get a homogeneous solution, followed by adding 25 μL solution of only one crosslinker under vortex. After 2 days of aging at 55 °C and then slowly cooling down to room temperature in another 2 days, the final single networks of IPN1-Zn^{2+}-Tpy or IPN1-Oxime were obtained.

250 μL of 10+10 wt.% single network of IPN1-Zn^{2+}-Tpy or IPN1-Oxime (**Scheme 4.3b**) were obtained by the same method but using twice the amount of mixed copolymers of P(T_2)-S with P(K_2)-S and twice the concentration of crosslinkers.

250 μL of single network of IPN2-Zn^{2+}-Tpy or IPN2-Oxime (**Scheme 4.4b**) were prepared at a total copolymer concentration of 5+5 wt.% (5 wt.% of P(T_4)-S with 5 wt.% of P(K_4)-S) by also employing the same method as for the 5+5 wt.% single IPN1 network.

Preparation of double network (DN) hydrogels.

In a typical experiment, 0.0125 g of P(T_4)-S with 0.025g of P($K_{0.4}$)-L1 or P($K_{0.4}$)-L2 were mixed and 215 μL of deionized water were added. The solution was placed at 35 °C overnight under stirring until the copolymers were completely dissolved to get a homogeneous solution. To this solution, 10 μL of bis-hydroxylamine solution (50 mmol/L) were added dropwise and vigorously vortexed for 1 min, followed by the addition of 25 μL of a $ZnCl_2$ solution (74.1 mmol/L) and shaking for another 1 min. The desired DN hydrogels of DN1 (**Scheme 4.5a**) or DN2 (**Scheme 4.6a**) were then obtained after 2 days

of aging at 55 °C and slowly cooling down to room temperature in an additional 2 days.

Preparation of single DN networks.

The DN-Zn^{2+}-Tpy single network was prepared from 5 wt.% P(T_4)-S singly crosslinked by Zn^{2+}-Tpy complexes in the presence of 10 wt.% P($K_{0.4}$)-L1 or P($K_{0.4}$)-L2. The DN-Oxime single network was prepared from 10 wt.% P($K_{0.4}$)-L1 or 10 wt.% P($K_{0.4}$)-L2 singly crosslinked by oxime bonds in the presence of 5 wt.% P(T_4)-S. Therefore, the DN1-Zn^{2+}-Tpy and DN1-Oxime were prepared from a mixture of 5 wt.% P(T_4)-S with 10 wt.% P($K_{0.4}$)-L1 copolymers (**Scheme 4.5b**), and the DN2-Zn^{2+}-Tpy and DN2-Oxime were prepared from a mixture of 5 wt.% P(T_4)-S with 10 wt.% P($K_{0.4}$)-L2 copolymers (**Scheme 4.6b**), by adding either Zn^{2+} or bis-hydroxylamine. These networks were created by the same procedure as the preparation of DN hydrogels but with the addition of only one type of crosslinkers.

Preparation of individual networks.

The 10 wt.% individual Zn^{2+}-Tpy network and individual oxime network (**Scheme 4.7**) were prepared similarly to the single networks described above. For example, 0.025 g pure P(T_4)-S was first dissolved in 200 μL of deionized water to obtain a homogeneous solution. Subsequently, 50 μL of a $ZnCl_2$ solution (74.1 mmol/L) was added to the above transparent solution and stirred, followed by the aging process. The 10 wt.% individual Zn^{2+}-Tpy network was thus obtained. Similarly, the 10% individual oxime network was prepared from 0.025 g of pure P(K_4)-S in 200 μL of water and 50 μL of bis-hydroxylamine solution (74.1 mmol/L) at the same concentration as the $ZnCl_2$ solution for the individual Zn^{2+}-Tpy network.

4.4.5. Rheological measurements

The rotational rheometer (MCR 301, Anton Paar) with a solvent trap equipment was used to conduct rheological measurements. All tests were conducted in parallel plate geometry, the bottom plate was a Peltier device controlling the system at a reference temperature of 25 °C. The gel samples, in the form of sheets with diameter 8 mm and thickness 0.2~0.5 mm, were set under an 8 mm diameter top plate geometry. A 15 mm diameter top plate geometry with distance 0.1~0.2 mm was used for solution samples. It can be seen that the samples used for rheological measurements were very small and therefore were susceptible to water evaporation during the experiments. In order to avoid/limit the effect of evaporation on the experimental data, as much water as possible was added around the sample on the static plate but making sure that it did not touch the tested sample. Two Teflon models were also set up as solvent traps. Under these conditions, a moist air atmosphere can be maintained around the sample for anywhere from a few to a dozen hours (the exact effective moisturising time would vary depending on the experimental operation), thus reducing evaporation from the sample.

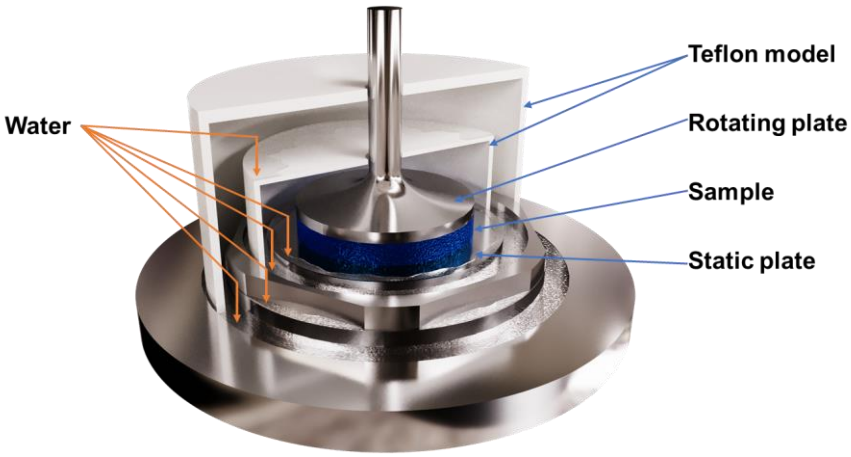

Figure 4.24. Solvent trap installation for rheological measurements.

The linear viscoelastic regimes of all samples were determined by oscillatory strain sweeps that were carried out with strain ranging from 0.01 to 1000% at a constant frequency of 2 rad/s unless otherwise specified. The dynamic properties of the samples were determined by oscillatory frequency sweeps (100-0.01 rad/s) at a fixed oscillatory strain of 2% strain, which is within the linear viscoelastic region. Reverse strain sweeps were also performed at a constant frequency of 0.2 rad/s, 2 rad/s and 20 rad/s, respectively. We estimate an accuracy of 10% on the mearued modulus values.

A pure PDMA [M_n: 36400 g/mol (Evaluated by monomer conversion), $Đ$: 1.37) was synthesized using the same method as for the synthesis of short chain copolymers. The oscillatory frequency sweeps (0.1-200 rad/s) were recorded at 140 °C, 150 °C, 160 °C, 170 °C and 180 °C for the PDMA polymer in the melt state. Based on these data, the entanglement molar mass Me of the linear PDMA melt was estimated to be 11000 g/mol with the method described in the textbook (Physical Properties of Polymers Handbook, 2nd ed.[55]).

4.5 Reference

[1] Sun, H.; Zhao, Y.; Wang, C.; Zhou, K.; Yan, C.; Zheng, G.; Huang, J.; Dai, K.; Liu, C.; Shen, C. Ultra-Stretchable, Durable and Conductive Hydrogel with Hybrid Double Network as High Performance Strain Sensor and Stretchable Triboelectric Nanogenerator. Nano Energy 2020, 76, 105035.

[2] Zhuo, S.; Zhao, Z.; Xie, Z.; Hao, Y.; Xu, Y.; Zhao, T.; Li, H.; Knubben, E. M.; Wen, L.; Jiang, L.; Liu, M. Complex Multiphase Organohydrogels With Programmable Mechanics Toward Adaptive Soft-Matter Machines. Sci. Adv. 2020; 6, 1464.

[3] Ryan, K. R.; Down, M. P.; Banks, C. E. Future of Additive Manufacturing: Overview of 4D and 3D Printed Smart and Advanced Materials and Their Applications. Chem. Eng. J. 2021, 403, 126162.

[4] Li, S.; Zhou, X.; Dong, Y.; Li, J. Flexible Self-Repairing Materials for Wearable Sensing Applications: Elastomers and Hydrogels. Macromol. Rapid Commun. 2020, 41, 2000444

[5] Matsuda T.; Kawakami R.; Namba R.; Nakajima T.; Gong J. P. Mechanoresponsive Self-Growing Hydrogels Inspired by Muscle Training. Science 2019, 363, 504-508.

[6] Li, C.; Iscen, A.; Palmer, L. C.; Schatz, G. C.; Stupp, S. I. Light-Driven Expansion of Spiropyran Hydrogels. J. Am. Chem. Soc. 2020, 142, 8447-8453.

[7] Dong, M.; Shi, B.; Liu, D.; Liu, J. H.; Zhao, D.; Yu, Z. H.; Shen, X. Q.; Gan, J. M.; Shi, B. L.; Qiu, Y.; Wang, C. C.; Zhu, Z. Z.; Shen, Q. D. Conductive Hydrogel for a Photothermal-Responsive Stretchable Artificial Nerve and Coalescing with a Damaged Peripheral Nerve. ACS Nano 2020, 14, 16565-16575.

[8] Liang, R.; Wang, L.; Yu, H.; Khan, A.; Amin, B. U.; Khan, R. U. Molecular Design, Synthesis and Biomedical Applications of Stimuli-Responsive Shape Memory Hydrogels. Eur. Polym. J. 2019, 114, 380-396.

[9] Rossow, T.; Seiffert, S. Supramolecular Polymer Gels with Potential Model-Network Structure. Polym. Chem. 2014, 5, 3018-3029.

[10] Golkaram, M.; Loos, K. A Critical Approach to Polymer Dynamics in Supramolecular Polymers. Macromolecules 2019, 52, 9427-9444.

[11] Podgórski, M.; Fairbanks, B. D.; Kirkpatrick, B. E.; McBride, M.; Martinez, A.; Dobson, A.; Bongiardina, N. J.; Bowman, C. N. Toward Stimuli-Responsive Dynamic Thermosets through Continuous Development and Improvements in Covalent Adaptable Networks (CANs). Adv. Mater. 2020, 32, 1906876.

[12] Perera, M. M.; Ayres, N. Dynamic Covalent Bonds in Self-Healing, Shape Memory, and Controllable Stiffness Hydrogels. Polym. Chem. 2020, 11, 1410-1423.

[13] Chakma, P.; Konkolewicz, D. Dynamic Covalent Bonds in Polymeric Materials. Angew. Chem., Int. Ed. 2019, 58, 9682-9695.

[14] Qin, B.; Yin, Z.; Tang, X.; Zhang, S.; Wu, Y.; Xu, J. F.; Zhang, X. Supramolecular Polymer Chemistry: From Structural Control to Functional Assembly. Prog. Polym. Sci. 2020, 100, 101167.

[15] Yang H.; Ghiassinejad S.; Van Ruymbeke, E.; Fustin, C. A. Tunable Interpenetrating Polymer Network Hydrogels Based on Dynamic Covalent Bonds and Metal-Ligand Bonds. Macromolecules, 2020, 53, 6956-6967.
[16] McBride, M. K.; Worrell, B. T.; Brown, T.; Cox, L. M.; Sowan, N.; Wang, C.; Podgorski, M.; Martinez, A. M.; Bowman, C. N. Enabling Applications of Covalent Adaptable Networks. Annu. Rev. Chem. Biomol. Eng. 2019, 10, 175-198.
[17] Nadgorny, M.; Collins, J.; Xiao, Z. Y.; Scales, P. J.; Connal, L. A. 3D-Printing of Dynamic Self-Healing Cryogels with Tuneable Properties. Polym. Chem. 2018, 9, 1684-1692.
[18] Li, Y.; Zhu, C.; Dong, Y.; Liu, D. Supramolecular Hydrogels: Mechanical Strengthening with Dynamics. Polymer 2020, 210, 122993.
[19] Fan, W.; Jin, Y.; Shi, L. Mechanically Robust and Tough Waterborne Polyurethane Films Based on Diselenide Bonds and Dual H-Bonding Interactions with Fast Visible-Light-Triggered Room-Temperature Self-Healability. Polym. Chem. 2020, 11, 5463-5474.
[20] Thompson, C. B.; Korley, L. T. J. 100th Anniversary of Macromolecular Science Viewpoint: Engineering Supramolecular Materials for Responsive Applications-Design and Functionality. ACS Macro Lett. 2020, 9, 1198-1216.
[21] Wang, S.; Urban, M. W. Self-Healing Polymers. Nat. Rev. Mater. 2020, 5, 562-583.
[22] Nele, V.; Wojciechowski, J. P.; Armstrong, J. P. K.; Stevens, M. M. Tailoring Gelation Mechanisms for Advanced Hydrogel Applications. Adv. Funct. Mater. 2020, 30, 2002759.
[23] Hu, X.; Zhou, J.; Daniel, W. F. M.; Vatankhah-Varnoosfaderani, M.; Dobrynin, A. V.; Sheiko, S. S. Dynamics of Dual Networks: Strain Rate and Temperature Effects in Hydrogels with Reversible H-Bonds. Macromolecules 2017, 50, 652-659.
[24] Wen, J.; Pan, M.; Yuan, J.; Wang, J.; Zhu, L.; Jia, Z.; Song, S. Facile Fabrication of Dual-Crosslinked Single Network Heterostructural Polyurethane Hydrogels with Superior Mechanical and Fluorescent Performance. React. Funct. Polym. 2020, 146, 104433.
[25] Yuan, Y.; Shen, S.; Fan, D. A physicochemical double cross-linked multifunctional hydrogel for dynamic burn wound healing: shape adaptability, injectable self-healing property and enhanced adhesion. Biomaterials 2021, doi:10.1016/j.biomaterials.2021.120838
[26] Li, Y.; Yang, L.; Zeng, Y.; Wu, Y.; Wei, Y.; Tao, L. Self-Healing Hydrogel with a Double Dynamic Network Comprising Imine and Borate Ester Linkages. Chem. Mater. 2019, 31, 15, 5576-5583.
[27] Ahmadi, M.; Löser, L.; Fischer, K.; Saalwächter, K.; Seiffert, S. Connectivity Defects and Collective Assemblies in Model Metallo-Supramolecular Dual-Network Hydrogels. Macromol. Chem. Phys. 2020, 221, 1900400.
[28] Silverstein, M. S. Interpenetrating Polymer Networks: So Happy Together? Polymer 2020, 207, 122929.
[29] Ishikawa, S.; Iijima, K.; Matsukuma, D.; Asawa, Y.; Hoshi, K.; Osawa, S.; Otsuka, H. Interpenetrating Polymer Network Hydrogels via a One-Pot and in Situ Gelation System Based on Peptide Self-Assembly and Orthogonal Cross-Linking for Tissue Regeneration. Chem. Mater. 2020, 32, 2353-2364.

[30] Haque, M. A.; Kurokawa, T.; Gong, J. P. Super Tough Double Network Hydrogels and Their Application as Biomaterials. Polymer 2012, 53, 1805-1822.
[31] Sun, T. L.; Kurokawa, T.; Kuroda, S.; Ihsan, A. B.; Akasaki, T.; Sato, K.; Haque, M. A.; Nakajima, T.; Gong, J. P. Physical Hydrogels Composed of Polyampholytes Demonstrate High Toughness and Viscoelasticity. Nat. Mater. 2013, 12, 932-937.
[32] Fu, X.; Hosta-Rigau, L.; Chandrawati, R.; Cui, J. Multi-Stimuli-Responsive Polymer Particles, Films, and Hydrogels for Drug Delivery. Chem. 2018, 4, 2084-2107.
[33] Cao, Z.-Q.; Wang, G.-J. Multi-Stimuli-Responsive Polymer Materials: Particles, Films, and Bulk Gels. Chem. Rec. 2016, 16, 1398-1435.
[34] Zhang, R.; Zhang, C.; Yang, Z.; Wu, Q.; Sun, P.; Wang, X. Hierarchical Dynamics in a Transient Polymer Network Cross-Linked by Orthogonal Dynamic Bonds. Macromolecules 2020, 53, 5937-5949.
[35] Xi, W.; Scott, T. F.; Kloxin, C. J.; Bowman, C. N. Click Chemistry in Materials Science. Adv. Funct. Mater. 2014, 24, 2572-2590.
[36] Xu, J.; Liu, Y.; Hsu, S.-H. Hydrogels Based on Schiff Base Linkages for Biomedical Applications. Molecules 2019, 24, 3005.
[37] Ahmadi, M.; Seiffert, S. Thermodynamic Control over Energy Dissipation Modes in Dual-network Hydrogels Based on Metal-ligand Coordination. Soft Matter 2020, 16, 2332-2341.
[38] Ahmadi, M.; Seiffert, S. Dynamic Model Metallo-Supramolecular Dual-Network Hydrogels with Independently Tunable Network Crosslinks. J. Polym. Sci. 2020, 58, 330-342.
[39] Xu, X.; Jerca, F. A.; Jerca, V. V.; Hoogenboom, R. Covalent Poly(2-Isopropenyl-2-Oxazoline) Hydrogels with Ultrahigh Mechanical Strength and Toughness through Secondary Terpyridine Metal-Coordination Crosslinks. Adv. Funct. Mater. 2019, 29, 1904886.
[40] Gong, J. P.; Katsuyama, Y.; Kurokawa, T.; Osada, Y. Double-Network Hydrogels with Extremely High Mechanical Strength. Adv. Mater. 2003, 15, 1155-1158.
[41] Hawke, L. G. D.; Ahmadi, M.; Goldansaz, H.; van Ruymbeke, E. Viscoelastic Properties of Linear Associating Poly(N-butyl acrylate) Chains. J. Rheol. 2016, 60, 297-310.
[42] Czarnecki, S.; Rossow, T.; Seiffert, S. Hybrid Polymer-Network Hydrogels with Tunable Mechanical Response. Polymers 2016, 8, 82.
[43] Kim, S.; Regitsky, A. U.; Song, J.; Ilavsky, J.; McKinley, G. H.; Holten-Andersen, N. In situ Mechanical Reinforcement of Polymer Hydrogels via Metal-Coordinated Crosslink Mineralization. Nat. Commun. 2021, 12, 667.
[44] Xu, X.; Jerca, F. A.; Jerca, V. V.; Hoogenboom, R. Self-Healing and Moldable Poly(2-isopropenyl-2-oxazoline) Supramolecular Hydrogels Based on a Transient Metal Coordination Network. Macromolecules 2020, 53, 6566-6575.
[45] Marco-Dufort, B.; Iten, R.; Tibbitt, M. W. Linking Molecular Behavior to Macroscopic Properties in Ideal Dynamic Covalent Networks. J. Am. Chem. Soc. 2020, 142, 15371-15385.
[46] Schmolke, W.; Ahmadi, M.; Seiffert, S. Enhancement of metallo-supramolecular dissociation kinetics in telechelic terpyridine-capped poly(ethylene glycol) assemblies in the semi-dilute regime. Phys. Chem. Chem. Phys. 2019, 21, 19623-19638.

[47] Yesilyurt, V.; Ayoob, A. M.; Appel, E. A.; Borenstein, J. T.; Langer, R.; Anderson, D. G. Mixed Reversible Covalent Crosslink Kinetics Enable Precise, Hierarchical Mechanical Tuning of Hydrogel Networks. Adv. Mater. 2017, 29, 1605947.
[48] Tan, C. S. Y.; Agmon, G.; Liu, J.; Hoogland, D.; Janeček, E.-R.; Appel, E. A.; Scherman, O. A. Distinguishing Relaxation Dynamics in Transiently Crosslinked Polymeric Networks. Polym. Chem. 2017, 8, 5336-5343.
[49] Vidavsky, Y.; Buche, M. R.; Sparrow, Z. M.; Zhang, X.; Yang, S. J.; DiStasio Jr, R. A.; Silberstein, M. N. Tuning the Mechanical Properties of Metallopolymers via Ligand Interactions: A Combined Experimental and Theoretical Study. Macromolecules, 2020, 53, 2021-2030.
[50] Zhang, X.; Vidavsky, Y.; Aharonovich, S.; Yang, S. J.; Buche, M. R.; Diesendruck, C. E.; Silberstein, M. N. Bridging Experiments and Theory: Isolating the Effects of Metal-Ligand Interactions on Viscoelasticity of Reversible Polymer Networks. Soft Matter 2020, 16, 8591-8601.
[51] Shi, W. H.; Pathiranage, T. M. S. K.; Marciel, A. B. Rheological properties of engineered protein polymer networks. MRS Bull. 2020, 45, 1048-1054.
[52] Gong, J. P. Why are double network hydrogels so tough? Soft Matter 2010, 6, 2583-2590.
[53] Mezger, T. G. The Rheology Handbook, 4th ed.; Vincentz Network: Hannover, 2014.
[54] Xu, D.; Hawk, J. L.; Loveless, D. M.; Jeon, S. L.; Craig, S. L. Mechanism of Shear Thickening in Reversibly Cross-Linked Supramolecular Polymer Networks. Macromolecules 2010, 43, 3556-3565.
[55] Mark, J. E. Physical Properties of Polymers Handbook, 2nd ed.; Springer: New York, 2007, pp. 448.

Chapter 5

Double Network Hydrogels with Contrasting Dynamic Crosslinking

Abstract

Two types of double network (DN) hydrogels were designed by either using a labile supramolecular first network with a second network based on stable dynamic covalent bonds, or using a less stable dynamic covalent bonding first network with a long-lifetime supramolecular network as the second network. Oscillatory shear rheology is used to study the two DN hydrogels and their corresponding sub-networks to compare their dynamic behaviors and oscillatory mechanical properties. The two DN hydrogels exhibit contrasting stress relaxation behaviors due to the exchange or dissociation of first dynamic network. Both DN hydrogels show higher elastic modulus than the sum moduli of the respective sub-networks. The self-healing properties of DN hydrogels are due to the synergetic contribution between the reversibility of dynamic bonds in the first network and the high deformability of the second network.

.

5.1 Introduction

As discussed in Chapter 2, the double network (DN) is a subset of the interpenetrating polymer network (IPN) and was introduced by Gong and coworkers in 2003 to improve the mechanical properties of polymer hydrogels.[1-4] Unlike a conventional IPN, a DN consists of two contrasting networks. The first network is rigid and brittle, and is formed by a densely crosslinked short-chain network, while the second network is soft, stretchable and is created by a loosely crosslinked long-chain network. The main weakness of classical DN hydrogels is that both networks are permanently crosslinked by covalent bonds and the fracture of the network is irreversible upon large deformations, thus reducing the overall fatigue resistance of the hydrogel and lacking self-healing mechanisms.[5, 6] To address these limitations, it has been attempted to replace static covalent bonds with dynamic bonds used as crosslinks.[7-10] The introduction of dynamic bonds into network enables the hydrogel to inherit some features of the bonds (e.g. stimulus responsiveness) and to regulate the dynamic behavior of the hydrogels (crosslinking dynamics, shear-thinning, moldability, etc.).[11, 12] The reversible dissociation/formation and exchange of dynamic bonds allow these bonds to be broken to dissipate energy and then the network can be restructured after the release of the deformation, thus effectively improving the mechanical properties of the material (e.g. enhanced elasticity, self-healing, fatigue resistance and self-recovery).[13-20] In general, supramolecular interactions are used as crosslinks for the first network and static covalent bonds are used as crosslinks for the second network.[21] Nevertheless, DN hydrogels prepared using dynamic covalent bonds have been rarely reported.[21-30] In Chapter 4, we have discussed DN hydrogels consisting of a supramolecular first network and of a dynamic covalent second network. In contrast, to our knowledge, DN hydrogels prepared from a dynamic covalent bond-based first network and a supramolecular second network has never been reported. It is interesting to develop this new dynamic DN hydrogel and to compare it with a DN hydrogel in which the two

networks are crosslinked by the inverse combination of dynamic bonds, i.e., a DN with a supramolecular first network and a dynamic covalent second network.

As illustrated in Chapter 3, the lifetimes and association constants of metal-terpyridine coordination bonds (M(II)-Tpy) can be varied by appropriate selection of metal ions,[32] and the stability of reversible C=N bonds can also be regulated by changing the nucleophile structure that reacts with the carbonyl electrophile.[33] Therefore, in this chapter, we attempted to construct two contrasting DN hydrogels based on the combination of metal-terpyridine coordination bonds and reversible C=N bonds, expecting to provide some clues for designing new DN hydrogels by the orthogonal incorporation of two types of dynamic bonds with significantly different dynamics and stabilities. To this aim, we developed two DN hydrogels for comparison. The first DN hydrogel (DN1) is fabricated by the addition of Zn^{2+} ions to highly functionalized short-chain polymers with terpyridine entities (Tpy) (the proportion of Tpy in the polymer chain is much higher than in the Tpy copolymers used in Chapter 4) to form the first network densely crosslinked by labile zinc(II)-terpyridine bis-complexes (Zn^{2+}-Tpy), and of a bis-hydroxylamine that would react with a long-chain polymers sparsely modified with ketone groups to create the second network loosely crosslinked by stable oxime bonds (**Figure 5.1**). In contrast, for the second DN hydrogel (DN2), a di-acylhydrazide can be used as crosslinkers to react with the ketone groups of a highly functionalized short-chain polymer to build the first network crosslinked by less stable acylhydrazone bonds, and the second network is produced by forming long-lifetime iron(II)-terpyridine bis-complexes (Fe^{2+}-Tpy) by the addition of Fe^{2+} ions to a Tpy sparsely functionalized long-chain polymer. In other words, the DN1 hydrogel consists of a first network crosslinked by more dynamic supramolecular interactions, and of second network crosslinked by stable dynamic covalent bonds. The DN2 hydrogel consists of a first network crosslinked by highly reversible dynamic covalent bonds and of a second network crosslinked by a supramolecular interaction of high bond energy.

As shown in **Figure 5.1**, our DNs are similar to conventional DN hydrogels, with the first network being highly crosslinked by a short-chain polymer and the second network being loosely crosslinked by a long-chain polymer.[1] However, our DNs differ from Gong's classical DNs in the preparation method, polymer compositions and types of crosslinking bonds. Firstly, Gong's DN hydrogels are synthesized from monomers by a two-step in situ polymerization, where the first network is first formed by polymerization followed by its immersion in a second monomer solution to highly swell it, and finaly form the second network by a second polymerization.[2] Our hydrogel preparation starts with two already formed copolymers, and subsequently, crosslinkers are added to the mixed copolymer solution to crosslink each of the two copolymers to form the DN. The order of addition of the crosslinker may affect the homogeneity and thus the mechanical properties of the gels. Secondly, the first network of Gong's DN is usually composed of polyelectrolytes, which ensures its high swelling and thus that the first network is highly extended. Therefore, when the DN is subjected to external forces, the stresses are first concentrated on the rigid and brittle first network, which acts as a sacrificial network to dissipate the stresses and thus improve the toughness of the hydrogel. Although our preparation method does not guarantee a full swelling of the first network the asymmetry in the crosslinking density of the two networks is nevertheless well present.

To this end, four copolymers based on poly(N,N-dimethyl acrylamide) (PDMA) with functional Tpy and ketone groups were prepared via reversible addition-fragmentation chain transfer (RAFT) polymerization. As shown in **Figure 5.1**, the short-chain copolymer PT-S and long-chain copolymer PK-L are used for preparing DN1 hydrogel, and the short-chain copolymer PK-S and long-chain copolymer PT-L are used for preparing DN2 hydrogel. Oscillatory shear rheology is used as the primary measurement to relate the contribution of two dynamic networks to the macroscopic frequency- and amplitude-dependent mechanical properties of the two as-prepared DN hydrogels. The dynamic responsiveness and self-healing properties of the DN hydrogels are also characterized by rheology.

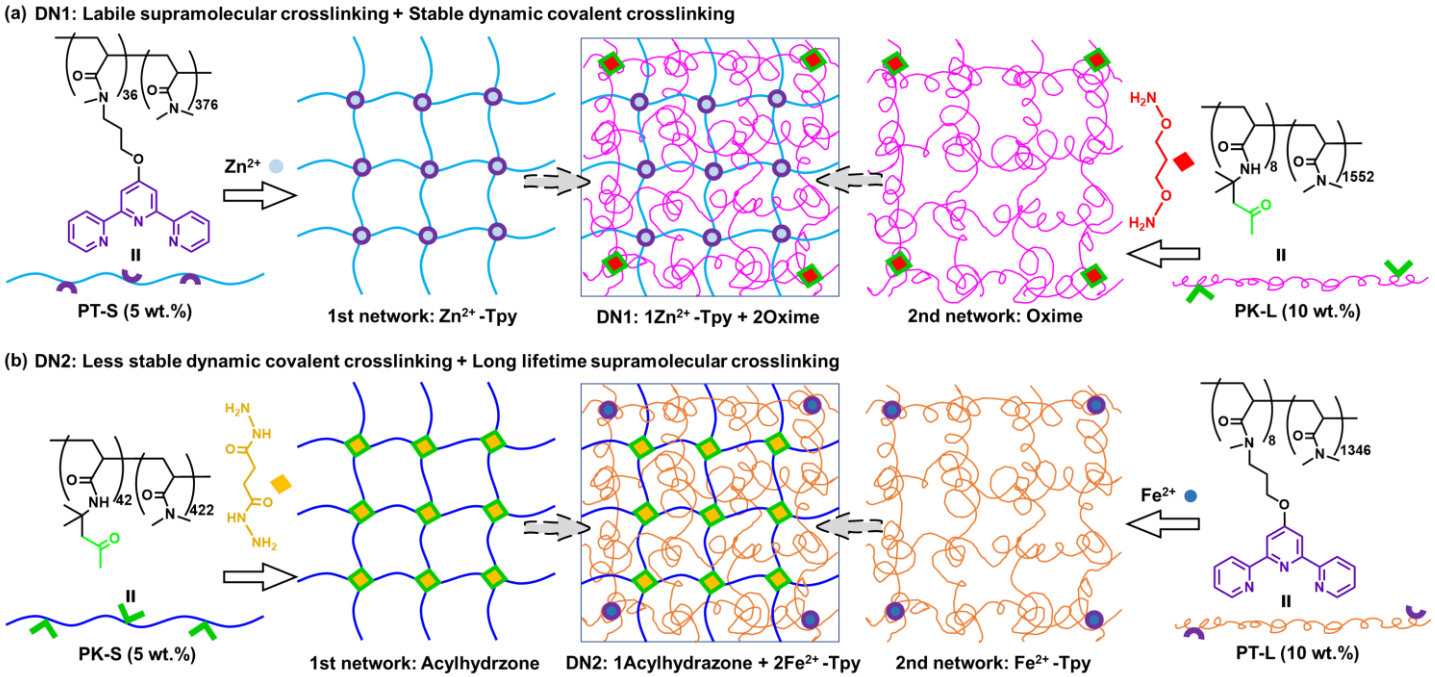

Figure 5.1. Schematic representation of two double network (DN) hydrogels based on the combinations of metal-terpyridine coordination bonds and reversible C=N bonds: (a) DN1: labile Zn^{2+}-Tpy crosslinks in the first network and stable oxime crosslinks in the second network, (b) DN2: less stable acylhydrazone crosslinks in the first network and long-lifetime Fe^{2+}-Tpy crosslinks in the second network.

5.2 Results and Discussion

5.2.1. Synthesis of hydrophilic functionalized copolymers

Table 5.1. Main characteristics of the hydrophilic functionalized copolymers.

Copolymer	Final ratio[a] (mol%)			M_n[b] (g/mol)	M_n[c] (g/mol)	$Đ$[c]	N_f/Chain[d]	
	Tpy	Ketone	DMA				Tpy	Ketone
PT-S	8.7	/	91.3	50600	58100	1.25	36	/
PK-L	/	0.5	99.5	155200	128900	1.43	/	8
PK-S	/	9.1	90.9	49000	52000	1.26	/	42
PT-L	0.5	/	99.5	136300	135300	1.36	8	/

[a] Calculated from the ^{1}H NMR spectra. [b] Evaluated by monomer conversion (^{1}H NMR). [c] Determined by SEC (polymethylmethacrylate standards). [d] Average number of functional groups per chain.

The aqueous poly(N,N-dimethyl acrylamide) (PDMA) was selected as the backbone polymer for preparing the functional copolymers. The terpyridine-functionalized monomer N-(3-([2,2':6',2''-terpyridin]-4'-yloxy)propyl)-N-methylacrylamide (TPy-AM) was synthesized as described in Chapter 4. The ketone containing monomer diacetone acrylamide (DAAM) was commercially available. A highly terpyridine-functionalized short-chain copolymer (PT-S) and a sparsely terpyridine-functionalized long-chain copolymer (PT-L) were synthesized via RAFT polymerization using TPy-AM and N,N-dimethyl acrylamide (DMA) by varying the ratios of the two monomers. In contrast, the highly ketone-functionalized short-chain copolymer (PK-S) and the sparsely ketone-functionalized long-chain copolymer (PK-L) were synthesized using DAAM and DMA. Details of the synthesis of these copolymers are shown in the Experimental Section and they were characterized by NMR and SEC (**Table 5.1**).

5.2.2. Preparation of networks

Unless otherwise stated, the amount of added crosslinkers (Zn^{2+}, Fe^{2+}, bis-hydroxylamine, di-acylhydrazide) was half an equivalent compared to the reaction sites (terpyridine groups or ketone groups) of the copolymers for preparing all networks. After the addition of the crosslinkers, the systems underwent an aging process at 55°C for two days and were gradually and slowly cooled to room temperature over two days to facilitate all crosslinking reactions and to obtain a stable and reproducible network.

Following our design, short-chain polymers are highly functionalized for the construction of the first network of DN hydrogels, while long-chain polymers are sparsely functionalized for the fabrication of the second network. In order to keep the DN in the gel state after one of the two networks has lost his crosslinks due to e.g. long timescales, high strain, etc., the concentration of the two individual networks must be higher than their respective minimum gelation concentrations. Therefore, the concentration of the long-chain polymer in the DN system should be higher than that of the short-chain polymer, which is also in line with the features of DN gels, i.e., the molar concentration of monomers in the second network should be much higher than that of the first network.[2] However, given the solubility of the long-chain polymer, the concentration of the short-chain polymer for DN hydrogels was fixed at 5 wt.%, and the concentration of the long-chain polymer at 10 wt.% in order to obtain homogeneous DN hydrogels. In such cases, the two individual networks of each DN hydrogel systems are hydrogels with concentrations slightly higher than the minimum gelation concentrations. The first individual network of DN1 was crosslinked by addition of Zn^{2+} ions to PT-S chains via the formation of Zn^{2+}-Tpy, and the second individual network of DN1 was crosslinked through the reaction of bis-hydroxylamine (O,O'-(propane-1,3-diyl)bis(hydroxylamine) dihydrochloride) with ketones between PK-L chains to form oxime bonds (**Scheme 5.1a**). Correspondingly, the

first individual network of DN2 was created by the formation of acylhydrazone bonds between di-acylhydrazine (succinic dihydrazide) and PK-S chains, and the second individual network of DN2 was crosslinked by the generation of Fe^{2+}-Tpy between Fe^{2+} and PT-L chains (**Scheme 5.1a**). The apparent mechanical properties observed by touching the hydrogels with tweezers revealed that the individual Zn^{2+}-Tpy network (5 wt.%) and individual acylhydrazone network (5 wt.%) were stiff and non-sticky hydrogels; the individual oxime network (10 wt.%) was a soft and sticky hydrogel; the individual Fe^{2+}-Tpy network (10 wt.%) was a soft and non-stick hydrogel.

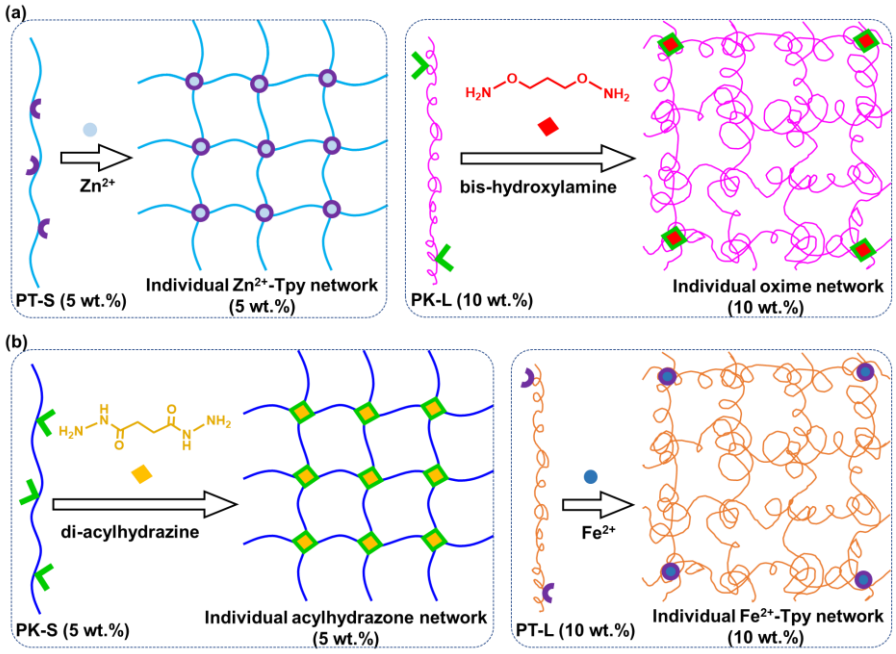

Scheme 5.1. (a) Preparation of individual networks of DN1 hydrogel system. (b) Preparation of individual networks of DN2 hydrogel system.

DN hydrogels consist of two interpenetrating polymer networks (IPNs), where only physical interactions between the two networks may exist,[34] but the presence of the polymer chains of one network may lead to steric hindrances or screening effects that affect the formation

of the other network.[35, 36] To learn the influence of the presence of the non-crosslinked polymer on the formation of the other network, single networks of each of DN hydrogels were also prepared for comparison with their individual networks and the resultant DN hydrogels. The single networks were thus formed with the same polymer composition as the corresponding DN hydrogels but with the addition of only one appropriate crosslinker, as in the case of the individual networks (**Scheme 5.2**). Similar to the individual networks without the presence of another non-crosslinked polymer, the corresponding single networks have the same apparent mechanical properties observed by touching the hydrogels with tweezers. For example, the single Zn^{2+}-Tpy network (5+10 wt.%) and single acylhydrazone network (5+10 wt.%) were stiff and non-sticky hydrogels.

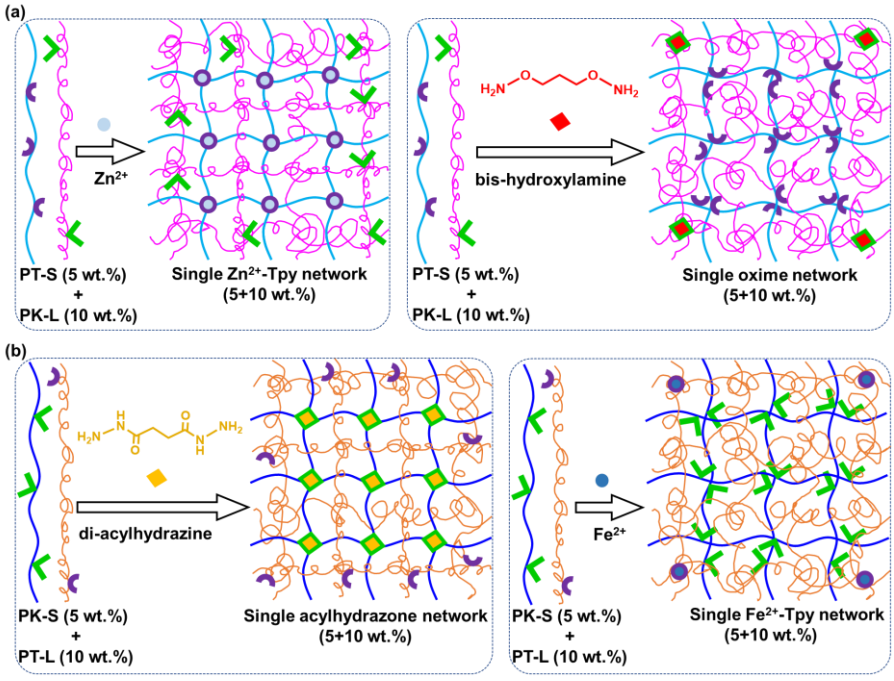

Scheme 5.2. (a) Preparation of single networks of DN1 hydrogel system. (b) Preparation of single networks of DN2 hydrogel system.

The DN1 and DN2 hydrogels were prepared by a "one-step" crosslinking method (**Scheme 5.3**). Since the formation of metal-terpyridine bis-complexes is usually fast and leads to almost immediate gelation that may limit the diffusion of the other crosslinker (used to form reversible C=N bonds), DN hydrogels were prepared by first mixing bis-hydroxylamine or di-acylhydrazine homogeneously into the mixed solution of the two copolymers before adding the Zn^{2+} or Fe^{2+} ions. After the addition of both crosslinkers for the two interpenetrating networks, an aging time of 2 days at 55 °C followed by a slow cooling down to room temperature for another 2 days was applied. DN1 and DN2 hydrogels were then obtained. The apparent mechanical properties observed by touching the hydrogels with tweezers revealed that the DN1 (5+10 wt.%) and DN2 (5+10 wt.%) were tough hydrogels.

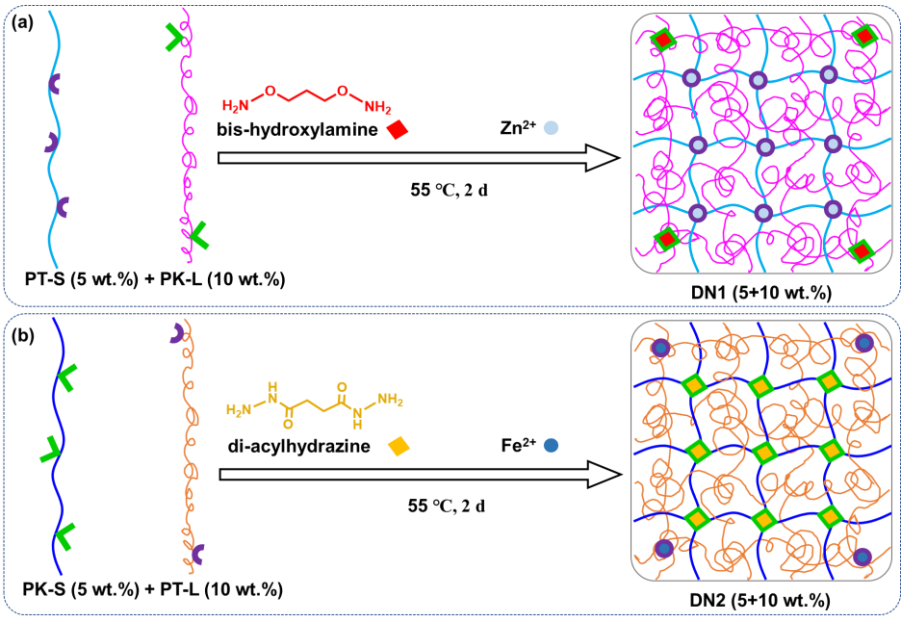

Scheme 5.3. Preparation of DN1 (a) and DN2 (b) hydrogels by the "one-step" crosslinking method.

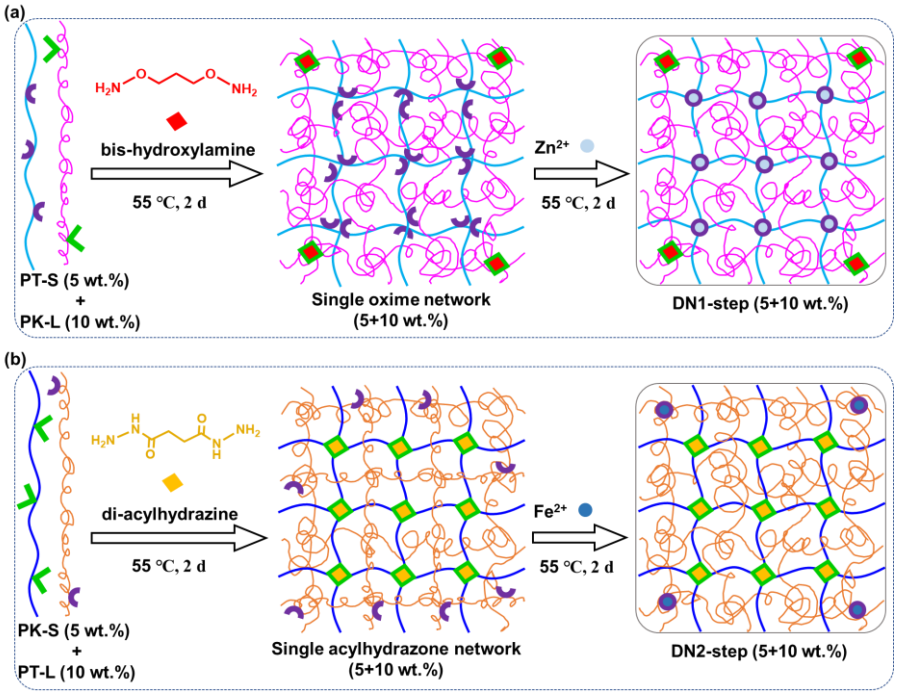

Scheme 5.4. Preparation of DN1-step (a) and DN2-step (b) hydrogels by the "two-step" crosslinking method.

Moreover, in classical DN hydrogels, the two networks are formed in steps, which may be beneficial to obtain more homogeneous hydrogels with better mechanical properties.[1, 34] Considering that the formation of reversible C=N bonds is slower than M(II)-Tpy, we also adopted a "two-step" crosslinking strategy of forming oxime or acylhydrazone networks before forming Zn^{2+}-Tpy or Fe^{2+}-Tpy networks (**Scheme 5.4**). The metal ions were added after bis-hydroxylamine or di-acylhydrazine was added and aged at 55 °C for two days to ensure the formation of the oxime or acylhydrazone networks. After the addition of metal ions, the systems were also aged at 55 °C for two days and then slowly (2 days) cooled to room temperature. The two DN hydrogels obtained by this "two-step" crosslinking method were named "DN1-step" and "DN2-step", which were distinguished and compared with the DN1 and DN2 hydrogels that

were obtained by the initial "one-step" crosslinking method. The apparent mechanical properties observed by touching the hydrogels with tweezers revealed that the DN1 (5+10 wt.%) was not a homogeneous hydrogel where the upper gel layer was soft and the lower gel layer was stiff, and DN2 (5+10 wt.%) was a tough hydrogel.

5.2.3. Rheological characterizations

To investigate the oscillatory mechanical and dynamic properties of the obtained DN hydrogels, DN1 and DN2 hydrogels as well as their corresponding individual and single networks, were probed by oscillatory shear rheology.

5.2.3.1. Individual networks of DN1 and DN2 systems

Since both DN hydrogels and their single networks were prepared from mixed copolymers, the formation of interchain crosslinks in one copolymer can be influenced by the presence of the other copolymer.[35, 36] Therefore, as a basis for all measurements, we first performed tests on the individual Zn^{2+}-Tpy and oxime networks used to construct DN1 hydrogels (**Scheme 5.1a**) as well as the individual acylhydrazone and Fe^{2+}-Tpy networks that make up the DN2 hydrogel (**Scheme 5.1b**). The results of the frequency sweeps on the four individual networks are presented in **Figure 5.2**.

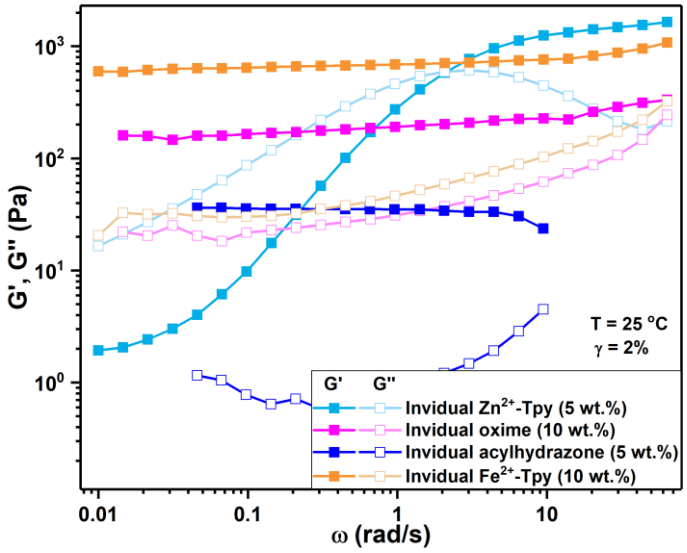

Figure 5.2. Oscillatory frequency sweeps performed on four individual networks of DN1 and DN2 (**Scheme 5.1**). The individual Zn^{2+}-Tpy and oxime networks are related to DN1, and the individual acylhydrazone and Fe^{2+}-Tpy networks are related to DN2.

As shown in **Figure 5.2**, the storage modulus (G') of the individual oxime and individual Fe^{2+}-Tpy networks is almost constant and always larger than the loss modulus (G'') over the whole experimental frequency window. It demonstrates that due to the stability of the oxime and Fe^{2+} -Tpy crosslinks, these two individual networks as the second networks of DN1 and DN2, respectively, are structurally stable and act like elastic gels. Interestingly, the first network of DN1, i.e., the individual Zn^{2+}-Tpy network, displayed a significant network relaxation behavior as evidenced by the observed crossover of G'-G'' at intermediate frequency, reflecting stress relaxation from strand exchange or dissociation due to the finiteness of the Zn^{2+}-Tpy bis-complexes lifetime.[37] This crossover marks the onset of the transition from solid-like behavior to liquid-like behavior of the gel that is observed at long timescales.[38, 39] Due to the dynamic reversibility of the acylhydrazone bonds, the first network of DN2, i.e. the individual acylhydrazone network, is also supposed to have a relaxation behavior.

This dynamic character will be proven later on in the chapter. The G' increase observed at close to 0.01 rad/s results from the solvent evaporation, as a consequence of the prolonged testing from high to low frequency. Compared to the gel samples of the other three individual networks, the gel samples of the individual acylhydrazone network is expected to dry more quickly at room temperature, despite the solvent trapping equipment used in the rheological tests, resulting in an increase in G' in the low frequency region. Therefore, the data for the individual acylhydrazone network in the low frequency region are not shown in **Figure 5.2**. The reason for the greater volatility of the individual acylhydrazone network sample is explained by its weak network property, which makes it difficult to retain moisture in it for long periods of time, as we can see from **Figure 5.2** where the plateau modulus of individual acylhydrazone network is only 33 Pa. Furthermore, the proportion of ketone hydrophobic blocks in the pure PK-S used for the individual acylhydrazone network is the highest compared to the other three individual networks prepared from pure copolymers (see **Table 5.1**). The greater number of hydrophobic groups may also lead to a poor water retention capacity of the individual acylhydrazone network. Nevertheless, there is a tendency for the G" to increase in the low frequency region, suggesting the onset of a relaxation of the network caused by acylhydrazone bond cleavage.

The four individual networks display significantly different plateau moduli (**Figure 5.2**), which is attributed to the differences in the formation of effective interchain crosslinks by the respective crosslinking bonds. **Table 5.2** summarizes the plateau moduli (G'_p) of the four individual networks obtained from the frequency sweep curves in the high frequency region before relaxation. Accordingly, the theoretical plateau moduli (G_N^0) of the four individual networks were calculated according to the Equation 4.1 in Chapter 4 and are listed in **Table 5.2** for comparison with the experimental plateau moduli. It can be seen that the experimental plateau moduli of the individual networks are all much lower than the theoretical plateau moduli, and therefore all showed very low crosslinking efficiency (**Table 5.2**). This may be due

to the presence of molecular defects and network imperfections, such as inhomogeneities in the network due to chain length and unreacted sites, as well as dangling chains and internal loops, which do not contribute to the practical elastic modulus of the network.[40, 41]

Table 5.2. Compositions, experimental and theoretical elastic plateau moduli of individual networks.

Sample	Copolymer[a]	M_{xx}[c] (g/mol)	G'$_p$[d] (Pa)	G_N^0 (Pa)	E$_c$[e] (%)
Individual Zn^{2+}-Tpy (5 wt.%)	PT-S (5 wt.%)	1400	1420	84600	1.7
Individual oxime (10 wt.%)	PK-L (10 wt.%)	19400	220	10500	2.1
Individual acylhydrazone (5 wt.%)	PK-S (5 wt.%)	1200	30	99200	0.03
Individual Fe^{2+}-Tpy (10 wt.%)	PT-L (10 wt.%)	17000	770	11900	6.5

[a] Copolymer used for crosslinking. [b] Concentration of added crosslinker (Zn^{2+}, bis-hydroxylamine, di-acylhydrazide or Fe^{2+}) is half of the concentration corresponding copolymer reaction sites. [c] Average molar mass between reaction sites on the corresponding copolymer. [d] Obtained from the plateau value of G' in the high-frequency domain of the frequency sweeps. [e] The crosslinking efficiency (E$_c$) is calculated by G'$_p$/G_N^0.

Although the crosslinking efficiency calculated from G_N^0 does not take into account the effect of dangling ends on the network, the value of the crosslinking efficiency can be used to roughly compare the tendency of different types of bonds to form effective elastic crosslinks in their individual networks. As discussed in Chapter 4, the estimated entanglement molar mass (M$_e$) of the linear PDMA melt is 11 kg/mol, which means that the minimum molar mass of PDMA copolymer to produce entanglement in an aqueous solution at 5 wt.% or 10 wt.% concentration is approximately 55 kg/mol or 110 kg/mol, and the critical entanglement molar mass is 2M$_e$ = 110 kg/mol or 220 kg/mol, respectively. This means that the 5 wt.% PT-S (50.6 kg/mol) and 10

wt.% PK-L (155.2 kg/mol) in DN1 as well as the 5 wt.% PK-S (49 kg/mol) and 10 wt.% PT-L (136.3 kg/mol) in DN2 are mostly unentangled. Nevertheless, we cannot exclude the possibility that some entanglements are trapped due to the crosslinking, which also contribute to the elastic modulus. As shown in **Table 5.2**, the crosslinking efficiency of the second networks was consistently higher than that of the first networks of DN1 and DN2, probably due to the fact that both PT-S and PK-S are highly functionalized, easily resulting in intramolecular crosslinking in the Zn^{2+}-Tpy or acylhydrazone individual networks. In addition, the lower concentration of the copolymers to build the first networks compared to the second networks may also be a reason for their low crosslinking efficiency. The copolymers forming respectively the first and the second networks in the two DNs are at the same concentrations and have comparable functionalization degrees, however, the crosslinking efficiency of the individual Fe^{2+}-Tpy network is higher than the oxime network, and the efficiency of the individual Zn^{2+}-Tpy network is higher than the acylhydrazone network. This can be explained by the higher effective crosslink formation for Zn^{2+}-Tpy and Fe^{2+}-Tpy bis-complexes, than for the reaction of ketone with acylhydrazone or hydroxylamine groups to form acylhydrazone or oxime bonds.[36] The higher crosslinking efficiency of metal-terpyridine coordination bonds compared to reversible C=N bonds may be explained by the steric hindrance effect of the crosslinkers. In the present work, the crosslinkers used to form M(II)-Tpy interchain crosslinks are Zn^{2+}, Fe^{2+}, and those used to form reversible C=N linkages are di-acylhydrazine and bis-hydroxylamine. In order to obtain an effective interchain M(II)-Tpy crosslink, the crosslinker Zn^{2+} or Fe^{2+} can directly associate with two interchain Tpy entities to form a bis-complex. In contrast, the two nucleophilic groups at each end of the di-acylhydrazine or bis-hydroxylamine crosslinker must react with two ketone groups on different chains respectively to lead to effective interchain crosslinking. Therefore, the different ways in which these two types of crosslinkers form effective interchain

crosslinks result in a higher crosslinking density in the Zn^{2+}-Tpy or Fe^{2+}-Tpy networks than in the acylhydrazone or oxime networks.

5.2.3.2. Single networks of DN1 and DN2 systems

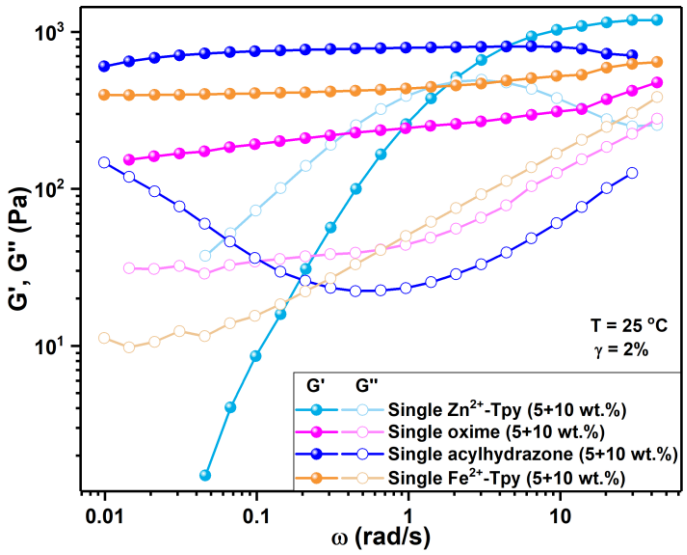

Figure 5.3. Oscillatory frequency sweeps performed on four single networks related to DN1 and DN2 (**Scheme 5.2**). The single Zn^{2+}-Tpy and oxime networks are related to DN1, and the single acylhydrazone and Fe^{2+}-Tpy networks are related to DN2.

Although the resultant DN1 and DN2 hydrogels are a combination of two individual networks, the crosslinking of each network in the two DN hydrogels is formed in the presence of another copolymer (**Scheme 5.3**). Accordingly, the rheological behavior of four single networks (**Scheme 5.2**), i.e., with the same polymer composition as the DN hydrogels but with only one polymer being crosslinked (see **Schemes 5.2** and **5.3**), and the results are presented in **Figure 5.3**. It can be seen from the figure that the rheological behaviors of the four single networks and their corresponding individual networks (see **Scheme 5.1** and **Figure 5.2**) are basically similar, i.e., the single oxime and the single Fe^{2+}-Tpy networks exhibit stable elastic solid behaviors, while

the single Zn^{2+}-Tpy and acylhydrazone have different relaxation behaviors.

In order to understand the effect of the presence of non-crosslinked copolymers on the single networks, the dynamic modulus as a function of frequency for the individual and single networks of the DN1 or DN2 systems are plotted in the same graph for comparison. As shown in **Figure 5.4a** (comparison of individual networks shown in **Scheme 5.1a** and single networks shown in **5.2a**), the moduli of the single Zn^{2+}-Tpy network are slightly lower than those of the individual Zn^{2+}-Tpy network, indicating that the "screening effect"[36] caused by the presence of the non-crosslinked 10 wt.% PK-L in the single Zn^{2+}-Tpy network diluted the effective crosslinking of the network. The moduli of the single oxime network are slightly higher than those of the individual oxime network, probably due to the fact that the PT-S copolymer highly functionalized with Tpy (8.7%, see **Table 5.1**), slightly contributes to the modulus value because of some π-π stacking or hydrophobic interactions between the Tpy moieties acting as crosslinks. In addition, the network relaxation time ($\tau_{Zn\text{-}Tpy}$) associated to the dissociation of Zn^{2+}-Tpy did not change in the single network (cf. the dashed line in **Figure 5.4a**), indicating that the non-crosslinked long-chain copolymer does not significantly affect the bond lifetime of Zn^{2+}-Tpy. In contrast, both individual and single oxime networks show a purely elastic response, with their G' being frequency independent and greater than G". This suggests that the oxime networks behave as pure chemical gels.[42]

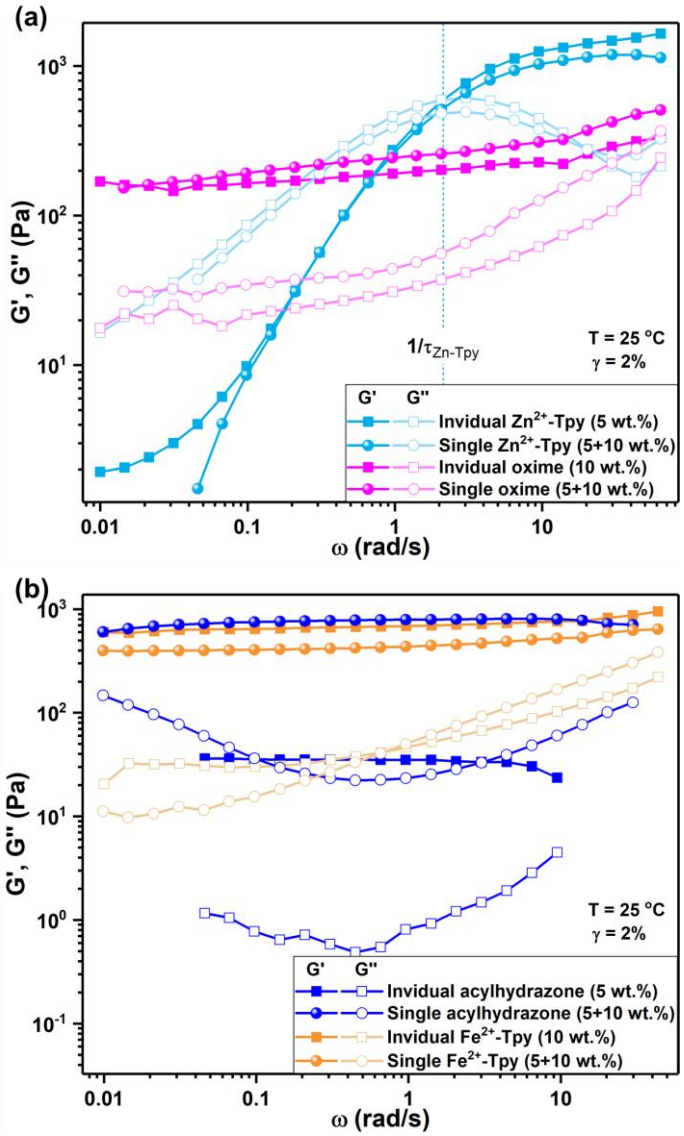

Figure 5.4. Comparison of dynamic moduli of individual and single networks for (a) DN1 and (b) DN2 systems.

Similarly to the comparison between the single and individual networks of the DN1 system, the presence of a non-crosslinked copolymer in the single networks of the DN2 system influences the level of the moduli of the single networks. As shown in **Figure 5.4b**

(comparison of individual networks shown in **Scheme 5.1b** and single networks shown in **5.2b**), the elastic modulus of the single acylhydrazone network is about 20 times higher compared to the individual acylhydrazone network. The self-assembled weak network formed by π-π stacking or hydrophobic interaction between Tpy entities in PT-L may slightly increase the modulus of the single network, like PT-S in single oxime networks. However, the great increase in modulus in the single acylhydrazone network is likely due to the presence of 10 wt% PT-L copolymer in the system, effectively preventing the formation of intrachain loops that exist in the individual acylhydrazone network, and more importantly causing the generation of more interchain crosslinks in the single acylhydrazone network. In the individual acylhydrazone network, the 5 wt.% pure PK-S is used, but this highly functionalized copolymer (9.1%, see **Table 5.1**) is prone to aggregation in aqueous solutions due to the hydrophobicity of the ketone side groups.[43] As a result, the addition of the di-acylhydrazine crosslinker tends to produce more intramolecular crosslinks, which make no contribution to the elastic modulus. For the single acylhydrazone network, which was prepared from mixed copolymer solution of 5 wt.% PK-S with 10 wt.% PT-L, the presence of PT-S may have prevented the aggregation of PK-S to some extent, promoting more intermolecular crosslinks after the addition of crosslinker. Therefore, the interchain crosslinking density of the single acylhydrazone network was much higher than that of the individual acylhydrazone network, which shows a 20-fold lower elastic modulus than the former. However, we cannot deny that the "screening effect" is still present in the single acylhydrazone network. The total polymer concentrations for the single acylhydrazone and single Zn^{2+}-Tpy networks are the same, and the 5 wt.% PK-S and PT-S used for the crosslinks have a similar functionalization degree (see **Table 5.1**). After two days of heating at 55 °C and two days of slow cooling, the more stable single acylhydrazone network was supposed to have a higher modulus than the labile single Zn^{2+}-Tpy network, but the opposite was

observed (**Figure 5.3**), suggesting that there should also be a "screening effect" in the single acylhydrazone network.

The moduli of the single Fe^{2+}-Tpy network are slightly lower than those of the individual Fe^{2+}-Tpy (**Figure 5.4b**), probably due to the "screening effect" caused by the presence of 5 wt.% PK-S, which reduced the interchain crosslinks in the single Fe^{2+}-Tpy network.

From the above, it is clear that the presence of Tpy copolymers that are not crosslinked by metal ions can increase the modulus of single oxime or acylhydrazone networks to varying levels, while the presence of non-crosslinked ketone copolymers can slightly decrease the modulus of single Zn^{2+}-Tpy or Fe^{2+}-Tpy networks. Therefore, the proposed "two-step" crosslinking strategy (**Scheme 5.4**) has the potential to yield stronger DN1 and DN2 hydrogels than the "one-step" crosslinking method (**Scheme 5.3**).

5.2.3.3. DN1 and DN2 hydrogels

The DN hydrogels can be obtained by the "one-step" (**Scheme 5.3**) or "two-step" (**Scheme 5.4**) crosslinking methods. However, it is not clear which of the two methods is better for preparing the DN hydrogels. To understand the effect of these two crosslinking strategies on the internal structure of the final DN hydrogels, oscillatory frequency sweeps were also performed on the DN hydrogels prepared by the two-step method. As shown in **Figure 5.5**, it is clear that the moduli of either DN1 or DN2 are higher than those of the DN1-step or DN2-step, demonstrating that it is easier to obtain more homogeneous DN hydrogels by the "one-step" crosslinking method. Therefore, the following discussion on DN hydrogels will be mainly based on the "one-step" crosslinking method to obtain DN1 or DN2 hydrogels.

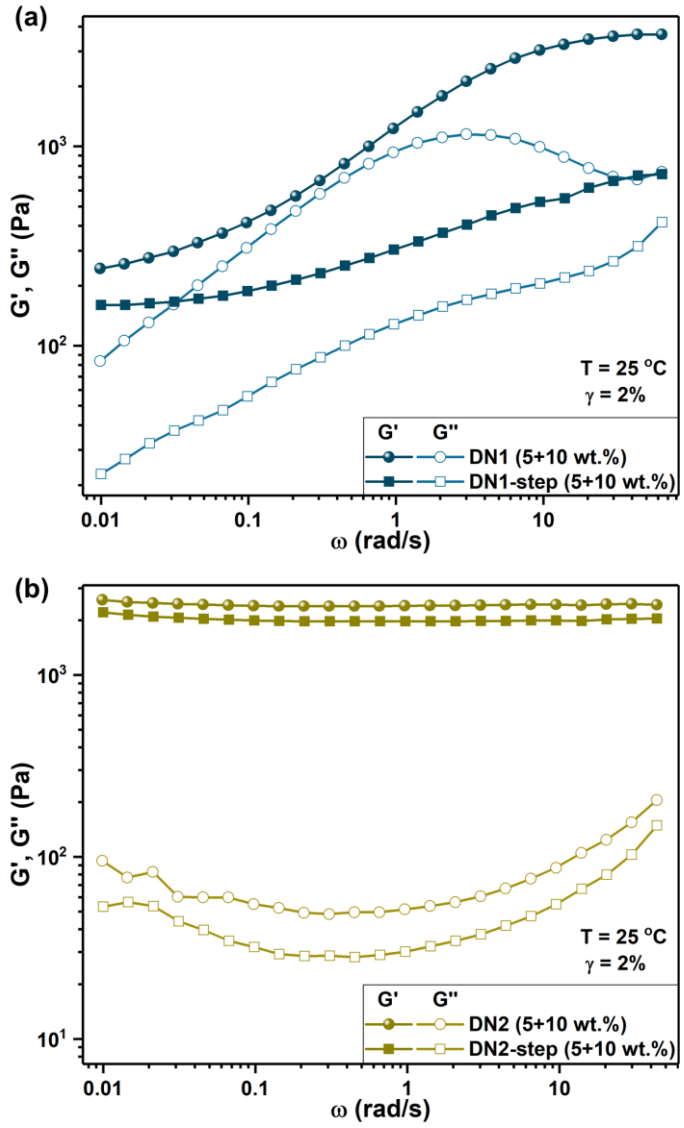

Figure 5.5. Comparison of dynamic moduli of (a) DN1 and DN1-step hydrogels as well as (b) DN2 and DN2-step hydrogels prepared by the "one-step" (**Scheme 5.3**) and "two-step" (**Scheme 5.4**) crosslinking methods, respectively.

Figure 5.6 shows the variation of the moduli of DN1 and DN2 hydrogels as a function of frequency. By carefully providing a continuous aqueous atmosphere within the solvent-trap equipment around the hydrogel samples tested in the rheometer, frequency sweeps

performed at 25 °C can be prolonged from 100 rad/s to 0.002 rad/s. Frequency sweeps performed in the lower frequency region are more likely to show the relaxation behavior of the dynamic networks at large time scales.[44] It can be seen from **Figure 5.6** that the G' of DN1 and DN2 hydrogels are always higher than G" throughout the experimental frequency range, indicating that these two DN hydrogels can maintain the solid-like elastic properties over a long time scale.

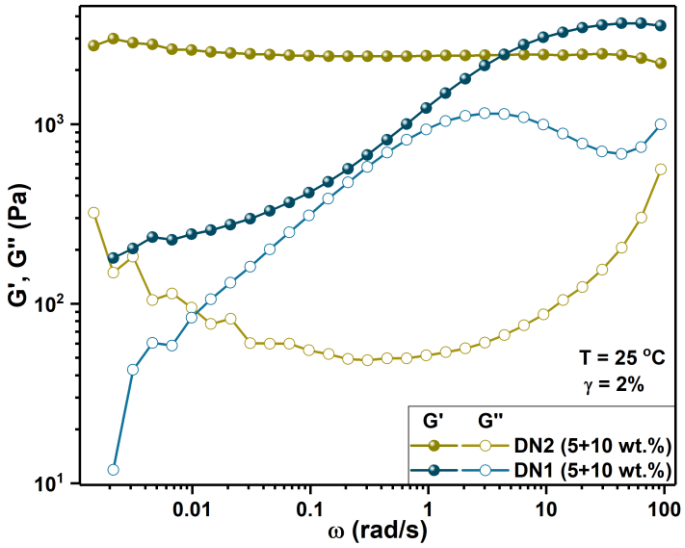

Figure 5.6. Comparison of dynamic moduli of DN1 and DN2 hydrogels (see **Scheme 5.3**).

As depicted in **Figure 5.6**, the DN1 hydrogel exhibits the typical viscoelastic solid behavior, where G' has two plateau moduli in the high and low frequency regions.[37] The plateau in the high-frequency region is attributed to both Zn^{2+}-Tpy and oxime crosslinks in DN1, while the plateau in the low-frequency region is mainly ascribed to oxime crosslinks due to the relaxation of the Zn^{2+}-Tpy network, as evidenced by the relaxation peak observed on the G" curve. In addition, a power law of $G' \sim \omega^{0.5}$ is observed in the transition region from high- to low-frequency, indicating that the relaxation process of DN1 hydrogels can be described by a sticky Rouse process.[45]

Careful prevention of water evaporation from the hydrogel sample during the test was still not able to completely prevent the evaporation of the DN2 hydrogel, so a slight increase in G' of the DN2 hydrogel is observed in the low frequency region (**Figure 5.6**). Nevertheless, DN2 exhibits an increase of G" at low-frequency, which was also observed in the individual and single acylhydrazone networks, indicating that the network relaxation behavior conferred by dynamic acylhydrazone bonds is still retained in the DN2 hydrogel.

The dynamic moduli of the DN1 and DN2 hydrogels and their respective two single networks were integrated into a graph for comparison, to further understand the effect of the single networks on the relaxation behavior and on the elastic modulus of the final DN hydrogels. As shown by the dashed line in **Figure 5.7**, the frequencies corresponding to the G" peak of the DN1 hydrogel and the G'-G" crossover point of the single Zn^{2+}-Tpy network are basically at the same position, indicating that the relaxation times of the DN1 hydrogel and of the single Zn^{2+}-Tpy network are basically the same. This also proves that the network relaxation in DN1 hydrogel is indeed caused by the dissociation of Zn^{2+}-Tpy crosslinks, and also indicates that the relaxation behavior induced by Zn^{2+}-Tpy is basically unaffected by the presence or not of 10 wt.% PK-L, crosslinked or not. Also, it is noticed that, after the dissociation of Zn^{2+}-Tpy crosslinks in DN1 hydrogel, the G' of DN1 in the low frequency region is always slightly higher than that of the single oxime network, indicating that the presence of Zn^{2+}-Tpy crosslinks in DN1 promotes the formation of more interchain oxime crosslinks due to the greater proximity (stronger confinement) of ketone groups.[41]

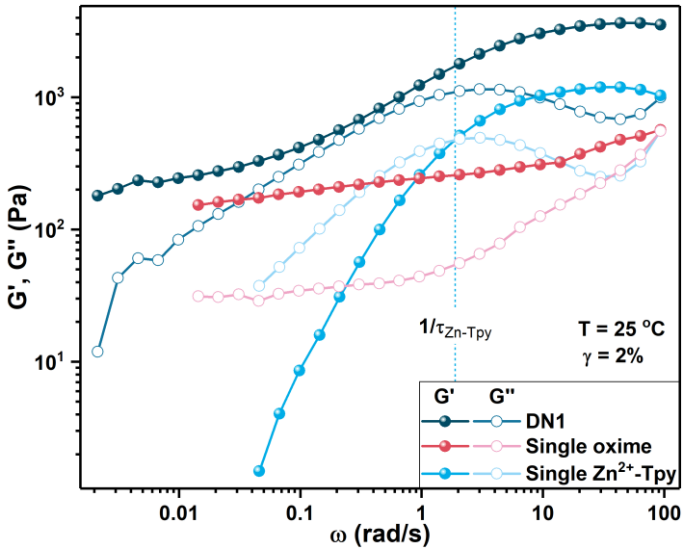

Figure 5.7. Comparison of the dynamic moduli of DN1 hydrogel and of its two single networks (see **Schemes 5.3a** and **5.2a**).

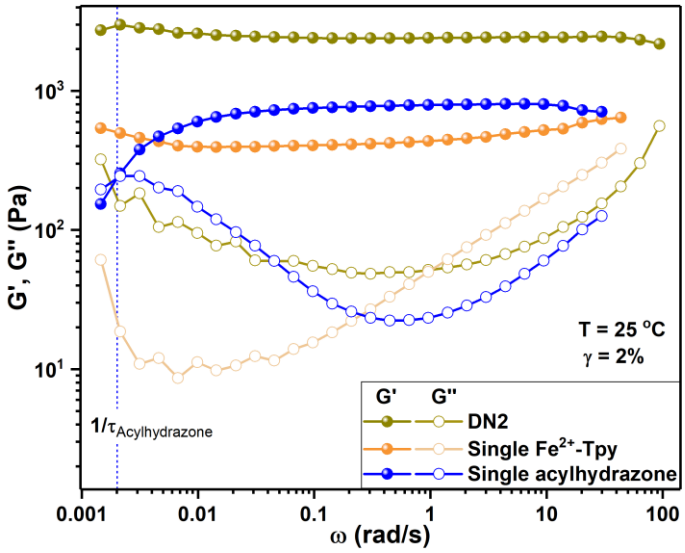

Figure 5.8. Comparison of the dynamic moduli of DN2 hydrogel and of its two single networks (see **Schemes 5.3b** and **5.2b**).

As shown in **Figure 5.8**, performing the oscillation frequency sweeps from 100 rad/s down to close to 0.001 rad/s, leads to the inevitable water evaporation from the samples due to the longer test time, and therefore the storage modulus of the DN2 hydrogel and of the single Fe^{2+}-Tpy network are marginally elevated in the low frequency region. Fortunately, we can still observe a G'-G" crossover at 0.002 rad/s for the single acylhydrazone network (dashed line in **Figure 5.8**) corresponding to the relaxation of acylhydrazone bonds. This clearly confirms the dynamic reversibility of the acylhydrazone networks.[19, 46] It also proves that the tendency of the G" curve to increase in the low frequency region for DN2 hydrogel does reflect the onset of the relaxation of the acylhydrazone network.

The relaxation time of the network can be estimated from the frequency at the G'-G" crossover point, from which the relaxation time of the single Zn^{2+}-Tpy network ($\tau_{Zn\text{-}Tpy} = 1/\omega_{Zn\text{-}Tpy} = 0.53$ s) (**Figure 5.7**) is much shorter than the relaxation time of the single acylhydrazone network ($\tau_{Acylhydrazone} = 1/\omega_{Acylhydrazone} = 500$ s) (**Figure 5.8**). This is reasonable because the reversible bond breaking and exchange process of acylhydrazone bonds is slow and the dissociation and exchange process of Zn^{2+}-Tpy bis-complexes is fast.[19,40] This different relaxation behavior of Zn^{2+}-Tpy in DN1 and acylhydrazone in DN2 further leads to a faster decrease of G' in DN1 hydrogels than in DN2 hydrogels on the timescales (**Figure 5.6**) since the oxime and Fe^{2+}-Tpy networks (both individual and single networks) are generally frequency independent. The results suggest that the stress relaxation behavior of DN hydrogels can be tuned by selecting fast dynamic supramolecular interactions or slow dynamic covalent bonds as crosslinks of the first network if the behavior of the second network is similar to that of a static chemical network. This provides a basis for the design of suitable dynamic DN hydrogels to meet the requirements of practical applications.

Furthermore, in order to compare the mechanical properties of the two crosslinking combinations of DN hydrogels compared to the

corresponding single networks, the plateau moduli (G'_p) of the DN1 and DN2 hydrogels and of their single networks, as well as the sum of the plateau moduli (G'_{sum}) of the single networks of each DN systems, are summarised in **Figure 5.9**. The values of the plateau modulus (G'_p) for the DN1 and DN2 hydrogels and for their corresponding single networks were obtained from the high frequency region of the frequency sweeps shown in **Figure 5.7** and **Figure 5.8**, respectively. For example, the G'_p of DN1, single Zn^{2+}-Tpy and oxime networks were taken from ~50 rad/s, ~30 rad/s and ~13 rad/s at a strain of 2% respectively (see **Figure 5.7**). The G'_p of DN2, single acylhydrazone and Fe^{2+}-Tpy networks were taken from ~20 rad/s, ~10 rad/s and ~10 rad/s at a strain of 2% respectively (see **Figure 5.8**). The G'_{sum} is a simple addition of the respective single networks for the DN1 and DN2 systems, respectively.

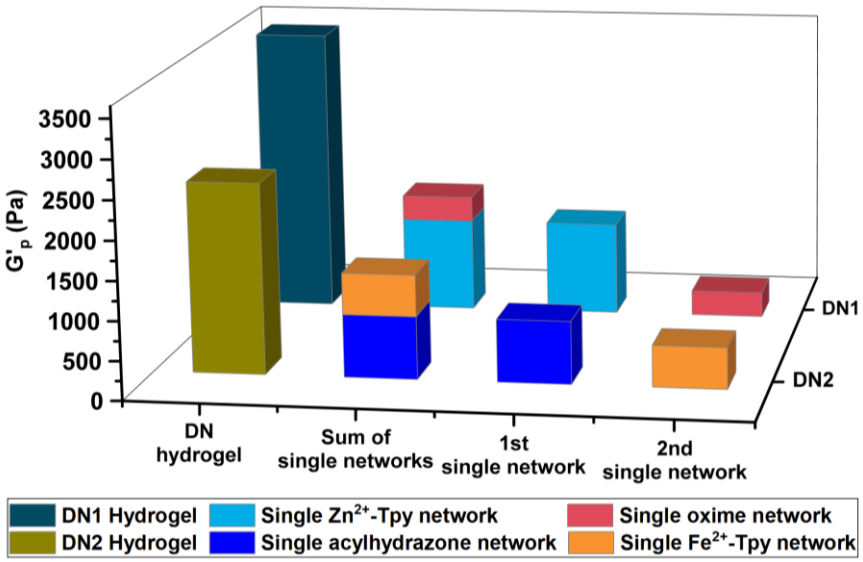

Figure 5.9. Summary of the plateau moduli of DN1 and DN2 hydrogels, and their corresponding single networks (1st single network and 2nd single network) (see **Schemes 5.2** and **5.3**) as well as the sum of plateau moduli (G'_{sum}) of the two single networks of each DN systems.

As shown in **Figure 5.7**, the first single network of the two DN hydrogels has a higher plateau modulus than the second single network, even though the first network has half the crosslinked polymer concentration of the second network. This is because the first network is densely crosslinked while the second network is loosely crosslinked and accordingly, the first single network has a higher crosslinking density than the second single network. Interestingly, the DN1 and DN2 hydrogels, in which both interpenetrated networks are crosslinked, exhibit higher elastic moduli than the sum of the moduli of the corresponding two single networks, indicating that the synergistic effect of the two asymmetric sub-networks enhanced the stiffness of the resultant DN hydrogels.[22, 29] Among them, the G'_p of DN1 hydrogel (3650 Pa) is about 2.4 times higher than the sum of the moduli (G'_{sum} = 1510 Pa) of single Zn^{2+}-Tpy network (1190 Pa) and single oxime network (320 Pa), and the G'_p of DN2 hydrogel (2440 Pa) is about 1.8 times higher than the sum of the moduli (G'_{sum} = 1330 Pa) of single acylhydrazone network (800 Pa) and single Fe^{2+}-Tpy network (530 Pa). This suggests that DN hydrogels constructed with a labile supramolecular first network and a stable reversible covalent second network are stronger than DN hydrogels composed of a slow dynamic reversible covalent first network and a stable supramolecular covalent second network, given comparable chain lengths, functionalization degree of the copolymers and polymer concentrations.

To investigate the stability and deformability of hydrogels under oscillatory strain, strain sweeps were performed on DN hydrogels and on the corresponding single networks. A strain sweep performed at a fixed frequency can provide the limiting strain and rupture strain of the hydrogel sample being tested. The rupture strain (γ_r) is defined as the strain amplitude at the critical G'-G" crossover point, and marks the transition of the gel from a solid-like to a liquid-like state. Therefore, the value of γ_r indicates the deformability of the hydrogel. The strain sweeps of DN1 hydrogel and of its two single networks are shown in **Figure 5.10**.

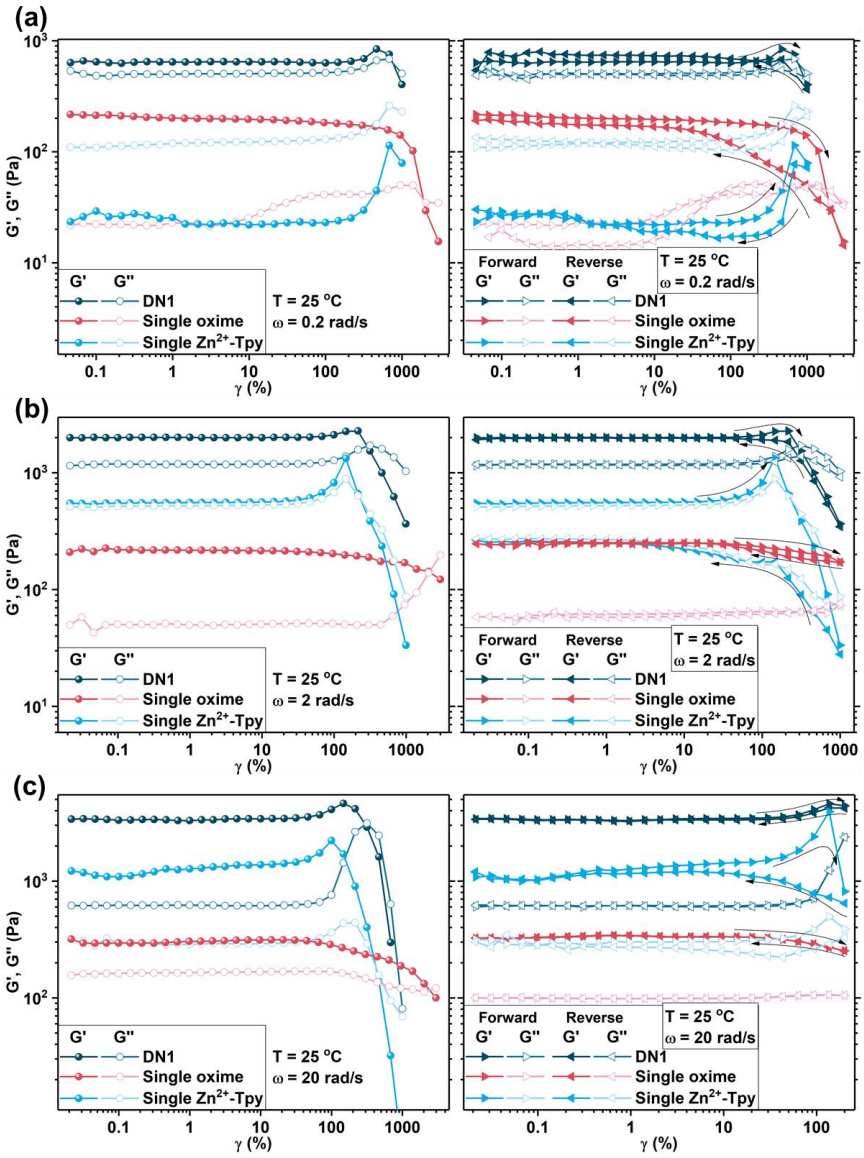

Figure 5.10. Oscillatory strain sweeps performed on the DN1 hydrogel and on its two single networks at a fixed frequency of (a) 0.2 rad/s, (b) 2 rad/s, and (c) 20 rad/s. The plots in the right panels are measured from a low strain up to the maximum strain amplitude without destroying the samples, and then from that high strain amplitude down to a low strain.

As can be seen from the results shown in **Figure 5.7**, it is clear that the DN1 hydrogel and its Zn^{2+}-Tpy network exhibit a relaxation

behavior around 1.88 rad/s due to the dissociation of Zn^{2+}-Tpy complexes. The strain sweeps were thus performed at a fixed frequency of 0.2 rad/s, 2 rad/s, and 20 rad/s, corresponding to the different states of the Zn^{2+}-Tpy crosslinks, i.e., after, close to, and before their dissociation, respectively. Thus, at 0.2 rad/s, in the linear regime, the modulus of DN1 hydrogel is mainly dominated by the single oxime network, with a smaller effect of the Zn^{2+}-Tpy network (see **Figure 5.10a**). On the other hand, strain sweeps at 2 rad/s do not allow the Zn^{2+}-Tpy network to fully dissociate, even at low strain amplitude (see **Figure 5.10b**).

As observed in **Figures 5.10b** and **5.10c**, the γ_r (single Zn^{2+}-Tpy network) < γ_r (single oxime network) (**Table 5.3**), demonstrating that the second network of the DN1 hydrogel, formed by loosely crosslinked long-chain copolymer, does have better deformation capability than the densely crosslinked short-chain first network. As expected, the DN1 hydrogel has a smaller γ_r than the single oxime network (second network). We also observe that while the exact value of γ_r for DN1 is close to that of the single Zn^{2+}-Tpy network (first network), its overall response shows that DN1 has a longer linear regime (**Figures 5.10b** and **5.10c**), despite its higher crosslinking density. This suggests that the dense Zn^{2+}-Tpy network in DN1 is broken first, at a strain amplitude similar to the single Zn^{2+}-Tpy network. However, the double network is able to withstand a larger deformation thanks to the presence of the second network, leading to a delay of the rupturing of the whole gel compared to the behavior of the single Zn^{2+}-Tpy network. In short, the presence of Zn^{2+}-Tpy gives DN1 a large elastic modulus, but breaks at rather low oscillatory strains, while the loose oxime network gives the sample a larger deformability.

Table 5.3. Strain parameters for DN1 and DN2 hydrogels, and for the corresponding single networks.

Sample	γ_L[a] (%)	γ_r[b] (%)	γ_{Max}[c] (%)
DN1	**35**	**290**	**1000**
Single Zn^{2+}-Tpy (1st network)	20	235	1000
Single oxime (2nd network)	30	2090	1000
DN2 (5+10 wt.%)	**45**	**1000**	**200**
Single acylhydrazone (1st network)	15	90	200
Single Fe^{2+}-Tpy (2nd network)	40	1110	200

[a] Obtained from the strain at which the G' starts to decrease/increase in the strain sweeps at a fixed frequency of 2 rad/s. [b] Obtained from the crossover of G' and G'' in the strain sweeps at a fixed frequency of 2 rad/s. [c] Maximum strain applied to the sample for reverse strain sweeps at a fixed frequency of 2 rad/s. Note: γ_{Max} is higher than γ_L to ensure that the applied strain is sufficient to partially break the gel network. With the exception of the single Zn^{2+}-Tpy sample, the applied high strain did not extrude the other samples from the two parallel plate geometries of the rheometer.

In addition, as displayed in **Figure 5.10**, shear thickening behaviors are found in DN1 and in the single Zn^{2+}-Tpy network, suggesting the reinforcement of DN1 hydrogel may be due to the chain stretching or the reorganization of the Zn^{2+}-Tpy network under strain, which leads to a mechano-induced homogenization.[48] To understand the reason of this shear thickening effect and to explore the contribution of the Zn^{2+}-Tpy and oxime crosslinks in the reversibility of the hydrogels, reverse strain-sweep measurements at a fixed frequency of 0.2 rad/s, 2 rad/s, and 20 rad/s were also performed and are illustrated in the right panels of **Figure 5.10**. Experiments were carried out by increasing the strain to the maximum strain amplitude achievable without expelling the sample from the geometry, and then reducing the strain for recovery. Clearly, there is no significant increase in G' for the single Zn^{2+}-Tpy network after the strain has been reduced to the initial strain amplitude. This suggests that the shear-thickening behaviors of the single Zn^{2+}-

Tpy network and of DN1 hydrogel under large strain is due mainly to chain stretching.[49]

Besides, for samples where G' can essentially recovers its initial level after strain reduction, a small hysteresis is observed at high strains, suggesting that some of the bonds broken by the high strain can reform upon strain reduction, but not at high deformation. The reverse strain sweeps performed at a fixed frequency of 20 rad/s (right panel of **Figure 5.10c**) reveals that modulus recovery in the single oxime network did not show hysteresis, which was only seen in the single Zn^{2+}-Tpy network and in the DN1 hydrogel. This suggests that the repairability of the gel network due to reversible bond re-formation is mainly attributed to the more dynamic first Zn^{2+}-Tpy network. In the previous discussion, we mentioned that oxime networks behave as static covalent networks even at long timescales, and that the presence of the highly Tpy functionalized PT-S in single oxime networks provides a weak network with a weak contribution through π-π stacking or hydrophobic interactions. The appearance of hysteresis in the strain recovery of a single oxime network at 0.2 rad/s (right panel of **Figure 5.10a**) is more likely to be due to the restructuring of the weak network of PT-S. Therefore, the recoverability of the DN1 hydrogel at 0.2 rad/s is due to the highly deformable second oxime network maintaining the integrity of the gel under high oscillatory strain and the restructuring of the PT-S weak network.

As shown in the right panel of **Figure 5.10b**, the DN1 hydrogel, single Zn^{2+}-Tpy and oxime networks were subjected to the same maximum oscillatory strain at a fixed frequency of 2 rad/s to verify recoverability. It can be seen that this maximum strain is less than the rupture strain of the single oxime network, and that the G' of the single oxime network returns to its initial level after the strain is reduced. This maximum strain is greater than the fracture strains of the DN1 and single Zn^{2+}-Tpy network. Interestingly, the G' of the DN1 hydrogel and oxime network are fully recovering their initial level after the strain is reduced, while the G' of the single Zn^{2+}-Tpy network does not recover

due to the sample being partially crushed out of the parallel plates. This suggests that the DN1 hydrogel has the large deformation capacity of the loose oxime network, while the dynamic Zn^{2+}-Tpy allows DN1 to recover quickly. The synergy effect of the interpenetrating Zn^{2+}-Tpy and oxime networks empowers the DN1 hydrogel to achieve full recovery. This also suggests that an alternative step-strain experiment can be carried out at a fixed frequency of 2 rad/s to verify the self-healing properties of DN1 hydrogels.

As shown in **Figure 5.11**, a large strain of 340% was applied, which is higher than the γ_r (290%) measured in a strain sweep at a fixed frequency of 2 rad/s, to completely break the hydrogel. The inversion of G' and G" of the hydrogel is indeed observed at such high magnitude of strain (340%), which indicates a rupture of the DN1 network. When the high strain is removed and a low strain (2%) is applied, the G' and G" are returned to values characteristic of a gel state (i.e. G' > G") within seconds, and back to the original level within 20s. Such self-healing cycles where strain is applied to force the network to fracture and then reform can be repeated at least 10 times. In connection with the above discussion on the reverse strain sweeps at a frequency of 2 rad/s, this highlights that the self-healing ability of the DN1 hydrogel is due to the synergistic effect of the exchange/reorganization of the Zn^{2+}-Tpy network (first network) and the high deformability of the oxime network (second network).

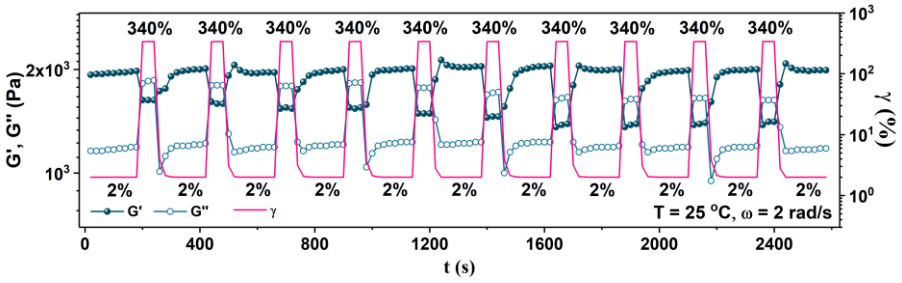

Figure 5.11. Oscillation time sweeps performed on DN1 hydrogels with alternating strain amplitudes. A strain of 340% is above γ_r and breaks the sample, while a strain of 2% is in the LVE range to allow the hydrogel to self-heal.

Finally, we also executed strain sweeps and reverse strain sweeps on the DN2 hydrogel and on its two single networks at a fixed frequency of 2 rad/s since those networks are generally stable in a broad frequency range. As shown in **Figure 5.12a** and **Table 5.3**, γ_r (single acylhydrazone network) < γ_r (DN2 hydrogel) < γ_r (single Fe^{2+}-Tpy network), and the γ_r of DN2 hydrogel is close to the single Fe^{2+}-Tpy network (second network). The loosely crosslinked Fe^{2+}-Tpy network protects the DN2 hydrogel from breaking under large oscillatory strains, thus delaying γ_r.

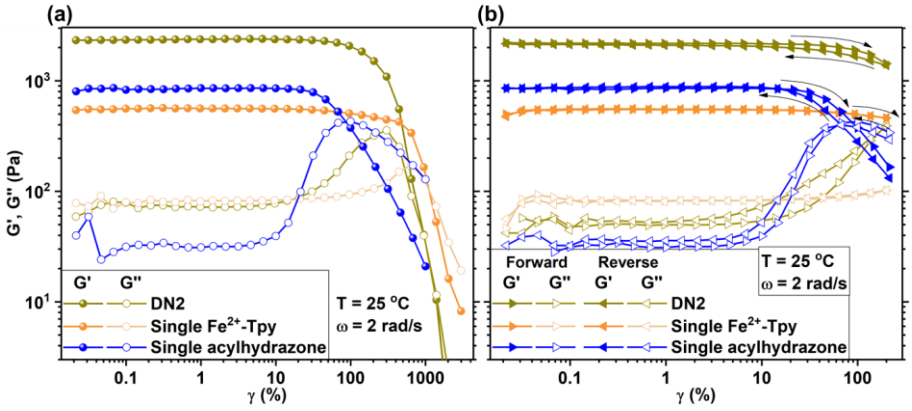

Figure 5.12. (a) Oscillatory strain sweeps and (b) reverse strain sweeps performed on the DN2 hydrogel and on its two single networks at a fixed frequency of 2 rad/s.

In addition, reverse strain sweeps were performed on DN2 and on its two single networks to learn about the recoverability of the DN2 hydrogel. The maximum strain applied to each sample was the maximum amplitude that ensured that the sample would not be expelled from the geometry during the tests. After applying a strain amplitude of up to 200% to the samples, and then reducing the strain, the G' of the DN2 and its two single networks fully recovered their initial levels (**Figure 5.12b**). The rupture strain of the single acylhydrazone network is 90% (**Table 5.3**), indicating that the acylhydrazone network has ruptured at the 200% oscillatory strain, which did not cause damage to the loose single Fe^{2+}-Tpy network. The small hysteresis of DN2 at high

strain suggests that the reorganization of the relatively more dynamic acylhydrazone network contributes to the recovery of this DN hydrogel. These results suggest that the self-recovery properties of DN2 hydrogels are due to the synergistic effect between the dynamic nature of the acylhydrazone bonds in the first network and the high deformability of the second network.

In summary, it is clear from the comparative results of the strain sweeps that the γ_r of DN1 is slightly greater than that of its single Zn^{2+}-Tpy network (first network), while the γ_r of DN2 is second to that of its Fe^{2+}-Tpy network (second network). This means that DN2 exhibits a greater γ_r (deformability) than DN1. As the first network of the DN hydrogel is densely crosslinked and the second network is loosely crosslinked, the first network of the DN should be damaged first followed by the second network under gradually increasing strain applied to the DN hydrogel.[2] Therefore, the stability of the first network of DN hydrogels is therefore a key factor in the deformation magnitude of DN hydrogels. The acylhydrazone linkages are more stable and have higher bond energies compared to Zn^{2+}-Tpy crosslinks, so that the first network of DN2 is more difficult to break than DN1, and thus DN2 hydrogel exhibits a greater deformability than DN1 hydrogel.

5.3 Conclusion

As a conclusion, we have developed two contrasting dynamic DN hydrogels by combining two distinct dynamics of supramolecular interactions and dynamic covalent bonds. The DN1 hydrogel is composed of a densely Zn^{2+}-Tpy crosslinked first network (made of supramolecular bonds) and a loosely oxime crosslinked second network (made of dynamic covalent bonds). The DN2 hydrogel is made up of a densely acylhydrazone crosslinked first network (made of dynamic covalent bonds) and a loosely Fe^{2+}-Tpy crosslinked second network (made of supramolecular bonds). The addition of two crosslinkers in one step to a mixed precursor copolymer solution makes it easier to obtain more homogeneous crosslinked hydrogels than the two-step crosslinking method.

Oscillatory shear rheology results revealed the contribution of two sub-networks of DN hydrogels to their dynamic and oscillatory mechanical properties. The more dynamic first networks in the two DN hydrogels are responsible for the stress relaxation behavior of the DN hydrogels over different timescales, and the more stable second networks protect the integrity of the hydrogel after the relaxation of the first network. Due to the difference in the lifetime of the first network, DN2 (dynamic covalent crosslinked first network) showed longer relaxation times than DN1 (supramolecular crosslinked first network). Interestingly, the DN1 hydrogel plateau modulus is 2.4 times higher than the sum of its two sub-network plateau moduli, and the DN2 hydrogel plateau modulus is 1.8 times the sum of its two sub-network plateau moduli, due to the differences in the formation of effective crosslinks in the sub-networks by the various dynamic bonds in the two DN hydrogels. This difference also results in a stiffer DN1 hydrogel compared to DN2, showing that the combination of dynamics in DN1 is more favorable. In addition, the loosely crosslinked second network interpenetrated in the DN is able to confer greater deformability to the DN hydrogel compared to the densely crosslinked first network. In

particular, the deformability of DN1 is only slightly greater than that of its first network, while the deformability of DN2 is close to that of its second network. This shows that the deformability of a dynamic DN hydrogel is determined not only by the stability of its first network, but also by the large deformability of the second network. We also demonstrated that the self-healing properties of both DN hydrogels are due to the reversibility of the Zn^{2+}-Tpy or acylhydrazone bonds in the first network and the high deformability of the second network.

In short, our results show that the combination of a supramolecular first network and a dynamic covalent second network produces a DN hydrogel that is stiffer but less deformable than a DN hydrogel combining a dynamic covalent first network and a supramolecular second network. Moreover, using dynamic bonds to prepare DNs not only provides hydrogels with tunable relaxation behaviors on different time scales, but also brings self-healing properties to the hydrogels. In future work, the macroscopic mechanical properties of such dynamic DN hydrogels (including tensile/compression strength, tensile/compression strain at break, Young's modulus, toughness, etc.) will also need to be evaluated to enable the comparison of their advantages and disadvantages with conventional static covalent DN hydrogels.

5.4 Experimental Section

All reagents and materials are the same as in Chapter 4 unless otherwise stated. The synthesis of terpyridine-functionalized monomer N-(3-([2,2':6',2''-terpyridin]-4'-yloxy)propyl)-N-methylacrylamide (TPy-AM) was described in Section 4.4.2.

5.4.1. Preparation and characterization of copolymers

Synthesis of short-chain poly(N,N-dimethylacrylamide) copolymer with ~9% terpyridine and with an approximate molecular weight of ~50 kDa, PT-S.

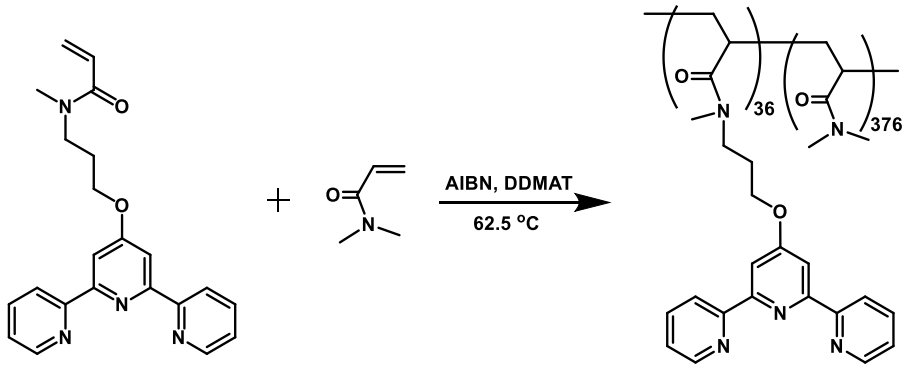

Scheme 5.5. Synthetic route of PT-S.

AIBN (0.9 mg, 0.0054 mmol), DDMAT (19.7 mg, 0.054 mmol), TPy-AM (1.49 g, 3.97 mmol) and DMA (3.542 g, 35.73 mmol) were dissolved in 7.2 mL of dry dioxane in a 25 mL round-bottom Schlenk-flask. The solution was degassed by five freeze-pump-thaw cycles, backfilled with argon and stirred in a preheated oil bath at 62.5 °C for 4 days. The polymerization was then stopped by opening the flask to air

and placing it in liquid nitrogen. The conversion of monomer was determined to be 55%, by comparing the integral ratio of the vinyl signal to the methylene proton of dioxane on the ^{1}H NMR spectrum. The viscous liquid was diluted with DCM and precipitated three times in 20-times volume excess diethyl ether, and the polymer was finally dried in a vacuum oven at 40 °C for 24 h. The product was characterized by ^{1}H NMR and GPC.

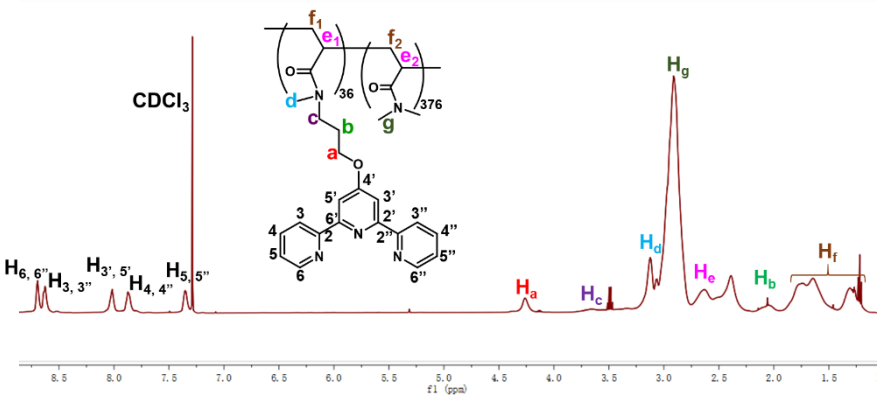

Figure 5.13. ^{1}H NMR spectrum of PT-S.

Synthesis of long-chain poly(N,N-dimethylacrylamide) copolymer with ~0.5% ketone and with an approximate molecular weight of ~155 kDa, PK-L.

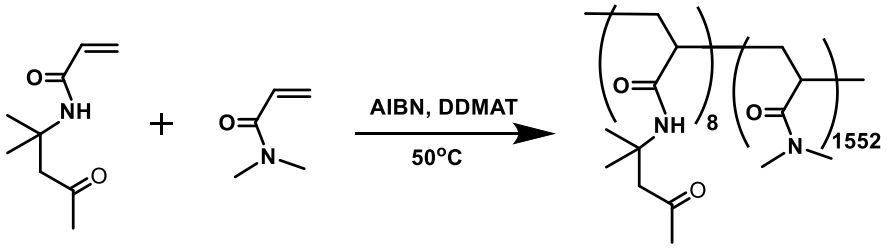

Scheme 5.6. Synthetic route of PK-L.

AIBN (0.6 mg, 0.0034 mmol), DDMAT (12.4 mg, 0.034 mmol), DAAM (115.1 mg, 0.68 mmol) and DMA (11.055 g, 111.52 mmol) were dissolved in 10 mL of dry dioxane in a 50 mL round-bottom Schlenk-flask. The solution was degassed by five freeze-pump-thaw cycles, backfilled with argon, and stirred in a preheated oil bath at 50 °C for 14.5 h. The polymerization was stopped by opening the flask to air and placing it in liquid nitrogen. The conversion of monomer was determined to be 58%, by comparing the integral ratio of the vinyl signals to the methylene proton of dioxane on the ^{1}H NMR spectrum. The viscous liquid was diluted with DCM and precipitated three times in 20-times volume excess of diethyl ether, and the polymer was finally dried in a vacuum oven at 40 °C for 24 h. The product was characterized by ^{1}H NMR and GPC.

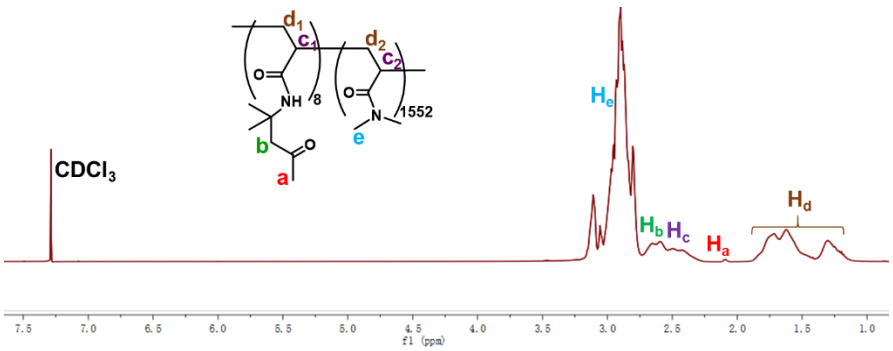

Figure 5.14. ^{1}H NMR spectrum of PK-L.

Synthesis of short-chain poly(N,N-dimethylacrylamide) copolymer with ~9% ketone and with an approximate molecular weight of ~50 kDa, PK-S.

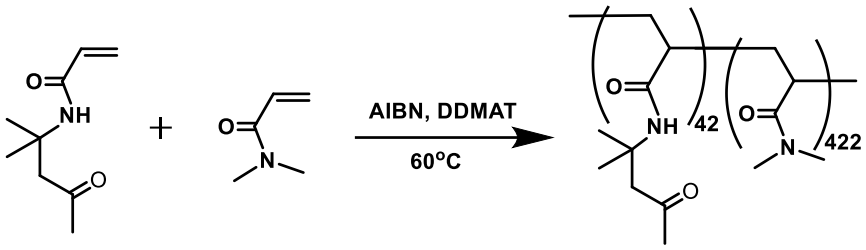

Scheme 5.7. Synthetic route of PK-S.

AIBN (0.9 mg, 0.0054 mmol), DDMAT (19.7 mg, 0.054 mmol), DAAM (671.8 mg, 3.97 mmol) and DMA (3.542 g, 35.73 mmol) were dissolved in 7.2 mL of dry dioxane in a 25 mL round-bottom Schlenk-flask. The solution was degassed by five freeze-pump-thaw cycles, backfilled with argon, and stirred in a preheated oil bath at 60 °C for 36 h. The polymerization was stopped by opening the flask to air and placing it in liquid nitrogen. The conversion of monomer was determined to be 70%, by comparing the integral ratio of the vinyl signals to the methylene proton of dioxane on the ^{1}H NMR spectrum. The viscous liquid was diluted with DCM and precipitated three times in 20-times volume excess of diethyl ether, and the polymer was finally dried in a vacuum oven at 40 °C for 24 h. The product was characterized by ^{1}H NMR and GPC.

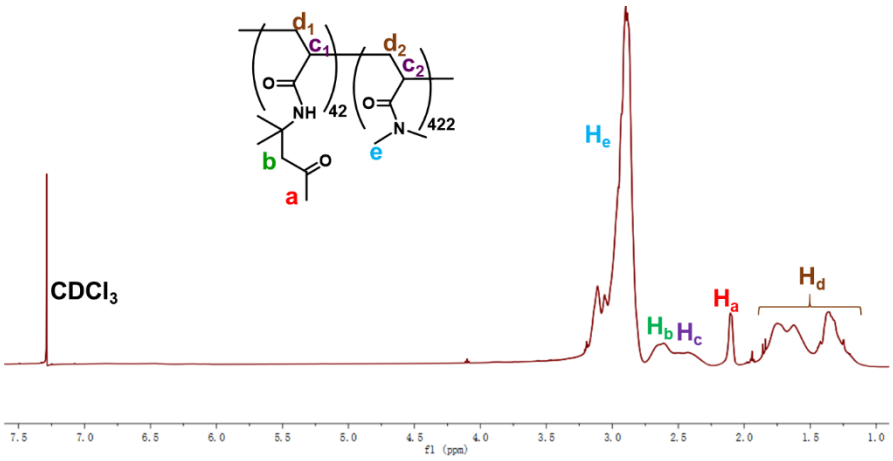

Figure 5.15. ^{1}H NMR spectrum of PK-S.

Synthesis of long-chain poly(N,N-dimethylacrylamide) copolymer with ~0.5% terpyridine and with an approximate molecular weight of ~136 kDa, PT-L.

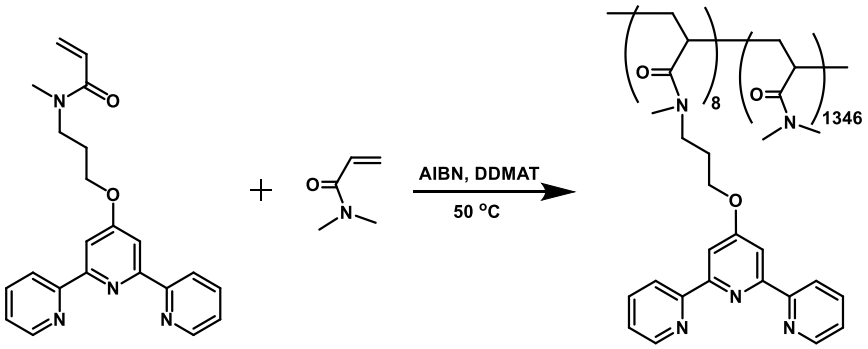

Scheme 5.8. Synthetic route of PT-L.

AIBN (0.6 mg, 0.0034 mmol), DDMAT (12.4 mg, 0.034 mmol), TPy-AM (255 mg, 0.68 mmol) and DMA (11.055 g, 111.52 mmol) were dissolved in 10 mL of dry dioxane in a 50 mL round-bottom Schlenk-flask. The solution was degassed by five freeze-pump-thaw cycles, backfilled with argon and stirred in a preheated oil bath at 50 °C

for 17 h. The polymerization was stopped by opening the flask to air and placing it in liquid nitrogen. The conversion of monomer was determined to be 45%, by comparing the integral ratio of the vinyl signals to the methylene proton of dioxane on the ^{1}H NMR spectrum. The viscous liquid was diluted with DCM and precipitated three times in 40-times volume excess diethyl ether, and the polymer was finally dried in a vacuum oven at 40 °C for 24 h. The product was characterized by ^{1}H NMR and GPC.

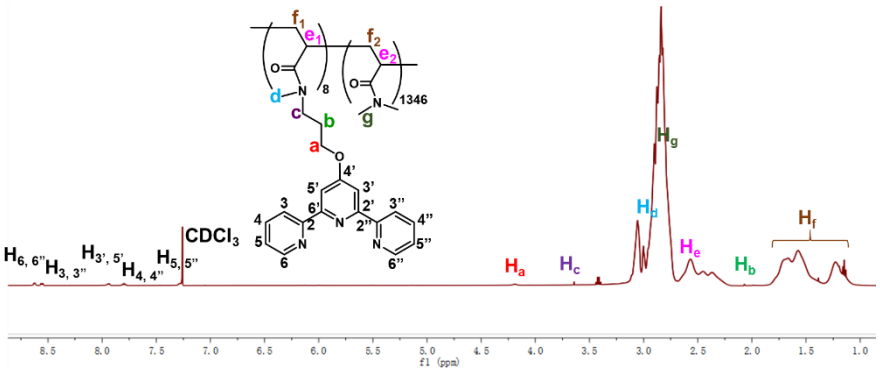

Figure 5.16. ^{1}H NMR spectrum of PT-L.

5.4.2. Preparation of networks

For the two DN hydrogels and their single or individual networks, the amount of added crosslinkers (di-acylhydrazine, bis-hydroxylamine or metal ions) was half an equivalent compared to the reactive sites (ketone or terpyridine groups) of the corresponding copolymers. $ZnCl_2$ was used to form the Zn^{2+}-Tpy crosslinks between PT-S chains for the first network of DN1, and bis-hydroxylamine (O,O'-(propane-1,3-diyl)bis(hydroxylamine) dihydrochloride) was used to react with ketone groups of PK-L for creating the oxime-crosslinked second network of DN1. A di-acylhydrazine (succinic dihydrazide) was employed to react with PK-S for producing the acylhydrazone-crosslinked first network of DN2, and $FeCl_2$ was employed to form the

Fe^{2+}-Tpy bridging between PT-L chains. Aqueous solutions of the four crosslinkers were prepared, and a certain amount was added to the polymer aqueous solutions to obtain the desired amount of crosslinker. The Fe^{2+} solution was dosed with 10 mol.% ascorbic acid to prevent the oxidation of Fe(II) to Fe(III).

Preparation of individual networks.

As shown in **Scheme 5.1**, the four individual networks were prepared from pure PT-S, PK-L, PK-S and PT-L, respectively. The procedure of preparation of the 5 wt.% individual Zn^{2+}-Tpy network will be illustrated as an example. In a typical experiment, 0.025 g of pure PT-S and 450 μL of deionized water were introduced in a clean and closed glass vial and the mixture was stirred overnight in a preheated water bath at 35°C to obtain a homogeneous solution. To the solution, 50 μL of a 176.8 mmol/L $ZnCl_2$ aqueous solution were then added and vortexed for 1 min. Finally, the individual Zn^{2+}-Tpy network (5 wt.%) was obtained by aging the sealed reaction sample in a preheated water bath at 55 °C for 2 days, followed by slow cooling to room temperature over 2 days. Using the same method, the individual oxime network (10 wt.%), the individual acylhydrazone network (5 wt.%), and the individual Fe^{2+}-Tpy network (10 wt.%) were prepared from the corresponding pure copolymers.

Preparation of single networks.

As shown in **Scheme 5.2**, the single Zn^{2+}-Tpy network (5+10 wt.%) and the single oxime network (5+10 wt.%) were prepared from mixed copolymers of 5 wt.% PT-S with 10 wt.% PK-L, while the single acylhydrazone network (5+10 wt.%) and the single Fe^{2+}-Tpy network (5+10 wt.%) were prepared from mixed copolymers of 5 wt.% PK-S with 10 wt.% PT-L. Typically, 0.075 g of a mixture of the copolymers (0.025 g short-chain copolymer and 0.050 g long-chain copolymer) were first dissolved in 450 μL of deionized water (35°C water bath, overnight), followed by the addition of 50 μL of a solution containing

the crosslinkers, and then strongly and rapidly vortexed to disperse evenly in the solution. After aging at 55°C for 2 days and slow cooling to room temperature within 2 days, the final single networks were obtained.

Preparation of double network (DN) hydrogels.

Generally, the DN hydrogels of DN1 and DN2 (**Scheme 5.3**) were prepared by a "one-step" crosslinking method. 0.075 g of the copolymer mixture (0.025 g short-chain copolymer and 0.050 g long-chain copolymer) and 400 μL deionized water were sealed in a glass vial and placed in a 35°C water bath overnight. To the homogeneous mixed polymer solution, 50 μL of bis-hydroxylamine or di-acylhydrazine crosslinker solution were first added, and quickly vortexed, followed by adding 50 μL of a $ZnCl_2$ or $FeCl_2$ solution, and vortexed, to the mixture. Finally, the DN1 and DN2 hydrogels were obtained after 2 days of heating at 55°C water bath and slow cooling to room temperature for additional 2 days.

To evaluate the effect of a stepwise crosslinking on DN hydrogels, DN1-step and DN2-step hydrogels (**Scheme 5.4**) were also prepared by a "two-step" crosslinking method. In the present preparation protocol, 50 μL of bis-hydroxylamine or di-acylhydrazine solution were first added to the homogeneous mixture of 400 μL H_2O and 0.075 g copolymer (0.025 g short-chain copolymer and 0.050 g long-chain copolymer) and aged for two days in a 55°C water bath to first form oxime or acylhydrazone crosslinked hydrogels. Subsequently, 50 μL of a $ZnCl_2$ solution were added to the surface of the oxime hydrogel and 50 μL of a $FeCl_2$ solution were added to the surface of the acylhydrazone hydrogel as shown in **Scheme 5.4**. The added metal ion solution was then homogeneously dispersed on the surface of the hydrogel by gentle shaking. Finally, the DN1-step and DN2-step hydrogels were obtained by aging in a 55°C water bath for additional 2 days and slowly cooling to room temperature in 2 days.

5.4.3. Rheological measurements

As described in Chapter 4, the rheological measurements were conducted on an Anton Paar-Physica MCR 301 rheometer with an 8 mm diameter top plate geometry. The bottom plate was a Peltier device controlling the system at a reference temperature of 25 °C. The freshly prepared gel samples with 8 mm diameter and 0.2~0.5 mm thickness were transferred onto the bottom plate for measuring.

The linear viscoelastic regions of all samples were determined by oscillatory strain sweeps (0.01-1000% strain) performed at a frequency of 2 rad s^{-1}. Unless otherwise stated, the dynamic properties of the samples were determined by oscillatory frequency sweep (100-0.01 rad s^{-1}) at 2% strain, which is within the linear viscoelastic region. For shear self-healing experiments, step-stain tests were performed at a fixed frequency of 2 rad s^{-1} by alternating the large strain (340%, 180 s) and the small stain (2%, 60 s). We estimate an accuracy of 10% on the mearued modulus values.

Due to the small amount of tested samples and the long duration (several hours) of the rheological experiments performed in this chapter, in particular the frequency sweeps, the solvent trapping device shown in **Figure 4.24** in Chapter 4 was also used in this chapter.

5.5 References

[1] Gong, J. P.; Katsuyama, Y.; Kurokawa, T.; Osada, Y. Double-Network Hydrogels with Extremely High Mechanical Strength. Adv. Mater. 2003, 15, 1155-1158.

[2] Gong, J. P. Why are double network hydrogels so tough? Soft Matter 2010, 6, 2583-2590.

[3] Chen, Q.; Chen, H.; Zhu, L.; Zheng, J. Fundamentals of double network hydrogels. J. Mater. Chem. B 2015, 3, 3654-3676.

[4] Zhang, W.; Liu, X.; Wang, J.; Tang, J.; Hu, J.; Lu, T.; Suo, Z. Fatigue of double-network hydrogels. Eng. Fract. Mech. 2018, 187, 74-93.

[5] Chen, Q.; Zhu, L.; Chen, H.; Yan, H.; Huang, L.; Yang, J.; Zheng, J. A Novel Design Strategy for Fully Physically Linked Double Network Hydrogels with Tough, Fatigue Resistant, and Self-Healing Properties. Adv. Funct. Mater. 2015, 25, 1598-1607.

[6] Chen, Q.; Wei, D.; Chen, H.; Zhu, L.; Jiao, C.; Liu, G.; Huang, L.; Yang, J.; Wang, L.; Zheng, J. Simultaneous Enhancement of Stiffness and Toughness in Hybrid Double-Network Hydrogels via the First, Physically Linked Network. Macromolecules 2015, 48, 8003-8010.

[7] Chen, Q.; Chen, H.; Zhu, L.; Zheng J. Engineering of tough double network hydrogels. Macromol. Chem. Phys. 2016, 217, 1022-1036.

[8] Xu, X.; Jerca, V. V.; Hoogenboom, R. Bioinspired double network hydrogels: from covalent double network hydrogels via hybrid double network hydrogels to physical double network hydrogels. Mater. Horiz. 2021, 8, 1173-1188.

[9] Maiz-Fernandez, S.; Perez-Alvarez, L.; Ruiz-Rubio, L.; Vilas-Vilela, J. L.; Lanceros-Mendez, S. Polysaccharide-Based In Situ Self-Healing Hydrogels for Tissue Engineering Applications. Polymers 2020, 12, 2261.

[10] Ye, J.; Fu, S.; Zhou, S.; Li, M.; Li, K.; Sun, W.; Zhai, Y. Advances in hydrogels based on dynamic covalent bonding and prospects for its biomedical application. Eur. Polym. J. 2020, 139, 110024.

[11] Gyarmati, B.; Szilágyi, B. Á.; Szilágyi, A. Reversible interactions in self-healing and shape memory hydrogels. Eur. Polym. J. 2017, 93, 642-669.

[12] Talebian, S.; Mehrali, M.; Taebnia, N.; Pennisi, C. P.; Kadumudi, F. B.; Foroughi, J.; Hasany, M.; Nikkhah, M.; Akbari, M.; Orive, G.; Dolatshahi-Pirouz, A. Self-Healing Hydrogels: The Next Paradigm Shift in Tissue Engineering? Adv. Sci. 2019, 6, 1801664.

[13] Podgórski, M.; Fairbanks, B. D.; Kirkpatrick, B. E.; McBride, M.; Martinez, A.; Dobson, A.; Bongiardina, N. J.; Bowman, C. N. Toward Stimuli-Responsive Dynamic Thermosets through Continuous Development and Improvements in Covalent Adaptable Networks (CANs). Adv. Mater. 2020, 32, 1906876.

[14] Li, Y.; Zhu, C.; Dong, Y.; Liu, D. Supramolecular hydrogels: mechanical strengthening with dynamics. Polymer 2020, 210, 122993.

[15] Wemyss, A. M.; Ellingford, C.; Morishita, Y.; Bowen, C.; Wan, C. Dynamic Polymer Networks: A New Avenue towards Sustainable and Advanced Soft Machines. Angew. Chem. 2021, 133, 2-14.

[16] Maiti, C.; Imani, K. B. C.; Yoon, J. Recent Advances in Design Strategies for Tough and Stretchable Hydrogels. ChemPlusChem 2021, 86, 601-611.

[17] Zhang, J.-Y.; Zeng, L.-H.; Feng, J. Dynamic Covalent Gels Assembled from Small Molecules: From Discrete Gelators to Dynamic Covalent Polymers. Chin. Chem. Lett. 2017, 28, 168-183.
[18] Perera, M. M.; Ayres, N. Dynamic covalent bonds in self-healing, shape memory, and controllable stiffness hydrogels. Polym. Chem. 2020, 11,1410-1423.
[19] Tang, S.; Richardson, B. M.; Anseth, K. S. Dynamic covalent hydrogels as biomaterials to mimic the viscoelasticity of soft tissues. Prog. Mater Sci. 2020, 100738. doi: 10.1016/j.pmatsci.2020.100738
[20] Zheng, N.; Xu, Y.; Zhao, Q.; Xie, T. Dynamic Covalent Polymer Networks: A Molecular Platform for Designing Functions beyond Chemical Recycling and Self-Healing. 2021, 121, 1716-1745.
[21] Rodell, C. B.; Dusaj, N. N.; Highley, C. B.; Burdick, J. A. Injectable and Cytocompatible Tough Double-Network Hydrogels through Tandem Supramolecular and Covalent Crosslinking. Adv. Mater. 2016, 28, 8419-8424.
[22] Le, X.; Lu, W.; Zheng, J.; Tong, D.; Zhao, N.; Ma, C.; Xiao, H.; Zhang, J.; Huang, Y.; Chen, T. Stretchable supramolecular hydrogels with triple shape memory effect. 2016, 7, 6715-6720.
[23] Yan, Y.; Li, M.; Yang, D.; Wang, Q.; Liang, F.; Qu, X.; Qiu, D.; Yang, Z. Construction of Injectable Double-Network Hydrogels for Cell Delivery. Biomacromolecules 2017, 18, 2128-2138.
[24] Zhou, F.; Hong, Y.; Zhang, X.; Yang, L.; Li, J.; Jiang, D.; Bunpetch, V.; Hu, Y.; Ouyang, H.; Zhang, S. Tough hydrogel with enhanced tissue integration and in situ forming capability for osteochondral defect repair. Appl. Mater. Today 2018, 13, 32-44.
[25] Xiao, H.; Lu, W.; Le, X. X.; Ma, C. X.; Li, Z. W.; Zheng, J.; Zhang, J. W.; Huang, Y. J.; Chen, T. A Multi-Responsive Hydrogel with a Triple Shape Memory Effect Based on Reversible Switches. Chem. Commun. 2016, 52, 13292-13295.
[26] Wang, L. L.; Highley, C. B.; Yeh, Y. C.; Galarraga, J. H.; Uman, S.; Burdick, J. A. Three-dimensional extrusion bioprinting of single- and double-network hydrogels containing dynamic covalent crosslinks. J. Biomed. Mater. Res., Part A 2018, 106, 865-875.
[27] Cho, I. S.; Ooya, T. Tuned cell attachments by double-network hydrogels consisting of glycol chitosan, carboxylmethyl cellulose and agar bearing robust and self-healing properties. Int. J. Biol. Macromol. 2019, 134, 262-268.
[28] Fu, B; Cheng, B.; Jin, X.; Bao, X.; Wang, Z.; Hu, Q. Chitosan-based double network hydrogels with self-healing and dual-responsive shape memory abilities. J. Appl. Polym. Sci. 2019, 136, 48247.
[29] Lv, Y.; Pan, Z.; Song, C.; Chen, Y.; Qian, X. Locust bean gum/gellan gum double-network hydrogels with superior self-healing and pH-driven shape-memory properties. Soft Matter 2019, 15, 6171-6179.
[30] Lei, K.; Li, Z.; Zhu, D.; Sun, C.; Sun, Y.; Yang, C.; Zheng, Z.; Wang, X. Polysaccharide-based recoverable double-network hydrogel with high strength and self-healing properties. J. Mater. Chem. B 2020, 8, 794-802.
[31] Aldana, A. A.; Houben, S.; Moroni, L.; Baker, M. B.; Pitet, L. M. Trends in Double Networks as Bioprintable and Injectable Hydrogel Scaffolds for Tissue Regeneration. 2021, doi: 10.1021/acsbiomaterials.0c01749
[32] Lewis C. L.; Dell, E. M.; A review of shape memory polymers bearing reversible binding groups. J. Polym. Sci., Part B: Polym. Phys. 2016, 54, 1340-1364.

[33] Zhang, Z.; He, C.; Chen, X. Hydrogels based on pH-responsive reversible carbon–nitrogen double-bond linkages for biomedical applications. Mater. Chem. Front., 2018, 2, 1765-1778.
[34] Silverstein, M. S. Interpenetrating polymer networks: So happy together? Polymer 2020, 207, 122929.
[35] Kheirabadi, M.; Shi, L.; Bagheri, R.; Kabiri, K.; Hilborn, J.; Ossipov, D. A. In situ forming interpenetrating hydrogels of hyaluronic acid hybridized with iron oxide nanoparticles. Biomater. Sci. 2015, 3, 1466-1474.
[36] Yang H.; Ghiassinejad S.; Van Ruymbeke, E.; Fustin, C. A. Tunable Interpenetrating Polymer Network Hydrogels Based on Dynamic Covalent Bonds and Metal-Ligand Bonds. Macromolecules, 2020, 53, 6956-6967.
[37] Shi, W. H.; Pathiranage, T. M. S. K.; Marciel, A. B. Rheological properties of engineered protein polymer networks. MRS Bull. 2020, 45, 1048-1054.
[38] Brassinne, J.; Stevens, A. M.; Van Ruymbeke, E.; Gohy, J.-F.; Fustin, C.-A. Hydrogels with dual relaxation and two-step gel-sol transition from heterotelechelic polymers. Macromolecules 2013, 46, 9134-9143.
[39] Brassinne, J.; Jochum, F.; Fustin, C.-A.; Gohy, J.-F. Revealing the supramolecular nature of side-chain terpyridine-functionalized polymer networks. Int. J. Mol. Sci. 2015, 16, 990-1007.
[40] Xu, X.; Jerca, F. A.; Jerca, V. V.; Hoogenboom, R. Self-Healing and Moldable Poly(2-isopropenyl-2-oxazoline) Supramolecular Hydrogels Based on a Transient Metal Coordination Network. Macromolecules 2020, 53, 6566-6575.
[41] Ahmadi, M.; Seiffert, S. Thermodynamic control over energy dissipation modes in dual-network hydrogels based on metal-ligand coordination. Soft Matter 2020, 16, 2332-2341.
[42] Czarnecki, S.; Rossow, T.; Seiffert, S. Hybrid polymer-network hydrogels with tunable mechanical response. Polymers 2016, 8, 82.
[43] Mukherjee, S.; Bapat, A. P.; Hill, M. R.; Sumerlin, B. S. Oximes as reversible links in polymer chemistry: dynamic macromolecular stars. Polym. Chem. 2014, 5, 6923-6931.
[44] Dawn, A.; Kumari, H. Low Molecular Weight Supramolecular Gels Under Shear: Rheology as the Tool for Elucidating Structure-Function Correlation. Chem. Eur.J. 2018, 24,762-776.
[45] Hawke, L. G. D.; Ahmadi, M.; Goldansaz, H.; van Ruymbeke, E. Viscoelastic Properties of Linear Associating Poly(N-butyl acrylate) Chains. J. Rheol. 2016, 60, 297-310.
[46] Deng G.; Tang C.; Li F.; Jiang, H.; Chen, Y. Covalent Cross-Linked Polymer Gels with Reversible Sol-Gel Transition and Self-Healing Properties. Macromolecules 2010, 43, 1191-1194.
[47] Xu, X.; Jerca, F. A.; Jerca, V. V.; Hoogenboom, R. Covalent Poly(2-Isopropenyl-2-Oxazoline) Hydrogels with Ultrahigh Mechanical Strength and Toughness through Secondary Terpyridine Metal-Coordination Crosslinks. Adv. Funct. Mater. 2019, 29, 1904886.
[48] Xu, D.; Craig, S. L. Strain Hardening and Strain Softening of Reversibly Cross-linked Supramolecular Polymer Networks. Macromolecules 2011, 44, 7478-7488.
[49] Xu, D.; Hawk, J. L.; Loveless, D. M.; Jeon, S. L.; Craig, S. L. Mechanism of Shear Thickening in Reversibly Cross-Linked Supramolecular Polymer Networks. Macromolecules 2010, 43, 3556-3565.

Chapter 6
Conclusion and Perspectives

6.1 Conclusion

The objective of this thesis was to develop polymer hydrogels crosslinked by the orthogonal combination of dynamic covalent bonds and supramolecular interactions. Reversible C=N bonds including acylhydrazone and oxime bonds were selected as the dynamic covalent linkages, while the metal-terpyridine coordination bonds, including Zn(II)-terpyridine (Zn^{2+}-Tpy) and Fe(II)-terpyridine (Fe^{2+}-Tpy) bis-complexes, were employed for the supramolecular crosslinks. In pursuit of the aim of combining the above two types of crosslinking into one gel system, three topological networks: interpenetrating polymer network (IPN), dual-crosslinked network (DCN) and IPN-derived double network (DN) hydrogels, have been designed and studied. Oscillatory rheological methods were used to investigate the dynamic and oscillatory mechanical properties of the hydrogels obtained.

In the literature review (Chapter 2), we learned that reversible C=N bonds and metal-terpyridine coordination bonds are the most easily regulated types of bonding in dynamic covalent and supramolecular chemistry, respectively. The reversible C=N bond is formed by the reaction of a carbonyl electrophile (aldehyde or ketone) with a nucleophile (amine, acylhydrazine, hydroxylamine). Thus, the stability and dynamic reversibility of the reversible C=N network can be tuned by changing the electrophilic and/or nucleophilic reagents. Due to the potential toxicity of aldehyde groups,[1, 2] which is not suitable for future bio-applications, and the fact that some aldehyde monomers usually

need to be stored at very low temperatures such as -20 °C to prevent oxidation,[3] this thesis has chosen to use low toxicity and room temperature stable ketone based monomers as reaction handles for copolymerization. Considering that ketones are less electrophilic than aldehydes, we have chosen acylhydrazides and hydroxylamines as crosslinkers to regulate the reversibility and stability of the reversible C=N bonds. Since the commercially available ketone monomers used belong to the acrylamide family, acrylamide-based Tpy monomers were therefore selected and synthesized in order to obtain copolymers in which the reaction sites (ketone, Tpy) were homogeneously dispersed along the chain. Considering the differences in the lifetime and bond strength of the different transition metal ions forming bis-complexes with terpyridine ligands, this thesis used Zn^{2+} and Fe^{2+} as crosslinkers for the supramolecular networks. The hydrophilic monomer of choice for copolymerization with ketones and/or Tpy monomers is N,N-dimethylacrylamide (DMA), thus PDMA provides the aqueous polymer backbone. Unlike other hydrophilic polymers in the acrylamide family, such as the hydrogen bonding of polyacrylamide and the thermo-responsiveness of poly(N-isopropylacrylamide), which can affect the mechanical or dynamic properties of hydrogels,[4, 5] PDMA is relatively inert. This allows the contribution of reversible C=N bonds and metal-terpyridine coordination bonds to the hydrogel to be investigated with little influence from the nature of the main chain polymer. As a result, commercially available ketone monomers, DMA as well as synthesized Tpy monomers from the acrylamide family, were used for the synthesis of functional copolymers.

In addition, we also demonstrated in Chapter 2, mainly using the example of reversible C=N bond-based hydrogels, that the incorporation of two different types of dynamic bonds as crosslinks into hydrogels allows for a choice of three network topologies: DCN, IPN and DN. DCN hydrogels are constructed from a short-chain (typically M_n < 60 kDa) copolymer containing two reaction handles by the formation of two types of crosslinks.[6, 7] Ensuring that the two functional reaction sites are homogeneously dispersed along the

polymer chain may require that both ketone and Tpy monomers have good solubility in the solvent of the copolymerization. Simple IPN hydrogels can be composed of two mono-functionalized short-chain copolymers cross-linked individually.[8] Thus the two copolymers functionalized with ketone or Tpy respectively can be prepared separately without considering the solubility of the two functional monomers together. In DN hydrogels, the first network is crosslinked by highly functionalized short-chain copolymers and the second network is connected by sparsely functionalized long-chain (generally M_n > 100 kDa) copolymers.[9, 10] As a result, there is a huge difference in the concentration of the two types of crosslinking in DN. The DN system is therefore not suitable for a systematic study of the respective contributions of the two different classes of crosslinks. Taken together, of the three network topologies: DCN, IPN and DN, IPN hydrogel is probably the easiest to implement.

In order to gain a preliminary understanding of the fundamental properties of hydrogels with the orthogonal combination of acylhydrazone/oxime bonds and Zn^{2+}-Tpy/Fe^{2+}-Tpy, the work in Chapter 3 investigated four IPN hydrogels based on two functionalized PDMA copolymers. The first copolymer bears ketone pendant groups and can be crosslinked by di-acylhydrazine or bis-hydroxylamine to form acylhydrazone or oxime networks. The second copolymer bears terpyridine side groups and can be crosslinked by Zn^{2+} or Fe^{2+} to obtain Zn^{2+}-Tpy or Fe^{2+}-Tpy networks. Therefore, four IPN hydrogels including stable oxime with a long-lifetime Fe^{2+}-Tpy (Oxime + Fe^{2+}-Tpy), or with a more dynamic Zn^{2+}-Tpy (Oxime + Zn^{2+}-Tpy) and a less stable acylhydrazone with a long-lifetime Fe^{2+}-Tpy (Acylhydrazone + Fe^{2+}-Tpy), or with a more dynamic Zn^{2+}-Tpy (Acylhydrazone + Zn^{2+}-Tpy), were prepared. The rheological results show that the obtained IPN hydrogels exhibit a higher modulus compared to the simple addition of the moduli of the single networks. Since the Zn^{2+}-Tpy network is able to show a relaxation behavior due to bond dissociation in experimental timescales,[11] the study of IPN hydrogels of Oxime + Zn^{2+}-Tpy and Acylhydrazone + Zn^{2+}-Tpy revealed that the partial relaxation takes

place through a sticky Rouse relaxation process. Because the oxime is pH-insensitive and acylhydrazone is pH-sensitive, the pH can be used as a stimulus to affect the dynamics of the IPN hydrogels. The rheological data showed that the oxime-based IPN hydrogels are the least affected by the pH change, while a low pH strongly influenced the stability of the acylhydrazone-based IPN hydrogels. In particular, the Acylhydrazone + Zn^{2+}-Tpy IPN, made of the two weakest bonds, exhibited reversible gel (pH: 6~7) to sol (pH: 1~2) transformation. Reverse strain sweeps on four IPN hydrogels measured from low to high, and then to low strain amplitude showed good reversibility, indicating that the reversible bonds present in IPN are forced to break under large oscillatory shear, but are able to re-form rapidly once the deformation is reduced. This demonstrated the self-healing ability of IPN hydrogels with the orthogonal combination of reversible C=N bonds and metal-terpyridine coordination bonds after a large deformation.

Building on these findings, we next sought to combine the labile zinc(II)-terpyridine coordination bonds and stable oxime bonds into DCN, IPN and DN hydrogels for comparison. In Chapter 4, a series of copolymers were synthesized and used to prepare DCN, IPN and DN hydrogels. We then compared the oscillatory mechanical properties and dynamic relaxation behavior of these three hydrogels and the corresponding single crosslinked sub-networks by oscillatory rheology. Compared to single oxime crosslinked networks, single Zn^{2+}-Tpy crosslinked network exhibit higher plateau moduli and thus dominate the stiffness of the hydrogels before the dissociation of Zn^{2+}-Tpy. Due to the finite lifetime of the Zn^{2+}-Tpy bis-complexes, the single Zn^{2+}-Tpy networks displayed stress relaxation behavior on a timescale probed in the experiment and therefore determined the dynamic relaxation behavior of the hydrogels. After dissociation of the Zn^{2+}-Tpy sub-networks in the low frequency region (long timescale), the hydrogel networks are supported by the stable oxime sub-networks maintaining their solid-like behaviors. Consequently, DCN, IPN and DN hydrogels crosslinked with both Zn^{2+}-Tpy and oxime showed

similar viscoelastic solid behaviors in the frequency sweeps. Unlike DCN, IPN and DN are composed of two independent interpenetrating networks, and the presence of one sub-network influences the formation of crosslinks in the other sub-network, reducing the density of effective crosslinks. This difference in effective crosslinking density between the different topologies results in higher elastic moduli for DCN than for IPN or DN, and in the present work the plateau modulus in the high frequency region is G'_p (DCN) > G'_p (IPN) > G'_p (DN). Compared to the single crosslinked sub-networks, the topological differences between DCN, IPN and DN result in different magnitudes of potential gain in modulus. Among them, the elastic moduli of hydrogels with both Zn^{2+}-Tpy and oxime crosslinks show a ~2-fold increase for DCN, ~3-fold for IPN, and ~3.6-fold for DN compared to the sum of the moduli of the respective sub-networks. In addition, we demonstrated that the order of deformability and stability of the hydrogels under oscillatory strain is generally DCN <IPN <DN. Finally, we proved that DCN, IPN and DN hydrogels can recover after partial damage by oscillatory strain, indicating their self-healing properties due to the dynamic reversibility of Zn^{2+}-Tpy.

In Chapter 5, we have developed two contrasting DN hydrogels by the combination of the metal-terpyridine coordination bonds and reversible C=N bonds. The two DN hydrogels differ in the bonds used to form the densely crosslinked first network and the loosely crosslinked second network. In one DN hydrogel, the first network is crosslinked by the labile Zn^{2+}-Tpy bis-complexes and the second network is crosslinked by the stable oxime bonds. In contrast, in the other DN hydrogel, the first network is crosslinked by the less stable acylhydrazone bonds and the second network is crosslinked by the long lifetime Fe^{2+}-Tpy bis-complexes. Oscillatory shear rheology results revealed that the more dynamic first networks (Zn^{2+}-Tpy or acylhydrazone) in the two DN hydrogels are responsible for the stress relaxation behavior of the DN hydrogels. The more stable second networks (oxime or Fe^{2+}-Tpy) protect the integrity of the hydrogel over a long timescale or under large oscillatory strain. The two DN hydrogels

showed higher plateau moduli than the sum of their corresponding two sub-network plateau moduli. In addition, the DN hydrogel crosslinked by Zn^{2+}-Tpy and oxime exhibits less deformability than the hydrogel crosslinked by acylhydrazone and Fe^{2+}-Tpy due to the more dynamic but unstable first network of Zn^{2+}-Tpy than of acylhydrazone. We also demonstrated that the self-healing properties of both DN hydrogels are due to a synergistic effect between the dynamic reversibility of the first network and the high deformability of the second network.

In brief, our study explored the dynamic behaviors and oscillatory mechanical properties of dynamic hydrogels from the perspective of dual dynamic bonds and network topologies. In terms of dynamic bonds, the relaxation behaviors of hydrogels caused by the dissociation of more dynamic supramolecular interactions are more likely to be observed on experimental timescales. Due to topological differences, DCN is more conducive to producing high elastic modulus hydrogels, while DN has a greater potential to increase elastic modulus compared to its single networks and is also more favorable to create deformable hydrogels. The elastic modulus and deformability of IPN lie between that of DCN and DN.

As we mentioned in the literature review part of Chapter 2, most of the current dynamic hydrogels are based only on supramolecular interactions or only on dynamic covalent bonds, with very few studies that choose to use a combination of these two different types of dynamic bonds. Our work has developed a precedent for a new class of dynamic bond combinations, namely the combinations of reversible C=N bonds and metal-terpyridine coordination bonds with tunable dynamics for the preparation of dynamic hydrogels. More importantly, our works systematically investigate the effect of three network topologies, namely DCN, IPN and DN, on the properties of gels. This question of selecting the most appropriate network topology may arise for any hydrogel system when introducing more than two dynamic bonds, but has never been discussed systematically in previous works. The results of our rheological studies show that topology does not significantly

affect the dynamic behavior of the hydrogels. However, topology strongly influences the elastic modulus of a hydrogel, by affecting the number of dynamic bonds that form effective crosslinks, and also determines the potential magnitude of modulus increase and deformability of the hydrogel. This thesis could provide the reader with ideas for designing other dynamic hydrogels with desired properties that combine multiple dynamic bonds.

The dynamic and oscillatory mechanical properties of all the above hydrogels and networks were determined by small amplitude oscillatory shear (SAOS) measurements in linear viscoelastic (LVE) range. To learn and compare in depth the properties of DCN, IPN and DN hydrogels with the orthogonal combination of reversible C=N bonds and metal-terpyridine coordination bonds, other measurements should also be considered in future work. In addition, applications of these hydrogels are also worth exploring.

6.2 Perspectives

Hydrogel structure

As our dual dynamically crosslinked hydrogels were prepared from side chain modified copolymers, the possible aggregation of the hydrophobic functional groups (ketones and terpyridines) in water is uncertain. The aggregation of these copolymers in aqueous solutions is most likely to appear before the addition of crosslinkers. For the terpyridines, once the divalent transition metal ions are added, the ionic nature of formed complexes strongly increase the hydrophilicity, and the pseudo-octahedral geometry of the bis-complexes also reduces possible π-π stacking. For ketone copolymers, the diacetone acrylamide (DAAM) units in the polymer chain are hydrophobic, but the hydrophobicity of the DAAM will be diminished by the hydrophilicity of the crosslinkers after the formation of acylhydrazone or oxime bonds.[12, 13] Such hydrophobic aggregation may affect the structure and properties of the hydrogels. For example, the aggregation of the hydrophobic groups may induce a large number of intra-chain crosslinks rather than effective inter-chain crosslinks, potentially reducing the elastic modulus of the gel, upon the addition of crosslinkers.[12] The local aggregation of polymers may also result in a final gel network that is not perfectly homogeneous, and in particular, the IPN and DN may not be homogeneous interpenetrating networks. Therefore, the hydrophobic aggregation of the copolymers in water before and after the addition of the crosslinkers directly affects the homogeneity of the hydrogel structure and thus the macroscopic mechanical properties of the hydrogel. A first important perspective would thus be to learn about the aggregation behaviors of the copolymers in solution, before the addition of the crosslinkers, and the microstructure of the hydrogels formed after the addition of the crosslinkers.

In order to observe the aggregation behaviors of copolymers in aqueous solutions, we can use DLS (dynamic light scattering).[12] Using the DLS we can obtain the hydrodynamic diameter (D_h) of the copolymers in water and in DMF (in which copolymers exist as completely dissolved unimers), at the same concentration. If the copolymers form aggregates in aqueous solution, the D_h measured in water will be much greater than that in DMF. The size of the aggregates can also be obtained from transmission electron microscopy (TEM) or atomic force microscopy (AFM) images. In the same way, DLS or SEM can also be used to characterize the microstructure of hydrogels to study the homogeneity of the hydrogel networks.[14] In addition, small-angle neutron scattering (SANS), which is particularly suitable for studying the structure of polymer networks in the 1~1000 nm range,[15] could also be used to investigate the microstructure of hydrogels.

Furthermore, the addition of crosslinkers leads to the bond formation, and this can be correlated with the crosslinking density of the hydrogels. Following the number of formed bonds would help to understand the contribution of the bonds to the elastic modulus. In Chapter 3, we have shown that ^{1}H NMR spectroscopy can demonstrate the formation of acylhydrazone and oxime bonds, but the characteristic peaks are broad, making it difficult to determine the amount of bond formation by integration. Additionally, we also demonstrated that the formation of effective crosslinks (in turn related to the elastic modulus) correlates with the polymer concentration, crosslinker concentration and the presence of non-crosslinked polymer. Therefore, to trace the formation of bonds in a specific system it is best to use in situ detection methods. With these in mind, Fourier-transform infrared (FTIR) and Raman spectroscopies could be used to follow bond formation by looking at characteristic peaks (e.g. ketone vs oxime, or free terpyridines vs complexed ones), and translating the area under a characteristic region to a molar quantity using a Beer's Law type analysis.[14] Other spectroscopies such as ultraviolet/visible absorption (UV-vis) could also be used to quantify the concentration of metal-terpyridine coordination bond formed.

Nonlinear shear measurements

The nonlinear viscoelastic properties of dynamic hydrogels under large shear deformations are also interesting to be explored. For highly viscous systems, such as entangled polymer solutions or polymer melts, rheological measurements at high shear rates may cause flow instabilities including wall slip, shear banding, and edge fracture. To reduce experimental errors caused by edge fracture in rheological shear measurements, the cone-partitioned-plate (CPP) geometry is one of the most effective methods.[16] As shown in **Figure 6.1**, a CPP setup consists of a top combination fixture and a bottom cone that is connected to the motor of the rheometer. The combination fixture is divided into two parts, an inner plate and an outer hollow plate surrounding the inner plate, the two plates being coaxial and separate. The inner plate is connected to the sensor of the rheometer and records the torque, while the outer hollow plate is connected to the instrument and is fixed. During the test, rupture generally occurs at the edge of the sample. As long as the rupture edge does not propagate into the measured central plate, the recorded torque is negligibly affected by the rupture of the sample at the extremity.

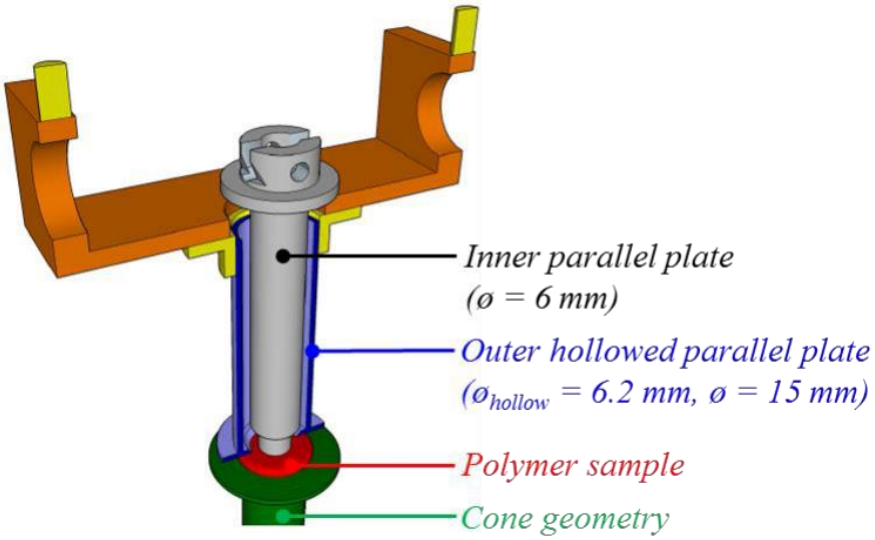

Figure 6.1. Schematic view of the cone-partitioned-plate (CPP) setup.[12]

Therefore, the CPP geometry allows measurement of the nonlinear shear flow properties of hydrogel samples. By using this method, reliable, artifact-free and bulk shear flow data could be obtained for DCN, IPN and DN hydrogels at high rates and/or strains.[17] From the conclusions in Chapter 4 it is clear that DN hydrogels have the greatest deformability. Starting the CPP measurements with both Zn^{2+}-Tpy and oxime crosslinked DN hydrogels first would be recommended.

Mechanical measurements

In addition to the rheological properties, the macro-mechanical properties of dynamic hydrogels are important to define whether the hydrogel can meet the requirements for certain applications. For example, the DN hydrogel in Chapter 4 has been shown to be stretchable (**Figure 6.2**). This property can be characterized by uniaxial tensile testing using a universal tensile tester. By performing uniaxial tensile/compression tests, the mechanical properties of the hydrogel, including tensile/compression strength, tensile/compression strain,

Young's modulus, toughness etc. can be obtained. In addition, it is possible to characterize the fatigue resistance of hydrogels by performing loading-unloading cyclic tensile/compression tests with preset testing parameters (e.g., strain, strain rate, etc.). [18] Therefore, the mechanical characterization of DCN, IPN and DN hydrogels can be performed not only to understand and compare the effect of different topologies on the mechanical properties of hydrogels crosslinked by dual dynamic bonds, but also to examine whether the hydrogels meet the mechanical requirements for practical applications.

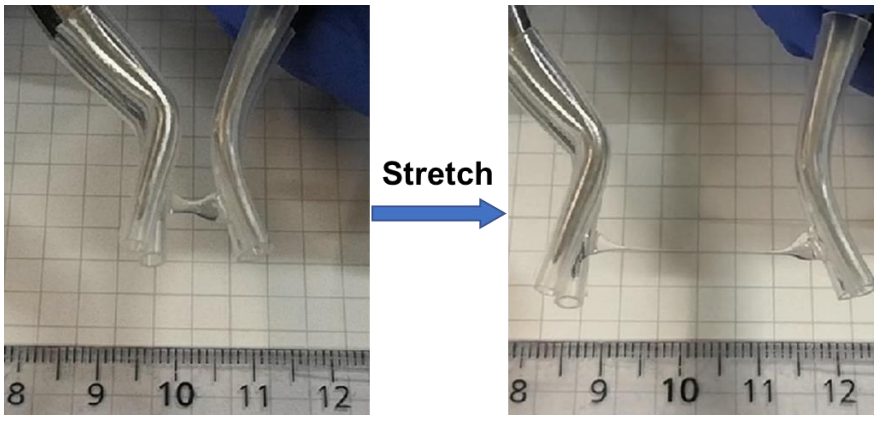

Figure 6.2. Photographs showing the stretchability of the both Zn^{2+}-Tpy and oxime crosslinked DN1 hydrogel in Chapter 4.

Applications

As discussed in the literature review in Chapter 2, hydrogels containing reversible C=N bonds may have many applications. For example, many acylhydrazone bonds constructed hydrogels exhibit injectability, which can be further developed for 3D printing applications. The acylhydrazone hydrogels prepared from ketone-functionalized PDMA polymers similar to this thesis also demonstrated the low toxicity of the hydrogels by in vitro cytotoxicity assays. [19, 20] In addition, Zn(II) cations are known to exhibit low toxicity, thus allowing

the use of Zn^{2+}-Tpy together with acylhydrazone crosslinking to prepare DCN, IPN or DN hydrogels to explore hydrogel applications in biomedicine. Importantly, the reversible C=N bond crosslinks in these hydrogels are acid degradable even though they are stable oxime bonds.[21] These suggest that hydrogels made of reversible C=N bonds and metal-ligand coordination bonds as crosslinks are promising for biomedical applications through 3D printing, and that the reversibility of dynamic bonds facilitates self-healing, recycling or reuse of the materials.

In conclusion, this thesis demonstrates for the first time that reversible C=N bonds and metal-terpyridine coordination bonds can be orthogonally combined to construct dynamic hydrogels. More importantly, three topological strategies for integrating two different types of dynamic bonds into hydrogels have been explored. The dynamic and oscillatory mechanical properties of three topological DCN, IPN and DN hydrogels have been systematically investigated and compared by rheology. Our investigations could provide insights not only into the selection of multiple dynamic bonds to fabricate dynamic networks, but also into the selection of suitable topologies to combine the two types of bonds to prepare polymeric materials. We hope that these studies will stimulate the design of dynamic polymer materials with the required properties for further applications.

6.3 Reference

[1] Spicer, C. D.; Pashuck, E. T.; Stevens, M. M. Achieving Controlled Biomolecule-Biomaterial Conjugation. Chem. Rev. 2018, 118, 7702-7743.

[2] Kölmel, D. K.; Kool, E. T. Oximes and Hydrazones in Bioconjugation: Mechanism and Catalysis. Chem. Rev. 2017, 117, 10358-10376.

[3] Patenaude, M.; Campbell, S.; Kinio, D.; Hoare, T. Tuning gelation time and morphology of injectable hydrogels using ketone-hydrazide cross-linking. Biomacromolecules 2014, 15, 781-790.

[4] Zhang, X.; Liu, K.; Liu, J.; Ding, Y.; Li, W.; Zhang, A. Thermoresponsive cryogels from dendronized interpenetrating polymer network showing dual-shape memory. Eur. Polym. J. 2020, 141, 110092.

[5] Gutierres, A.; Pascual, S.; Fontaine, L.; Piogé, S.; Benyahia, L. The effect of metal ions on the viscoelastic properties of thermosensitive sol-to-gel reversible metallo-supramolecular hydrogels. Polym. Chem. 2018, 9, 2494-2504.

[6] Liu, Y.; Liu, Y.; Wang, Q.; Han, Y.; Chen, H.; Tan, Y. Doubly Dynamic Hydrogel Formed by Combining Boronate Ester and Acylhydrazone Bonds. Polymers 2020, 12, 487.

[7] Zhao, J.; Diaz-Dussan, D.; Wu, M.; Peng, Y. Y.; Wang, J.; Zeng, H.; Duan, W.; Kong, L.; Hao, X.; Narain, R. Dual-Cross-Linked Network Hydrogels with Multiresponsive, Self-Healing, and Shear Strengthening Properties. Biomacromolecules 2021, 22, 2, 800-810.

[8] Wang, Y.; Yu, H.; Yang, H.; Hao, X.; Tang, Q.; Zhang, X. An Injectable Interpenetrating Polymer Network Hydrogel with Tunable Mechanical Properties and Self-Healing Abilities. Macromol. Chem. Phys. 2017, 218, 1700348.

[9] Fu, B; Cheng, B.; Jin, X.; Bao, X.; Wang, Z.; Hu, Q. Chitosan-based double network hydrogels with self-healing and dual-responsive shape memory abilities. J. Appl. Polym. Sci. 2019, 136, 48247.

[10] Lei, K.; Li, Z.; Zhu, D.; Sun, C.; Sun, Y.; Yang, C.; Zheng, Z.; Wang, X. Polysaccharide-based recoverable double-network hydrogel with high strength and self-healing properties. J. Mater. Chem. B 2020, 8, 794-802.

[11] Ahmadi, M.; Seiffert, S. Dynamic model metallo-supramolecular dual-network hydrogels with independently tunable network crosslinks. J. Polym. Sci. 2020, 58, 330-342.

[12] Mukherjee, S.; Bapat, A. P.; Hill, M. R.; Sumerlin, B. S. Oximes as reversible links in polymer chemistry: dynamic macromolecular stars. Polym. Chem. 2014, 5, 6923-6931.

[13] Guo, Z.; Gu, H.; He, Y.; Zhang, Y.; Xu, W.; Zhang, J.; Liu, Y.; Xiong, L.; Chen, A.; Feng, Y. Dual dynamic bonds enable biocompatible and tough hydrogels with fast self-recoverable, self-healable and injectable properties. Chem. Eng. J. 2020, 388, 124282.

[14] Danielsen, S. P. O.; Beech, H. K.; Wang, S.; El-Zaatari, B. M.; Wang, X.; Sapir, L.; Ouchi, T.; Wang, Z.; Johnson, P. N.; Hu, Y.; Lundberg, D. J.; Stoychev, G.; Craig, S. L.; Johnson, J. A.; Kalow, J. A.; Olsen, B. D.; Rubinstein, M. Molecular characterization of polymer networks. Chem. Rev. 2021, 121, 8, 5042-5092.

[15] Yu, G.; Yan, X.; Han, C.; Huang, F. Characterization of supramolecular gels. Chem. Soc. Rev., 2013, 42, 6697-6722.
[16] Costanzo, S.; Huang, Q.; Ianniruberto, G.; Marrucci, G.; Hassager, O.; Vlassopoulos, D. Shear and Extensional Rheology of Polystyrene Melts and Solutions with the Same Number of Entanglements. Macromolecules 2016, 49, 10, 3925-3935.
[17] Snijkers, F.; Vlassopoulos, D. Cone-partitioned-plate geometry for the ARES rheometer with temperature control. J. Rheol. 2011, 55, 1167-1186.
[18] Wang, W.; Narain, R.; Zeng, H. Chapter 10: Hydrogels. In Polymer science and nanotechnology; Narain, R. Ed.; Elsevier, 2020, pp 203-244.
[19] Garcia, F. P.; Rippe, M.; Companhoni, M. V. P.; Stefanello, T. F.; Louage, B.; Van Herck, S.; Sancey, L.; Coll, J. L.; De Geest, B. G.; Vataru Nakamura, C.; Auzely-Velty, R. A versatile method for the selective core-crosslinking of hyaluronic acid nanogels via ketone-hydrazide chemistry: from chemical characterization to in vivo biodistribution. Biomater. Sci. 2018, 6, 1754-1763.
[20] Hou, F.; Xi, B.; Wang, X.; Yang, Y.; Zhao, H.; Li, W.; Qin, J.; He, Y. Self-healing hydrogel with cross-linking induced thermo-response regulated light emission property. Coll. Surf. B Biointerfaces 2019, 183, 110441.
[21] Sims, M. B.; Patel, K. Y.; Bhatta, M.; Mukherjee, S.; Sumerlin, B. S. Harnessing Imine Diversity To Tune Hyperbranched Polymer Degradation. Macromolecules 2018, 51, 356-363.